Charles University in Prague

Faculty of Science

Ph.D. Program: Immunology

Mgr. Iva Šplíchalová

The utility of Toll-like receptor 2 in defining the progenitors of definitive embryonic hematopoiesis

Využití Toll-like receptoru 2 při definování embryonálních definitivních hematopoetických progenitorů

Ph.D. Thesis

Supervisor: RNDr. Dominik Filipp, CSc.

Laboratory of Immunobiology

Institute of Molecular Genetics of the ASCR, v.v.i.

Prague, 2020

DECLARATION

I hereby declare that this thesis is a presentation of my original research work. Wherever the contribution of others is involved, every effort is made to indicate this clearly, with reference to the literature and acknowledgement of collaborative research and discussions. This thesis contains no material that has been submitted previously, in whole or in part, for the award of any other academic degree or diploma.

Prague,

Signature:

ACKNOWLEDGMENTS

ABSTRACT

Hematopoiesis is a vital process in which red blood cells and cells of the immune system are formed. It is initiated during early embryonic development when we find hematopoietic progenitors in separate anatomical sites. Embryonic hematopoiesis comprises three successive and partly overlapping waves of progenitors with a different hematopoietic potential. The primary anatomical place where hematopoiesis takes place shortly before the birth is the bone marrow (BM). Since at this time point of development BM is already populated by hematopoietic stem cell (HSCs) progenitors, it becomes also the site of hematopoiesis in adulthood. However, the bone marrow is not the only place where hematopoietic progenitors emerge and develop. The Yolk sac (YS) and the Aorta-Gonad-Mesonephros (AGM) region are the initial sites of the appearance of the three waves of progenitors in the early embryogenesis. These progenitors and their descendants play an indispensable role during the development of an individual. Because there are no specific markers that would unambiguously characterize progenitors of these individual waves, their physical separation and hence also functional characterization is still incomplete.

Recent studies have shown that Toll-like receptors (TLRs) are expressed on adult HSCs. The stimulation of HSC via TLRs leads to the preferential generation of myeloid lineages. We have shown that TLR2 is expressed on progenitors of the second hematopoietic wave, erythro-myeloid progenitors (EMPs). Since such TLR2 expression allowed the distinction between emerging EMP precursors from the preceding wave of precursors of primitive erythropoiesis, we characterize in detail the emergence, fate, and function of EMPs during early embryogenesis. We were able to show that the progenitors of EMPs emerge much earlier than previously described in the literature. Using various novel transgenic models we have also demonstrated the indispensability of $TLR2^+$ EMPs for embryonic development.

Both embryonic and hematopoietic progenitors and cells in the adult traverse through the body via navigation which is based on the interaction between their chemokine receptors and their ligands. One such molecule is the chemokine

CXCR4. Using a transgenic mouse model we have shown that CXCR4 hyperactivation has no impact on embryonic hematopoiesis, but affected adult hematopoiesis. The work conducted on medullary thymic epithelial cells also showed that TLR9-regulated expression of chemokines is critical for the process of establishment of central tolerance, specifically, the recruitment of monocyte-derived dendritic cells to the thymic medulla and the generation of regulatory T cells.

This dissertation thesis revolves around three already published articles and one article that has been already submitted and is currently under revision. The first part of this thesis provides a literature overview of embryonic and adult hematopoiesis as well as the structure and function of TLRs. The following chapter defines the main objectives of this work. The three above mentioned papers and one attached manuscript represent the results and specific discussion to each part of my experimental work. The last part of my thesis containing the chapters General discussion and Conclusions summarizes the main output and novelty of presented work. We believe that the presented work will contribute to a better and more comprehensive understanding of both embryonic as well as adult hematopoiesis.

ABSTRAKT

Krvetvorba, též hematopoéza je životně nepostradatelný proces, při kterém se tvoří červené krvinky a buňky imunitního systému. Její počátek sahá již do embryogeneze, kdy v různých anatomických místech nalézáme hematopoetické progenitory. Embryonálí hematopoéza je složená ze tří vln progenitorů, jejichž vznik se časově překrývá a vyznačují se různým potenciálem tvorby svých dceřinných buněk. Krátce před narozením můžeme kompletní hematopoézu nalézt v kostní dřeni, která je díky přítomnosti hematopoetických kmenových buněk (HSCs) hlavním místem krvetvorby v dospělém jedinci. Avšak kostní dřeň není jediné místo, kde hematopoetické progenitory vznikají a vyvýjí se. Žloutkový váček a Aorta-Gonad Mesonephros jsou místa, ve kterých dochází k vzniku prvních progenitorů tří krvetvorných vln a to již během embryogeneze. Tyto progenitory a jejich dceřinné buňky hrají nepostradatelnou roli během vývoje jedince. Protože neexistuje jedinečný marker, který by byl exkluzivní pro progenitory jednotlivých vln jejich separace a následná funkční charakterizace není doposud kompletní.

Nedávné studie ukázaly, že Toll like receptory (TLRs) jsou exprimované na HSCs v kostní dřeni. Jejich stimulací dochází k přednostnímu vzniku myeloidních krevních linií. V naší práci jsme ukázali, že TLR2 lze nalézt na progenitorech druhé embryonální hematopoetické vlny, takzvaných erytro-myeloidních progenitorech (EMPs). Exprese TLR2 na EMPs umožňuje jejich odlišení od hematopoetických progenitorů první vlny, která produkuje primitivní erytrocyty. Díky tomuto zjištění jsme byli schopni detailně charakterizovat vznik a funkci EMPs během ranné embryogeneze. Navíc jsme ukázali, že progenitory EMPs vznikají mnohem dříve, než bylo popsáno v literatuře. Za použití několika nových myších modelů jsme demonstrovali nepostradatelnost TLR2$^+$ EMPs pro vývoj embrya. Jak embryonální tak hematopoetické progenitory a buňky v dospělém jedinci se pohybují na základně inerakcí migratorních molekul a jejich ligandů. Jednou takovou molekulou je chemokinový receptor CXCR4. Za použití transgenního myšího modelu, kde dochází ke zvýšené expresi a aktivaci této molekuly jsme demostrovali, že hyperaktivace CXCR4 nemá zásadní vliv na průběh embryonální hematopoézy, avšak ovlivňuje průběh hematopoézy v dospělci. Poslení práce, která

se zabývala funkcí medulárních epitelialních buněk v brzlíku taktéž poukázala na nepostradatelnost TLRs a chemokinové signalizace. V práci jsme ukázali, že TLR9 řízená exprese chemokinů je nepostradatelná k ustanovení centrální tolerance, zejména pro vstup dendritických buněk derivovaných z monocytů do meduly a následnému vzniku regulačních T lymfocytů.

Předložená disertační práce vznikla na základě tří opublikovaných prací a jedné práce, která je v revizi. První část je věnována úvodu, ve který popisuje embryonální a dospělou hematopoézu a strukturu TLRs. Následuje definování cílů disertační práce spolu s výsledky, které zahrnují tři opublikované práce a jednu, která je v revizním řízení. Práce je zakončená diskuzí a závěry, které shrnují hlavní poznatky a objevy našeho výzkumu. Tato práce by měla posloužit k lepšímu pochopení jak embryonální hematopoézy tak té dospělé.

TABLE OF CONTENTS

LIST OF ABBREVIATIONS

AA4.1   CD93, C-type lectin transmembrane receptor

AGM   Aorta-gonad mesonephros

AIRE   Autoimmune regulator

APC   Antigen-presenting cells

BM   Bone marrow

CAT   Cooperative antigen transfer

CD11b   Integrin alpha M

CD31   Platelet endothelial cell adhesion molecule

CD41   Integrin alpha-Iib

CD45   Protein tyrosine phosphatase, receptor type, C

CD144   VE-cadherin

CD201   Endothelial protein C receptor

c-kit   Tyrosine-protein kinase KIT

CLPs   Common lymphoid progenitors

CMPs   Common myeloid progenitors

Csf1r   Colony-stimulating factor 1 receptor CSF1R

cTECs   Cortical thymic epithelial cells

CX3CR1   Fractalkine receptor

CXCR4   C-X-C chemokine receptor type 4

DAMPs   Damage-associated molecular patterns

DCs   Dendritic cells

DDs   Death domains

DN   Double negative

DP   Double positive

DT   Diphtheria toxin

E   Embryonic day

EHT   Endothelial to hematopoietic transition

EMP   Erythro-myeloid progenitor

F4/80   EGF-like module-containing mucin-like hormone receptor-like 1

FcRγ	Fc receptor gamma
FL	Fetal liver
Hlf	Hepatic leukemia factor
HSC	Hematopoietic stem cell
Il	Interleukin
INF	Interferon
LRRs	Leucine-rich repeats
LT-HSCs	Long term hematopoietic stem cells
mDCs	Migratory dendritic cells
MHC	Major histocompatibility complex I and II
MMPs	Multipotent progenitors
mTECs	Medullary thymic epithelial cells
Myd88	Myeloid differentiation primary response 88
NF-kB	Nuclear factor kappa-light-chain-enhancer of activated B cells
NPCs	Neuronal progenitor cells
OH	Hydroxy-tamoxifen
PAMPs	Pathogen-associated molecular patterns
pDCs	Plasmacytoid dendritic cells
PRRs	Pattern recognition receptors
RAG	V(D)J recombination-activating genes recombinases
Runx1	Runt-related transcription factor 1
ST-HSCs	Short term hematopoietic stem cells
tDCs	Thymic dendritic cells
T reg	T regulatory cell
TCR	T-cell receptor
TF	transcription factor
TLRs	Toll-like receptors
TRAs	Tissue-restricted antigens
TRIF	TIR-domain-containing adapter-inducing interferon-β
WBP1L	WW domain-binding protein 1-like

1. OVERVIEW OF THE LITERATURE

1.1. INTRODUCTION

Before the establishment of the adult hematopoiesis, the embryonic hematopoiesis occurs. Embryonic hematopoiesis is a dynamic process that takes place in different anatomical locations where the progenitors of each wave appear. The progenitors, their progeny, and mature cells seed developing organs and contribute to the proper development. Before birth, the hematopoietic stem cells (HSCs) seeds the bone marrow (BM) where they expand and establish the pool of adult hematopoiesis. To this day, only a subset of tissue-resident macrophages is considered to be derived from the embryonic progenitor, called erythro-myeloid progenitor (EMP) which came before the establishment of the adult hematopoietic system (Perdiguero et al., 2015; Schulz et al., 2012; Yona et al., 2013).

Embryonic hematopoiesis can be divided into three waves based on the appearance of progenitors with different hematopoietic potential. The first and second waves originate from the yolk sac (YS) and give rise mainly to the erythrocytes and macrophages (Ferkowicz et al., 2003; Perdiguero et al., 2015). Part of the embryo-derived macrophages, originating from the YS, persists till adulthood to became tissue-resident macrophages in adult organs. The third wave originates from the embryo proper (EP) and gives rise to HSCs (Yokomizo and Dzierzak, 2010) which later seed the fetal liver (FL) (Ema and Nakauchi, 2000; Kumaravelu et al., 2002) and shortly before birth colonize BM (Mendelson and Frenette, 2014). The potential of the HSCs is not lineage-restricted as observed for hematopoietic progenitors originating from YS. They generate erythrocytes, myeloid cells as well as T and B lymphocytes (Kumaravelu et al., 2002; Muller et al., 1994), which are later subjected to negative selection in the thymus and BM, respectively.

Toll-like receptors (TLRs) are evolutionarily conserved receptors present even in lower animals. They were firstly described in 1985 on fruit flu Drosophila melanogaster and named Toll (Anderson et al., 1985)and only a few years later in human (Medzhitov et al., 1997) with the main function to recognize exogenous pathogen-associated molecular patterns (PAMPs) (Li et al., 2014; Mariano et al.,

2014) and endogenous damage-associated molecular patterns (DAMPs) (Kariko et al., 2004; Liu-Bryan et al., 2005; Shi et al., 2003; Vabulas et al., 2001). It has been shown that TLRs are expressed on adult HSCs in the bone marrow where their stimulation under inflammatory conditions preferentially drives the hematopoiesis towards the generation of myeloid lineage (De Luca et al., 2009; Megias et al., 2012). We have shown, that TLR2 is expressed on EMPs and HSCs in the embryo and can be used as the marker for the genetic lineage tracing of its progeny. Also, we have described the importance of TLR signaling in the thymic generation of T regulatory cells.

1.2. ORIGIN OF EMBRYONIC HEMATOPOIESIS

One of the closest and readily available system for studying mammalian hematopoietic system is a mouse model. This is largely due to the number of embryos, relatively fast progress of the pregnancy, and the same anatomical locations as in humans where the progenitors of each hematopoietic wave appear.

A routine classification of embryonic waves is based on the anatomical sites where the progenitor cells are generated and with respect to the time of their appearance. Based on these criteria, embryonic hematopoiesis can be divided into three waves. The first transient wave is extra-embryonic and appears between embryonic day (E) 7.25 to E7.5 in the YS within blood islands and displays a restricted hematopoietic potential to generate mainly the first erythroid cells (Ferkowicz et al., 2003; Isern et al., 2011). The second transient hematopoietic wave emerges at E8.25-8.5 in the YS (Perdiguero et al., 2015). The timing of its appearance is not the only attribute by which we can distinguish it from the very first wave. The hematopoietic potential of progenitors is also different in comparison to that of the first wave. It can give rise to the erythroid as well as myeloid cells (mainly macrophages) and due to this capacity, these progenitors are referred to as erythro-myeloid progenitors (EMP) (Frame et al., 2016; Palis et al., 1999; Perdiguero et al., 2015). As the embryo is growing, the EMPs and macrophages expand in YS, migrate to and colonize developing FL (McGrath et al., 2015; Mukouyama et al., 1999). The only described

product of this wave that persists during the postnatal life are macrophages. They infiltrate forming fetal organs and give rise to the tissue-resident macrophages (Schulz et al., 2012; Yona et al., 2013).

The third and the ultimate wave of embryonic hematopoiesis, represented by HSCs, develops in the EP (Garcia-Porrero et al., 1995; Garcia-Porrero et al., 1998; Yokomizo and Dzierzak, 2010). The HSCs are generated in the form of clusters within the arterial regions (Yokomizo and Dzierzak, 2010), which are readily detectable at E10.5 (Medvinsky and Dzierzak, 1996). Shortly thereafter they migrate to the FL which serves as a niche for their expansion and differentiation and where they develop along with EMPs (Ema and Nakauchi, 2000; Kumaravelu et al., 2002). HSCs migrate to BM shortly before birth where they reside and generate progenitor cells of all hematopoietic lineages throughout mammalian adult life (Mendelson and Frenette, 2014). Adult hematopoiesis replaces embryonic one shortly after the birth.
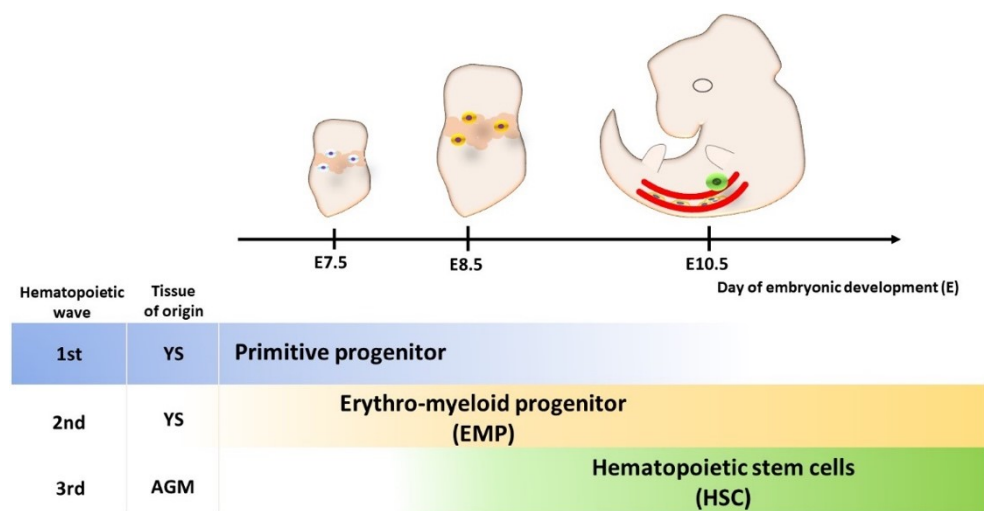
Figure 1. The appearance of hematopoietic progenitors in the mouse embryo. *Schematics of developing mouse embryos at stages E7.5, E8.5, and E10.5, showing sites of the appearance of hematopoietic progenitors from each embryonic wave. The YS is the site where EMPs originate. These progenitors belong to the first and second waves of hematopoiesis. The third wave is characterized by the appearance of HSCs at E10.5 in the embryo proper within the major vitelline arteries such as vitelline, umbilical arteries, and mainly AGM. YS= Yolk Sac, AGM= Aorta-Gonad Mesonephros Adapted from (Costa et al., 2012; Perdiguero and Geissmann, 2016).*

1.2.1. FIRST HEMATOPOIETIC WAVE

The earliest events related to the hematopoiesis starts to occur around E7.25 in the hemogenic angioblast of the YS blood islands (Isern et al., 2011). The process is also called primitive hematopoiesis due to the production of mainly nucleated erythroid cells which are called primitive (Tober et al., 2007). This wave possesses the ability to generate predominantly primitive erythrocytes and megakaryocytes (McGrath et al., 2003; Palis et al., 1999; Tober et al., 2007) which are the first hematopoietic cells produced in the embryo (Costa et al., 2012). Primitive erythrocytes remain nucleated with megaloblastic morphology during the whole lifespan, with crucial function to carry the oxygen during a fast-growing phase of the embryo when the oxygen diffusion would be insufficient to support such growth. The spectrum of expression of hemoglobin genes in primitive erythrocytes differs from that observed in erythrocytes produced in the following waves. These hemoglobin genes have different amino acid sequences and, importantly, they differ in the ability to bind oxygen. The primitive erythrocytes express embryonic-like hemoglobins: ζ, α and preferentially $\beta H1$ and $\varepsilon \gamma$ globin chains over the $\beta 1$ and $\beta 2$ ones in the comparison to the definitive erythrocytes (McGrath et al., 2011; Palis, 2014) which will be mentioned below. Failure in the porocess of primitive erythropoiesis results in early embryonic lethality around E10.5 as it was demonstrated by the genetic disruption of transcription factors important for primitive erythrocytes generation such as Gata-1, Gata-2, Lmo2 or Scl in combination with Lyl1 (Fujiwara et al., 1996; Chiu et al., 2018; Tsai et al., 1994).

In vivo studies performed in zebrafish and *in vitro* research in mouse suggest that the first hematopoietic wave can also give rise to macrophages which can colonize embryonic brain and establish there a pool of tissue-resident macrophages – refer to as microglia (Bertrand et al., 2005; Herbomel et al., 1999). There is no specific marker, which can precisely distinguish progenitors of these cells, therefore, the notion that these macrophages originate from the primitive wave remains to be experimentally tested.

Figure 2. Primitive and adult erythrocytes. The image depicts the primitive nucleated and relatively large erythrocyte isolated at E12.5 from the peripheral blood of embryo (the two darker cells) and non-nucleated small definitive erythrocytes isolated from adult peripheral blood for the comparison. Blood smear stained with May-Grünwald Giemsa staining. Scale bar represents 10 μm. The picture was prepared by the author.

1.2.2. SECOND HEMATOPOIETIC WAVE

Shortly after the appearance of the first hematopoietic wave, the second so-called pro-definitive hematopoietic wave appears in the YS. Predominant cell progenitors are EMPs, followed by the presence of lymphoid progenitors with B cell (Godin et al., 1993; Hadland et al., 2017) and T cell potential (Luis et al., 2016; Yokota et al., 2006). To this date, the first appearance of EMPs was observed in a range between E8.25-E8.5 (McGrath et al., 2015; Palis et al., 1999). The EMPs are the hematopoietic progenitors with lineage-restricted potential and capability to produce erythrocytes, granulocytes, megakaryocytes, mast cells, and macrophages (McGrath et al., 2015; Mukouyama et al., 1999). Their hematopoietic potential was assessed by a cell tracing approach (Perdiguero et al., 2015) combined with methocell cultivation assays (McGrath et al., 2015; Perdiguero et al., 2015).

The most important cells originating from EMPs during embryonic development are transient definitive like erythrocytes and macrophages. Transient definitive like erythrocytes are necessary for the oxygenation of enlarging embryo and the macrophages which are later the source of long-lived tissue-resident macrophages such as liver Kuppfler cells (Klein et al., 2007), epidermal Langerhans cells (Schulz et al., 2012) and pleural macrophages (Jenkins et al., 2011) which persist through the life of an individual with self-renewal capacity (Perdiguero et al., 2015; Schulz et al., 2012). Later studies showed, that even microglia may originate from EMPs

(Kierdorf et al., 2013; Mass et al., 2017; Perdiguero et al., 2015) which is in contrast with previous-studies showing their origin from embryonic monopotent (Palis et al., 1999) progenitor originating from the first wave of embryonic hematopoiesis. The EMPs originate from YS hepatic leukemia factor (Hlf)-independent but the Runt-related transcription factor 1 (*Runx1*)-dependent hemogenic endothelium (Frame et al., 2016; Yokomizo et al., 2019). The differentiation of EMPs to the pre-macrophages is happening in Cx3cr1 dependent manner (Mass et al., 2016) which enables them to travel through the developing body. YS EMPs and pre-macrophages traffic through the bloodstream to colonize developing embryo (Stremmel et al., 2018). The majority of EMPs migrate to the FL where they reside during embryonic development and where they expand (Chen et al., 2011; McGrath et al., 2015). The most studied factor which is crucial for EMPs, their proliferation, and survival in the FL, is the tyrosine kinase (c-kit) and its signaling machinery (Azzoni et al., 2018; Ding et al., 2012). Defects in c-kit signaling lead to embryonic lethality with severe anemia (Azzoni et al., 2018; Ding et al., 2012) suggesting the definitive-like erythroid cell differentiation block (Broudy, 1997). Disruption of the production of EMPs or definitive-like erythroid cells leads to embryonic lethality between E13.5 - E15.5 (Chen et al., 2011; Mucenski et al., 1991).
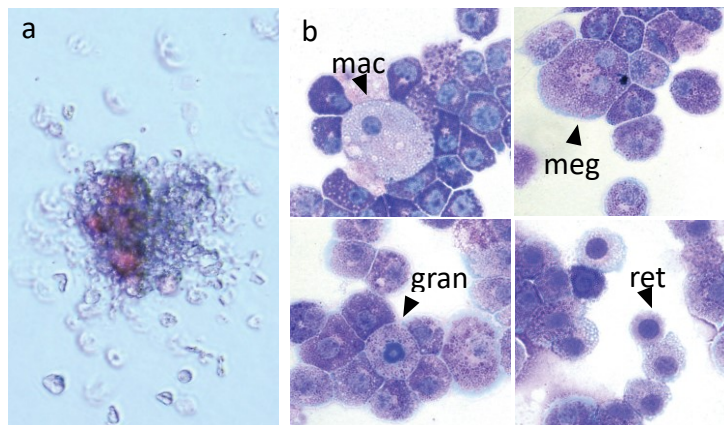

Figure 3. Erythro-myeloid colony and its progenitor cells. *(a) EMP colony at day 7. (b) Morphology of cells at day 14 generated from EMP showing macrophage (mac), megakaryocyte (meg), granulocyte (gran), and red cell progenitor (ret). Cells were stained with May-Grünwald-Giemsa staining. The picture was prepared by the author.*

1.2.3. THIRD HEMATOPOIETIC WAVE

The third embryonic hematopoietic wave generates HSCs in EP. Embryonic HSCs play a pivotal role in the establishment of the adult hematopoietic system. HSCs are for the first time during ontogenesis generated in the inner endothelium of Aorta-Gonad Mesonephros (AGM) in EP through the trans-differential process called endothelial to hematopoietic transition (EHT) (Chen et al., 2009; Zovein et al., 2008), which means that they originate from the endothelial cells with hematopoietic potential. The process of HSC generation from endothelial cells is in comparison to the EHT of EMPs Hlf-dependent (Yokomizo et al., 2019). The origin of HSCs in embryo was confirmed by the cell fate tracing systems using Runx1 in a time-controlled manner (Chen et al., 2009), vital imaging with Ly6A (Boisset et al., 2010) or VE-cadherin (Zovein et al., 2008) transgenic mouse strains. The hemogenic endothelial cells in the AGM acquire the rounded shape and form cell aggregates called the hematopoietic clusters, containing HSCs (Yoshimoto et al., 2008), which are situated to the lumen of the vessels (Yokomizo and Dzierzak, 2010). Because HSCs appears after the blood circulation is established, the possibility, that the progenitors of HSCs can be generated in different anatomical location is still under consideration (Eliades et al., 2016; Tanaka et al., 2014). Hematopoietic clusters contain HSCs precursors at E10-11. Interestingly, at E10-11, within 700 hematopoietic clusters, we can found approximately 2 functional HSCs (Kumaravelu et al., 2002; Yokomizo and Dzierzak, 2010; Zhou et al., 2016).

HSCs do not stay in AGM forever, they migrate into the FL, which serves as the site of their expansion and differentiation (Ema and Nakauchi, 2000). In mammals HSCs from the third embryonic wave posses the ability to produce all progenitors for differentiated and mature functional hematopoietic cells and exhibit the capacity to self-renew after transplantation into the conditioned recipient (Ivanovs et al., 2011). HSCs are the main source of the hematopoietic cells in adults. Their progeny supplies BM, thymus, and all secondary lymphoid organs with hematopoietic cells (Zovein et al., 2008). The disruption of functional HSCs in embryo results in lethality shortly before or after birth (Ding et al., 2012; Zhao et al., 2017).
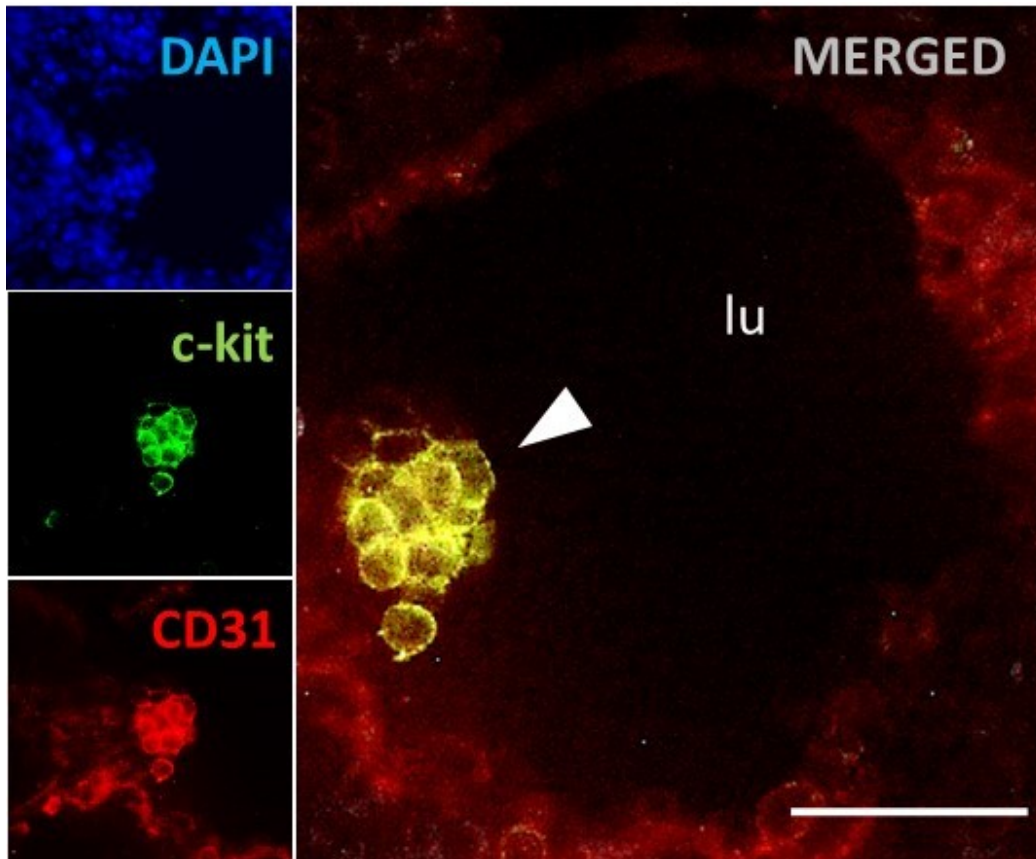
Figure 4. HSC cluster within the E10.5 AGM. *The microscopic image of a hematopoietic cluster is CD31⁺(red) and c-kit⁺(green) and is attached (white arrowhead) is CD31⁺(red) and c-kit⁺(green) to the endothelial CD31⁺ (red) cells within the aortic wall. Hematopoietic cluster is oriented into the aortic lumen (lu). DAPI was used for nuclear staining. Scale bar represents 50 μm. The picture was prepared by the author.*

1.2.4. DIFFICULTIES IN THE IDENTIFICATION OF HEMATOPOIETIC PROGENITORS IN EMBRYO

To identify the hematopoietic progenitors of each embryonic wave is crucial for a better understanding of their relationships and the potential to contribute to the adult hematopoietic system. There is not one specific marker which would alone define the progenitor of each wave or even any reliable method which will unambiguously confirm that the cell which we study belongs to one or the other hematopoietic wave. To properly define progenitor of each wave we should combine the time of

their appearance during development, anatomical location, the presence of a surface or intracellular markers, and assessment of its hematopoietic potential.

If we want to establish the hematopoietic potential of the progenitor cells, the easiest way is to use genetic cell tracing systems. For example, by employing the constitutive or inducible Cre recombinase under the promoter of the gene encoding the marker of studied cell subset. Cre recombinase can activate the expression of fluorescent protein, used for the identification of this population. This allows the sorting of a targeted subset of progenitors with the subsequent assessment of their hematopoietic potential using *in vitro* clonogenic assays. Via combining more of the surface markers with a lineage tracing fluorescent signal, the definition of the wave-relevant progenitor is more accurate.

First observations concerning the embryonic hematopoietic waves were performed using the surface markers on the cells with their detection by the microscopic or flow cytometry methods. In these days, the combination of transgenic mice strains and surface markers is the most commonly used method for the identification of embryonic hematopoietic progenitors. Primitive progenitors of the first embryonic wave express low levels of c-kit and CD41 (Ferkowicz et al., 2003). EMPs can be defined as c-kit$^+$ CD45^{low} (Kierdorf et al., 2013), but this population will also contain the pre-macrophages (macrophages which are not mature). It is possible to combine these two markers with C-type lectin transmembrane receptor AA4.1 (Perdiguero et al., 2015). Another possibility of how to identify EMPs is the combination of c-kit, CD41, FcRγ expression (McGrath et al., 2015). For targeting the early EMPs, the detection of colony-stimulating factor 1 receptor (CSF1R) (Perdiguero et al., 2015; Schulz et al., 2012) expression can be added. Both primitive progenitors and EMPs can be found in the YS and later they seed the FL and other organs.

In the case of HSCs, they are generated in the AGM in EP at E10.5-11.5. But the isolation of AGM is not sufficient because EMPs migrate from the YS to EP trough the vasculature which opens at E8.5 and thus the contamination of AGM by EMPs can occur. Another difficulty is when we want to identify HSCs in FL because it is also seeded by progenitors from YS. The phenotype of the HSCs is changing very

dynamically. All HSCs express c-kit, also, the earliest HSCs express CD41 (Mikkola et al., 2003) and CD34 (Ogawa et al., 2001). With their maturation, the expression of CD41 (Ferkowicz et al., 2003) and CD34 is downregulated, the expression of CD45 and CD144 starting to be apparent. (North et al., 2002). Based on these phenotypical characteristics the phenotype of the transplantable HSCs isolated from AGM is $CD31^+c\text{-}kit^+CD144^+CD41^{low}$ and $CD45^-$. A recent study showed that the addition CD201 to the upper mention phenotypical pannel leads to the higher purity of HSCs and improves transplantation efficiency into the irradiated recipients (Zhou et al., 2016). Known phenotypical markers for the progenitors of each wave are summarized in Figure 5.

Precursor	Hematopoietic wave	Localization	Embryonic day	Phenotype
Primitive progenitor	first	YS	7.0-7.5	$c\text{-}kit^{low}$ $CD41^{low}$
EMP	second	YS	8.0-8.5	$c\text{-}kit^+$ $CD41^+$ $FcR\gamma^+$ $AA4.1^+$ $CSF1R^+$ $CD45^{low}$
HSC	third	AGM vitelline arteries umbilical arteries	10.5-11.5	$CD31^+$ $c\text{-}kit^+$ $CD144^+$ $CD201^+$ $CD41^{low}$ $CD45^-$

Figure 5. Phenotypic markers defining progenitors of each embryonic wave

Table showing the name of the progenitor of each embryonic wave, anatomical localization of their appearance, embryonic day of their first appearance, and possible surface markers that can be used for their phenotypical analysis. Tyrosine-protein kinase KIT (c-kit), Integrin alpha-IIb (CD41), Fc receptor gamma (FcRγ), CD93 (AA4.1), colony-stimulating factor 1 receptor (CSF1R), protein tyrosine

phosphatase, receptor type, C (CD45), platelet endothelial cell adhesion molecule (CD31), VE-cadherin (CD144), endothelial protein C receptor (CD201). Adapted from (Ferkowicz et al., 2003; Gomez Perdiguero et al., 2015; Kierdorf et al., 2013; McGrath et al., 2015; Mikkola et al., 2003; North et al., 2002; Ogawa et al., 2001; Schulz et al., 2012; Zhou et al., 2016).

Thus, there is a need for new progenitor markers which can assist in more precise distinction and separation of hematopoietic progenitors originating from each of the embryonic waves.

1.2. ORIGIN OF ADULT HEMATOPOIETIC CELLS

The generation of functional hematopoietic cells is a continuous process. Adult hematopoiesis takes place in the bone marrow under unperturbed conditions. In the case of disruption of the bone marrow homeostasis, for example by the injury, infection, or hematopoietic malignancy, the hematopoiesis can transiently move to the liver or spleen. On the top of the adult hematopoietic system, or tree, are the repopulating long term HSCs (LT-HSCs) (Spangrude et al., 1988) which are immature cells capable to replenish all hematopoietic lineages in the lethally irradiated recipient after transplantation (Liu et al., 2012). LT-HSCs produce short term HSCs (ST-HSCs) with limited self-renewal activity which differentiate into the multipotent progenitors (MPPs) which lose the ability of self-renewal but they retain the ability of multipotency. MPPs are still able to differentiate into the hematopoietic progenitor of megakaryocyte, erythroid or myeloid cells called common myeloid progenitors (CMPs) and later into granulo-myeloid precursors (GMPs) or megakaryocyte-erythrocyte progenitors (MEPs) (Akashi et al., 2000). Another descendant population generated from MPPs is a common lymphoid progenitor (CLP) which gives rise to lymphoid cells (Kondo et al., 1997). All hematopoietic progenitor cells are generated in BM. But it does not mean that all their daughter cells are already fully functional. For example, T cells that originate from BM HSCs, need to be differentiated, mature, and be educated in the thymus

to become functional. The origin of adult hematopoietic cells is depicted as a hematopoietic tree in Figure 6.
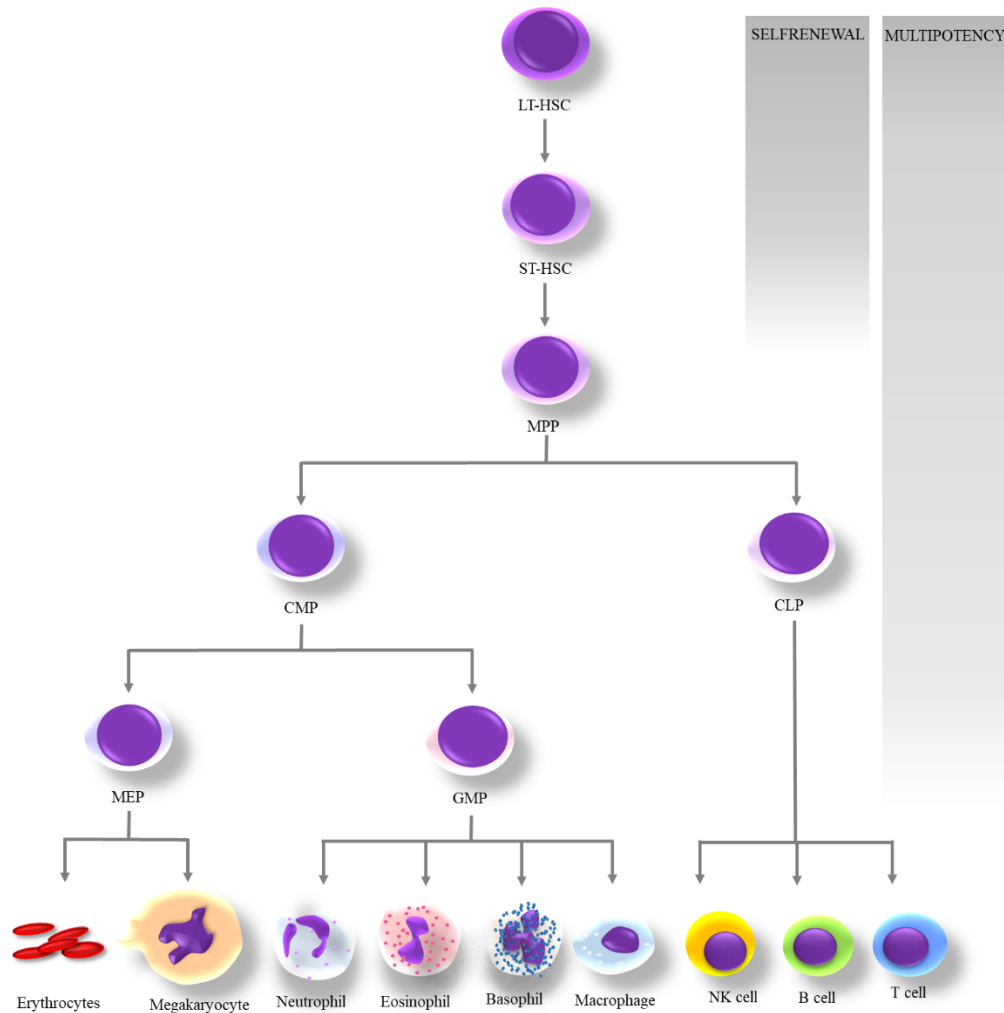
Figure 6. Hematopoietic tree. *Simplified hematopoietic tree describing the origin of hematopoietic cells with a depiction of their self-renewal ability and multipotency. Long term HSC (LT-HSC), short term HSCs (ST-HSC), multipotent progenitor (MPP), common myeloid progenitor (CMP), the granulo-myeloid precursor (GMP), megakaryocyte-erythrocyte progenitor (MEP), common lymphoid progenitor (CLP). Adapted from (Akashi et al., 2000; Kondo et al., 1997; Spangrude et al., 1988).*

1.3.1. ORIGIN OF TISSUE-RESIDENT MACROPHAGES

The majority of hematopoietic cells in adults originate from bone marrow HSCs except for the tissue-resident macrophages. Tissue-resident macrophages originate from YS progenitors and seed the tissues of their residency to perform homeostatic functions such as phagocytosis of unfitting cells, microorganisms, and metabolic waste together with the production of growth factors and bioactive molecules (Truman et al., 2008; Willenborg et al., 2012). In the past, it was thought that tissue-resident macrophages are differentiated monocytes from the blood circulation originating from HSCs in bone marrow (van Furth, 1980; van Furth and Cohn, 1968). New studies showed that the majority of tissue-resident macrophages originate from the YS (Perdiguero et al., 2015). They are generated from EMPs through the pre-macrophage stage (Mass et al., 2016), distinct from the monocytes (Mass et al., 2016; Takahashi et al., 1989). It has been shown that pre-macrophages upregulate Cx3Cr1 expression (Mass et al., 2016) and Cx3Cr1 knock-out embryos posses lower numbers of macrophages in limbs and head till E10.5 which suggest that pre-macrophages colonize the embryonic tissues in Cx3Cr1 dependent manner and acquire typical macrophage markers such as EGF-like module-containing mucin-like hormone receptor-like 1 (F4/80) or Integrin alpha M (CD11b) (Stremmel et al., 2018). Immediately after the colonization of embryonic tissues at E10.5, they acquire core adult-type resident macrophage program (genes characteristic for core adult-type macrophage program are depicted in Figure 7.) in all tissues simultaneously (Mass et al., 2016), but the surrounding microenvironment shapes their phenotype and function with the time (Lavin et al., 2014). To this date, only the tissue-resident macrophages in the brain, called microglia are considered to be a pure population of YS derived macrophages (Perdiguero et al., 2015). In the case of other tissue-resident macrophages, they are usually a mixed population of YS macrophages, fetal monocytes, and BM progenitors (Guilliams et al., 2013; Hoeffel et al., 2012; Merad et al., 2002).

Transcription factors	Phagocytosis	Pathogen recognition receptors	Chemokine receptors	Cytokine receptors
Atf3	C3ar1	Clec7a	Ccr1	Csf1r
Cebp α,β	C5ar1	Tlr1,4,7,8,13	Cx2cr1	Csf2ra
Ifr 1,5,8,9	FcRγ1,3,4		Cx3cr1	Il4ra
Stat 1,3,5b,6	Mertk			Il10rb
PU.1	Mrc1			Infgr2
PPAR-γ	Stab1			Tnfrs1b, 11a
Mafb				

Figure 7. Genes upregulated when EMPs transit to the macrophages. *Table showing the core macrophage adult-type resident macrophage genes which are upregulated when EMPs transit through the pre-macrophage to the macrophage stage. These genes are upregulated simultaneously in all embryonic tissues starting E10.5. Adapted from (Mass et al., 2016).*

1.3.1.1. HOW YS MACROPHAGES COLONIZE THE TISSUES

YS EMPs and pre-macrophages traffic through the bloodstream to colonize FL and other embryonic peripheral organs during a restricted time window (Stremmel et al., 2018). The crucial attribute is functional heartbeat which establishes the circulation and is indispensable for the distribution of cells. Embryos lacking the heartbeat had accumulated EMPs and macrophages in the YS without any of them in EP (Lux et al., 2008). When the hematopoietic cells from YS reach the bloodstream they distribute to the place of residence. This migration pattern likely depends on receptor-ligand interactions. The chemokine receptors responsible for the migration of adult myeloid cells (Ccr2, Ccr3, Ccr5, Ccr7, Cxcr2, Cxcr4, and Cx3cr1) were detected also in embryonic macrophages in early stages of development except the CXCR2 and CXCR7 (Mariani et al., 2019) which might be expressed later. Their ligands are usually produced by the endothelial cells in the target destination where the macrophages should migrate (Mariani et al., 2019). The most expressed chemokine receptor is CX3CR1 followed by the expression CXCR4 (Mariani et al., 2019; Mass et al., 2016; Stremmel et al., 2018). The deletion of the latter results in the accumulation of EMPs and mainly macrophages

in the YS at the expense of EMPs and macrophages in the EP (Stremmel et al., 2018). This suggests the worsening of the migration capacity of these cells. Changes in the distribution of cells during embryogenesis are compensated during development and adult mouse is viable without any significant complications.

1.3.2. T CELL DEVELOPMENT

T cells originate from bone marrow HSCs (Donskoy and Goldschneider, 1992). In the beginning, MPPs and later CLPs are formed and migrate to the thymus via bloodstream where they finally differentiate and mature into several types of T cells. Their maturation process is dependent on various cell types of interaction and signaling molecules (Boehm et al., 2003; Silva-Santos et al., 2005). The T cell precursors seed the thymic cortex as double-negative (DN). They do not possess any of the typical phenotypic markers, such as T-cell receptor (TCR) for antigen recognition, nor CD4 or CD8 co-receptors. In the beginning, the rearrangement of the TCR occurs due to the activity of the V(D)J recombination-activating genes recombinases 1 and 2 (RAG). The precursor cells start to co-express CD4 and CD8 and they are called double-positive (DP) cells (Godfrey et al., 1993; Stritesky et al., 2013).

Another function of the thymus is to select T cells which would not recognize the host-own structures (self-antigens) by TCR and thus prevent the development of the autoimmune reaction. The set of processes and mechanisms that lead to the generation of functional T cells with limited self-reactivity is collectively called as central tolerance (Mayerova and Hogquist, 2004). The process begins in the thymic cortex when T cells are in the DN stage and are subjected to positive selection. Cortical thymic epithelial cells (cTECs) express molecules of major histocompatibility complex I and II (MHC) with the main function to bind antigens and present them to the developing T cells via their TCR. If the TCR recognizes the antigen with low affinity, then T cells survive. If T cell recognizes antigen expressed by MHC I, the expression of CD8 remains and the CD4 is down-regulated. These cells are called cytotoxic T cells. In case that TCR recognizes

antigen in MHC II, expression of CD4 remains and CD8 is downregulated. Cells are called T helper cells. Cells that are unable to bind to any self-antigen presented by cTECs die by apoptosis (Bevan, 1997; Hogquist, 2001).

Only T cells that survived positive selection expressing either CD4 or CD8 (single positive T cells, SP) migrate to the inner part of the thymus (medulla) to undergo the process called negative selection. The main output of negative selection is to eliminate potentially self-reactive T cells. The medulla is filled by antigen-presenting cells such as dendritic cells (DCs) or medullary thymic epithelial cells (mTECs) with the ability to present self-antigens called tissue-restricted antigens (TRAs) under the control of transcription autoimmune regulator called AIRE (Anderson et al., 2002). Recently it has been shown, that not only mTECs can present TRAs but even DCs which acquire the TRAs from mTECs by the process called cooperative antigen transfer (Leventhal et al., 2016; Perry et al., 2014) which suggest that TRAs can be presented directly (by mTECs) or indirectly (DCs) in MHC context. The presentation of TRAs by APC can results in the deletion of self-reactive T cells (Barclay and Mayrhofer, 1981, 1982; Klein et al., 1998) or the reprogramming to the T regulatory (T reg) cells. Importantly T regs modulate immune system function by the maintenance of the tolerance to self-antigens and thus prevent the autoimmune disease (Aschenbrenner et al., 2007; Bains et al., 2013).

1.4. TOLL-LIKE RECEPTORS

Toll-like receptors (TLRs) are highly conserved structures identified even in low animals such as Amoeba (Chen et al., 2007) or Nematoda *Caenorhabditis elegans* (Tenor and Aballay, 2008). They were firstly described in 1985 on fruit flu Drosophila melanogaster and named Toll (Anderson et al., 1985) and only a few years later in humans (Medzhitov et al., 1997). These findings meant a big revolution in the field of innate immunity by adding the missing piece into the whole picture of host-pathogen interactions.

The immune system is a very complex array of various types of host cells that collectively protect the body against various infectious diseases. The trigger(s) which activate the immune system can be invading pathogens or structures released during tissue damage. The easiest way how to inform the immune system about the invasion of a pathogen into the host environment is to recognize them by the pattern recognition receptors (PRRs). Various immune cells express PRRs such as Toll-like receptors (TLRs). TLRs are densely expressed in the cells of the innate immune system and play a critical role in the very early stages of infection.

The structure of TLRs is now very well described. They are type I transmembrane protein composed of distinct domains at their N- and C- terminal parts. The extracellular N-terminal part is necessary for the pathogen recognition and consists of the leucine-rich repeats (LRRs) and cysteine-rich domains. The C-terminal transmembrane and cytosolic or intracellular Toll/IL-1R like (TIR) part is necessary for recruiting signaling adaptor proteins leading to downstream signaling (Medzhitov et al., 1997; Rock et al., 1998) due to the. Currently, 10 humans and 13 mice TLRs have been described (Du et al., 2000; Chuang and Ulevitch, 2001; Rock et al., 1998).

By their nature, the ligands of TLRs can be divided into exogenous and endogenous. TLRs recognize exogenous pathogen-associated molecular patterns (PAMPs) (Li et al., 2014; Mariano et al., 2014) for a purpose to induce inflammatory immune responses. Endogenous ligands are termed also as damage-associated molecular patterns (DAMPs). They are usually released during tissue damage from stressed or necrotic cells. DAMPs include the components of the extracellular matrix, heat shock proteins, RNA, or purine metabolites (Kariko et al., 2004; Liu-Bryan et al., 2005; Shi et al., 2003; Vabulas et al., 2001). Due to the recognition of PAMPs or DAMPs by TLRs, the innate immune responses are set off (Akira, 2006) which also plays an instructive role for the initiation of adaptive immune responses (Liu and Zhao, 2007).

An important role in the recognition of TLR's ligands plays their cellular localization. TLRs which are localized on the cell surface of host cells (TLR1, 2, 4, 5 and 6) recognize mainly components of the microbial membranes. On the other

hand, TLRs which are expressed within intracellular vesicles (TLR3, 7, 8, 11 and 13), recognize nucleic acids from pathogens (mainly viruses) phagocytosed or internalized by the cell (Takeda et al., 2003).

1.4.1. TOLL-LIKE RECEPTOR SIGNALING

Ligand recognition by TLRs leads to the series of events that activate various transcription factors that are responsible for the induction of genes encoding various protective molecules. Upon ligand recognition, TLRs dimerize and intracellular adaptor proteins are recruited to TIR-domain of TLR which triggers the downstream signaling. The adaptor proteins for TLRs are MyD88 (Hultmark, 1994; Muzio et al., 1997), TRIF (Yamamoto et al., 2003a), MAL/TIRAP (Horng et al., 2002), MAL, and TRAM (Yamamoto et al., 2003b). Based on the adaptor proteins involved in the TLRs signaling, we can divide them as Myd88-dependent and Myd88-independent. All TLRs, except TLR3, signal via MyD88. In addition, TLR3 and TLR4 use TIR-domain-containing adaptor-inducing interferon-β (TRIF) signaling (Yamamoto et al., 2003b). The activation of TLRs leads to the activation of transcription factors (TF): AP1, IRFs or/and NF-κB. The activation AP1 TF leads to the transcription of genes encoding proteins involved in cell signaling. Activation of IRFs TF leads to the transcription of interferons (IFNs) which serve as the defense mechanism against viral infections. Active TF NF-κB initiates the transcription of genes for the pro-inflammatory cytokines: tumor necrosis factor α (TNFα) which induces apoptosis, pro-IL1β, and pro-Il-18. Pro-IL-1β and pro-Il-18 are released to the cytoplasm in the inactive form and processed into to the active forms by the cascade of caspases. Active Il-1β activates leukocytes and Il-18 serves as the chemoattractive molecule for the leukocytes (De Nardo, 2015; Kawasaki and Kawai, 2014). The type of response depends on the adaptor protein or their combination involved in TLRs signaling.

In the case of Myd88-dependent signaling, after the TLRs dimerization, Myd88 forms a complex with IRAK kinases. IRAK1 is released from the Myd88 complex after its activation (Jiang et al., 2002). Active IRAK complex associates with

TRAF6 ubiquitin ligase and ubiquitinates itself and TAK1 protein kinase complex and activates it. Active TAK1 activates NF-KB and MAPK pathway (Ninomiya-Tsuji et al., 1999). MAPK pathway activation leads to the AP-1 TF.

Myd88-independent signaling uses different proteins for its activation. In the beginning, TRIF interacts with TRAF6 and TRAF3. Active TRAF recruits the TBK1 and IKKi kinases together with NEMO, which is necessary for IRF3 phosphorylation. IRF3 dimerizes and after its translocation into the nucleus induces expression of IFN I related genes. On the other hand, active TRAF6 recruits the RIP-1 kinase which then activates the TAK1 complex. TRAF6 activation leads to the activation of NF-κB, MAPKs and genes for inflammatory cytokines.

1.4.2. CELLS EXPRESSING TOLL-LIKE RECEPTORS

TLRs are usually expressed on the cells which form the interphase between the host and environment, such as the immune, epithelial and endothelial cells as well as keratinocytes (Andonegui et al., 2009; Baker et al., 2003; Price et al., 2018), where they serve as the sensors for PAMPs and danger or damage signals. In the case of immune cells, TLRs are expressed by the innate immune cells such as macrophages, monocytes, dendritic cells, granulocytes and NK cells (Applequist et al., 2002; Zarember and Godowski, 2002). The expression of TLRs was even described in adaptive immune cells such as B (Bourke et al., 2003) and T cells (Crellin et al., 2005; Komai-Koma et al., 2004). Interestingly, recent studies showed that adult BM HSCs express a battery of TLRs in steady-state and their stimulation leads to the preferential differentiation of these cells into myeloid lineages (De Luca et al., 2009; Nagai et al., 2006; Sioud et al., 2006).

Since the detection methods are more robust and highly sensitive, the evidence for the expression of TLRs in immune-privileged tissues also started to accumulate. For example, the pregnancy is described as the state of immune suppression from the immunological point of view. Recent studies showed that the inner villous cytotrophoblast layer of the placenta express TLRs (Patni et al., 2009; Pudney et al., 2016). The expression of TLRs was also confirmed on neuronal cells of the

fetus (Lathia et al., 2008; Okun et al., 2010) and adults (Rolls et al., 2007), in the eye (Feng et al., 2017) or at the Sertoli cells in testes (Riccioli et al., 2006) and even in spermatozoa (Palladino et al., 2008). Findings made by recent studies indicate, that TLR signaling may be involved even in mammalian embryonic development.

1.4.3. TOLL-LIKE RECEPTORS IN DEVELOPMENT

TLRs are best known for their evolutionary conserved and universal function in innate immunity. Interestingly, the first TLRs were described not as the PRRs involved in immune recognition, but as the crucial component of dorsoventral patterning during development of Drosophila embryo (Anderson and Nusslein-Volhard, 1984)and later in sensory neurons differentiation in *Caenorhabditis elegans* (Brandt and Ringstad, 2015). Drosophila TLRs are called *Toll* and bind endogenous protein ligands such as Spz, DNT1 or DNT2 involved in development (Foldi et al., 2017; Zhu et al., 2016). Unfortunately, the mammalian endogenous ligands (except pathogens and ligands released during tissue injury) have not been yet precisely characterized. Some recent studies suggest that TLR signaling may play a role also in mammalian development. Based on the RNA sequencing of EP (without YS) the RNA expression of TLRs was confirmed in the ectoderm of E7.0 mice embryos (Pijuan-Sala et al., 2019), which is the earliest evidence for the TLRs presence. Unfortunately, the data showing the protein expression of TLRs on embryos younger than E10.5 are missing. Regarding the studies showing the involvement of TLR signaling in the adult brain, specifically on neuronal cells (Leow-Dyke et al., 2012; McCarthy et al., 2017; Rolls et al., 2007), the importance of TLR signaling in the mouse embryo is studied mainly in neuronal cells. Embryonic protein expression of TLRs was described at neuronal cells starting E13.5 (Barak et al., 2014) and indispensability of TLRs in the mammal neuronal progenitor cells (NPCs) fate decision between glial versus neuronal cells was described (Lathia et al., 2008; Okun et al., 2010; Shechter et al., 2008). These processes are influenced mainly by the TLR2 versus TLR4 balance. Mice lacking the expression of TLR2 produce only astrocytes from NPCs. On the other hand,

TLR4 knock-out mice lack the presence of astrocytes, and neurons are preferentially generated from NPCs (Rolls et al., 2007).

Unfortunately, the data showing TLR signaling involvement in embryonic immune system development are far from being complete. In case of embryonic hematopoiesis, the RNA expression of various TLR signaling molecules was described in E9.5 EMPs, among which the TLR2 and its adaptor protein Myd88 were the highest (Mass et al., 2016). However, the protein expression has been described so far only on E10.5 embryonic macrophages (Balounova et al., 2014; Mass et al., 2016) in which the downstream signaling activated upon exogenous ligand stimulation was also reported (Balounova et al., 2014). On the other hand, the exact reason for TLR expression in very early embryonic development has not been thus far explained and substantiated properly.

2. THESIS AIMS

The main aim of the thesis is to characterize the expression, function, and experimental utility of TLR2 in embryonic hematopoiesis. The presented work also concerns the role of TLRs in the establishment of central tolerance and the involvement of chemokine signaling in embryonic and adult hematopoiesis.

 The specific goal of the presented work is to describe the TLR2 as a novel marker of the second and third embryonic hematopoietic waves which in the combination with c-kit marker provides so far, the most specific and reliable phenotypic feature for their isolation and detail functional characterization.

Such phenotypic determination of progenitors of EMPs and HSCs allows to address several specific questions:

I)   Where and when is the TLR2 expressed during embryonic hematopoiesis? Can TLR2 be used for the physical separation of progenitors of the fist, second, and third embryonic hematopoietic waves?

II)   Are the TLR2$^+$ EMPs indispensable for embryo survival?

III)   Does the disruption of CXCR4 signaling influence the migratory potential of progenitor cells and embryonic macrophages?

IV)   What is the role of TLR signaling in the establishment of central tolerance?

3. RESULTS

The list of applicant's publications and a manuscript directly linked to the presented thesis:

Balounová J*, **Šplíchalová I***, Dobešová M, Kolář M, Fišer K, Procházka J, Sedlacek R, Jurisicova A, Sung HK, Kořínek V, Alberich-Jorda M, Godin I, Filipp D. Toll-like receptor 2 expression on c-kit+ cells tracks the emergence of embryonic definitive hematopoietic progenitors. **Nat Commun. 2019 Nov 15;10(1):5176.** doi: 10.1038/s41467-019-13150-0. **(*shared first author)**.

Iva Šplíchalová, Jana Balounová, Matouš Vobořil, Tomáš Brabec, Radislav Sedlacek and Dominik Filipp. Deletion of TLR2$^+$ erythro-myeloid progenitors leads to embryonic lethality. Submitted, currently under review/revision.

Borna S, Drobek A, Kralova J, Glatzova D, **Splichalova I**, Fabisik M, Pokorna J, Skopcova T, Angelisova P, Kanderova V, Starkova J, Stanek P, Matveichuk OV, Pavliuchenko N, Kwiatkowska K, Protty MB, Tomlinson M. G, Alberich-Jorda M, Korinek V, Brdicka T. Transmembrane adaptor protein WBP1L regulates CXCR4 signalling and murine haematopoiesis. **J Cell Mol Med. 2019; 00:1–13**.

Vobořil, M., Brabec, T., Dobeš, J. **Šplíchalová I.,** Březina J., Čepková A., Dobešová M., Aidarova A., Kubovčiak J., Tsyklauri O., Štěpánek O., Beneš V., Sedláček R., Klein L., Kolář M., Filipp D., Toll-like receptor signaling in thymic epithelium controls monocyte-derived dendritic cell recruitment and Treg generation. **Nat Commun 11, 2361 (2020).** https://doi.org/10.1038/s41467-020-16081-3

The applicant also co-authored the paper describing the upregulation of TLRs and its related molecules in the intestine of piglets by the *L. amylovorus, L. mucosae, E. coli Nissle 1917 and S. Typhimurium*:

Splichal, I.; Donovan, S.M.; Jenistova, V.; **Splichalova, I**.; Salmonova, H.; Vlkova, E.; Neuzil Bunesova, V.; Sinkora, M.; Killer, J.; Skrivanova, E.; Splichalova, A. High Mobility Group Box 1 and TLR4 Signaling Pathway in Gnotobiotic Piglets Colonized/Infected with *L. amylovorus*, *L. mucosae*, *E. coli* Nissle 1917 and *S.* Typhimurium. **Int. J. Mol. Sci. *2019, 20, 6294*.**

3.1. TOLL-LIKE RECEPTOR 2 EXPRESSION ON C-KIT$^+$ CELLS TRACKS THE EMERGENCE OF EMBRYONIC DEFINITIVE HEMATOPOIETIC PROGENITORS

It has been known, that embryonic hematopoiesis proceeds through three waves of progenitors. The first, primitive wave begins around E7.25 arises in the YS and give rise to primitive nucleated erythrocytes and megakaryocytes (Tober et al., 2007). Some studies showed that even the first wave of macrophages may originate from very early primitive progenitor (Bertrand et al., 2005; Herbomel et al., 1999). The second wave so-called transient definitive appears at E 8.25. Progenitors of EMPs and LMPs emerges from hemogenic endothelium of YS (Boiers et al., 2013; Frame et al., 2016; McGrath et al., 2015). In the end, the third wave called definitive starts at E10.5 in the EP. The HSCs start to emerge from hemogenic endothelium of the ventral floor of the dorsal aorta it the AGM region (Taoudi and Medvinsky, 2007). How the embryonic development progress, the progenitors migrate trough the embryonic body and differentiate into the precursor cells, with the latter populating BM, spleen or thymus (Christensen et al., 2004; Kumaravelu et al., 2002; McGrath et al., 2015).

The unique marker which can characterize progenitor of each wave does not exist. We usually recognize progenitors by the combination of markers. But the contamination of progenitors by the more mature cells is still present due to the small number of markers. This contamination can influence the output of the research very significantly and can lead to the misinterpretation of data at the end. Another way how to characterize embryonic hematopoietic progenitors is by the usage of the cell tracing that previously employed Tie2, Runx1 or c-kit reporters with constant expression or time-dependent inducible approach (Busch et al., 2015; Perdiguero et al., 2015). The combination of surface markers with the cell tracing reporters can provide better resolution for the separation of distinct progenitor cells and its progeny. The identification of progenitor originating from YS or AGM is due to anatomical separation much less complicated, but the problems persist if we want to discriminate progenitors of the first and second waves. Both progenitors originate from and coexist in the YS as well as share a set of known phenotypic

markers such as c-kit, Tie2, CD31 and CD41 (Ferkowicz et al., 2003; Frame et al., 2016; Lugus et al., 2009). Even the integration of cell tracing systems which were mentioned above does not provide sufficient resolution in the tracing of the first and second wave of hematopoietic progenitors. `for this reason, we still do not have convincing data which would confirm or disprove the origin of tissue-resident macrophages. Thus, there has been an urgent need for additional surface markers which will clarify the potential of embryonic hematopoietic progenitors and elucidate the developmental and functional relationship between hematopoietic waves.

In this study, we described the nowel marker of embryonic hematopoiesis. It is TLR2, a highly conserved surface protein with the main function to recognize microbial products in adults and which is signaling in Myd88- and Triff-dependent manner. The expression of TLR2 starts to be apparent on progenitor cells in YS at E7.5. Interestingly the E7.5 TLR2$^+$c-kit$^+$ cells possess functional attributes of EMPs and not progenitors of the first hematopoietic wave which suggests that these precursors of EMPs are present earlier than it was described. In addition, this finding sheds new light on the origin of tissue-resident macrophages, mainly microglia.

By the genetic labeling of progenitors with active TLR2 promoter we have shown, that the TLR2 program is initiated not only in the YS EMPs precursors but also in the pre-HSCs in the AGM at E8.5 which means that the TLR2 expression is initiated exclusively in definitive hematopoietic progenitors and not in primitive progenitors. These findings suggest that the expression of TLR2 represents one of the oldest and evolutionary conserved ontogenetic programs.

ARTICLE

Toll-like receptor 2 expression on c-kit$^+$ cells tracks the emergence of embryonic definitive hematopoietic progenitors

Jana Balounová[1,2,11], Iva Šplíchalová[1,3,11], Martina Dobešová[1], Michal Kolář[4], Karel Fišer [5], Jan Procházka[2], Radislav Sedlacek[2], Andrea Jurisicova[6], Hoon-ki Sung[7], Vladimír Kořínek[8], Meritxell Alberich-Jorda[9], Isabelle Godin [10] & Dominik Filipp [1]*

Hematopoiesis in mammalian embryos proceeds through three successive waves of hematopoietic progenitors. Since their emergence spatially and temporally overlap and phenotypic markers are often shared, the specifics regarding their origin, development, lineage restriction and mutual relationships have not been fully determined. The identification of wave-specific markers would aid to resolve these uncertainties. Here, we show that toll-like receptors (TLRs) are expressed during early mouse embryogenesis. We provide phenotypic and functional evidence that the expression of TLR2 on E7.5 c-kit$^+$ cells marks the emergence of precursors of erythro-myeloid progenitors (EMPs) and provides resolution for separate tracking of EMPs from primitive progenitors. Using in vivo fate mapping, we show that at E8.5 the *Tlr2* locus is already active in emerging EMPs and in progenitors of adult hematopoietic stem cells (HSC). Together, this data demonstrates that the activation of the *Tlr2* locus tracks the earliest events in the process of EMP and HSC specification.

[1] Laboratory of Immunobiology, Institute of Molecular Genetics of the Czech Academy of Sciences, Prague, Czech Republic. [2] Czech Centre for Phenogenomics & Laboratory of Transgenic Models of Diseases, Institute of Molecular Genetics of the Czech Academy of Sciences, Prague, Czech Republic. [3] Department of Cell Biology, Faculty of Science, Charles University, Prague, Czech Republic. [4] Laboratory of Genomics and Bioinformatics, Institute of Molecular Genetics of the Czech Academy of Sciences, Prague, Czech Republic. [5] Childhood Leukaemia Investigation Prague, 2nd Faculty of Medicine, Charles University, Prague, Czech Republic. [6] Samuel Lunenfeld Research Institute, Mount Sinai Hospital, Toronto, ON, Canada. [7] The Hospital for Sick Children Research Institute, Toronto, ON, Canada. [8] Laboratory of Cell and Developmental Biology, Institute of Molecular Genetics of the Czech Academy of Sciences, Prague, Czech Republic. [9] Laboratory of Hematooncology, Institute of Molecular Genetics of the Czech Academy of Sciences, Prague, Czech Republic. [10] Institute Gustave Roussy PR1, INSERM U1170, Villejuif, France. [11] These authors contributed equally: Jana Balounová, Iva Šplíchalová. *email: dominik.filipp@img.cas.cz

Mammalian hematopoiesis proceeds through three successive waves of progenitors. The first, referred to as the primitive wave, arises in the yolk sac (YS) at E7.25 and consists of progenitors of primitive nucleated erythrocytes (EryP) and megakaryocytes (Mk)[1–3]. Monopotent progenitors of macrophages (MFs) are also considered to be part of this wave[4,5]. At E8.5, a second, transient definitive wave of erythro-myeloid progenitors (EMPs) and lympho-myeloid progenitors (LMPs) emerges from the YS hemogenic endothelium (HE)[6–8]. Ultimately, around E10.5, hematopoietic stem cells (HSCs) emerge from the HE of the ventral floor of the dorsal aorta in the aorta–gonad–mesonephros region (AGM)[9,10]. Commencing from E9.5, EMPs from YS and other hemogenic tissues[11] and at E10.5 HSCs from AGM, start to seed and expand in the forming fetal liver (FL). Subsequently, these progenitors migrate and differentiate to tissue-resident MFs, with the latter populating the bone marrow (BM), spleen, or thymus[4,6,12–14].

Hematopoietic commitment in YS and AGM occurs independently of each other via the endothelial to hematopoietic transition (EHT) of Runx1 expressing cells, and is traceable by the appearance of CD41 on the surface of c-kit^{+} cells[8,15–17]. Due to differences in the timing of their appearance, lineage potential and combinatorial dependency on developmental factors, such as Runx1, c-myb, and Notch, the progenitors of the primitive erythropoiesis are considered to be distinct from EMPs and HSCs which exhibit definitive hematopoietic potential[18]. This is in agreement with the observation that primitive erythropoiesis occurs in Runx1 deficient embryos, although EMPs, HSCs, and also MFs are absent[8,19,20]. However, other studies have suggested that these hematopoietic waves not only share their progenitors but also phenotypic markers, such as c-kit and CD41[3,8,21]. Due to low temporal resolution, lineage-tracing experiments that employ Tie2, Runx1, and c-Kit reporters have failed to track the separate emergence of primitive versus EMP-derived MFs[22–24]. Thus, identification of additional surface markers would be vital in revealing the developmental and functional relationship between hematopoietic waves.

Toll-like receptors (TLRs) recognize various structures of microbes and are crucial for triggering immune responses to infections[25,26]. TLR stimulation of adult BM HSCs during infection redirects BM hematopoiesis toward the increased production of myeloid cells, demonstrating their role in hematopoietic homeostasis under inflammatory conditions[27–29]. So far, only a few studies have analyzed the expression of TLRs in embryonic development[30–32], leaving the ontogeny of TLR expression in pre-circulation embryos unknown.

We show here that TLR2 is expressed on E7.5 c-kit^{+} YS cells, which co-express the hematopoietic emergence markers Runx1 and CD41 and exhibit the functional attributes of EMPs. In addition, E8.5 TLR2^{+} c-kit[+] EMPs respond to TLR2 stimulation in a MyD88-dependent manner. By genetic labeling of progenitors with active Tlr2-regulatory elements, we have determined their contribution to definitive hematopoietic lineages. Altogether, co-expression of TLR2 and c-kit serves as a reliable marker to track the emergence of EMPs and HSCs as well as the tracing of their origin, emergence, fate, lineage potential, and function.

Results

E7.5 YS-derived TLR2^{+}c-kit^{+} cells are emerging precursors of EMPs.
We have previously shown that TLRs are expressed in E10.5 YS-derived MFs[33]. After deeper analysis, we detected the transcripts of Tlrs and their adaptors already at E7.5 (Supplementary Fig. 1a). At this time point, TLR protein expression, exemplified by TLR2, showed a scattered pattern of distribution

across the YS. Anatomically, TLR2[LOW] cells were most abundant in the YS and posterior primitive streak (PPS), where cells undergo epithelial to mesenchymal transition (Fig. 1a; Supplementary Movie 1).

The localization of TLR2^{+} cells within the PPS and YS suggests an association with early hematopoiesis. To focus exclusively on embryonically derived cells, we used crosses between wild-type (Actb[wt/wt]) and actin-β[EGFP] (Actb[EGFP/wt]) transgenic mice to distinguish cells of maternal and embryonic origin based on their EGFP expression (Supplementary Fig. 1b). This data confirmed that maternal MFs at ~E8.5–9.5 are replaced by embryo-derived ones[5] and that TLR2^{+}CD11b^{−}CD45^{−} cells, already present at E7.5, are indeed of embryonic origin.

At E7.5, a large proportion of embryonic Actb[EGFP]TLR2^{+}CD45^{−} cells also co-expressed c-kit, a hallmark of hematopoietic progenitors. TLR2^{+}c-kit^{+} cells were largely restricted to YS, with significantly lower numbers in the embryo proper (EP) (Fig. 1b). Importantly, only TLR2^{+}c-kit^{+} cells from YS, but not those from EP, were positive for the early hematopoietic marker, CD41[3] (Fig. 1c). Similarly, TLR2^{+}c-kit[+] progenitors isolated from YS, but not EP, expressed mRNA encoding Runx1, an obligatory transcription factor (TF) required for the emergence of definitive hematopoiesis (Fig. 1d). Runx1 was also expressed by the YS-derived TLR2^{−}c-kit[+] population, which was also positive for CD41 (Fig. 1c). This is consistent with the emergence of hematopoietic progenitors exclusively among c-kit^{+} cells in the YS[8].

Next, we tested whether the expression of TLR2 on E7.5 c-kit^{+} cells marks progenitors with an early commitment to a hematopoietic fate. Using Actb[EGFP] embryos, we gated on YS-derived embryonic TLR2^{+} or TLR2^{−} cells and analyzed the kinetics of their c-kit and CD45 expression. At E7.5, TLR2^{+} cells separated into two subsets: one expressing high levels of c-kit while the other was c-kit^{−} (Fig. 1e, top panels). During the specification of the TLR2^{+} subset toward the CD45^{+} cells, we observed three stages: (i) at E8.5, the c-kit^{−} subset increased its c-kit expression with virtually all TLR2^{+} cells becoming c-kit^{+}; (ii) at E9.75, TLR2^{+}c-kit^{+}CD45^{−} cells acquired CD45 surface expression; and (iii) concomitantly downregulated c-kit. In contrast, the TLR2^{−} phenotype was associated with low/negative c-kit expression. However, despite the upregulation of c-kit expression in some cells at E8.5–9.5, the entire TLR2^{−} subset remained CD45 negative (Fig. 1e, bottom panels).

Consistent with the observed transition to hematopoietic fate, TLR2^{+}c-kit^{+} cells expressed higher levels of endothelial, hematopoietic, and myeloid markers as well as TFs typical for EHT in comparison with the TLR2^{−}c-kit^{+} subset (Supplementary Fig. 1c, d). During their maturation toward the CD45^{+} stage, the expression of myeloid markers increased while endothelial markers such as Tie2 and Cd31 were downregulated, a distinctive feature of EHT. It is of note, that Gata1, a TF required for the generation of primitive erythroblasts[34], was the only gene which was preferentially expressed in TLR2^{−}c-kit^{+} cells (Supplementary Fig. 1d). These data imply that in E7.5–10.5 YS, the process of hematopoietic maturation toward CD45^{+} stage is restricted to TLR2^{+}c-kit^{+} progenitors.

To establish if the developmental progression of E7.5 TLR2^{+}c-kit^{+} progenitors is cell autonomous, we assessed their hematopoietic potential in a clonogenic assay at days 5 and 12 (Fig. 1f; Supplementary Fig. 2a, b). After 5 days of culture, only c-kit^{+} cells gave rise to visible colonies with those derived from TLR2^{+}c-kit^{+} cells being more abundant. Importantly, erythroid colonies from E7.5 TLR2^{−}c-kit[+] progenitors expressed significantly higher ratio between embryonic and adult globins than their TLR2^{+}c-kit[+] counterparts (Supplementary Fig. 2b). When scored at 12 days of culture, both c-kit[+] subsets produced erythroid and megakaryocytic colonies (E/Mk). However, a critical distinction between

41
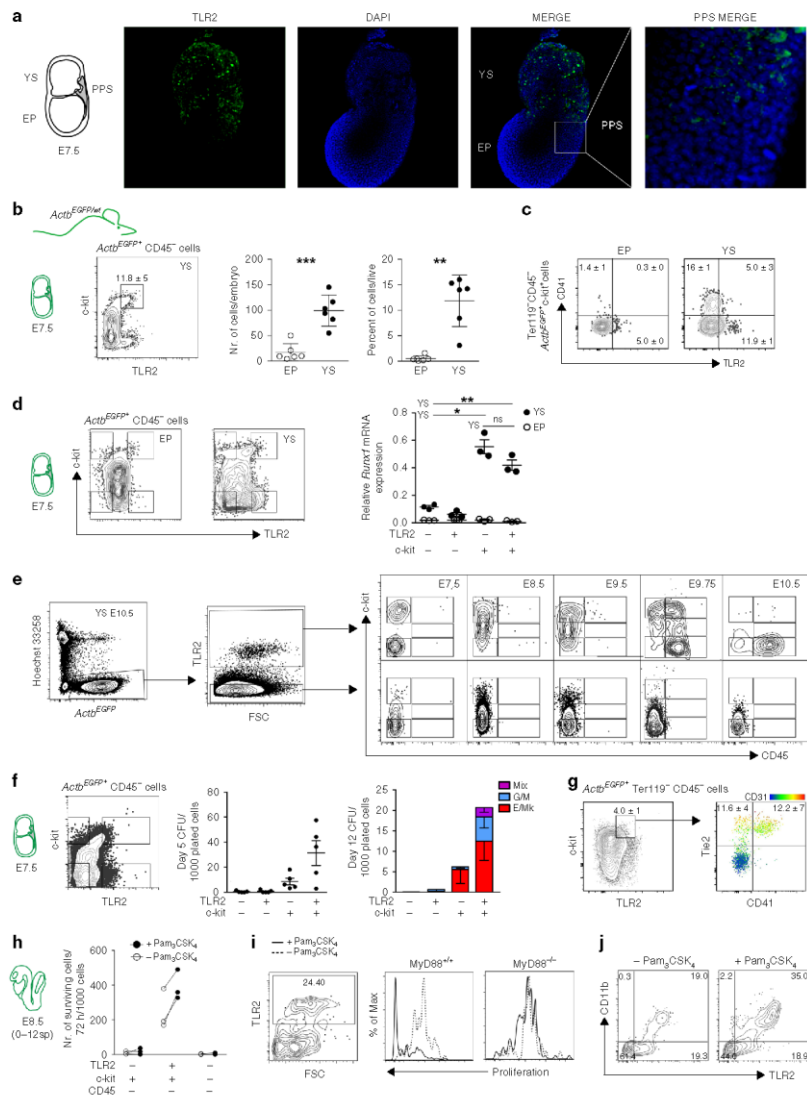
TLR2−c-kit+ and TLR2+c-kit+ progenitors was that only the latter gave rise to mixed colonies (Mix) (Fig. 1f; Supplementary Fig. 2b). In five independent experiments, apart from the occasional monopotent myeloid colonies (G/M), mixed colonies from TLR2−c-kit+ progenitors were never observed. This

principal distinction of EMPs, signified by TLR2 expression on their c-kit+ precursors, was functionally discernable despite the fact that a fraction of both TLR2+c-kit+, and to a lesser extent, TLR2−c-kit+ subsets, co-expressed Tie2, CD31 along with CD41 (Fig. 1g; Supplementary Fig 2c, middle row), suggesting their

42

Fig. 1 Early YS-derived TLR2$^+$ c-kit$^+$ cells exhibit features of EMP precursors. **a** Immunofluorescence of E7.5 embryos revealed the presence of TLR2$^+$ cells (green) predominantly in YS. Weaker TLR2 staining was also detected in PPS (white insert). Nuclei were stained with DAPI (blue). YS yolk sac, EP embryo proper, PPS posterior primitive streak. A representative image is shown ($n = 2$ independent experiments with at least four embryos per experiment). **b–j** $Actb^{EGFP/wt}$ embryos (see Supplementary Fig. 1b) were used to analyze cells of embryonic origin. **b** Quantification of $Actb^{EGFP}$+CD45$^-$c-kit$^+$TLR2$^+$ cells in E7.5 EP and YS (mean ± SD; $n = 6$; **$p \leq 0.01$, ***$p \leq 0.001$; paired, two-tailed t test). **c** Surface co-expression of TLR2 with CD41 determined on E7.5 $Actb^{EGFP}$+CD45$^-$c-kit$^+$ cells obtained from EP or YS. **d** $Runx1$ mRNA expression normalized to $Gapdh$ levels in four sorted subsets of E7.5 embryonic $Actb^{EGFP}$+CD45$^-$ cells with combinatorial expression of c-kit and TLR2 (mean ± SD; $n = 3$; *$p \leq 0.05$, **$p \leq 0.01$; paired, two-tailed t test). **e** E7.5- E10.5 YS $Actb^{EGFP}$+ cells of either TLR2$^+$ or TLR2$^-$ phenotype were analyzed for the expression of c-kit and CD45 by FCM. **f** E7.5 $Actb^{EGFP}$+Lin$^-$ cells (Lin = CD3$^-$Gr-1$^-$CD11b$^-$B220$^-$Ter119$^-$) were sorted based on their c-kit and TLR2 expression (see sorting strategy in Supplementary Fig. 2a), plated in a methylcellulose medium M3434 (StemCell Technologies) and assessed for their CFU potential (mean ± SEM; $n = 5$). **g** YS-derived E7.5 $Actb^{EGFP}$+Ter119$^-$CD45$^-$c-kit$^+$TLR2$^+$ cells were analyzed for Tie2, CD41, and CD31 expression. See full gating strategy in Supplementary Fig. 2c. **h–j** Sorted E8.5 $Actb^{EGFP}$+ cells were plated on OP-9 stromal cells in the presence or absence of the TLR2 agonist Pam$_3$CSK$_4$ (1 μg/ml) and analyzed by FCM after 72 h ($n = 3$). **h** Survival analysis of sorted E8.5 TLR2$^{+/-}$c-kit$^{+/-}$CD45$^-$cells. **i** The proliferation history of E8.5 TLR2$^+$c-kit$^+$CD45$^-$ cells sorted from MyD88$^{+/+}$ or MyD88$^{-/-}$ embryos was assessed by the dilution of a proliferation dye in TLR2$^+$ cells (see also Supplementary Fig. 2d). **j** $Actb^{EGFP}$+ cells recovered from cultures of $Actb^{EGFP}$+TLR2$^+$ c-kit$^+$ CD45$^-$ cells stimulated, or unstimulated, with Pam$_3$CSK$_4$ were analyzed for CD11b and TLR2 expression. Source data are provided as a Source Data file

common hemogenic endothelial ancestry and hematopoietic fate. However, while t-SNE analysis revealed that these two subsets displayed a continuum of Tie2, CD31, and CD41 surface expression, it was the TLR2$^+$c-kit$^+$ subset which formed a tight cluster (red dots) with the highest expression of these markers (Supplementary Fig. 2c, bottom panel). Taken together, the expression of TFs, endothelial, and hematopoietic markers and the outcome from clonogenic assay link TLR2$^-$c-kit$^+$ progenitors to primitive erythro/megakaryopoiesis. In contrast, TLR2 expression on E7.5 c-kit$^+$ YS progenitors accompanied by the high expression of Tie2, CD31 and CD41 predicates the acquisition of functional competence for multi-lineage EMP potential. Thus, TLR2 expression allows for the unequivocal distinction of emerging precursors of EMPs among coexisting progenitors of primitive erythropoiesis.

TLR2 stimulation of TLR2$^+$c-kit$^+$ precursors enhances the production of myeloid cells. When E8.5 $Actb^{EGFP}$+ cells of either TLR2$^+$c-kit$^+$, TLR2$^-$c-kit$^+$, or TLR2$^-$c-kit$^-$ phenotypes were co-cultured with OP-9 stroma in the presence or absence of the TLR2 agonist, Pam$_3$CSK$_4$, both TLR2$^-$ populations failed to survive. However, ~39 and 24% of $Actb^{EGFP}$+ cells that were either stimulated or not stimulated with Pam$_3$CSK$_4$, respectively, were recovered from co-cultures with TLR2$^+$c-kit$^+$ progenitors (Fig. 1h). The increased survival after TLR2 stimulation correlated with a higher rate of proliferation that was fully dependent on MyD88, the adaptor protein which is required for TLR2 signaling (Fig. 1i; Supplementary Fig. 2d). In addition, Pam$_3$CSK$_4$-stimulated cells showed a more efficient myeloid differentiation rate measured by the expression of CD11b (Fig. 1j). This data, as well as the findings of a previous report, suggest that the capacity of activated TLRs to nudge the output of hematopoiesis toward myelo/granulopoiesis is inherent to all progenitors of definitive hematopoiesis, ontogenetically commencing with the emergence of TLR2$^+$c-kit$^+$ precursors of EMPs[29].

$Tlr2$ locus is efficiently activated in erythro-myeloid progenitors. To follow the fate of cells with an active $Tlr2$ locus, we generated a $Tlr2^{Cre}$ mouse strain by BAC recombineering. In adult animals, $Tlr2$ activation labeled all hematopoietic lineages and their progenitors with no significant bias (Supplementary Fig. 3). To determine the first ontogenetic time point of $Tlr2$-driven labeling, we looked at the emergence of $Tlr2^{Cre}$EYFP$^+$ cells in E7.5–E10.5 embryos. Due to the expected delay caused by Cre-
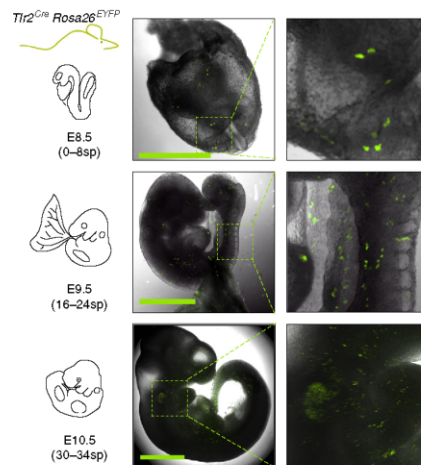

Fig. 2 Lineage tracing shows early activation of $Tlr2$ locus in hematopoietic progenitors. Spatial microscopic analysis of E8.5–E10.5 $Tlr2^{Cre}$EYFP$^+$ cells; scale bar = 1 mm. Representative image is shown ($n = 3$ independent experiments with 3–6 embryos per experiment)

mediated recombination followed by EYFP labeling, the first $Tlr2^{Cre}$EYFP$^+$ cells appeared at E8.5 (0–8sp) (Fig. 2).

If TLR2 expression marks the emergence of EMP precursors, then EMPs and their progeny with a sufficiently activated $Tlr2$ promoter should be genetically labeled in the $Tlr2$-driven reporter mice. Thus, we first assessed the phenotype and frequency of labeled cells by combining Ter119, c-kit, CD41, and FcRγ surface markers to discriminate erythroid and myeloid precursors[6]. The analysis of $Tlr2^{Cre}$EYFP$^+$ cells at E8.5, E9.5 YS, and EP revealed the presence of five distinct populations that represented the most abundant $Tlr2^{Cre}$EYFP$^+$ subsets (Supplementary Fig. 4a). At E8.5, $Tlr2^{Cre}$EYFP$^+$ cells accounted for an average 6.9% of the total cells, among which non-hematopoietic cells and primitive erythrocytes (EryP) each represented ~40%. Subsets of c-kit$^+$FcRγ$^+$ (MFp), c-kit$^+$CD41$^+$ (Mkp), and c-kit$^+$CD41$^+$FcRγ$^+$ (EMPs) phenotypes
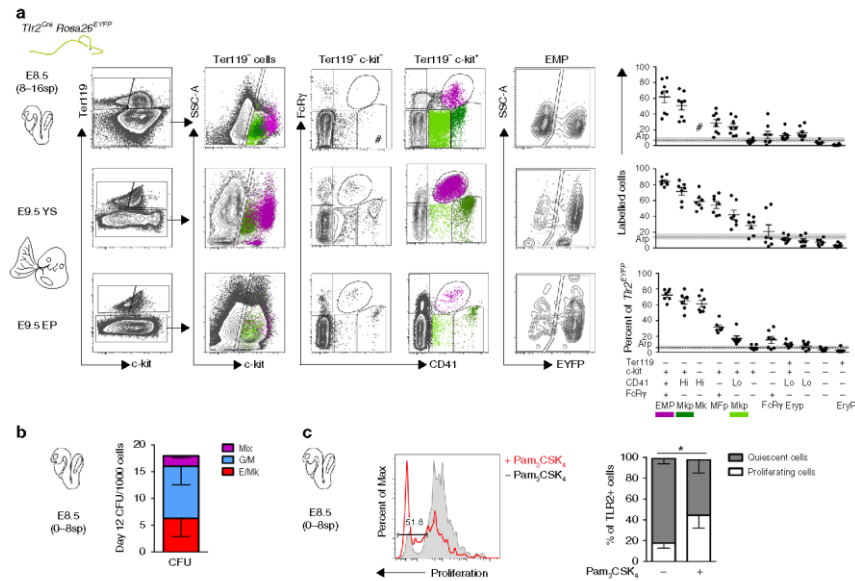
43

Fig. 3 Lineage tracing shows activation of *Tlr2* locus predominantly in EMPs. **a** Embryonic hematopoietic precursors were analyzed by FCM for frequency of labeling in E8.5 and E9.5 *Tlr2*^Cre^*Rosa26*^EYFP^ embryos (mean ± SEM; n = 7–9; arp, average recombination probability is equal to mean ± SEM (gray zone) labeling efficiency of all live cells; EMP, erythro-myeloid progenitor; Mkp, megakaryocyte progenitor; Mk, megakaryocyte; MFp, macrophage progenitor; FcRγ, FcRγ+ cells; Eryp, Ery progenitor; EryP, primitive erythrocyte; # insufficient cell count for statistical analysis). **b** Sorted E8.5 *Tlr2*^Cre^EYFP+Lin− cells (see Supplementary Fig. 4g) were plated in a methylcellulose medium and assessed for their differentiation potential at day 12 of culture (mean ± SEM; n = 8). **c** The proliferation history of sorted *Tlr2*^Cre^EYFP+Lin− cells cultured in the presence (red open histogram) or absence (gray closed histogram) of Pam₃CSK₄ (1 µg/ml) on ST-2 stroma was assessed by the dilution of proliferation dye in TLR2+ cells after 72 h (mean ± SEM; n = 3; *p < 0.05; paired, one-tailed t test). Source data are provided as a Source Data file

collectively represented the remaining ~20% of *Tlr2*^Cre^EYFP+ cells (Supplementary Fig. 4a). While being at E8.5 the least frequent population among *Tlr2*^Cre^EYFP+ subsets, YS EMPs, which expressed the highest levels of c-kit, exhibited the highest labeling efficiency (~60%, Fig. 3a, top scatterplot) attesting to the preferential and robust activation of their *Tlr2* locus. Other populations, Mkp, MFp, and by E9.5 also CD41+ Mk, were also preferentially labeled well above the average recombination probability (arp) threshold. In contrast, EryPs were negligibly labeled (Fig. 3a, scatterplots). In the E9.5 YS, due to their expansion, EMPs accounted for 17–38% of all *Tlr2*^Cre^EYFP+ cells with even higher labeling efficiency (< 80%) (Supplementary Fig. 4a and Fig. 3a, middle scatterplots). Consistent with previous reports, at E9.5, only a fraction of TLR2+ EMPs were found in EP compared to YS (Supplementary Fig. 4b) confirming that these cells emerge in YS[4,35].

Interestingly, when maternally-derived FcRγ+ MFs (mMFs) were discounted, nearly one-half of the minute population of E8.5 FcRγ+ cells (eFcγ) was also *Tlr2*-labeled (Supplementary Fig. 4c). However, as these cells, in contrast to mMFs (Supplementary Fig. 1b, right panel), were virtually all CD45−CD11b− (Supplementary Fig. 4c) they could not be considered *bona-fide* MFs. Moreover, since they represented merely 0.3% of all *Tlr2*-labeled

cells, it is impossible at this junction to make any statement about their origin and affiliation to a certain hematopoietic wave and lineage. However, *Tlr2*^Cre^EYFP+ tissue-resident MFs were microscopically detectable in the E11.5 head and FL (Supplementary Fig. 4d). In addition, and consistent with the activation of *Tlr2* locus in the progenitors of EMPs, while E11.5 FL early erythroid progenitors (Early E)[36] were labeled almost as efficiently as FL and circulating EMPs, circulating and FL EryPs were labeled with only background and sub-background frequencies, respectively (Supplementary Fig. 4e, f).

Functionally, *Tlr2*^Cre^EYFP+Lin− cells isolated from E8.5 (0–8sp) embryos (Supplementary Fig. 4g) exhibited the potential to generate erythroid, myeloid, and mixed colonies (Fig. 3b). In addition, E8.5 *Tlr2*^Cre^EYFP+Lin− cells responded to TLR2 triggering by an enhanced proliferation rate (Fig. 3c). Thus, the expression of functional TLR2 accompanies the emergence of EMPs in vivo.

E8.5 *Tlr2*-labeled progenitors contribute to embryonic hematopoiesis. To follow the developmental fate of cells with active *Tlr2* locus in a time controlled manner, we generated a *Tlr2*^CreERT2^ mouse BAC strain (Supplementary Fig. 5a). In this model, *Cre* expression and the generation of EYFP+ cells was
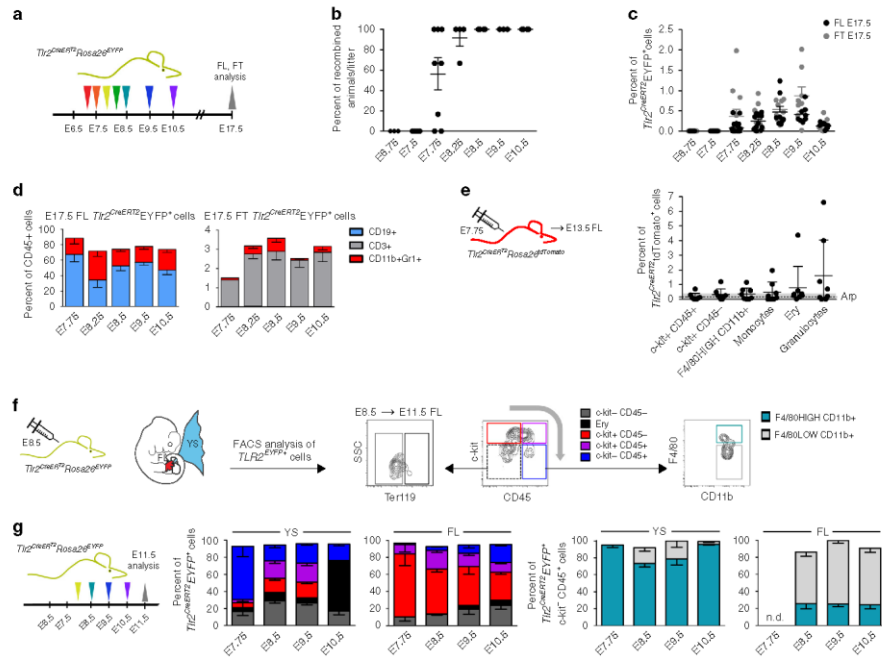
44

Fig. 4 At E7.75, *Tlr2*-labeled progenitors contribute to embryonic and fetal hematopoiesis. **a** Experimental design of the fate mapping of cells with an active *Tlr2* locus. **b** The percentage of EYFP+ embryos among all *Tlr2CreERT2Rosa26EYFP* embryos in the same litter pulsed with one dose of 4-OHT from E6.75 to E10.5 was analyzed at E17.5 by FCM (mean ± SEM; $n = 3–8$ litters). **c** Percentage of *Tlr2CreERT2*EYFP+ cells in E17.5 fetal liver (FL, black dots) and E17.5 fetal thymus (FT, gray dots) in embryos described in (**b**); (mean ± SEM; $n = 6–21$ embryos). **d** The hematopoietic fate of *Tlr2CreERT2*EYFP+ cells pulsed with one dose of 4-OHT from E7.75 to E10.5 was determined in E17.5 FL and FT by FCM; (mean ± SEM; $n = 4–8$). **e** Labeling of hematopoietic populations (including granulocytes and monocytes) was determined in E13.5 FL of *Tlr2CreERT2Rosa26tdTomato* embryos pulsed with a single dose of 4-OHT at E7.75 (mean ± SEM; $n = 8$; arp = average recombination probability assessed in Ter119⁻c-kit⁻CD45⁻ cells. **f** Gating strategy to identify the contribution of *Tlr2CreERT2*EYFP+ cells to indicated hematopoietic populations in E11.5 YS and FL. **g** Fate tracing of E11.5 *Tlr2CreERT2*EYFP+ cells pulsed with one dose of 4-OHT from E7.75 to E10.5 (mean ± SEM; $n = 5–15$) was analyzed by FCM according to (**f**). Source data are provided as a Source Data file

accomplished within 18 h upon 4-hydroxy tamoxifen (4-OHT) administration (Supplementary Fig. 5b). The first *Tlr2CreER-T2Rosa26EYFP* recombined embryos were found when 4-OHT was applied at E7.75 (Fig. 4a, b), resulting in the appearance of labeled cells in the FL and thymus (FT) (Fig. 4c). A single 4-OHT pulse at E7.75, E8.5, E9.5, or E10.5 marked hemato-poietic progenitors that in E17.5 FL and FT gave rise to all main hematopoietic lineages (Fig. 4d; Supplementary Fig. 5c) with the highest labeling efficiencies at E8.5 and E9.5 (Fig. 4c). Moreover, consistent with the initiation of TLR2 expression in the precursors of EMPs at E7.5, when pulsed at E7.75, myeloid cells, including Ly6G+ granulocytes and Ly6C+ monocytes, were labeled in E13.5 *Tlr2CreERT2Rosa26tdTomato* FL (Fig. 5e; Supplementary Fig. 5d), supportive evidence of their early EMP origin. It is of note, that in the absence of 4-OHT, no labeling was observed (Supple-mentary Fig. 5e). This data confirm that the E7.75 embryo already contains a fully committed pool of multi-lineage progenitors of EMP and LMP.

We next investigated the fate of *Tlr2CreERT2*EYFP+ cells. We pulsed *Tlr2CreERT2Rosa26EYFP* embryos from E7.75 to E10.5 with a single dose of 4-OHT and assessed the phenotype of *Tlr2CreERT2*EYFP+ cells at E11.5 in YS and FL by flow cytometry (FCM) (Fig. 4f, g). When pulsed between E7.75 and E9.5, *Tlr2CreERT2*EYFP+ cells at their c-kit+ stage colonized FL where they retained mostly a c-kit+ phenotype with only a fraction differentiating to c-kit+CD45+ cells. In YS, *Tlr2CreERT2*EYFP+ cells differentiated to c-kit+CD45+ and CD45+ cells, a vast majority of which were F4/80HIGHCD11b+ MFs. In contrast, a minute CD45+ myeloid population in FL was predominantly F4/80LOWCD11b+. Importantly, the highest labeling efficiency of E11.5 FL cells was achieved upon labeling from E7.5 to E8.5 (Supplementary Fig. 5f). These results imply that the wave of E7.5–8.5 *Tlr2CreERT2*EYFP+ EMP precursors contributed the most to the pool of hematopoietic cells differentiating in the FL.

When tracing the fate of cells labeled by *Tlr2* at E8.5 at later stages of development (E12.5–E15.5; Supplementary Fig. 5g), we
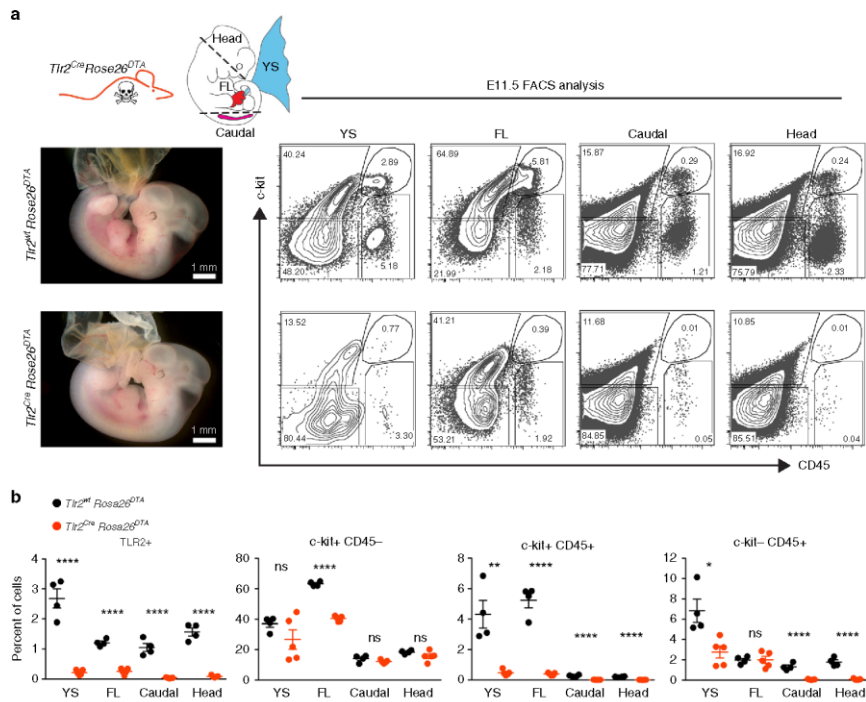
Fig. 5 *Tlr2*-driven production of DTA efficiently deletes hematopoietic cells in E11.5 embryos. **a** Representative images of E11.5 *Tlr2^{wt}Rosa26^{DTA}* and *Tlr2^{Cre}Rosa26^{DTA}* embryos ($n = 4$ independent experiments with 3–8 embryos of each genotype per experiment). FCM analysis (**a**) and its quantification (**b**) of TLR2+, c-kit+CD45−, c-kit+CD45+, and c-kit−CD45+ cell subsets in the YS, FL, caudal part, and head of dissected E11.5 *Tlr2^{wt}Rosa26^{DTA}* (upper panel) and *Tlr2^{Cre}Rosa26^{DTA}* (lower panel) embryos (mean ± SEM; $n = 4$–5; ****$p ≤ 0.0001$, *$p < 0.05$; paired, two-tailed *t* test). Scale bar = 1 mm. Source data are provided as a Source Data file

observed that c-kit+ cells gradually disappeared from YS as the number of myeloid and erythroid cells increased. Starting from E12.5, the number of labeled erythroid cells in FL increased at the expense of c-kit+ as well as c-kit+CD45+ progenitors, attesting for the relocalization of the main site of erythropoiesis from YS to FL.

Tlr2-driven production of diphtheria toxin efficiently deletes EMPs. To determine the phenotype of embryos that lack TLR2+ cells, we employed a *Rosa26^{DTA}* reporter strain whereby the activation of the diphtheria toxin (DTA) module causes cell death (Fig. 5a). Depletion of TLR2+ cells from E11.5 *Tlr2^{Cre}Rosa26^{DTA}* embryos was highly efficient (Fig. 5a, b, left scatterplot; Supplementary Fig. 6a) and caused lethality before E13.5 (Supplementary Fig. 6b). At E11.5, the absence of TLR2+ cells translated into a significant decrease of myeloid cells as well as their progenitors in the YS, head, and caudal part of the embryo (Fig. 5a, b). By E11.5, c-kit+CD45+ progenitors had vanished in all compartments. Consistent with *Tlr2* activity in tissue MFs, microglia were also efficiently depleted (Supplementary Fig. 6c). While the depletion of TLR2+ cells did not affect the counts of EryPs in

E12.5 peripheral blood, it caused severe defects in FL definitive hematopoiesis (Supplementary Fig. 6d, e). E12.5 *Tlr2^{Cre}Rosa26^{DTA}* livers were pale and had reduced cellularity as compared with livers of wt animals. In addition, EMPs and MFs were virtually absent and the counts of Early E, as well as erythroid cells were severely decreased (Supplementary Fig. 6e). Thus, while primitive erythropoiesis remained intact, EMP-derived erythropoiesis was severely affected upon depletion of TLR2+ cells. It is of note, that even though *Tlr2* locus is activated also in some non-hematopoietic cells, their numbers were not affected by *Tlr2* driven depletion, strongly advocating that lethality was caused by aberrant EMP-dependent hematopoiesis. Thus, the *Tlr2* locus is activated in the earliest YS-derived c-kit+ precursors of EMPs which in *Tlr2^{Cre}Rosa26^{DTA}* embryos, due to DTA toxicity, largely fail to mature to the erythro-myeloid progenitor stage and beyond.

Tlr2 locus is active in hematopoietic clusters emerging from the mouse aorta. Analysis of adult *Tlr2^{Cre}Rosa26^{EYFP}* mice BM showed that the *Tlr2* locus is active in phenotypical LT-HSC (Supplementary Fig. 3d). To determine whether it is also active in

46
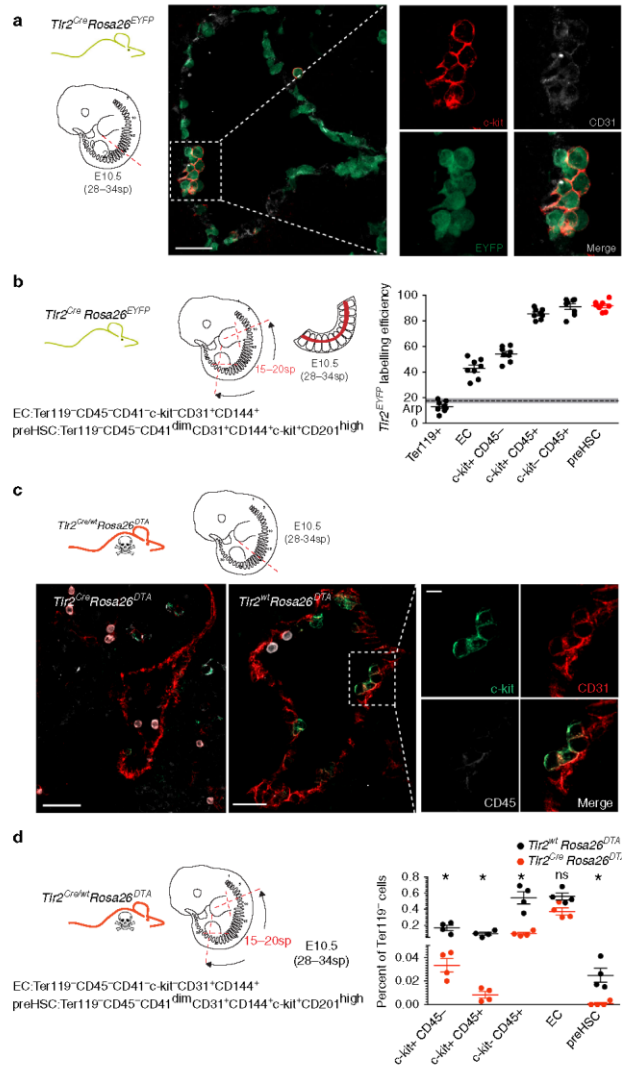
HSCs during embryonic development, we imaged the aortic sections of E10.5 $Tlr2^{Cre}Rosa26^{EYFP}$ embryos (28–34sp) where intra-aortic hematopoietic clusters (IAHCs) emerged from the CD31$^+$ endothelium[10,37]. In addition to endothelial cells at the lining of the aorta, IAHCs were also labeled (Fig. 6a). Moreover, in the aortic parts of these embryos, pre-HSCs[38] showed the most efficient labeling among all populations tested (98% ± 4.0 SD) as opposed to endothelial cells which were only partially labeled (40% ± 7.5 SD) (Fig. 6b; Supplementary Fig. 7a). This suggests that activation of the $Tlr2$ locus in blood cells occurred at the time

47

Fig. 6 E10.5 aortic pre-HSC activate their *Tlr2* locus. **a** Cryosections of E10.5 (28–34sp) dorsal aortae with intra-aortic hematopoietic clusters (IAHCs) were analyzed from *Tlr2^{Cre}Rosa26^{EYFP}* embryos by staining for EYFP (green), c-kit (red) and CD31 (white). A representative image is shown (*n* = 5 independent experiments with 1–2 embryos per experiment). **b** Aortic regions were dissected from E10.5 *Tlr2^{Cre}Rosa26^{EYFP}* embryos (28–34sp), and hematopoietic populations as well as endothelial cells were analyzed for their labeling efficiency by FCM. The gating strategy for each indicated subset adopted from ref., [38] is shown in Supplementary Fig 7a. **c** Sections of E10.5 (28–34sp) aortae were taken from *Tlr2^{Cre}Rosa26^{DTA}* (left panel) and *Tlr2^{wt}Rosa26^{DTA}* (middle and right panels) embryos and stained for c-kit (green), CD31 (red), and CD45 (white) to identify IAHCs. Scale bar represents 50 μm. A representative image is shown (*n* = 5 independent experiments with 1–2 embryos of each genotype per experiment). **d** Aortic regions were disected from E10.5 *Tlr2^{wt}Rosa26^{DTA}* (black dots) and *Tlr2^{Cre}Rosa26^{DTA}* (red dots) embryos (28–34sp). Hematopoietic populations as well as endothelial cells were analyzed for their frequencies by FCM (mean ± SEM; *n* = 4; *$p < 0.05$; paired, two-tailed *t* test). Gating strategy is shown in Supplementary Fig. 7b. Source data are provided as a Source Data file

of HSCs specification. In addition, the emergence of IAHCs was disrupted in *Tlr2^{Cre}Rosa26^{DTA}* embryos (Fig. 6c) where pre-HSCs were absent (Fig. 6d; Supplementary 7b).

E8.5 HSC progenitors with an active *Tlr2* locus contribute to adult hematopoiesis. To address if early *Tlr2^{CreERT2}*EYFP^+ progenitors contribute to adult hematopoiesis, we pulsed *Tlr2^{CreERT2}Rosa26^{EYFP}* embryos from E6.75 to E10.5 with a single dose of 4-OHT and monitored *Tlr2^{CreERT2}*EYFP^+ cells in the peripheral blood (PB) of animals until 16 weeks of age (Fig. 7a). While the first time point of PB labeling of all three main hematopoietic lineages occurred at ~E7.75–8.0, it persisted for only the first 4 weeks of life, thus targeting EMPs and LMPs (Fig. 7a). The highest efficiency of labeling was achieved when pulsed at E8.5 (Fig. 7a), whereby *Tlr2^{CreERT2}*EYFP^+ cells contributed to all three main hematopoietic lineages in all hematopoietic tissues tested at 16 weeks of age (Fig. 7b; Supplementary Fig. 8a). When the E15.5 FL of these mice were analyzed, ST-HSC, multipotent progenitors (MPP), and LT-HSCs were labeled at the highest frequencies (Fig. 7c). Moreover, E8.5 *Tlr2*-labeled Lin^− BM cells (*n* = 8) engrafted primary, lethally irradiated recipients for more than 16 weeks (Fig. 7d; Supplementary Fig. 8b) Then, lineage-depleted *Tlr2^{CreERT2}*EYFP^+ sorted cells isolated from BM of primary recipients 16-weeks after transplantation engrafted secondary adult lethally irradiated recipients giving rise to all three hematopoietic lineages (Fig. 7d; Supplementary Fig. 8c) demonstrating their ability to self-renew. These data imply that *Tlr2^{CreERT2}*EYFP^+cells that give rise to HSCs activated their *Tlr2* locus as early as E8.5. This stage so far represents one of the earliest known events in the HSC specification process.

Discussion

Our study has established that the expression of TLR2 on c-kit^+ cells allows for the discrimination of emerging multi-lineage precursors of EMPs from c-kit^+ progenitors of the primitive erythroid wave, both of which are present in E7.5 embryos. Notably, phenotypic analysis and clonogenic assay demonstrated that only TLR2^+c-kit^+ but not TLR2^−c-kit^+ cells are able to mature to CD45^+ hematopoietic cells and produce mixed colonies. The data from *Tlr2^{CreERT2}Rosa26^{EYFP}* and *Tlr2^{Cre}Rosa26^{EYFP}* embryos confirmed that the *Tlr2* locus in hematopoietic precursors is activated at ~E7.5, which is followed at E8.5 by the emergence of the first EYFP-labeled c-kit^+ cells exhibiting essential EMP characteristics. Importantly, genetic ablation of these progenitors with active *Tlr2* locus left the primitive erythropoiesis intact. This data is in agreement with previously reported labeling of EMPs by 4-OHT at E7.75 in *Csf1r^{MeriCreMer}* embryos[22]. Indeed, *Tlr2* expressing cells were enriched in the hematopoietic progenitor cluster identified by single cell profiling of E7.75 cells[39]. Consistent with the co-expression of TLR2 on c-kit^+ progenitors shown in this study, the emergence of the earliest pre-HSCs at E8.5 can be visualized by lineage tracing using both *Tlr2*- and *c-Kit*-based reporter systems[24].

The co-expression of TLR2 and c-kit markers as the earliest signature of emerging EMPs precursors aids to clarify the sequence and developmental relationships among early hematopoietic waves. Since it has been assumed that the primitive and EMP waves emerge successively at E7.5 and E8.5, respectively[40], preferential labeling of brain microglia over other tissue resident MFs at E7.5 using *Runx1*, *Tie2*, or *c-Kit* drivers[22–24], has led some to propose that they originated from the primitive wave. Our data supports an alternative view that, due to their appearance at E7.5, c-kit^+TLR2^+ precursors of EMPs could represent the main source of progenitors for brain microglia, fetal, and adult tissue-resident MFs as well as fetal definitive erythrocytes[4,41]. The brain vasculature develops early, hence it becomes a primary sink of migrating precursors of EMPs[42]. In line with previous reports, we also showed that EMPs, the precursors of which expressed TLR2 between E7.75 and E8.5, were the main source of cells seeding FL, where they expanded and differentiated mostly to monocyte-like F4/80^{LOW}CD11b^+ myeloid cells, whereas beyond FL they preferentially produced F4/80^{HIGH}CD11b^+ tissue resident MFs[6,22]. Thus, while our data advocates a shared endothelial origin and an overlapping expression pattern of *Runx1*, CD41, Tie2, and CD31 between E7.5 progenitors of the primitive and EMP waves, it is the acquisition of TLR2 and the enhanced expression of CD41, Tie2 and CD31 on the background of c-kit that marks the initiation of the ontogenetic program which endows early progenitors with the acquisition of multi-lineage erythro-myeloid potential. Endogenous labeling of cells with an active *Tlr2* locus showed that EryPs were labeled only at a very low efficiency, hardly overcoming the background labeling level, suggesting that the activation of the *Tlr2* locus occurs predominantly and most robustly in emerging EMPs and their progeny. Thus, the contribution of *Tlr2*-labeled EryPs to their total pool is negligible as is the effect of their depletion on early embryonic erythropoiesis. At E8.5, ~60–90% of EMPs were labeled by *Tlr2* activation, followed by progenitors of MFs, Mks, and Eryps.

Functionally analogous to the situation in adult BM[29], stimulation of E8.5 TLR2^+c-kit^+ progenitors and E8.5 *Tlr2^{Cre}*EYFP^+c-kit^+Lin^− cells by the TLR2 ligand enhanced their proliferation rate as well as differentiation to myeloid cells in a *MyD88*-dependent manner. However, as TLR2^+ embryonic progenitors were still able to proliferate and differentiate into myeloid cells regardless of ligand stimulation, TLR2-generated signals seemed to be dispensable for normal embryonic myelopoiesis under noninflammatory conditions. Presently, no evidence for the impaired development of myeloid cells at steady-state in *Tlr2^{−/−}* or *MyD88^{−/−}* mice has been reported[43,44]. Thus, the early activation of the *Tlr2* locus and its dispensability for the process of embryonic development, makes *Tlr2* regulatory elements a suitable target for the generation of experimental models for fate mapping of the earliest steps in embryonic hematopoiesis.
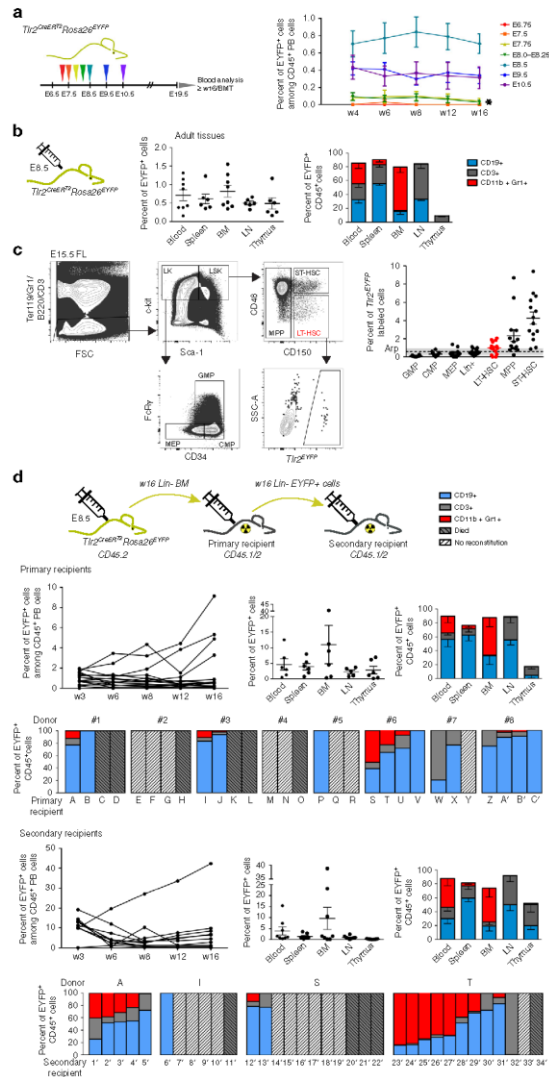
At E8.5, in $Tlr2^{CreERT2}Rosa26^{EYFP}$ embryos, in addition to EMPs, HSC progenitors were labeled at the highest efficiency, which correlates with the expression of $Tlrs$ on hematopoietic cluster cells in $Ly6a^{GFP}$ transgenic animals[32]. EMPs and HSCs originate from distinct populations of endothelial cells[17], yet the onset of their $Tlr2$ promoter activity at E8.5 seems to be

ontogenetically synchronized. The indication that the activation of the inflammatory expression program occurs during EHT[32,45], together with our finding that TLR2 stimulation of the earliest TLR2+c-kit+ YS precursors as well as BM-derived HSCs[29] augmented their myeloid fate, suggests that the mechanism of TLR-driven hematopoiesis under inflammatory conditions is not only

49

Fig. 7 Progenitors with active *Tlr2* locus labeled at E8.5 contribute to adult hematopoiesis. **a** *Tlr2^CreERT2Rosa26^EYFP* embryos pulsed with a single dose of 4-OHT between E6.75-E10.5 were monitored postpartum for the presence of *Tlr2^CreERT2*EYFP+ cells in their peripheral blood (PB) up to 16 weeks of age (mean ± SEM; *n* = 9–25; ^ indicates short-term hematopoietic potential which persisted for only the first 4 weeks of life. **b** Percentage of *Tlr2^CreERT2*EYFP+ cells, labeled at E8.5, and their contribution to the main CD45+ lineages in different hematopoietic organs is shown (mean ± SEM; *n* = 5–7; see gating strategy in Supplementary Fig. 8a). **c** *Tlr2^CreERT2Rosa26^EYFP* embryos were pulsed with a single dose of 4-OHT at E8.5, and labeling efficiency of indicated hematopoietic populations was analyzed in E15.5 FL by FCM. LT-HSC gate is shown as an example. **d** *Tlr2^CreERT2Rosa26^EYFP* embryos were pulsed with a single dose of 4-OHT at E8.5. At 16 weeks of age, Lin-depleted BM (CD45.2) (w16 Lin⁻ BM; see Supplementary Fig. 8b) was transferred to lethally irradiated primary recipients (CD45.1/2) along with support BM cells (0.5 × 10^6 CD45.1), and the level of *Tlr2^CreERT2*EYFP+ cells was monitored in PB of primary recipients until week 16 (upper left panel). The percentage of *Tlr2^CreERT2*EYFP+ cells, their organ distribution and fate in primary recipients is shown (mean ± SEM; *n* = 6). Bar graphs show the reconstitution success and fate of *Tlr2^CreERT2*EYFP+ cells in primary recipients (A–C') of BM from eight individual donors (#1–8). Sorted *Tlr2^CreERT2*EYFP+ cells (see Supplementary Fig. 8c) from Lin-depleted BM of 16-week old primary recipients were transferred to secondary, lethally irradiated recipients (CD45.1/2) along with support BM cells (0.5 × 10^6, CD45.1) and the frequency of *Tlr2^CreERT2*EYFP+ cells in PB was monitored until week 16 (the outcome of BMT from one primary recipient (donor T) is shown (secondary recipients, upper row, left panel). The percentage of *Tlr2^CreERT2*EYFP+ cells, their organ distribution and fate in secondary recipients is shown (mean ± SEM; *n* = 8). Bar graphs on the bottom indicate the reconstitution success and fate of *Tlr2^CreERT2*EYFP+ cells in secondary recipients (1'−34') of BM from four primary recipients. Source data are provided as a Source Data file

operational in adult but also in embryonic hematopoietic progenitors. Indeed, a number of studies has reported that proinflammatory cytokines are important players in HSCs specification in the mouse and zebrafish[32,46,47]. In this scenario, TLR expression represents one of the oldest, evolutionary conserved and ontogenetically synchronized genetic programs activated during hematopoietic specification.

Taken together, the *Tlr* expression program is not only operational in embryonic and adult hematopoietic progenitors, endothelial cells, and MFs regardless of their origin[33] but it is initiated in the earliest YS-derived definitive hematopoietic progenitors as well as ancestors of HSCs.

Methods

Animals. CD1 and C57Bl/6J mice were maintained at the animal facility of the Institute of Molecular Genetics in Prague (IMG). pCAGEGFPMos3 mice expressing EGPP under the control of the *Actb* promoter, here referred to as *Actb^EGFP* mice were generated and provided by Petr Svoboda[48]. *MyD88^−/−* mice (B6.129P2 (SJL)-*Myd88^tm1.1Defr*/J) and *Rosa26^DTA* (B6.129P2-Gt(ROSA)26Sor^tm1(DTA)Lky/J) reporter mice were purchased from The Jackson Laboratory. *Rosa26^tdTomato* (B6;129S6-Gt(ROSA)26Sortm14(CAG-tdTomato) Hze/J) and *Rosa26^EYFP* (B6.129 × 1-Gt(ROSA)26Sortm1(EYFP)Cos/J) reporter mice were provided by V. Korinek. *Tlr2^Cre* and *Tlr2^CreERT2* transgenic mice were generated by inserting Cre and *Cre^ERT2* cassettes, respectively, under the control of the *Tlr2* promoter by BAC recombineering[49]. Murine BAC clone RP23-455P23 encompassing *Tlr2* gene with extensive upstream (46 kb) and downstream (123 kb) sequences was obtained from the BAC resource depository at CHORI. By homologous recombination, the openreading frame of *Tlr2* exon 3 was substituted with *Cre* and *Cre^ERT2* cDNA, respectively. BAC DNA for pronuclear injection was prepared using the QIAGEN Large-Construct Kit and analyzed by pulsed-field gel electrophoresis. The pronuclear injection of the construct (1 ng/µl) into mouse zygotes was carried out at the Transgenic Unit of IMG. Founders were identified by PCR amplification of tail DNA with specific primers for *Tlr2^Cre* transgenic and wt alleles: *Tlr2F* (common) 5′-AGCCATAGGCCACATCTAGT-3′, *Tlr2CreR* 5′-GTATGCTCAGAAAACGC CTG-3′ (470b), and *Tlr2wtR* 5′-AAAAAGCGATGTTACCCC-3′ (784b) and backcrossed to C57BL/6 mice. All experiments included littermate controls with the minimum sample size of three animals. Embryonic development was estimated by considering the day of vaginal plug formation as embryonic day 0.5 (E0.5) and staged using standard criteria[50]. To obtain E7.5 embryos, we used E7.5 time pregnant females and strictly selected only those embryos that were at the neural plate stage (NPS) with no visible signs of allantoic bud or structure, with an apparent cranial limit furrow and pointy node (i.e. E7.25–7.5, on rare occassion up to 7.75). All embryos, which were older than those without the "allantois bud stage" of NPS, were excluded from CPU assays experiments. In various other experiments, somite pairs were counted to determine embryo age more accurately. All experiments were approved by the ethical committee of the IMG.

Cell suspension preparation. Time pregnant females were killed by cervical dislocation, and embryos were dissected from uteri. E7.5–8.5 embryos were carefully stripped of maternal decidua, Reichart's membrane and ectoplacental cone. For flow cytometry (FCM) and qPCR analysis and cell sorting, cells from E7.5-E8.5 dissected embryos were pooled from one litter. E9.5-12.5 embryos were separated from extraembryonic membranes (YS and amnion), and single embryos were analyzed unless stated otherwise. Embryos were washed in Hank's balanced saline solution (HBSS) and dissociated using 1 mg/ml dispase (Invitrogen) in HBSS for 10 min at 37 °C with occasional gentle pipetting. The reaction was stopped by washing in 2% FCS in HBSS. Embryonic suspensions were then passed through a 50-µm cell strainer. Peripheral blood of adult animals was collected from the facial vein into PBS EDTA solution, and red blood cells were lysed in ACK solution.

Flow cytometry and cell sorting. After Fc receptor blocking (in experiments where FcRγ was not stained) by rat anti mouse FcRγ antibody (2.4G2; Biolegend), single-cell suspensions were stained with conjugated monoclonal antibodies for 30 min on ice. Where appropriate, cells were further incubated with streptavidin conjugates for 20 min. The full list of antibodies and secondary reagents used can be found in the reporting summary. Fluorescence data were acquired using LSRII flow cytometer (BD Biosciences). FCM analysis was performed using FlowJo software (FlowJo, LCC). Cell debris and dead cells were excluded from the analysis based on scatter signals and viability dye fluorescence (Hoechst 33258 (Sigma-Aldrich), Sytox-blue, Fixable viability dye eFluor780 (Thermo Fisher Scientific)). Cell sorting was performed with an Influx cell sorter (BD Biosciences). For t-SNE and hierarchical clustering analysis, raw or pre-gated FCS3.0 files were exported from acquisition software and imported into R environment where all subsequent analyses were carried out[51].

t-SNE. For dimensionality reduction and subsequent population choices across all measured parameters, we used Barnes-Hut implementation of t-Distributed Stochastic Neighbour Embedding (t-SNE)[52]. In Fig. S1H, a tSNE map was built using a tSNE plugin in FlowJo software (FlowJo, LCC).

Hierarchical clustering analysis for flow cytometry. Agglomerative unsupervised Hierarchical clustering analysis (HCA) was performed using Mahalanobis distance measure and Mahalanobis-based custom linkage[53]. From the resulting hierarchy, the clusters (cell populations) were selected based on dendrogram topology and a matrix of parameters scatterplots.

Gene expression analysis. The total RNA from whole embryos or sorted cells was isolated using a RNeasy Plus Micro Kit (Qiagen) and was reverse transcribed using Premium RevertAid (Fermentas) and random hexamers (Fermentas). Quantitative RT-PCR (qPCR) was performed using the LightCycler 480 SYBR Green I Master mix on a LightCycler 480 instrument (Roche). Each sample was tested in triplicate. The relative amounts of mRNA were calculated using LightCycler 480 1.5 software with *Casc3* or *Gapdh* mRNA levels as a reference gene. Primers were designed using UPL software (Roche). Intron-spanning assays were used when possible. Primer efficiencies were calculated using LightCycler 480 1.5 software. Primer sequences are listed in Supplementary Table 1. Data were analyzed using Prism 5.03 software (GraphPad). The expression level of different *Tlrs* and their adaptors highlighted in Supplementary Fig. 1a precluded the effect of primer efficiency factor.

Tracking cells of maternal and embryonic origin. To follow the cells of embryonic origin, we crossed wt CD1 females with *Actb^EGFP* males. Only EGFP+ embryos were included in subsequent analysis. Due to paternal inheritance, all *Actb^EGFP* cells were considered to be of embryonic origin (Supplementary Fig. 1b, left panel). To follow maternal cells, *Actb^EGFP/wt* females were crossed with wt CD1 males. Maternally derived *Actb^EGFP* cells were analyzed in wt embryos that did not inherit the maternal EGFP allele (~50%) (Supplementary Fig. 1b, right panel).

50

In vitro assays. Distinct subpopulations of E7.5 or E8.5 embryonic $Actb^{EGFP+}$ cells were sorted based on their TLR2, c-kit, and CD45 surface expression, plated on a semi-confluent layer of OP-9 cells[54] (gift from J.C. Zuniga-Pflucker) or ST-2 cells[55] (gift from L. Klein) and cultured in RPMI containing 5% PCS (Sigma-Aldrich). E7.5 sorted cells were supplemented with recombinant cytokines IL-3 (1 ng/ml), SCF (50 ng/ml) GM-CSP (3 ng/ml), and M-CSP (10 ng/ml) (Biolegend). A thousand cells from each E8.5 sorted $Actb^{EGFP+}$ population labeled with Cell Proliferation Dye eFluor® 670 (eBioscience) were co-cultured with OP-9 cells in the presence or absence of 1 μg/ml Pam_3CSK_4 (Invivogen) for 72 h. The total number of surviving $Actb^{EGFP+}$ cells were normalized to 10,000 events obtained by FCM analysis. E8.5 $Tlr2^{Cre}EYFP^+$ Lin$^-$ cells were sorted, stained with Cell Proliferation Dye eFluor® 670 (eBioscience) and cultured in the presence or absence of Pam_3CSK_4 (1 μg/ml) on ST-2 stroma. The proliferation history of embryonic cells was determined by the dilution of Cell Proliferation Dye® eFluor 670 according to the manufacturer's instructions.

Colony-forming cell assay. Sorted E7.5 or E8.5 cells were plated on methylcellulose medium M3434 GF (Stem Cell Technologies) according to the manufacturer's instructions. Cultures were maintained at 37 °C in humidified air with 5% CO_2. Hematopoietic colonies were scored at days 5 and 12. For EryP clonogenic assays, M3434 was supplemented with 3U/ml erythropoietin and 10% PCS. Microscopic images were acquired using Nikon Diaphot 300 equipped with $10\times$/ 0.25 or Plan $20\times$/0.4 objectives.

Single-colony qPCR. Individual erythroid colonies were imaged and individually transferred to 5 μl of lysis buffer (0.1 % BSA in RNAse free water supplemented with RNAse inhibitors) and instantly frozen on dry ice. Cell lysate was then used for reverse transcription (Superscript III RT, Thermo Fisher Scientific). qPCR was performed using the LightCycler 480 SYBR Green I Master mix in a LightCycler 480 instrument (Roche).

Whole embryo ex vivo imaging. $Tlr2^{Cre}EYFP^+$ cells in E8.5-E10.5 $Rosa26^{EYFP}Tlr2^{Cre}$ embryos were imaged with a Nikon AZ-100 confocal microscope equipped with a $\times4$ objective. Images of E7.5 $Actb^{EGFP}$ embryos and E11.5 $Tlr2^{wt}Rosa26^{DTA}$ and $Tlr2^{Cre}Rosa26^{DTA}$ embryos were acquired using a Olympus SZX9 StereoZoom microscope equipped with a DF PLAPO 1xPF objective and a DP72 digital camera.

Whole mount embryo immunohistochemistry and imaging. E7.5 embryos were dissected from decidua, washed several times in ice-cold PBS, fixed overnight in PHEM fixative (80 mM PIPES, 5 mM EGTA, 1 mM $MgCl_2$, 25 mM HEPES at pH of 7.2, 3.7% formaldehyde, purified 0.1% Triton X-100) at 4 °C, and then rinsed three times in PBS. Embryos were blocked in PBS supplemented with 10% goat serum for 1 h. The primary antibody, purified rat anti-mouse TLR2 (clone 6C2, eBioscience) was added at a final concentration of 5 μg/ml for overnight at 4 °C and developed with the secondary goat anti-rat IgG labeled with Alexa 488. The isotype control antibody produced no specific staining. Embryos were then embedded with Vectashield mounting medium with 4′,6-diamino-2-phentlindole (DAPI) (Vector Laboratories) and prepared for scanning. Signals were visualized and digital images were obtained using a Zeiss LSM 780 equipped with two photon, argon and helium–neon lasers. For 3D image, individual confocal planes (25–30 planes in 1–2 μm intervals) were projected to generate a single stacked 3D-reconstructed image using Imaris 7.3 (Bitplane).

Preparation of aortic regions for imaging and FCM analysis. Caudal parts of E10.5 embryos including somites were cut between forelimbs and hindlimbs. These parts and the aortae were gently flushed with HBSS using a syringe to remove blood cells. Aortic regions were either washed and fixed in 3.7% PFA in PBS for subsequent imaging or digested with dispase for FCM analysis.

Immunofluorescence of embryonic sections and imaging. Embryos were fixed with 3.7% PFA in PBS overnight at 4 °C, washed in PBS, transferred to 30% sucrose and mounted in OCT for freezing and sectioning. Sections (8–10-μm thick) were postfixed in 3.7% PFA in PBS, permeabilized in methanol for 10 min at −20 °C (except for phalloidin staining), then blocked in 5% BSA in 1% BSA 0.1% Triton-X100 (PBT) and stained with antibodies in 1% BSA PBT. The complete list of antibodies and secondary reagents used can be found in the NR reporting summary. The coverslips were mounted using Vectashield containing DAPI (Vector Laboratories). Sections were imaged with Leica DM6000 epifluorescence microscope equiped with HCX PL APO 10.0×0.40, HCX PL APO 20×0.7 and HCX PL APO 40×0.75 objectives or with a Dragonfly 503 spinning disc confocal microscope and/or equipped with a HC PL APO $20\times$/ 0.75 IMM objective.

Continuous labeling of *Tlr2* progenitors. For fate-mapping analysis of *Tlr2* precursors, $Rosa26^{EYFP}$ or $Rosa26^{tdTomato}$ females were crossed with $Tlr2^{Cre}$ males. The indicated tissues from embryos and adult P1 mice were analyzed by PCM and imunofluorescence.

Pulse labeling of *Tlr2* progenitors. For genetic cell labeling of embryonic cells, we crossed $Rosa26^{EYFP}$ reporter mice with tamoxifen-inducible $Tlr2^{CreERT2}$ mice. Recombination was induced by a single i.p. injection of 1.5 mg 4-hydroxytamoxifen (4-OHT; H6278; Sigma) into pregnant females from E6.75 to E10.5. When 4-OHT was administered after E9.5, the delivery was assisted by C-section at E20.5 and pups were transferred to foster mothers.

Embryonic lethality assay. $Rosa26^{DTA/DTA}$ females were crossed with $Tlr2^{Cre/wt}$ males to obtain litters with equal numbers of wt ($Tlr2^{wt/wt}Rosa26^{DTA/wt}$) and tg ($Tlr2^{Cre/wt}Rosa26^{DTA/wt}$) genotypes, if no lethality occurs. Litters were scored for phenotype (normal growth, growth retardation, resorbtions) from E9.5 to E13.5.

Analysis of embryonic peripheral blood. E11.5- E12.5 embryos were carefully removed from decidua and placenta, and washed three times in PBS. Upon placing intact embryos in individual wells containg 0.02% EDTA in PBS, umbilical vessels were cut and embryos were bled out. Cell suspensions were collected and spun for subsequent analyses (counting and PCM analysis).

May Grunwald Giemsa staining of frozen sections and blood smears. In total, 8-μm thin cryosections prepared from E12.5 FLs, and smears from PB were stained with May Grunwald Giemsa (MGG) stain (Diapath) according to the manufacturer's intructions and imaged with a Leica DM6000 microscope equipped with a 40x objective. Images were processed in ImageJ.

Transplantation of *Tlr2*-labeled BM cells into lethally irradiated mice. $Rosa26^{EYFP}Tlr2^{CreERT2}$ embryos were pulsed with 4-OHT at E8.5. After 16 weeks, lineage-depleted BM (CD45.2) was transferred to lethally irradiated (2×7.5 Gy delivered by orthovoltage X-ray instrument T-200; Wolf-Medizintechnik) recipients (CD45.1/2) along with support (0.5×10^6 CD45.1) BM cells. Recipient mice were maintained on antibiotic water (gentamycin, 1 mg/ml) for 10 days. Sixteen weeks after primary cell transfer, BM was isolated and after lineage depletion, $Tlr2$EYFP$^+$ cells were sorted and transferred to secondary lethally irradiated recipients (CD45.1/2) along with support (0.5×10^6 CD45.1) BM cells. The percentage of EYFP labeled cells and their contribution to CD45$^+$ hematopoietic lineages in different organs was determined 16 weeks after induction or BM transfer, respectively.

Whole-body imaging. The total fluorescence of tdTomato in adult $Rosa26^{tdTomato}$ $Tlr2^{Cre}$ animals was acquired by Xtreme whole body imager (Bruker). Fluorescence spectra of excitation wavelengths from 420 nm to 540 nm with 580–629 nm emission filter were measured. Multispectral analyzer software (Bruker) was used to distinguish non-specific body autofluorescence from the specific tdTomato signal.

Quantification and statistical analysis. Data was statistically analyzed using Prism 5.03 software (GraphPad). The statistical tests used are indicated in the corresponding Figure legends.

Reporting summary. Further information on research design is available in the Nature Research Reporting Summary linked to this article.

Data availability

The authors declare that all data supporting the findings of this study are available within the article and its supplementary information files or from the corresponding author upon reasonable request. The source data underlying Figs. 1, 3, 4, 5, 6 and 7, as well as Supplementary Figs. 1, 2, 3, 3e – heatmap, 4, 5 and 6 are provided as a Source Data file.

References

1. Tober, J. et al. The megakaryocyte lineage originates from hemangioblast precursors and is an integral component both of primitive and of definitive hematopoiesis. *Blood* **109**, 1433–1441 (2007).
2. Xu, M.-j et al. Evidence for the presence of murine primitive megakarycytopoiesis in the early yolk sac. *Blood* **97**, 2016–2022 (2001).
3. Ferkowicz, M. J. et al. CD41 expression defines the onset of primitive and definitive hematopoiesis in the murine embryo. *Development* **130**, 4393–4403 (2003).
4. Palis, J., Robertson, S., Kennedy, M., Wall, C. & Keller, G. Development of erythroid and myeloid progenitors in the yolk sac and embryo proper of the mouse. *Development* **126**, 5073–5084 (1999).

51

5. Bertrand, J. Y. et al. Three pathways to mature macrophages in the early mouse yolk sac. *Blood* **106**, 3004–3011 (2005).
6. McGrath, K. E. et al. Distinct sources of hematopoietic progenitors emerge before HSCs and provide functional blood cells in the mammalian embryo. *Cell Rep.* **11**, 1892–1904 (2015).
7. Boiers, C. et al. Lymphomyeloid contribution of an immune-restricted progenitor emerging prior to definitive hematopoietic stem cells. *Cell Stem Cell* **13**, 535–548 (2013).
8. Frame, J. M., Fegan, K. H., Conway, S. J., McGrath, K. E. & Palis, J. Definitive hematopoiesis in the yolk sac emerges from wnt-responsive hemogenic endothelium independently of circulation and arterial identity. *Stem Cells* **34**, 431–444 (2016).
9. Muller, A. M., Medvinsky, A., Strouboulis, J., Grosveld, F. & Dzierzakt, E. Development of hematopoietic stem cell activity in the mouse embryo. *Immunity* **1**, 291–301 (1994).
10. Taoudi, S. & Medvinsky, A. Functional identification of the hematopoietic stem cell niche in the ventral domain of the embryonic dorsal aorta. *Proc. Natl Acad. Sci. USA* **104**, 9399–9403 (2007).
11. Dzierzak, E. & Speck, N. A. Of lineage and legacy: the development of mammalian hematopoietic stem cells. *Nat. Immunol.* **9**, 129–136 (2008).
12. Kumaravelu, P. et al. Quantitative developmental anatomy of definitive haematopoietic stem cells/long-term repopulating units (HSC/RUs): role of the aorta-gonad-mesonephros (AGM) region and the yolk sac in colonisation of the mouse embryonic liver. *Development* **129**, 4891–4899 (2002).
13. Ema, H. & Nakauchi, H. Expansion of hematopoietic stem cells in the developing liver of a mouse embryo. *Blood* **95**, 2284–2288 (2000).
14. Christensen, J. L., Wright, D. E., Wagers, A. J. & Weissman, I. L. Circulation and chemotaxis of fetal hematopoietic stem cells. *PLoS Biol.* **2**, E75 (2004).
15. Chen, M. J., Yokomizo, T., Zeigler, B. M., Dzierzak, E. & Speck, N. A. Runx1 is required for the endothelial to haematopoietic cell transition but not thereafter. *Nature* **457**, 887–891 (2009).
16. Lancrin, C. et al. The haemangioblast generates haematopoietic cells through a haemogenic endothelium stage. *Nature* **457**, 892–895 (2009).
17. Chen, M. J. et al. Erythroid/myeloid progenitors and hematopoietic stem cells originate from distinct populations of endothelial cells. *Cell Stem Cell* **9**, 541–552 (2011).
18. Gomez Perdiguero, E. & Geissmann, F. Development and maintainance of resident macrophages. *Nat. Immunol.* **17**, 2–8 (2016).
19. Okuda, T., van Deursen, J., Hiebert, S. W., Grosveld, G. & Downing, J. R. AML1, the target of multiple chromosomal translocations in human leukemia, is essential for normal fetal liver hematopoiesis. *Cell* **84**, 321–330 (1996).
20. Yokomizo, T. et al. Requirement of Runx1/AML1/PEBP2αB for the generation of haematopoietic cells from endothelial cells. *Genes Cells* **6**, 13–23 (2001).
21. Lugus, J. J., Park, C., Ma, Y. D. & Choi, K. Both primitive and definitive blood cells are derived from Flk-1+ mesoderm. *Blood* **113**, 563–566 (2009).
22. Gomez Perdiguero, E. et al. Tissue-resident macrophages originate from yolk-sac-derived erythro-myeloid progenitors. *Nature* **518**, 547–551 (2015).
23. Ginhoux, F. et al. Fate mapping analysis reveals that adult microglia derive from primitive macrophages. *Science* **330**, 841–845 (2010).
24. Sheng, J., Ruedl, C. & Karjalainen, K. Most tissue-resident macrophages except microglia are derived from fetal hematopoietic stem cells. *Immunity* **43**, 382–393 (2015).
25. Akira, S., Takeda, K. & Kaisho, T. Toll-like receptors: critical proteins linking innate and acquired immunity. *Nat. Immunol.* **2**, 675–680 (2001).
26. Medzhitov, R. Recognition of microorganisms and activation of the immune response. *Nature* **449**, 819–826 (2007).
27. De Luca, K. et al. The TLR1/2 agonist PAM3CSK4 instructs commitment of human hematopoietic stem cells to a myeloid cell fate. *Leukemia* **23**, 2063–2074 (2009).
28. Megias, J. et al. Direct Toll-like receptor-mediated stimulation of hematopoietic stem and progenitor cells occurs in vivo and promotes differentiation toward macrophages. *Stem Cells* **30**, 1486–1495 (2012).
29. Nagai, Y. et al. Toll-like receptors on hematopoietic progenitor cells stimulate innate immune system replenishment. *Immunity* **24**, 801–812 (2006).
30. Harju, K., Glumoff, V. & Hallman, M. Ontogeny of Toll-like receptors Tlr2 and Tlr4 in Mice. *Pediatr. Res* **49**, 81–83 (2001).
31. Kaul, D. et al. Expression of Toll-like receptors in the developing brain. *PLoS ONE* **7**, e37767 (2012).
32. Li, Y. et al. Inflammatory signaling regulates embryonic hematopoietic stem and progenitor cell production. *Genes Dev.* **28**, 2597–2612 (2014).
33. Balounova, J. et al. Toll-like receptors expressed on embryonic macrophages couple inflammatory signals to iron metabolism during early ontogenesis. *Eur. J. Immunol.* **44**, 1491–1502 (2014).
34. Pevny, L. et al. Development of hematopoietic cells lacking transcription factor GATA-1. *Development* **121**, 163–172 (1995).
35. Lux, C. T. et al. All primitive and definitive hematopoietic progenitor cells emerging before E10 in the mouse embryo are products of the yolk sac. *Blood* **111**, 3435–3438 (2008).
36. Azzoni, E. et al. Kit ligand has a critical role in mouse yolk sac and aorta-gonad-mesonephros hematopoiesis. *EMBO Rep.* **19**, e45477 (2018).
37. Boisset, J. C. et al. In vivo imaging of haematopoietic cells emerging from the mouse aortic endothelium. *Nature* **464**, 116–120 (2010).
38. Zhou, F. et al. Tracing haematopoietic stem cell formation at single-cell resolution. *Nature* **533**, 487–492 (2016).
39. Scialdone, A. et al. Resolving early mesoderm diversification through single-cell expression profiling. *Nature* **535**, 289 (2016).
40. Kierdorf, K., Prinz, M., Geissmann, F. & Gomez Perdiguero, E. Development and function of tissue resident macrophages in mice. *Semin. Immunol.* **27**, 369–378 (2015).
41. Hoeffel, G. et al. C-Myb(+) erythro-myeloid progenitor-derived fetal monocytes give rise to adult tissue-resident macrophages. *Immunity* **42**, 665–678 (2015).
42. Stremmel, C. et al. Yolk sac macrophage progenitors traffic to the embryo during defined stages of development. *Nat. Commun.* **9**, 75 (2018).
43. Adachi, O. et al. Targeted disruption of the MyD88 gene results in loss of IL-1- and IL-18-mediated function. *Immunity* **9**, 143–150 (1998).
44. Takeuchi, O. et al. Differential roles of TLR2 and TLR4 in recognition of gram-negative and gram-positive bacterial cell wall components. *Immunity* **11**, 443–451 (1999).
45. McKinney-Freeman, S. et al. The transcriptional landscape of hematopoietic stem cell ontogeny. *Cell Stem Cell* **11**, 701–714 (2012).
46. Espin-Palazon, R. et al. Proinflammatory signaling regulates hematopoietic stem cell emergence. *Cell* **159**, 1070–1085 (2014).
47. Sawamiphak, S., Kontarakis, Z. & Stainier, D. Y. Interferon gamma signaling positively regulates hematopoietic stem cell emergence. *Developmental cell* **31**, 640–653 (2014).
48. Nejepinska, J. et al. dsRNA expression in the mouse elicits RNAi in oocytes and low adenosine deamination in somatic cells. *Nucleic Acids Res.* **40**, 399–413 (2012).
49. Sharan, S. K., Thomason, L. C., Kuznetsov, S. G. & Court, D. L. Recombineering: a homologous recombination-based method of genetic engineering. *Nat. Protoc.* **4**, 206–223 (2009).
50. Downs, K. M. & Davies, T. Staging of gastrulating mouse embryos by morphological landmarks in the dissecting microscope. *Development* **118**, 1255–1266 (1993).
51. Team, R. D. C. R.: *A Language and Environment for Statistical Computing.* the R Foundation for Statistical Computing (2011).
52. van der Maaten, L. & Hinton, G. Visualizing Data using t-SNE. *J. Mach. Learn. Res.* **9**, 2579–2605 (2008).
53. Fiser, K. et al. Detection and monitoring of normal and leukemic cell populations with hierarchical clustering of flow cytometry data. *Cytom. Part A: J. Int. Soc. Anal. Cytol.* **81**, 25–34 (2012).
54. Nakano, T., Kodama, H. & Honjo, T. Generation of lymphohematopoietic cells from embryonic stem cells in culture. *Science* **265**, 1098–1101 (1994).
55. Ogawa, M. et al. B cell ontogeny in murine embryo studied by a culture system with the monolayer of a stromal cell clone, ST2: B cell progenitor develops first in the embryonal body rather than in the yolk sac. *EMBO* **7**, 1337–1343 (1988).

Author contributions

D.F. and J.B. designed and supervised the experiments, wrote the paper. J.B., LS., and M. D. performed experiments. M.K. and K.F. performed bioinformatic analyses. V.K. provided reporter mouse strains and Cre^{ERT2} cassette, and M.A.J. supervised the BM transfer experiments. J.P. performed whole body imaging. J.B. and R.S. generated mouse *Tlr2*-transgenic models. LG. designed and supervised colony assay and adviced on multiple experiments. A.J and H.S. performed two-photon microscopy imaging.

52

Competing interests

The authors declare no competing interests.

Additional information

Supplementary Information accompanies this paper at https://doi.org/10.1038/s41467-019-13150-0.

Correspondence and requests for materials should be addressed to D.F.

Peer review information *Nature Communications* thanks the anonymous reviewers for their contribution to the peer review of this work Peer reviewer reports are available.

Reprints and permission information is available at http://www.nature.com/reprints

Publisher's note Springer Nature remains neutral with regard to jurisdictional claims in published maps and institutional affiliations.

53

3.2. DELETION OF TLR2$^+$ ERYTHRO-MYELOID PROGENITORS LEADS TO EMBRYONIC LETHALITY

Early embryonic hematopoiesis in mammals is defined by three successive waves of hematopoietic progenitors which exhibit a distinct hematopoietic potential and provide continuous support for the development of the embryo and adult organism. Although the functional importance each of these waves has been analyzed, their spatio-temporal overlap and the lack of wave-specific markers hinders the accurate separation and assessment of their functional roles during early embryogenesis. We have recently shown that TLR2, in combination with c-kit, represents the earliest signature of emerging precursors of the second wave, erythro-myeloid precursors (EMPs). Since the onset of *Tlr2* expression distinguishes EMPs from primitive progenitors which coexist in the yolk sac from E7.5, we generated a novel transgenic "knock in" mouse model suitable for inducible targeted depletion of TLR2$^+$ EMPs. In this model, the red fluorescent protein and diphtheria toxin receptor sequences are linked via a P2A sequence and inserted into the *Tlr2* locus before its stop codon. Using this model, we show that a timely-controlled deletion of TLR2$^+$ EMPs results in a marked decrease in both erythroid as well as myeloid lineages and, consequently, in embryonic lethality at E12.5. These findings validate the importance of EMPs in embryonic development.

3.2.1. INTRODUCTION

During ontogenesis, three timely-defined waves of progenitors appear in several anatomical locations of the mouse conceptus (McGrath et al., 2015; Palis, 2014; Silver and Palis, 1997). The first, the transient wave, appears at embryonic day (E) 7.25 in the blood islands of the yolk sac (YS) (Ferkowicz et al., 2003). These monopotent progenitors give rise to primitive nucleated erythrocytes and megakaryocytes (Palis et al., 1999; Tober et al., 2007). Studies performed on zebrafish and mice suggest that progenitors of the first hematopoietic wave can also give rise to monopotent macrophages (Bertrand et al., 2005; Herbomel et al., 1999). The second wave starts around E8.5 and gives rise to Erythro-Myeloid progenitors (EMPs) (Epelman et al., 2014; Chen et al., 2011; Perdiguero et al., 2015). These progenitors originate from the cells of the hemogenic endothelium in the YS which undergo the process denoted as endothelial to hematopoietic transition (EHT) (Chen et al., 2011). EMPs downregulate endothelial markers such as *Tie2* and *Cd31* during EHT, with concomitant upregulation of the markers of hematopoietic lineages, and are phenotypically defined as c-kit$^+$ CD41$^+$ and FcRγ^+ (McGrath et al., 2015). The distinctive feature of EMPs is their capacity to give rise not only to myeloid, erythroid, and megakaryocyte colonies but also to mixed erythro-myeloid colonies in a clonogenic assay (Perdiguero et al., 2015). Upon establishment of blood circulation at ~E8.5, EMPs migrate to the embryo proper (EP) via the blood stream and colonize the fetal liver (FL) (Lux et al., 2008; Stremmel et al., 2018). Here, they expand and differentiate to definitive erythroid cells (EryD) and F4/80^{low} CD11b$^+$ myeloid cells (Chen et al., 2011; McGrath et al., 2015) or, alternatively, migrate directly to other tissues where they differentiate to F4/80^{high} CD11b$^+$ tissue-resident macrophages (14, 15). These tissue resident macrophages are necessary for proper embryonic development (Munoz-Espin et al., 2013; Paolicelli et al., 2011; Yosef et al., 2018) and can potentially persist in the tissue throughout the life of an organism (Hoeffel et al., 2015; Schulz et al., 2012). Hence, the progenitors of the second wave are also referred to as embryonic definitive hematopoietic progenitors. The third hematopoietic wave is established around E9.5-10.5 in the Aorta-Gonad Mesonephros region (AGM) (Medvinsky and Dzierzak, 1996; Yokomizo and

Dzierzak, 2010) where hematopoietic cell clusters transiently emerge from the hemogenic endothelium to generate the first adult-type hematopoietic stem cells (HSCs). HSCs then migrate to the FL which serves as a niche for their expansion (Ema and Nakauchi, 2000; Kumaravelu et al., 2002). Shortly before birth, HSCs seed the BM where they generate cells of all hematopoietic lineages throughout an adult's life (Mendelson and Frenette, 2014).

Importantly, identification of genes controlling the development and production of early hematopoietic progenitors has provided tools for the study of the physiological role of each of the three hematopoietic waves. Specifically, the genetic disruption of transcription factors (TFs) which are important for primitive erythrocytes such as *Gata-1*, *Gata-2*, *Lmo2* or *Scl* in combination with *Lyl1* caused early embryonic lethality around E10.5 (Fujiwara et al., 1996; Chiu et al., 2018; Tsai et al., 1994). Similarly, the disruption of HSC development driven by the c-kit ligand, *kitl*, and the epigenetic regulator *Uhrf1* resulted in lethality during the perinatal period (Ding et al., 2012; Zhao et al., 2017). On the other hand, a specific disruption of EMP wave turned out to be more problematic. It has been shown that the abrogation of *c-myb*, tyrosine kinase *c-Kit* or *Runx1* TF signaling, all of which are important for the emergence of EMPs and their survival in FL, led to severe anemia and embryonic lethality from E12.5 to E15.5 (Azzoni et al., 2018; Ding et al., 2012; Chen et al., 2011; Mucenski et al., 1991). However, a spatio-temporal overlap in the expression of these genes within the other two hematopoietic waves or their more restricted role in determining the development of certain lineages, makes the attribution of embryonic lethality solely to EMPs somewhat ambiguous (Ginhoux et al., 2010; Gomez Perdiguero et al., 2015; Sheng et al., 2015).

We recently reported that fully functional Toll-like receptors (TLRs) are expressed not only on mature E10.5 embryonic YS-derived macrophages (Balounova et al., 2014) but also on the earliest precursors of EMPs (Balounova et al., 2019). These precursors display a TLR2$^+$c-kit$^+$ phenotype and coexist in E7.5 YS with TLR2$^-$c-kit$^+$ precursors of the primitive wave. The coexpression of TLR2 on c-kit$^+$ progenitors along with TIE2, CD31, and CD41 surface markers seems to predicate

the acquisition of functional competence for their multi-lineage EMP potential (Balounova et al., 2019). Since TLR2 expression allowed the distinction between emerging EMP precursors from precursors of primitive erythropoiesis, we used the TLR2 promoter activity ($Tlr2^{Cre}$ strain) to genetically ablate TLR2$^+$ cells. The depletion of embryonic cells by Tlr^{Cre}-mediated expression of diphtheria toxin resulted in embryonic lethality before E13.5, suggesting that embryos died due to improper development of EMPs (Balounova et al., 2019). In this genetic model, $TLR2^{Cre}$-mediated ablation targeted all cells with an active $Tlr2$ locus, including those which ultimately failed to express surface TLR2, hence could be distinctly different from EMPs and their precursors. To obviate this limitation, we report here the generation of a novel knock-in mouse strain suitable for tracking and depletion of cells expressing TLR2 on the protein level. Using this animal model, we have shown that the production of EMPs and their progenies is critical for the survival of the embryos before the establishment of definitive adult hematopoiesis.

3.2.2. RESULTS

3.2.2.1. PHENOTYPIC EMPs EXPRESS TLR2

A recent report suggested that at E8.5, the emergence of EMPs can be monitored by their expression of CD16/32 and CD41 surface markers which predict their differentiation to the erythroid as well as myeloid lineages (McGrath et al., 2015). Indeed, we found that c-kit$^+$ CD16/32$^+$ CD41$^+$ EMPs (Supplementary Fig. 1) first appeared at low frequencies in the YS at E8.5 and dramatically increased in numbers by E9.5. Importantly, these phenotypical EMPs together with the above markers also coexpressed surface TLR2 (Fig. 1A). Consistent with the notion that EMPs originate in the YS and subsequently colonize the embryo via circulation, we first detected TLR2$^+$ EMPs in the embryo proper (EP) at E9.5 (Fig. 1A and B). To confirm the functional competence of these EMPs in terms of their capacity to produce mixed hematopoietic colonies (Chen et al., 2011; McGrath et al., 2015), we sorted Ter119$^-$ c-kit$^+$ CD16/32$^+$ CD41$^+$ TLR2$^+$ cells from the E8.5 YS and performed a clonogenic assay. At day seven of cultivation, we observed mixed

colonies each containing both erythroid and myeloid lineages (Fig. 1C). At day 14, once their size and cellularity increased, we validated the presence of relevant hematopoietic lineages that formed these mixed colonies (Fig. 1D). This data confirmed that TLR2 is coexpressed on phenotypical EMPs.
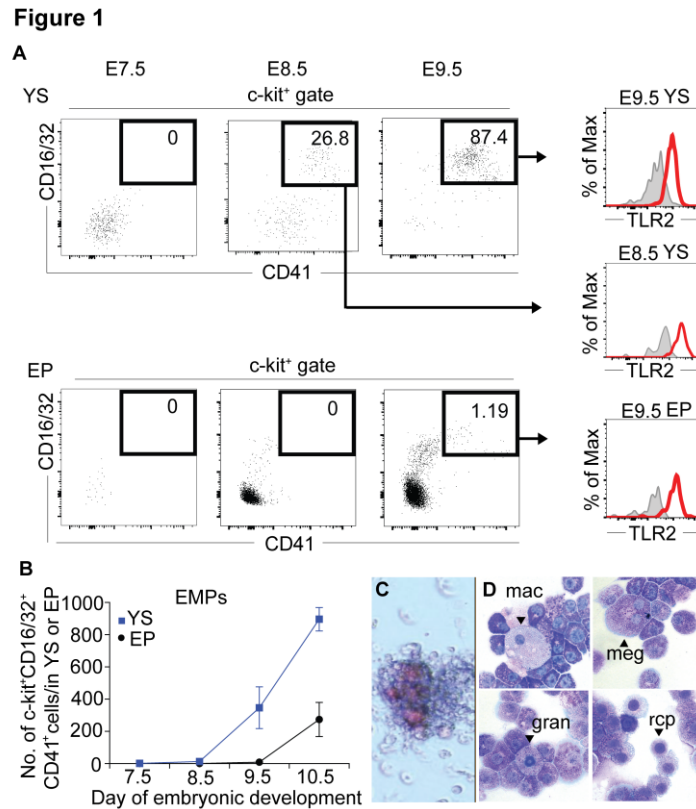

Figure 1. Erythro-myeloid progenitors express TLR2. (A) Expression of TLR2 (red histogram) is readily detectable on emerging phenotypical EMPs (Ter119⁻ c-kit⁺ CD16/32⁺ CD41⁺, black gates) at E8.5 in YS and at E9.5 in EP (grey histograms represent the FMO controls). (B) Kinetics of appearance of EMPs in the YS and EP (mean ± SEM, n=24-36 embryos per each time point). (C) Morphology of an erythro-myeloid colony derived from EMPs on day seven of CFU clonogenic assay. TLR2⁺ c-kit⁺ CD16/32⁺ CD41⁺ cells were sorted and plated for CFU assay. (D) Morphology of cells derived from EMPs at day 14 of CFU clonogenic assay showing the presence of macrophages (mac), megakaryocytes (meg), granulocytes (gran), erythroblasts (ery), and red blood cell progenitors (rcp). Cells were stained by May-Grünwald-Giemsa staining.

3.2.2.2. GENERATION OF NOVEL TRANSGENIT MOUSE MODEL SUITABLE FOR DEPLETION OF TLR2$^+$ CELLS

To visualize the emergence of cells expressing TLR2 at the protein level and to investigate the effect of their deletion during embryonic development, we generated a novel *Tlr2* knock-in reporter mouse model which also allows for the inducible elimination of TLR2$^+$ cells which we refer to as the *Tlr2^{Dtr}* mouse model. In this model, the red fluorescent protein (RFP) and diphtheria toxin receptor (DTR) sequences were linked via a P2A sequence and inserted into the *Tlr2* locus before its stop codon using CRISPR/Cas9 technology (Fig. 2A, see Experimental procedures for details). The expression of DTR and RFP transgenes was first confirmed in adult bone marrow (BM) and BM-derived dendritic cells (Supplementary fig. 2A and B). Similarly, as illustrated in Fig. 2B, the expression of RFP in adult peritoneal macrophages was readily detectable. The functionality of the DTR cassette was tested by the intraperitoneal (i.p.) administration of diphtheria toxin (DT) which is transported to the interior of cells by DTR, resulting in cell death by the inhibition of protein synthesis (Collier, 2001). In the peritoneum, a majority of TLR2$^+$ cells also coexpressed the macrophage marker F4/80 (Supplementary fig. 2C). 24 hours upon administration of DT, we observed the complete absence of the F4/80$^+$ macrophage compartment in the peritoneum (Fig. 2D and E) and liver (Supplementary fig. 2D). In contrast to adult cells, the fluorescence intensity of RFP on embryonic TLR2$^+$ cells in *Tlr2^{Dtr}* embryos was weaker but reproducible (Fig. 2C). Unfortunately, such a dim signal was insufficient to microscopically visualize and map their emergence during the earliest embryonic hematopoietic development. Thus, in the following experiments, we took advantage of the sensitivity of the DTR system for TLR2$^+$ cell-specific deletion in the early embryo to determine the importance of the EMP wave in embryonic development.
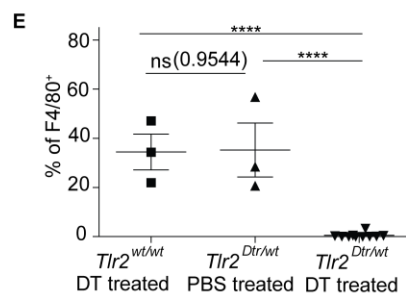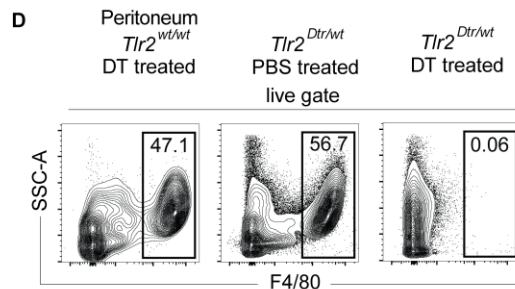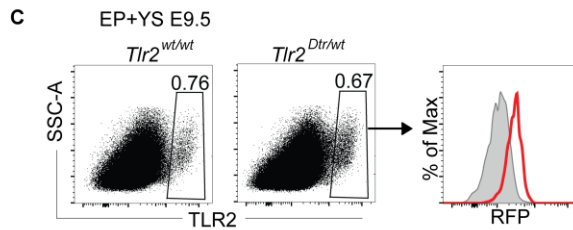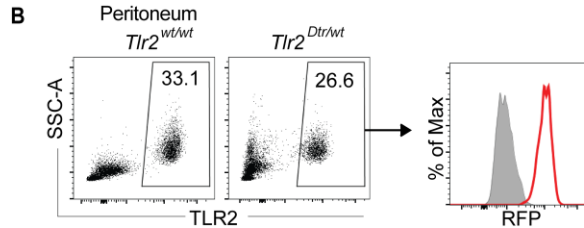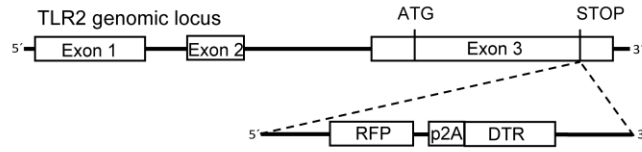
Figure 2

A   Scheme of construct

Figure 2. Generation of novel Tlr2^{Dtr} mouse model suitable for the depletion of TLR2^{+} cells. *(A) Scheme of the construct used for the generation of Tlr2^{Dtr} transgenic mouse strain. RFP p2A-DTR (Red fluorescent protein–p2A–Diphtheria toxin receptor) sequence was inserted before the stop codon of the Tlr2 gene. 23-nt sequence containing the stop codon was chosen as the CRISPR target. (B and C) Representative comparative analysis of RFP fluorescence intensity between TLR2^{+}*

*cells isolated by peritoneal lavage of 6-week old Tlr2^{wt/wt} mice (grey histogram) versus Tlr^{Dtr/wt} (red histogram) (B) and TLR2^+ cells isolated from Tlr2^{wt/wt} (grey histogram) and Tlr^{Dtr/wt} (red histogram) E9.5 embryos (pooled YS and EP) (C). (D) DT-mediated removal of TLR2 expressing F4/80^+ macrophages from the peritoneal cavity in 6-week old Tlr2^{Dtr/wt} mice. DT-treated Tlr2^{wt/wt} and PBS-treated Tlr2^{Dtr/wt} adult mice served as controls. (E) Statistical analysis in D was performed by unpaired two-tailed Student's t-test, ****p≤0.0001, mean ± SEM, n=3 for each of the control settings and n=10 for DT-treated Tlr^{Dtr/wt} condition).*

3.2.2.3. ABLATION OF TLR2^+ CELLS LEADS TO THE REDUCTION OF EMP NUMBERS

First, we assessed whether the depletion of TLR2^+ cells altered the frequency of emerging EMPs in early embryos. For this purpose, *Tlr2^{wt/wt}* females were crossed with *Tlr2^{Dtr/wt}* males to obtain *Tlr2^{Dtr/wt}* and *Tlr2^{wt/wt}* embryos in the same litter, the latter being used as controls (Fig. 3A). Time-pregnant females were i.p. double injected with DT over a 24-hour period, at E8.5 and E9.5 The embryos were then analysed 24 (at E10.5) and 48 hours later (at E11.5) (Fig. 3B). Flow cytometric analyses of TLR2^+ cells from E10.5 YS samples showed a significant depletion of EMPs from *Tlr2^{Dtr/wt}* compared to *Tlr2^{wt/wt}* controls (Fig. 3C-F).

It has been shown that EMPs originate from endothelial cells of the YS which undergo EHT. To exclude the possibility that the endothelial cells themselves express TLR2 and thus are sensitive to DT treatment, we tested the integrity of the YS vascular system. Notably, after DT-mediated depletion of TLR2^+ cells, the YS tissue stained with a marker of endothelial cells, CD31, showed no apparent alteration in its cellularity and structure (Fig. 3G). This indicated that TLR2-driven DTR expression failed to occur in YS vasculature, and thus the administration of DT targeted emerging EMPs but not vascular endothelial cells from which EMPs originate.

When the liver develops, blood circulation is already established and EMPs can migrate to EP and populate the liver (Lux et al., 2008; Stremmel et al., 2018). This process starts around E8.5 and peaks at E10.5 (Stremmel et al., 2018). Therefore, we tested the prediction that the loss of EMPs in the YS translates to a decrease in EMPs counts in the FL. To this end, cell suspensions from E11.5 FL were stained for markers of EMPs and early erythroid progenitors (Azzoni et al., 2018; Balounova et al., 2019) (for a full gating strategy see Supplementary fig. 3). Importantly, FL EMPs were depleted with a similar efficiency as those in the YS. Furthermore, the decrease in EMPs was paralleled by the decrease of early erythroid progenitors (Fig. 3H-J). Together, this data showed that the TLR^{DTR} mouse model is suitable for the depletion of early emerging EMPs.
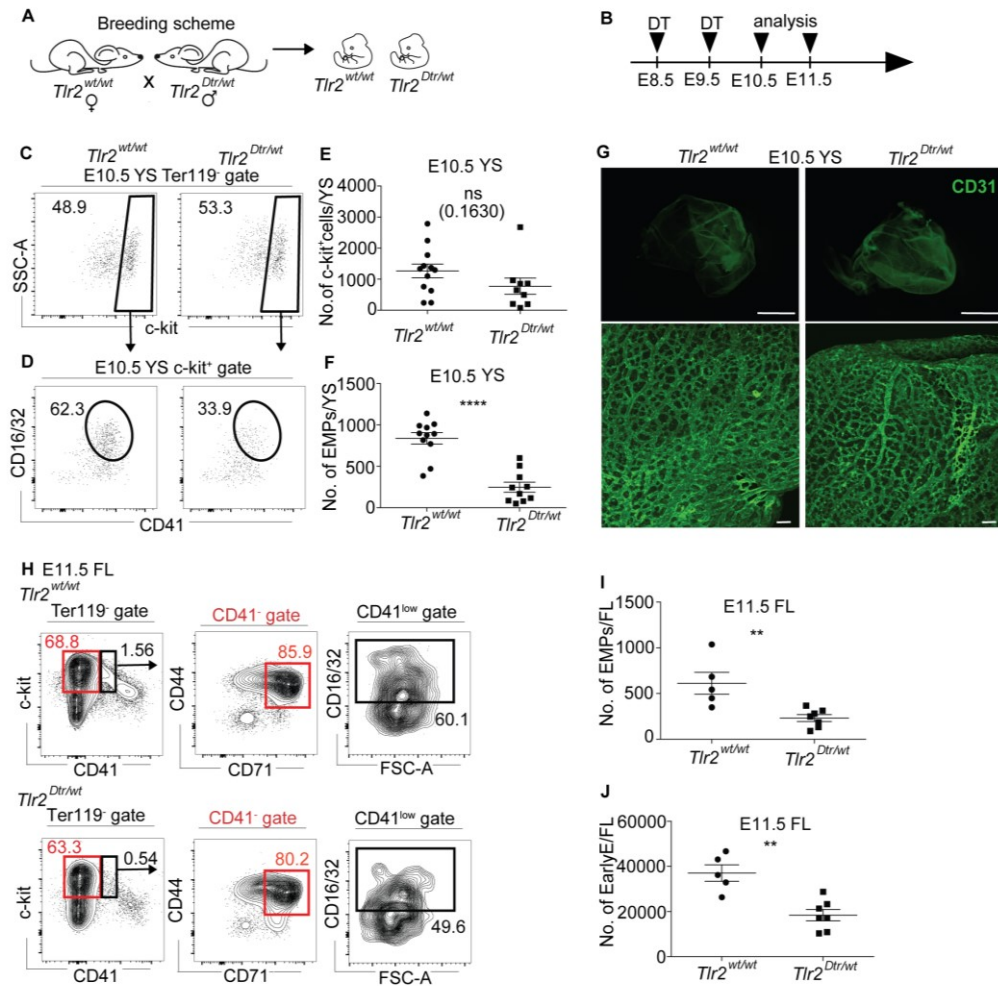
Figure 3

***Figure 3. EMPs are depleted in Tlr2^{Dtr/wt} embryos upon DT administration.** (A) Schematics of breeding of transgenic Tlr2^{Dtr/wt} male with Tlr2^{wt/wt} female. Wild-type embryos obtained in the same litter served as internal controls. (B) Timeline of the experiment. 600ng of DT was administered i.p. into time-pregnant females at E8.5 and E9.5 (DT double treatment). Embryos were analyzed at E10.5 and E11.5. (C, D) Gating strategy for the enumeration of YS-derived c-kit+ cells and phenotypic EMPs (Ter119⁻ c-kit+ CD16/32+ CD41+), respectively. (E, F) Graphs show the quantification of C and D, respectively (mean ± SEM, n=19-20 independent samples of YS for each displayed condition, ****p≤0.0001, ns = not significant, unpaired two-tailed Student's t-test. (G) YS isolated from E10.5 Tlr2^{wt/wt} and Tlr2^{Dtr/wt} DT double treated embryos (Fig.3B) were stained for CD31 and imaged (green) (upper panels, scale bar represents 500μm) with their details (lower panel, scale bar represents 50 μm). (H) Gating strategy for EMPs (black gates) and early*

erythroid progenitors (Early E) (red gate) in E11.5 fetal liver (FL). Quantification of EMP (I) and Early E (J) in E11.5 FL (shown in H) (mean ± SEM, n=5-7 independent samples of FL for each displayed condition, **p≤0.01, ns = not significant, unpaired two-tailed Student's t-test).

3.2.2.4. LOSS OF EMPs LEADS TO A DECREASE OF EMBRYONIC MACROPHAGES AND ERYTHROCYTES

EMPs serve as the source of erythroid and myeloid cells which upon differentiation and maturation from these progenitors execute important functions necessary for proper embryonic development (Epelman et al., 2014; Chen et al., 2011; Perdiguero et al., 2015; Yosef et al., 2018). Thus, using the protocol for DT administration shown in Fig. 3B, we next assessed how the targeted depletion of $TLR2^+$ cells translates to a specific decrease of mature myeloid and erythroid cells at E10.5 and E11.5 in the YS, and EP. First, we observed a significant decrease of $TLR2^+$ cells in both the YS and EP from $Tlr2^{Dtr/wt}$ compared to control $Tlr2^{wt/wt}$ embryos (Fig. 4A, B and 4F, G, respectively). This decrease was more pronounced two days after DT administration, i.e. at E11.5 (Fig. 4B and G). To assess if the loss of $TLR2^+$ cells also impacts EMP-derived mature cells, we enumerated erythroid cells which would guarantee the proper oxygenation of tissues during development. Gating on $Ter119^+$ cells, we observed no significant decrease of erythroid cells in the E10.5 YS (Fig. 4A and C). This is consistent with the fact that at this time point, all $Ter119^+$ erythrocytes represent EryP generated from the first wave of embryonic hematopoiesis and not from EMPs (Fraser et al., 2007; Kingsley et al., 2004). A similar situation was observed at E10.5 EP (Fig. 4F and H). However, at E11.5 erythroid cells were dramatically decreased in EP (Fig. 4F bottom panels and H) but not in the YS (Fig. 4A bottom panels and C). We also assessed the changes in the frequencies of $F4/80^+CD11b^+$ macrophages (for gating strategy see Supplementary fig. 4) in E10.5 and E11.5 embryos. As predicted, their decreased values in the YS and EP were readily detectable (Fig. 4D, E and 4I, J, respectively). This shows that in contrast to EryP which differentiate in the YS and blood stream,

the erythroid cells of EMP origin which expand and mature in the FL (McGrath et al., 2011) are efficiently depleted.
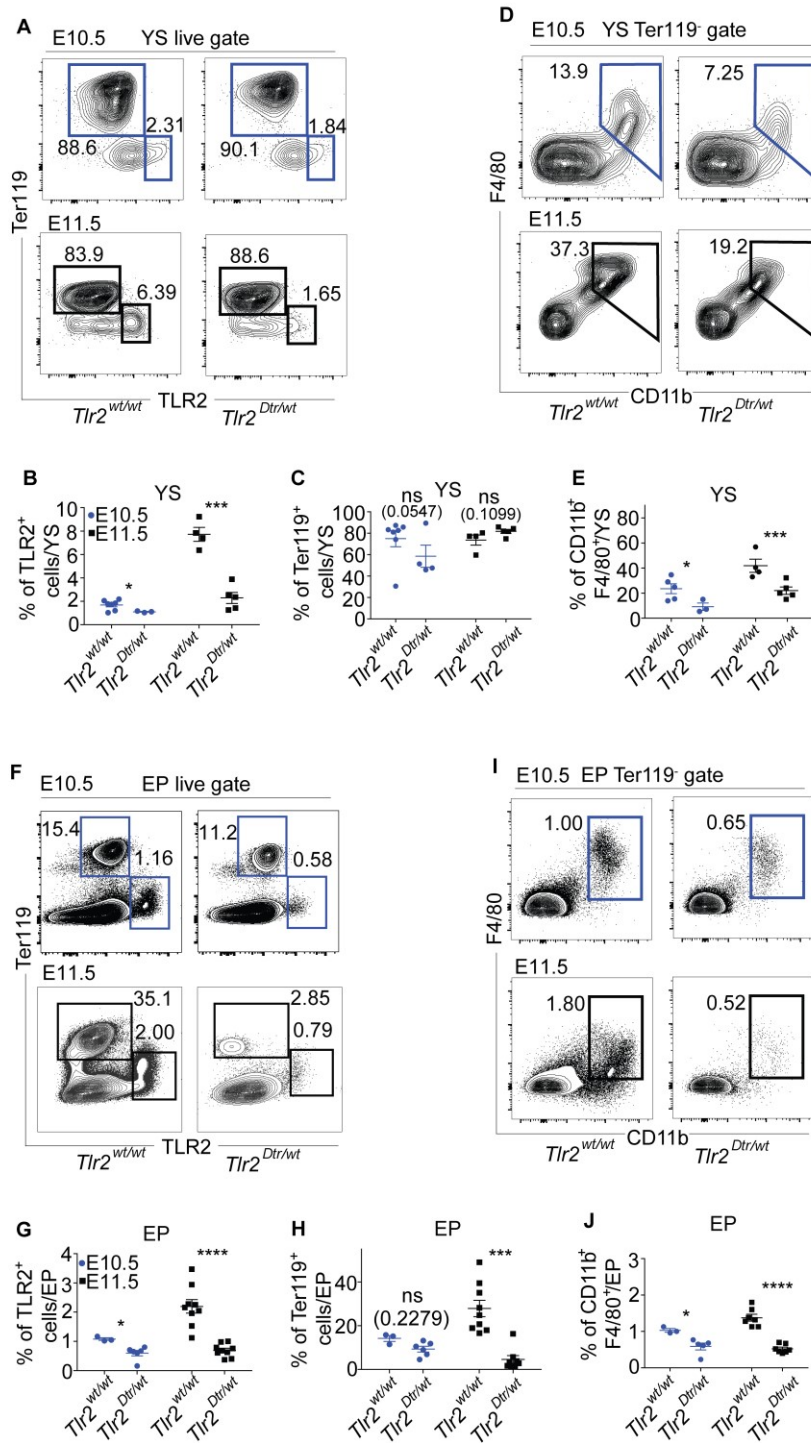
Figure 4. DT-mediated depletion of embryonic macrophages and erythrocytes in Tlr2^{Dtr/wt} mice. *Time-pregnant females bearing Tlr2^{Dtr/wt} and Tlr2^{wt/wt} embryos were treated as shown in Figure 3B. (A) Gating strategy for enumeration of E10.5 (blue) and E11.5 (black) YS-derived Ter119^+ erythroid and total TLR2^+ cells as well as*

CD11b⁺F4/80⁺ embryonic macrophages (D) in Tlr2$^{wt/wt}$ and Tlr2$^{DTR/wt}$ embryos. (B) Quantification of TLR2⁺ cells, (C) erythroid cells, and (E) CD11b⁺ F4/80⁺ embryonic macrophages in YS shown in A and D, respectively (mean ± SEM, n=3-6 independent samples of YS for each displayed item, ***p≤0.001, ns = not significant, unpaired two-tailed Student's t-test. (F) Gating strategy for enumeration of E10.5 (blue) and E11.5 (black) erythroid cells (Ter119⁺) and total TLR2⁺ cells as well as CD11b⁺ F4/80⁺ macrophages (I) in EP of Tlr2$^{wt/wt}$ and Tlr2$^{Dtr/wt}$ embryos. Quantification of (G) TLR2⁺ cells, (H) erythroid cells, and (J) CD11b⁺ F4/80⁺ macrophages (J) in EP shown in F and I, respectively (mean ± SEM, n=3-9 independent samples of EP for each displayed condition, *p<0.05, ***p<0.001, ****p<0.0001, n.s.= not significant, unpaired two-tailed Student's t-test).

3.2.2.5. LOSS OF EMBRYONIC MACROPHAGES DOES NOT INFLUENCE A GENERATION OF HSCs IN AGM

The presence of the YS-derived embryonic macrophages has been suggested to be essential for the generation of pre-HSC in the AGM (Mariani et al., 2019). To test this, we took advantage of our *Tlr2$^{Dtr/wt}$* knock-in mice treated with DT, where the deletion of EMPs was accompanied by a significant decrease in embryonic macrophages. The presence of pre-HSCs was determined in the AGM regions of embryos treated and untreated with DT by either hematopoietic cell staining of cryosections and flow cytometry. The intra-aortic hematopoietic clusters in macrophage depleted *Tlr2$^{Dtr/wt}$* aortic regions were formed normally (Fig. 5A) and the number of pre-HSCs in E10.5 AGM were largely comparable to their *Tlr2$^{wt/wt}$* littermates (Fig. 5B and C). Thus, our results show that decreased number of EMP-derived embryonic macrophages has no apparent effect on the generation of HSCs.
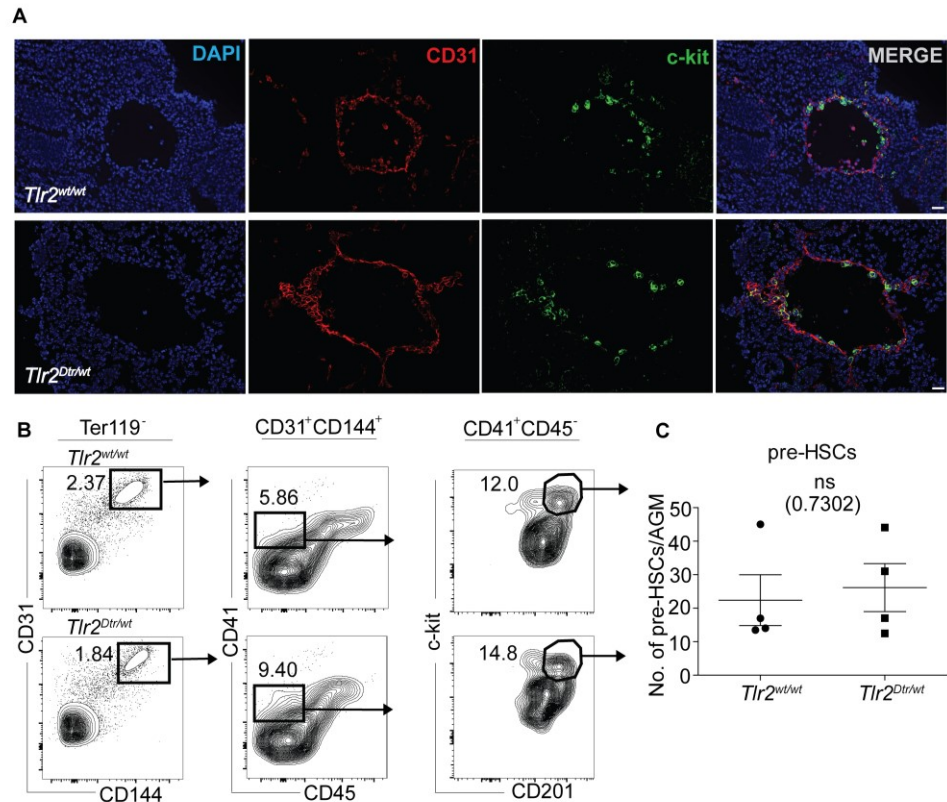
Figure 5

Figure 5. Generation of HSCs is intact in DT-treated Tlr2$^{Dtr/wt}$ mice. *Time-pregnant females bearing Tlr2$^{Dtr/wt}$ and Tlr2$^{wt/wt}$ embryos were treated as shown in figure 3B. (A) Visualization of hematopoietic clusters in AGM containing pre-HSCs by staining for CD31 (red), c-kit (green) and cell nuclei (DAPI). The scale bar represents 50 μm. (B) Pre-HSCs in AGM from DT double treated E10.5 Tlr2$^{wt/wt}$ and Tlr2$^{Dtr/wt}$ embryos were identified as CD31$^+$ CD144$^+$ CD41^{low} CD45$^-$ c-kit$^+$ CD201$^+$ cells. Numbers beside the gates show frequencies. The gating strategy shown in Supplementary fig. 5 was adopted from previous reports (Balounova et al., 2019; Zhou et al., 2016). (C) Quantification of pre-HSCs shown in B (mean ± SEM, 4 embryos per genotype, unpaired two-tailed Student's t-test, ns = not significant).*

3.2.2.6. THE DEPLETION OF TLR2$^+$ CELLS IS EMBRYONICALLY LETHAL

Considering the importance of EMP hematopoietic wave for the survival of the embryo (Chen et al., 2011), we asked whether the depletion of TLR2$^+$ cells would have any physiological consequences. We noted that pregnant mice treated with DT at E8.5 and E9.5 (Fig. 3A and B) failed to give birth to $Tlr2^{Dtr/wt}$ transgenic pups (Fig. 6A). This suggested that the depletion of TLR2$^+$ cells caused embryonic lethality. To identify the developmental stage at which the onset of lethality occurred, we analyzed double DT treated (at E8.5 and E9.5) embryos from E10.5 to E14.5 (Fig. 6B). Since the number of $Tlr2^{Dtr/wt}$ and $Tlr2^{wt/wt}$ embryos obtained from crosses between $Tlr2^{wt/wt}$ females and $Tlr2^{Dtr/wt}$ males at 11.5 were comparable and consistent with the expected Mendelian distribution 1:1, we used the percentage of $Tlr2^{Dtr/wt}$ embryos per all embryos found as a reference for establishing approximate day of lethality of $Tlr2^{Dtr/wt}$ embryos. As shown in Fig. 6B, this percentage dropped dramatically from about 55% at E11.5 to ~19% and ~6% at E12.5 and E13.5, respectively. At E14.5 no viable transgenic $Tlr2^{Dtr/wt}$ embryos were found. A detailed examination of E12.5 embryos showed that in more than half of the cases, the $Tlr2^{Dtr/wt}$ embryos were all already dead with signs of severe anemia and retardation of development (Fig. 6C, bottom right panel). Importantly, the deletion of TLR2$^+$ cells did not result in the significant diminishment of a minuscule subset of TLR2$^+$ non-hematopoietic cells (Supplementary fig. 6). The most likely explanation is that these cells were not yet positive or they only expressed very low levels of TLR2 at E8.5-E9.5 and thus were not subjected to elimination. However, given the low cellularity of this cell subset it is unlikely that even if eliminated, they would have any impact on embryonic survival. Thus, our data strongly suggests that it is the targeted removal of TLR2$^+$ EMPs and myeloid cells at E8.5-9.5 which critically contributed to embryonic lethality by E12.5.
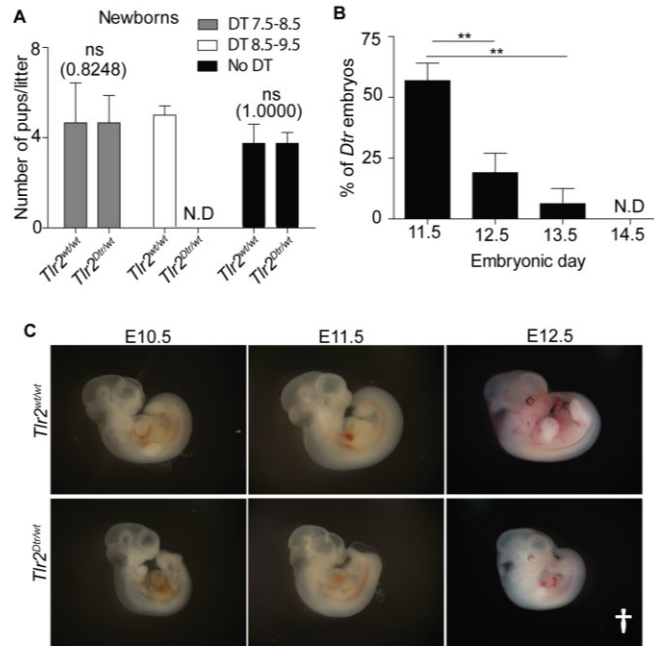
Figure 6

***Figure 6. The depletion of TLR2$^+$ cells at E8.5-9.5 is embryonically lethal.** (A) Untreated (black bars) and DT (double treated) time pregnant females at E7.5 and E8.5 (grey bars) showed no changes in the number of newborns with Tlr2$^{Dtr/wt}$ and Tlr2$^{wt/wt}$ genotypes. On the other hand, the administration of DT at E8.5 and E9.5 resulted in the complete absence of newborns with Tlr2$^{Dtr/wt}$ genotype (white bars) (mean ± SEM, n = 4-5 litters per indicated treatment, unpaired two-tailed Student's t-test, ns = not significant). (B) Percentage of viable Tlr2$^{Dtr/wt}$ (Dtr) embryos among all viable embryos after DT double treatment at E8.5 and E9.5, assessed between E11.5 and E14.5 (mean ± SEM, n =7 litters for E11.5, n =10 litters for E12.5; n = 4 litters for E13.5 and n=3 litters for E14.5, **p≤0.01, N.D.= non-detectable, unpaired two-tailed Student's t-test). (C) The morphology of Tlr2$^{wt/wt}$ and Tlr2$^{Dtr/wt}$ embryos double treated with DT at E8.5 and E9.5 microscopically examined between E10.5-E12.5. The white cross-mark denotes a deceased embryo.*

3.2.3. DISCUSSION

We have recently shown, that coexpression of TLR2 and c-kit on the precursors of EMPs by E7.5 serves as a suitable combinatorial surface marker for distinguishing emerging precursors of EMPs from the first embryonic wave (Balounova et al., 2019). Consistent with this observation, we have shown that phenotypic EMPs that express c-kit$^+$ CD16/32$^+$ and CD41$^+$ markers (McGrath et al., 2015) also display TLR2 on their surface. These TLR2$^+$ EMPs isolated from E8.5 YS were capable of producing hematopoietic colonies with a mixed erythro-myeloid potential (Gomez Perdiguero et al., 2015; McGrath et al., 2015). Thus both, TLR2$^+$c-kit$^+$ CD16/32$^+$CD41$^+$ EMPs at E8.5 as well as their TLR2$^+$c-kit$^+$ EMP precursors (Balounova et al., 2019) are evenly capable of producing mixed colonies, attesting that TLR2 expression parallels the acquisition of EMP functional capabilities in early embryonic development.

To assess the physiological importance of EMPs in embryonic development, we generated a new knock-in $Tlr2^{Dtr}$ mouse model suitable for depletion of cells expressing TLR2 during embryonic development. In contrast to the $Tlr2^{Cre}Rosa26^{DTA}$ model (Balounova et al., 2019), where all cells with an active $Tlr2$ locus were deleted, DT treatment of $Tlr2^{Dtr/wt}$ embryos removed only cells which expressed TLR2 at the protein level at the time of DT administration.

In $Tlr2^{Dtr/wt}$ embryos, the number of TLR2$^+$ EMPs was decreased upon the administration of DT at E8.5 and E9.5. The reason why such treatment failed to delete EMPs completely is that EMPs are constantly replenished from the YS and during their emergence TLR2 expression is often low and only gradually increasing, allowing early EMPs escape this elimination process. Also, EMPs can be generated between E10.5-E11.5 when DT levels subside and become biologically inefficient. Technical obstacles, such as organ distribution and bioavailability of i.p. injected DT in pregnat females could also contribute to incomplete deletion of EMPs in this model. Importantly, the DT-mediated decrease of YS EMPs in E10.5 $Tlr2^{Dtr/wt}$ mice was not accompanied by the apparent destruction of YS hemogenic endothelium, supporting the notion that TLR2 is

sufficiently expressed only on cells phenotypically defined as EMPs and their myeloid progenies but not on *bona-fide* endothelial cells.

YS-derived EMPs seed the FL where they start to produce hematopoietic cells (Gomez Perdiguero et al., 2015). Indeed, depletion of EMPs in the YS translated to a marked drop of c-kit$^+$ CD16/32$^+$ CD41$^+$ EMPs followed by the decrease of both c-kit$^+$ CD41$^-$CD44$^+$ CD71$^+$ early erythroid progenitors as well as CD11b$^+$ F4/80$^+$ macrophages in the FL and EP. Thus, our data is in line with previous reports suggesting that the embryonic lethality observed around E12.5 was caused by the decrease in EMPs with a subsequent reduction of erythroid cells and embryonic macrophages which are essential for proper oxygenation and complex developmental processes of embryo (Azzoni et al., 2018; Balounova et al., 2019; Plein et al., 2018).

It has been suggested that bone marrow-resident macrophages are important cellular components of the HSC niche where they contribute to the regulation of HSC mobilization and function (McCabe and MacNamara, 2016). Additionally, and in the context of this work, it has been proposed that embryonic macrophages could also be involved in the generation of functional HSCs from AGM in the mouse and zebrafish embryo (Mariani et al., 2019; Travnickova et al., 2015). In contrast, our data showed that at E10.5 the generation of HSC clusters was not affected by the diminished numbers of EMP-derived macrophages. However, the possibility that the diminishment of embryonic macrophages in our setting was not sufficient to unravel their functional involvement in this process cannot be excluded.

Together, this and our previous studies demonstrated that TLR2 can be effectively used as the marker of EMPs and their progeny. Since TLRs, as well as their signaling adaptor protein MyD88 knock-out models show no developmental phenotype, TLR2 represents a suitable molecular tool for genetic manipulation of early hematopoietic progenitors which express this gene. While the exploration of *Tlr2^{Dtr}* model in this study was restricted to the phenotype and function of EMPs at early embryonic stages, the coupled expression of TLR2, DTR and RFP in this mouse model allows for its effective implications in studies concerning the origin,

emergence, fate mapping and targeted deletion of TLR2^{+} cells not only in embryonic and fetal development but in adult animals. Another interesting question is whether TLR2, or any other pattern-recognition receptor (Li et al., 2014; Mariano et al., 2014) expressed on emerging EMPs (Balounova et al., 2019) which recognize pathogen-associated molecular patterns or danger-associated molecular patterns (Liu-Bryan et al., 2005; Shi et al., 2003; Vabulas et al., 2001), could be initially primed by endogenous ligands and thus provide activation signals to emerging components of immune system. Further investigation using available mouse models with manipulated *Tlr2* locus could provide invaluable insight into these and other related questions.

3.2.4. MATERIALS AND METHODS

Mice

For time pregnant females, the day of vaginal plug formation was considered as embryonic day 0.5 (E0.5). Embryos were strictly staged by standard criteria (Downs and Davies, 1993). Experiments were approved by the ethical committee of the IMG.

Generation of *Tlr2^Dtr* knock-in mouse strain

Tlr2^Dtr knock-in transgenic mouse was generated by inserting the RFP-p2A-DTR construct in front of the stop codon of TLR2 exon 3 via the Crisp/Cas9 system (Fig. 2A). Specifically, each part of the TLR2-RFP-p2A-DTR construct was ligated to the pBluescript II SK plasmid. The TagRFP-T (RFP) fragment with the peptide linker was ligated into the HindIII restriction site at the 3′-end of *Tlr2* exon 3. The 5'-end of the synthesized p2A-DTR fragment was ligated to the 3'end of RFP using the EcoRI restriction site and its 3'-end was integrated in front of the stop codon of the *Tlr2* Exon 3 via BamHI. This construct was then re-cloned into the pMSCV vector. Cas9 mRNA was prepared in a single step by *in vitro* transcription from the plasmid. The pronuclear injection of Cas9 mRNA, CRISPR gRNA sequence 5'-GAGAACTGCAATAAAGTCCTAGG-3', and the targeting of the construct into

C57BL/6 mouse zygotes was performed at the Transgenic Unit of IMG. Zygotes were transferred into the oviducts of pseudo-pregnant females.

Genotyping

PCR genotyping of $Tlr2^{Dtr}$ mice or embryos was performed using three primers. The first set of primers were designed to detect the presence of the 3'-end of the $Tlr2$ wt allele: (Tlr2-F: GAACTCTGACCCGCCCTTTA; $Tlr2$-R: CCAGTCAGTGCGACATAGGG). The second set was used to detect the $Tlr2$ transgenic allele: (Tlr2-F: GAACTCTGACCCGCCCTTTA; RFP-R: GGGCGAAGAGCTGATTAAGG). The size of the PCR products obtained were 643 bp and 434 bp for the wt and transgenic allele, respectively.

Processing of tissues for flow cytometry

Timed pregnant females were euthanized by cervical dislocation. Embryos were removed from the uterus and washed with 4°C phosphate-buffered saline (PBS). To obtain a single-cell suspension, the YS from E7.5 – E11.5 embryos or FL were transferred to Hank's Balanced Salt Solution (HBSS) containing 1mg/ml Dispase and incubated at 37°C for 10 minutes with occasional pipetting. To stop the dissociation process, embryos were washed in ice-cold PBS supplemented with 2mM EDTA and 3% FSC. The cell suspension was then passed through a 50μm cell strainer and centrifuged at 380g for 7min at 4°C.

Flow cytometry and cell sorting

After Fc receptor blocking (in experiments where CD16/32 was not stained) with rat anti-mouse CD16/32 antibody, single-cell suspensions were stained with fluorochrome conjugated or biotinylated monoclonal antibodies for 30 min on ice. Where appropriate, cells were washed and incubated with an APC-labelled streptavidin conjugate for 20 min. The full list of antibodies can be found in Supplementary Table 1. Samples were analyzed using the LSRII flow cytometer (BD Biosciences). FCM analysis was performed using FlowJo software (FlowJo, LCC). Cell debris and dead cells were excluded from the analysis based on their scatter signals and with viability dye staining, Hoechst 33258 (Sigma-Aldrich).

Colony Forming Assay

Colony forming unit (CFU-C) clonogenic assay was performed in Methocult M3434 medium (Stem Cell Technologies) as described elsewhere (Jung et al., 2000). E8.5 embryos were staged by somite counting. The YS were isolated, pooled, and the resulting cell suspension was prepared for cell sorting as described above. Live cells were gated on the basis of the Hoechst 33258 signal. Cells were sorted into FCS-coated tubes filled with Methocult M3434 and directly plated in culture dishes according to the manufacturer's instructions. At day 14, colonies were picked, washed once, transferred onto slides using *Cytospin* centrifugation and subsequently stained with May-Grünwald-Giemsa for morphological evaluation.

Immunofluorescence imaging and analysis

E10.5 and E11.5 embryos were fixed overnight in 4% paraformaldehyde (Sigma-Aldrich) at 4°C. After fixation, embryos were incubated overnight at 4°C in 30% sucrose dissolved in PBS and then embedded in OCT compound (Vendor). Cryoblocks were cut at a thickness of 10μm and then blocked with PBS containing 5% BSA (w/v) and 0.1% Triton X-100 for 1 hour at room temperature. Samples were stained overnight at 4°C with c-kit, CD31 or/and F4/80 primary antibodies, washed, then incubated with the appropriate secondary antibodies for 1 hour at room temperature in dark. Cell nuclei were stained with DAPI. Samples were mounted with Vectashield mounting medium and visualized using a Leica DM6000 epifluorescence microscope. Images were processed using Image J software.

Depletion of TLR2 positive cells in embryos

The initial assessment of the functionality of theTLR2-RFP-DTR cassette in $Tlr2^{Dtr}$ *mice* (Fig. 2D) was performed by intraperitoneal (i.p.) injection of a single-dose (600ng in 100 μl of PBS) of *Diphtheria toxin* (DT, Sigma Aldrich) into 6-week old animals and its effect was analyzed after 24 hours. To deplete TLR2$^+$ cells in early embryogenesis, C57Bl/6J wild type (wt) females were crossed with $Tlr2^{Dtr/wt}$ males to obtain embryos of both wt and transgenic phenotypes. 600ng of DT was administered i.p. to C57Bl/6J time-pregnant females at E8.5 and E9.5. DT double

treated embryos were removed from the uterus and depletion of TLR2 cells was analyzed microscopically and by flow cytometry at the indicated time points. The dosage of DT was optimized to obtain the most significant decrease of TLR2$^+$ cells without apparent toxic side effect.

Gene expression analysis by qRT-PCR

Total RNA from bone marrow cells was extracted using RNeasy Plus Micro Kit (Qiagen) and reverse transcribed using RevertAid transcriptase and random hexamers (ThermoFisher). Quantitative RT-PCR (qRT-PCR) was performed using the LightCycler 480 SYBR Green I Master mix (Roche) on a LightCycler 480 II (Roche). Each sample was tested in technical duplicates. Gene expression was calculated by relative quantification using the housekeeping gene, *Gapdh*. Primers were designed using Primer-BLAST (NCBI, NIH).

Generation of bone marrow-derived dendritic cells

Mouse femurs were isolated, Bone marrow was flushed from isolated mouse femurs with a 27G needle with cold RPMI and dissolved. Red blood cells were depleted with ACK lysis buffer. The cell suspension was centrifuged at 380g for 7 min at 4°C. Cells were cultured at a concentration of 10^6 cells/ml in RPMI supplemented with 5ng/ml GM-CSF. The medium was replaced at day three of cultivation. Cells were collected at day seven of cultivation for the experiment.

Preparation of aortic region for FACS analysis

The caudal region was isolated from E10.5 embryos. The AGM region was gently removed by tweezers and digested by Dispase (1mg/ml) to obtain a cell suspension for FACS analysis.

3.2.5. REFERENCES

1. Silver, L., and Palis, J. (1997) Initiation of murine embryonic erythropoiesis: a spatial analysis. *Blood* **89**, 1154-1164

2. McGrath, K. E., Frame, J. M., Fegan, K. H., Bowen, J. R., Conway, S. J., Catherman, S. C., Kingsley, P. D., Koniski, A. D., and Palis, J. (2015) Distinct Sources of Hematopoietic Progenitors Emerge before HSCs and Provide Functional Blood Cells in the Mammalian Embryo. *Cell Rep* **11**, 1892-1904

3. Palis, J. (2014) Primitive and definitive erythropoiesis in mammals. *Front Physiol* **5**, 3

4. Ferkowicz, M. J., Starr, M., Xie, X., Li, W., Johnson, S. A., Shelley, W. C., Morrison, P. R., and Yoder, M. C. (2003) CD41 expression defines the onset of primitive and definitive hematopoiesis in the murine embryo. *Development* **130**, 4393-4403

5. Palis, J., Robertson, S., Kennedy, M., Wall, C., and Keller, G. (1999) Development of erythroid and myeloid progenitors in the yolk sac and embryo proper of the mouse. *Development* **126**, 5073-5084

6. Tober, J., Koniski, A., McGrath, K. E., Vemishetti, R., Emerson, R., de Mesy-Bentley, K. K., Waugh, R., and Palis, J. (2007) The megakaryocyte lineage originates from hemangioblast precursors and is an integral component both of primitive and of definitive hematopoiesis. *Blood* **109**, 1433-1441

7. Bertrand, J. Y., Jalil, A., Klaine, M., Jung, S., Cumano, A., and Godin, I. (2005) Three pathways to mature macrophages in the early mouse yolk sac. *Blood* **106**, 3004-3011

8. Herbomel, P., Thisse, B., and Thisse, C. (1999) Ontogeny and behaviour of early macrophages in the zebrafish embryo. *Development* **126**, 3735-3745

9. Epelman, S., Lavine, K. J., and Randolph, G. J. (2014) Origin and functions of tissue macrophages. *Immunity* **41**, 21-35

10. Perdiguero, E. G., Klapproth, K., Schulz, C., Busch, K., de Bruijn, M., Rodewald, H. R., and Geissmann, F. (2015) The Origin of Tissue-Resident

Macrophages: When an Erythro-myeloid Progenitor Is an Erythro-myeloid Progenitor. *Immunity* **43**, 1023-1024

11. Chen, M. J., Li, Y., De Obaldia, M. E., Yang, Q., Yzaguirre, A. D., Yamada-Inagawa, T., Vink, C. S., Bhandoola, A., Dzierzak, E., and Speck, N. A. (2011) Erythroid/myeloid progenitors and hematopoietic stem cells originate from distinct populations of endothelial cells. *Cell Stem Cell* **9**, 541-552

12. Yosef, N., Vadakkan, T. J., Park, J. H., Poche, R. A., Thomas, J. L., and Dickinson, M. E. (2018) The phenotypic and functional properties of mouse yolk-sac-derived embryonic macrophages. *Dev Biol* **442**, 138-154

13. Munoz-Espin, D., Canamero, M., Maraver, A., Gomez-Lopez, G., Contreras, J., Murillo-Cuesta, S., Rodriguez-Baeza, A., Varela-Nieto, I., Ruberte, J., Collado, M., and Serrano, M. (2013) Programmed cell senescence during mammalian embryonic development. *Cell* **155**, 1104-1118

14. Paolicelli, R. C., Bolasco, G., Pagani, F., Maggi, L., Scianni, M., Panzanelli, P., Giustetto, M., Ferreira, T. A., Guiducci, E., Dumas, L., Ragozzino, D., and Gross, C. T. (2011) Synaptic pruning by microglia is necessary for normal brain development. *Science* **333**, 1456-1458

15. Hoeffel, G., Chen, J., Lavin, Y., Low, D., Almeida, F. F., See, P., Beaudin, A. E., Lum, J., Low, I., Forsberg, E. C., Poidinger, M., Zolezzi, F., Larbi, A., Ng, L. G., Chan, J. K., Greter, M., Becher, B., Samokhvalov, I. M., Merad, M., and Ginhoux, F. (2015) C-Myb(+) erythro-myeloid progenitor-derived fetal monocytes give rise to adult tissue-resident macrophages. *Immunity* **42**, 665-678

16. Schulz, C., Gomez Perdiguero, E., Chorro, L., Szabo-Rogers, H., Cagnard, N., Kierdorf, K., Prinz, M., Wu, B., Jacobsen, S. E., Pollard, J. W., Frampton, J., Liu, K. J., and Geissmann, F. (2012) A lineage of myeloid cells independent of Myb and hematopoietic stem cells. *Science* **336**, 86-90

17. Medvinsky, A., and Dzierzak, E. (1996) Definitive hematopoiesis is autonomously initiated by the AGM region. *Cell* **86**, 897-906

18. Yokomizo, T., and Dzierzak, E. (2010) Three-dimensional cartography of hematopoietic clusters in the vasculature of whole mouse embryos. *Development* **137**, 3651-3661

19. Kumaravelu, P., Hook, L., Morrison, A. M., Ure, J., Zhao, S., Zuyev, S., Ansell, J., and Medvinsky, A. (2002) Quantitative developmental anatomy of definitive haematopoietic stem cells/long-term repopulating units (HSC/RUs): role of the aorta-gonad-mesonephros (AGM) region and the yolk sac in colonisation of the mouse embryonic liver. *Development* **129**, 4891-4899

20. Ema, H., and Nakauchi, H. (2000) Expansion of hematopoietic stem cells in the developing liver of a mouse embryo. *Blood* **95**, 2284-2288

21. Mendelson, A., and Frenette, P. S. (2014) Hematopoietic stem cell niche maintenance during homeostasis and regeneration. *Nat Med* **20**, 833-846

22. Chiu, S. K., Saw, J., Huang, Y., Sonderegger, S. E., Wong, N. C., Powell, D. R., Beck, D., Pimanda, J. E., Tremblay, C. S., and Curtis, D. J. (2018) A novel role for Lyl1 in primitive erythropoiesis. *Development* **145**

23. Tsai, F. Y., Keller, G., Kuo, F. C., Weiss, M., Chen, J., Rosenblatt, M., Alt, F. W., and Orkin, S. H. (1994) An early haematopoietic defect in mice lacking the transcription factor GATA-2. *Nature* **371**, 221-226

24. Fujiwara, Y., Browne, C. P., Cunniff, K., Goff, S. C., and Orkin, S. H. (1996) Arrested development of embryonic red cell precursors in mouse embryos lacking transcription factor GATA-1. *Proc Natl Acad Sci U S A* **93**, 12355-12358

25. Mucenski, M. L., McLain, K., Kier, A. B., Swerdlow, S. H., Schreiner, C. M., Miller, T. A., Pietryga, D. W., Scott, W. J., Jr., and Potter, S. S. (1991) A functional c-myb gene is required for normal murine fetal hepatic hematopoiesis. *Cell* **65**, 677-689

26. Ding, L., Saunders, T. L., Enikolopov, G., and Morrison, S. J. (2012) Endothelial and perivascular cells maintain haematopoietic stem cells. *Nature* **481**, 457-462

27. Azzoni, E., Frontera, V., McGrath, K. E., Harman, J., Carrelha, J., Nerlov, C., Palis, J., Jacobsen, S. E. W., and de Bruijn, M. F. (2018) Kit ligand has

a critical role in mouse yolk sac and aorta-gonad-mesonephros hematopoiesis. *EMBO Rep* **19**

28. Zhao, J., Chen, X., Song, G., Zhang, J., Liu, H., and Liu, X. (2017) Uhrf1 controls the self-renewal versus differentiation of hematopoietic stem cells by epigenetically regulating the cell-division modes. *Proc Natl Acad Sci U S A* **114**, E142-E151

29. Balounova, J., Vavrochova, T., Benesova, M., Ballek, O., Kolar, M., and Filipp, D. (2014) Toll-like receptors expressed on embryonic macrophages couple inflammatory signals to iron metabolism during early ontogenesis. *Eur J Immunol* **44**, 1491-1502

30. Balounova, J., Splichalova, I., Dobesova, M., Kolar, M., Fiser, K., Prochazka, J., Sedlacek, R., Jurisicova, A., Sung, H. K., Korinek, V., Alberich-Jorda, M., Godin, I., and Filipp, D. (2019) Toll-like receptor 2 expression on c-kit(+) cells tracks the emergence of embryonic definitive hematopoietic progenitors. *Nat Commun* **10**, 5176

31. Collier, R. J. (2001) Understanding the mode of action of diphtheria toxin: a perspective on progress during the 20th century. *Toxicon* **39**, 1793-1803

32. Stremmel, C., Schuchert, R., Wagner, F., Thaler, R., Weinberger, T., Pick, R., Mass, E., Ishikawa-Ankerhold, H. C., Margraf, A., Hutter, S., Vagnozzi, R., Klapproth, S., Frampton, J., Yona, S., Scheiermann, C., Molkentin, J. D., Jeschke, U., Moser, M., Sperandio, M., Massberg, S., Geissmann, F., and Schulz, C. (2018) Yolk sac macrophage progenitors traffic to the embryo during defined stages of development. *Nat Commun* **9**, 75

33. Mariani, S. A., Li, Z., Rice, S., Krieg, C., Fragkogianni, S., Robinson, M., Vink, C. S., Pollard, J. W., and Dzierzak, E. (2019) Pro-inflammatory Aorta-Associated Macrophages Are Involved in Embryonic Development of Hematopoietic Stem Cells. *Immunity* **50**, 1439-1452 e1435

34. Gomez Perdiguero, E., Klapproth, K., Schulz, C., Busch, K., Azzoni, E., Crozet, L., Garner, H., Trouillet, C., de Bruijn, M. F., Geissmann, F., and Rodewald, H. R. (2015) Tissue-resident macrophages originate from yolk-sac-derived erythro-myeloid progenitors. *Nature* **518**, 547-551

35. Okun, E., Griffioen, K. J., Son, T. G., Lee, J. H., Roberts, N. J., Mughal, M. R., Hutchison, E., Cheng, A., Arumugam, T. V., Lathia, J. D., van Praag, H., and Mattson, M. P. (2010) TLR2 activation inhibits embryonic neural progenitor cell proliferation. *J Neurochem* **114**, 462-474

36. McCabe, A., and MacNamara, K. C. (2016) Macrophages: Key regulators of steady-state and demand-adapted hematopoiesis. *Exp Hematol* **44**, 213-222

37. Travnickova, J., Tran Chau, V., Julien, E., Mateos-Langerak, J., Gonzalez, C., Lelievre, E., Lutfalla, G., Tavian, M., and Kissa, K. (2015) Primitive macrophages control HSPC mobilization and definitive haematopoiesis. *Nat Commun* **6**, 6227

38. Mariano, V. S., Zorzetto-Fernandes, A. L., da Silva, T. A., Ruas, L. P., Nohara, L. L., Almeida, I. C., and Roque-Barreira, M. C. (2014) Recognition of TLR2 N-glycans: critical role in ArtinM immunomodulatory activity. *PLoS One* **9**, e98512

39. Li, J. Y., Liu, Y., Gao, X. X., Gao, X., and Cai, H. (2014) TLR2 and TLR4 signaling pathways are required for recombinant Brucella abortus BCSP31-induced cytokine production, functional upregulation of mouse macrophages, and the Th1 immune response in vivo and in vitro. *Cell Mol Immunol* **11**, 477-494

40. Liu-Bryan, R., Scott, P., Sydlaske, A., Rose, D. M., and Terkeltaub, R. (2005) Innate immunity conferred by Toll-like receptors 2 and 4 and myeloid differentiation factor 88 expression is pivotal to monosodium urate monohydrate crystal-induced inflammation. *Arthritis Rheum* **52**, 2936-2946

41. Shi, Y., Evans, J. E., and Rock, K. L. (2003) Molecular identification of a danger signal that alerts the immune system to dying cells. *Nature* **425**, 516-521

42. Vabulas, R. M., Ahmad-Nejad, P., da Costa, C., Miethke, T., Kirschning, C. J., Hacker, H., and Wagner, H. (2001) Endocytosed HSP60s use toll-like receptor 2 (TLR2) and TLR4 to activate the toll/interleukin-1 receptor signaling pathway in innate immune cells. *J Biol Chem* **276**, 31332-31339

43. Downs, K. M., and Davies, T. (1993) Staging of gastrulating mouse embryos by morphological landmarks in the dissecting microscope. *Development* **118**, 1255-1266

44. Jung, S., Aliberti, J., Graemmel, P., Sunshine, M. J., Kreutzberg, G. W., Sher, A., and Littman, D. R. (2000) Analysis of fractalkine receptor CX(3)CR1 function by targeted deletion and green fluorescent protein reporter gene insertion. *Mol Cell Biol* **20**, 4106-4114

3.2.6. SUPPORTING INFORMATION
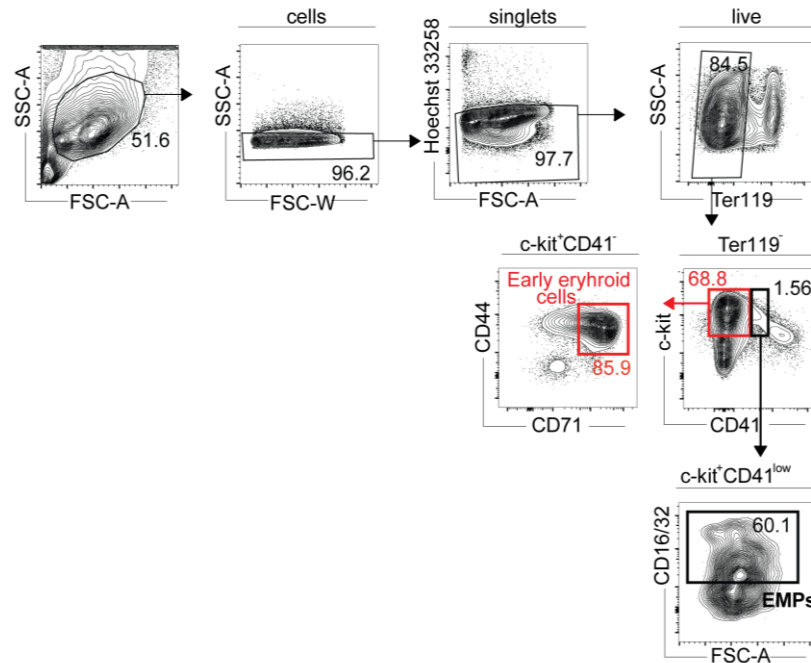
Supplementary Figure 1
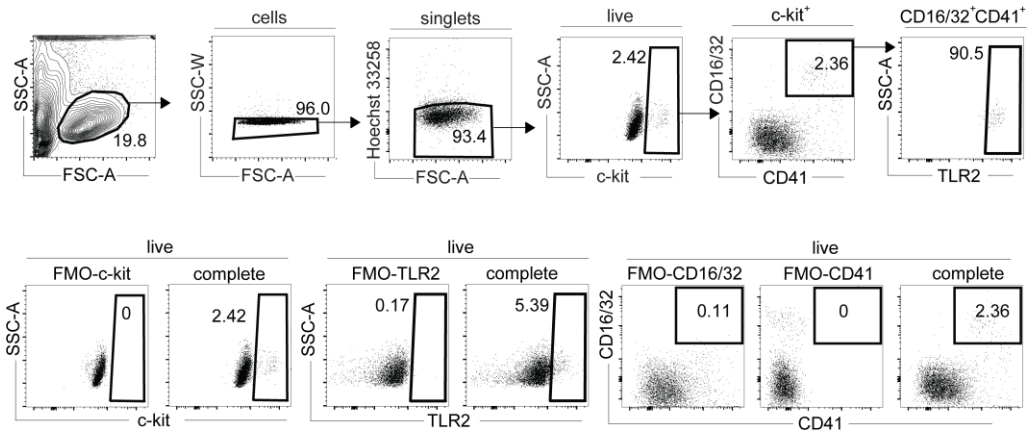
Supplementary Figure 1. Gating strategy for EMPs. *Gating strategy (upper panels) with relevant FMO controls (lower panels) are provided. Cells were gated as singlets, live, with c-kit$^+$ CD16/32$^+$ CD41$^+$ phenotype. Nearly all EMPs fall into or on the borderline of TLR2 positivity (upper panel). Gating strategy is shown on E9.5 YS.*
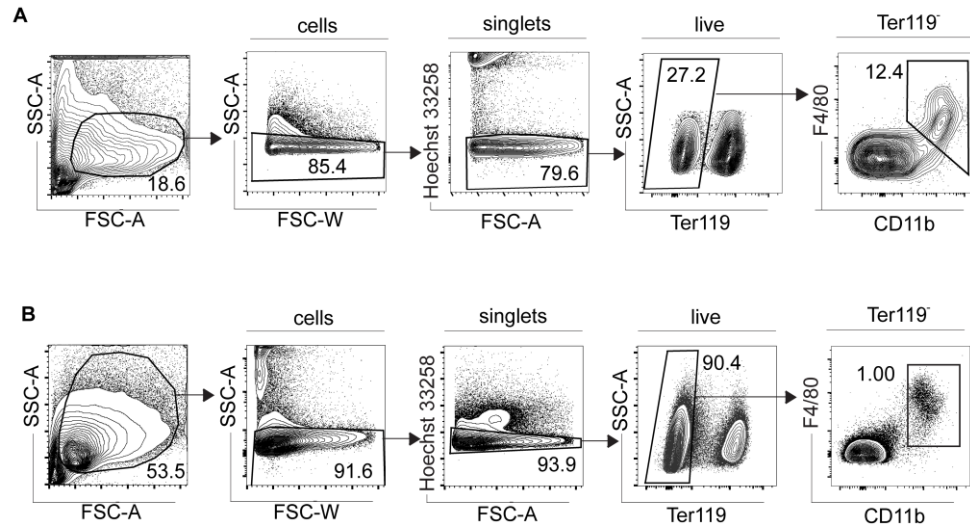
Supplementary Figure 2
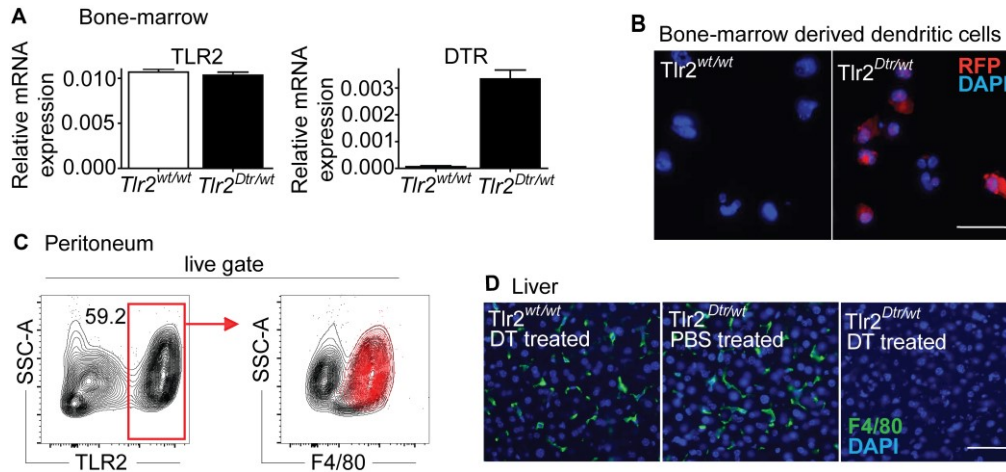
Supplementary Figure 2. Tlr2^Dtr mouse model for efficient depletion of TLR2+ cells. *(A) Expression of Tlr2 and Dtr mRNA in the bone marrow isolated from Tlr2^wt/wt and Tlr2^Dtr/wt mice. Total RNA was isolated from bone marrow. Obtained values were normalized to the expression of a reference gene, Gapdh (n=3). (B) Expression of RFP assessed by fluorescent microscopy (antibody staining-describe) of bone marrow-derived dendritic cells generated from Tlr2^wt/w (left panel) and Tlr2^Dtr/wt (right panel) animals (we do not know how you have generated DCs). Scale bar represents 25um (C) Cells from peritoneal lavage were gated on TLR2+. Nearly all F4/80+ mouse peritoneal macrophages coexpress TLR2+ . (D) Depletion of F4/80+ cells in the liver after intraperitoneal injection of DT. Samples were analyzed 24 hours after injection. Scale bar represents 50 μm.*
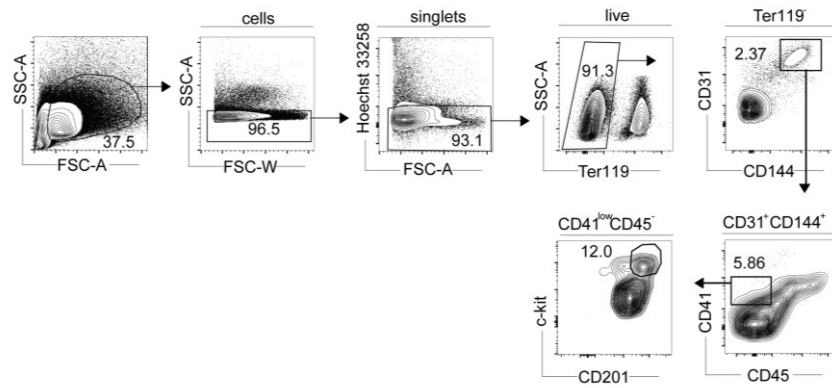
Supplementary Figure 3

Supplementary Figure 3. Gating strategy for EMPs and Early erythroid progenitors in the fetal liver. *Singlets and live cells were first gated for Ter119⁻ phenotype. This subset was then separated into c-kit⁺CD41⁻ subpopulation (red gate) used for the identification of Early erythroid cells of c-kit⁺ CD41⁻ CD44⁺ CD71⁺ phenotype and c-kit⁺CD41⁺ subset (black gate) used for the identification EMPs of c-kit⁺ CD41⁺ CD16/32⁺ phenotype.*
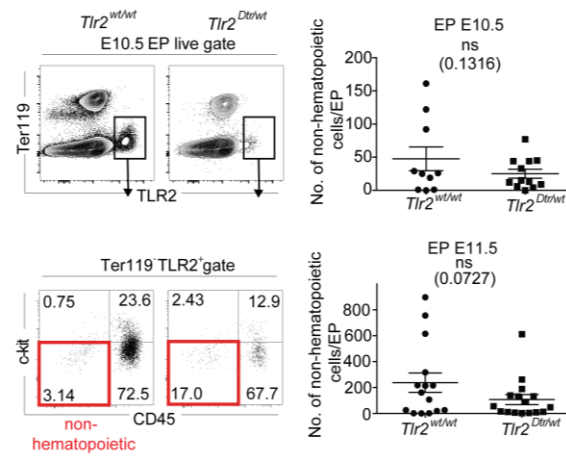
Supplementary Figure 4

Supplementary Figure 4. *Gating strategy for embryonic macrophages.* *Embryonic macrophages were gated as follows: cells, singlets, live, Ter119⁻ and CD11b⁺ F4/80⁺ population. A representative sample from E10.5 YS (A) and EP (B) is shown.*

Supplementary Figure 5

Supplementary Figure 5. Gating strategy for pre-HSCs isolated from the AGM.
E10.5 AGM was isolated and the cell suspension prepared. We gated on cells,
singlets, Ter119⁻, CD31⁺ CD144⁺, CD41^{low} CD45⁻ and then finally on the c-kit⁺
CD201⁺ population.

Supplementary Figure 6

***Supplementary Figure 6. DT-mediated elimination of TLR2+ cells does not
impact the cellularity of TLR2+ lineage⁻ cells.** DT was administered i.p. into time-
pregnant females of Tlr2wt/wt and Tlr2Dtr/wt mice at E8.5 and E9.5. Gating strategy
for non-hematopoietic TLR2+ CD45⁻c-kit⁻ cells (red gates) at E10.5 in EP is shown
(left dot plots). The quantification of the presence of these cells in EP at E10.5 and
E11.5 is provided in the scatter graphs, n=3, 2-4 embryos of the same genotype per
experiment (unpaired two-tailed Student's t-test), ns=not significant.*

Table 1. List of used antibodies

Antibodies used for flow cytometry

Antibody	Clone	Conjugate	Dilution	Company
CD11b	M1/70	A700	1/300	Sony
c-kit	2B8	FITC	1/200	Biolegend
CD16/32 (FcγRIII/II)	24G2	-	1/200	Biolegend
CD45	30-F11	PerCP-Cy5-5	1/300	Biolegend
CD282 (TLR2)	T2.5	Biotin	1/150	Biolegend
F4/80	BM8	PE-Cy-7	1/300	eBioscience
Ter119	Ter-119	Qdot605	1/300	Biolegend
Ter119	Ter-119	PB	1/300	Biolegend
Streptavidin	-	APC	1/400	Biolegend
CD45	30-F11	A700	1/250	eBioscience
c-kit	ACK2	PE	1/250	eBioscience
CD31	390	FITC	1/250	eBioscience
CD41	MWReg30	APC-Cy7	1/200	Biolegend
CD201	eBio 1560	PerCP-A710	1/200	Invitrogen
CD144	BV13	PE-Cy-7	1/250	Biolegend

Antibodies used for immunofluorescence

Antibody	Clone	Conjugate	Dilution	Company
F4/80,goat	Cl:A3-1		1/500	BIO RAD
c-kit, goat	polyclonal		1/750	RaD Systems
Iba1, goat	polyclonal		1/500	Abcam
CD31, rat	MEC 13.3 (RUO)		1/200	BD Biosciences
donkey anti rat	polyclonal	Alexa594	1/500	Invitrogen
chicken anti goat	polyclonal	Alexa488	1/500	Invitrogen

3.3. TRANSMEMBRANE ADAPTOR PROTEIN WBP1L REGULATES CXCR4 SIGNALLING AND MURINE HAEMATOPOIESIS

WW domain-binding protein 1-like (WBP1L) also known as an outcome predictor of acute leukemia 1 (OPAL1) is associated with childhood acute lymphoblastic leukemia. Its mRNA increase correlates with the favorable outcome of this disease and puts him into the group of the potential prognostic markers (Ross et al., 2003; Yeoh et al., 2002). This protein is still not well characterized and nothing is known about its physiological function.

Borna et. al. showed that WBP1L is the negative regulator of chemokine receptor CXCR4 in broad hematopoietic subsets by its interaction with NEDD4-family ubiquitin ligases. In the end, these processes regulate CXCR4 ubiquitination and its expression. WBP1L deficiency resulted in the alterations in B cell development and enhanced bone marrow transplantation efficiency. These data showed that WBP1L is a newly characterized regulator of CXCR4 signaling.

The expression of CXCR4 mRNA in embryo was firstly described in 1999 (McGrath et al., 1999). CXCR4 is starting to be increased together with CX3CR1 from E10.0 to E10.5 on embryonic macrophages in YS and surrounding the AGM region. Their ligands were increased on endothelial cells in the AGM region which attract them there (Mariani et al., 2019). These findings suggest that embryonic macrophages using receptor-ligand interactions for tracking as adult myeloid cells. It has been shown, that migration of embryonic pre-macrophages and macrophages to the developing organs is happening in the CX3CR1 dependent manner (Stremmel et al., 2018). We predicted that in the mice with WBP1L deletion the CXCR4 activity will be dysregulated and may influence the migration of embryonic macrophages from YS to the EP. We have found that the frequencies of embryonic macrophages are increased in YS from E10.5 but the frequencies of macrophages in the EP were unchanged.

In the case of adults, the impaired WBP1L function resulted in the perturbation of B cell development, increased ability of bone marrow stem and progenitor cells

reconstitution after the transplantation and increased progenitor cell homing into the bone marrow. It is still unclear if some of these phenotypes can be attributed to the CXCR4 hyperactivity.

Applicant's contribution: FACS analysis of embryonic YS and EP at E10.5 and E11.5. The analysis of c-kit+CD45-, c-kit+CD45+ (contains EMPs) and c-kit-CD45+ populations and embryonic macrophages.

ORIGINAL ARTICLE

Transmembrane adaptor protein WBP1L regulates CXCR4 signalling and murine haematopoiesis

Simon Borna[1,2] | Ales Drobek[1] | Jarmila Kralova[1] | Daniela Glatzova[1,2,3] |
Iva Splichalova[4] | Matej Fabisik[1,2] | Jana Pokorna[1] | Tereza Skopcova[1] |
Pavla Angelisova[1] | Veronika Kanderova[5] | Julia Starkova[5] | Petr Stanek[6] |
Orest V. Matveichuk[7] | Nataliia Pavliuchenko[1,2] | Katarzyna Kwiatkowska[7] |
Majd B. Protty[8] | Michael G. Tomlinson[9] | Meritxell Alberich-Jorda[10] |
Vladimir Korinek[11] | Tomas Brdicka[1]

[1]Laboratory of Leukocyte Signaling, Institute of Molecular Genetics of the Czech Academy of Sciences, Prague, Czech Republic

[2]Faculty of Science, Charles University, Prague, Czech Republic

[3]Department of Biophysical Chemistry, J. Heyrovsky Institute of Physical Chemistry of the Czech Academy of Sciences, Prague, Czech Republic

[4]Laboratory of Immunobiology, Institute of Molecular Genetics of the Czech Academy of Sciences, Prague, Czech Republic

[5]CLIP - Childhood Leukaemia Investigation Prague and Department of Pediatric Hematology and Oncology, Second Faculty of Medicine, Charles University, Prague, Czech Republic

[6]Second Faculty of Medicine, Charles University, Prague, Czech Republic

[7]Laboratory of Molecular Membrane Biology, Nencki Institute of Experimental Biology, Warsaw, Poland

[8]Institute of Biomedical Research, University of Birmingham, Birmingham, UK

[9]School of Biosciences, University of Birmingham, Birmingham, UK

[10]Laboratory of Hematooncology, Institute of Molecular Genetics of the Czech Academy of Sciences, Prague, Czech Republic

[11]Laboratory of Cell and Developmental Biology, Institute of Molecular Genetics of the Czech Academy of Sciences, Prague, Czech Republic

Correspondence
Tomas Brdicka, Institute of Molecular Genetics of the Czech Academy of Sciences, Videnska 1083, 14220 Prague, Czech Republic.
Email: tomas.brdicka@img.cas.cz

Present address
Majd B. Protty, Sir Geraint Evans Cardiovascular Research Building, Cardiff University, Cardiff, UK

Funding information
European Regional Development Fund, Grant/Award Number: CZ.1.05/1.1.00/02.0109 and OPPK (CZ.2.16/3.1.00/21547); Grantová Agentura České Republiky, Grant/Award Number: 16-07425S and P302-12-G101; H2020 Marie Skłodowska-Curie

Abstract

WW domain binding protein 1-like (WBP1L), also known as outcome predictor of acute leukaemia 1 (OPAL1), is a transmembrane adaptor protein, expression of which correlates with *ETV6-RUNX1* (t(12;21)(p13;q22)) translocation and favourable prognosis in childhood leukaemia. It has a broad expression pattern in haematopoietic and in non-haematopoietic cells. However, its physiological function has been unknown. Here, we show that WBP1L negatively regulates signalling through a critical chemokine receptor CXCR4 in multiple leucocyte subsets and cell lines. We also show that WBP1L interacts with NEDD4-family ubiquitin ligases and regulates CXCR4 ubiquitination and expression. Moreover, analysis of *Wbp1l*-deficient mice revealed alterations in B cell development and enhanced efficiency of bone marrow cell transplantation. Collectively, our data show that WBP1L is a novel regulator of CXCR4 signalling and haematopoiesis.

1 | INTRODUCTION

WW domain binding protein 1-like (WBP1L) also known as outcome predictor of acute leukaemia 1 (OPAL1) has attracted attention because of a report showing that its elevated expression at mRNA level correlates with favourable outcome in childhood acute lymphoblastic leukaemia (ALL).[1] These data suggested that it could potentially serve as a prognostic marker. Later, it was shown that its levels are particularly increased in B cell progenitor ALL (BCP-ALL) with chromosomal translocation t(12;21)(p13;q22), which results in expression of *ETV6-RUNX1* fusion transcription factor.[2,3] In BCP-ALL, this translocation is associated with good prognosis, which likely explains the correlation between WBP1L expression and favourable outcome.[2] However, it is not known whether WBP1L functionally contributes to it.

ETV6, a fusion partner in *ETV6-RUNX1*, is a transcriptional repressor and *WBP1L* is one of its target genes.[4–6] In general, ETV6 targets are of high interest because of critical importance of ETV6 in haematopoiesis and its involvement in leukaemia. Around 30 fusions of *ETV6* to different partner genes and a number of mutations in *ETV6* have been identified so far, many of them implicated in various haematological malignancies of myeloid and lymphoid origin.[7,8] In addition, its critical role in normal haematopoiesis has been revealed in studies of ETV6-deficient mice, which show profound defects in haematopoietic stem and progenitor cell function and inability of these cells to reconstitute haematopoiesis after bone marrow transplantation.[9,10]

Bioinformatic sequence analysis revealed that WBP1L is a transmembrane adaptor protein with a very short extracellular/luminal part followed by a single transmembrane domain and a larger cytoplasmic tail.[11] Although relatively short, the extracellular/luminal part presumably forms a small compact domain held together by disulphide bridges formed among cysteines in the C*C*CC*CC motif.[11] The cytoplasmic part of WBP1L contains several potential interaction motifs corresponding to the consensus sequence of WW domain binding motifs L-P-X-Y or P-P-X-Y.[11]

Except for the limited bioinformatics analysis, WBP1L protein remained completely uncharacterized. Its physiological function has been unknown and whether it has any functional features that may link it to normal haematopoiesis or neoplasia has never been investigated. Here, we show that it binds several members of the NEDD4-family of ubiquitin ligases and that its deficiency results in enhanced surface expression and signalling of critical chemokine receptor CXCR4. WBP1L deficiency also results in alterations in B cell development and altered dynamics of stem and progenitor cells in the bone marrow. Taken together, we establish the role of WBP1L in CXCR4 signalling and in normal haematopoiesis. These findings also form the basis for further research on its potential role in leukaemia.

2 | MATERIALS AND METHODS

2.1 | Protein isolation, detection and quantification assays

Immunoprecipitations (IP) and immunoblotting were performed essentially as reported with adjustments described in online supplement. Western blot quantifications were carried out using Azure c300 imaging system (Azure Biosystems) and Aida Image Analysis software (Elysia-raytest). WBP1L expression in B cell lines was analysed by size exclusion chromatography-microsphere-based affinity proteomics analysis described in detail here,[3] and the data were quantified using Matlab (MathWorks). Tandem purification of WBP1L was based on the following publication[12] with modifications described in online supplement. WBP1L palmitoylation was analysed using metabolic labelling with palmitic acid analogue 17ODYA followed by reaction with biotin-azide and enrichment on streptavidin-coupled beads as described in detail in online supplement.

2.2 | Antibodies

Antibodies are listed in Tables S1 and S2. WBP1L antisera were generated by immunization of rabbits with KLH-conjugated peptide from WBP1L C-terminus while WBP1L monoclonal antibodies were prepared by standard hybridoma technology after immunization of mice with recombinant C-terminal part of murine WBP1L protein as described in online supplement.

2.3 | Cloning, qPCR, DNA transfection, virus preparation and cell infection

cDNA was generated using Quick-RNA kit (Zymo Research), revert aid reverse transcriptase (Thermo-Fisher) and oligo-dT primer. qPCR reactions were run on LightCycler 480 Instrument II using LightCycler 480 SYBR Green I Master mix (Roche). List of qPCR primers is in Table S3. For construct preparation see online supplement and Table S4. Phoenix cell transfection, virus generation and cell transduction were performed as described.[13] For lentivirus production, the procedure was to a minor extent modified as described in online supplement. Infected cells were sorted on Influx (BD) or selected on G418 (Thermo-Fisher).

2.4 | Mouse experiments, homing assays

Wbp1l$^{-/-}$ mice (*Wbp1l*$^{tm2a(EUCOMM)Hmgu}$) on C57Bl/6J genetic background were obtained from International Mouse Phenotyping Consortium. In these mice, gene trap flanked by FRT sites followed by coding region of exon 5 surrounded by LoxP sites were inserted into *Wbp1l* locus by homologous recombination (*Wbp1l*$^{-/-}$). Mice were bred in specific pathogen free conditions. To obtain inducible *Wbp1l*$^{fl/fl}$*CreERT* mice, we crossed animals of the *Wbp1l*$^{-/-}$ strain to *B6.Cg-Tg (ACTFLPe)9205 Dym/J* mice to remove the gene trap, and subsequently, to *B6.129-Gt(ROSA)26Sor*$^{tm1(cre/ERT2)Tyj}$*/J* animals. Both mouse strains were purchased from the Jackson Laboratory (Bar Harbor). To achieve *Wbp1l* deletion, mice were injected intraperitoneally with five daily doses of 2 mg of tamoxifen (Merck) in corn oil (Merck). For homing and transplantation assays, congenic *Ly5.1 (C57BL/6NCr)* or *Ly5.1/Ly5.2 (C57Bl/6J)* heterozygote recipients were sublethally (three Grey) or lethally (seven Grey) irradiated, followed by injection of transplanted cells into the tail vain. For experiments we used 8- to 12–week-old sex and age matched animals. Housing of mice and in vivo experiments were performed in compliance with local legal requirements and ethical guidelines. The Animal Care and Use Committee of the Institute of Molecular Genetics approved animal care and experimental procedures (Ref. No. 69/2014, 6/2016).

2.5 | Transwell migration

1×10^5 Cells in DMEM with 0.2% BSA were plated in the upper well of 5µm pore Transwell apparatus (Corning). After 4 hours, migrated cells in the bottom well were counted using a flow cytometer (LSRII; BD).
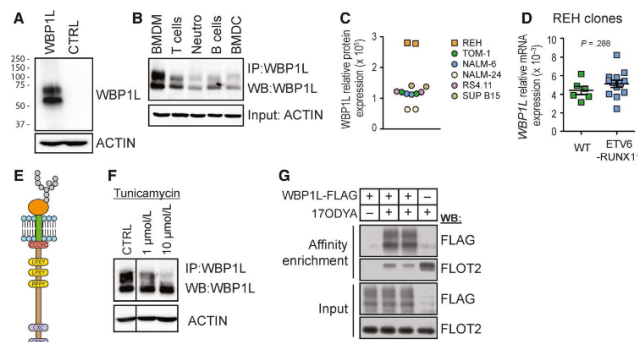

FIGURE 1 WBP1L is a palmitoylated glycoprotein, broadly expressed in haematopoietic cells. (A) Verification of new WBP1L rabbit antisera specificity on the lysates of HEK293 cells transfected or not with WBP1L construct. (B) Western blot analysis of WBP1L expression in murine leucocyte subsets. T cells (CD3$^+$), B cells (CD43$^-$, CD11b$^-$) and neutrophils (Ly6G$^+$) were isolated from the spleen or bone marrow. Bone marrow-derived macrophages (BMDM) and bone marrow-derived dendritic cells (BMDC) were differentiated in vitro from murine bone marrow. N = 3. (C) Expression of WBP1L in BCP-ALL cell lines was probed using size exclusion chromatography-microsphere-based affinity Proteomics method. Expression in *ETV6-RUNX1*$^+$ B cell line REH and *ETV6-RUNX1*$^-$ lines TOM-1, NALM-6, NALM-24, RS4.11 and SUB B15 was probed by two antibody clones to WBP1L (OPAL-01, OPAL-02) and quantified as an area under the curve on parts of chromatograms representing fractions corresponding to WBP1L (N = 1 per antibody clone). (D) Expression of *WBP1L* mRNA in different *ETV6-RUNX1*$^{-/-}$ REH clones from two independent sources of REH cells. Data are plotted as $2^{-\Delta ct}$ (N = 3). (E) Schematic representation of WBP1L structure and conserved sequence motifs (F) Analysis of WBP1L glycosylation in BMDM. BMDM treated or not with 1 or 10 µmol/L tunicamycin (overnight) were subjected to WBP1L immunoprecipitation followed by immunoblotting with WBP1L antisera. β-actin was stained in the corresponding cell lysates (N = 2). Irrelevant lines from the blot image were removed and replaced with a vertical dividing line. (G) Analysis of palmitoylation of WBP1L. HEK293 cells expressing WBP1L-FLAG-STREP were metabolically labelled with palmitate analogue 17ODYA and lysed. 17ODYA labelled proteins were tagged in a click chemistry reaction with biotin-azide, purified on streptavidin-coupled beads and analysed for the presence of WBP1L with anti-FLAG antibody (upper panel) or FLOTILLIN-2 as a representative of endogenous palmitoylated proteins (middle upper panel). WBP1L expression in cell lysates (middle lower panel) and comparable loading were verified by immunoblotting with antibodies to FLAG-tag (WBP1L) or FLOTILLIN-2, respectively (N = 3)

2.6 | Statistics

Results represent means ± SEM. If not specified otherwise, P-values were calculated using two-tailed Student's t test, one-way ANOVA or Q test. N represents number of animals or values per group or number of independent experiments.

3 | RESULTS

3.1 | WBP1L is a palmitoylated glycoprotein broadly expressed in haematopoietic cells

Analysis of WBP1L protein and mRNA expression in murine and human haematopoietic system with a newly generated polyclonal rabbit antibody (Figure 1A) and with Genevestigator tool, respectively, revealed that WBP1L is broadly expressed across multiple human and murine haematopoietic cell subsets (Figure 1B and S1). In addition and in agreement with previous reports of deregulated WBP1L expression in ETV6-RUNX1+ BCP-ALL, we have found elevated levels of WBP1L protein in REH cell line, which is derived from ETV6-RUNX1+ BCP-ALL. (Figure 1C and S2A). Interestingly, the genetic deletion of ETV6-RUNX1 in

REH cells (Figure S2B,C) did not alter WBP1L expression in these cells (Figure 1D).

Imaging of murine bone marrow-derived macrophages transduced with retroviral vector coding for murine WBP1L fused to EGFP revealed relatively broad distribution of WBP1L-EGFP within these cells. We have observed co-localization with plasma membrane, Golgi, endoplasmic reticulum, and to a limited extent with lysosomes and/or other acidic organelles (Figure S3). On the other hand, no co-localization with mitochondria could be detected (Figure S3).

The N-terminal part of WBP1L protein is highly conserved among major vertebrate classes (Figure S4). This region contains several conserved motifs, including potential N-glycosylation (NXS) and palmitoylation sites (Figure 1E and S4). Indeed, we could confirm that WBP1L is both glycosylated and palmitoylated (Figure 1F,G).

3.2 | WBP1L interacts with NEDD4-family E3 ubiquitin ligases

Cytoplasmic part of WBP1L contains three WW domain binding motifs ([L/P]PXY) (Figure 1E and S4). It has been speculated that they may interact with WW domains of NEDD4-family ubiquitin ligases.[11]
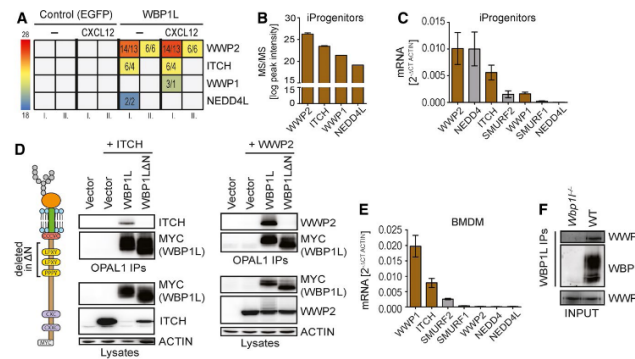

FIGURE 2 WBP1L binds multiple NEDD4-family E3 ubiquitin ligases. (A) Data from two independent mass spectrometry analyses (I. and II.) of WBP1L binding partners. Wbp1l−/− monocyte/macrophage progenitors were transduced with the constructs coding for WBP1L-FLAG-STREP or EGFP with the same tag. The cells were stimulated for 2 min with CXCL12 or left untreated. Tagged proteins with their binding partners were isolated by tandem purification and subjected to mass spectrometry analysis. The data are presented as colour-coded intensities obtained by label-free quantification of NEDD4-family E3 ubiquitin ligases. Values represent number of peptides used for intensity calculation/ number of unique peptides. Samples, where no peptides from a particular E3 ligase were detected, are coloured in grey (B) Label-free quantification of interacting E3 ligases from mass spectrometry experiment. Combined average intensities from both CXCR4 stimulated and non-stimulated samples are plotted (experiment I. form (A) only). (C) mRNA expression of NEDD4-family E3 ubiquitin ligases in immortalized monocyte/macrophage progenitors (iProgenitors). Plotted in brown are those ligases that interacted with WBP1L in mass spectrometry experiments (N = 3). (D) WBP1L interaction with NEDD4-family E3 ligases is dependent on WW binding motifs in WBP1L N-terminus. HEK293 cells were transfected with WBP1L-Myc or WBP1LΔN-Myc (with segment containing all WW binding motifs deleted) together with ITCH or WWP2. Following WBP1L immunoprecipitation, the isolated material and the original lysates were immunoblotted with antibody to ITCH or WWP2 and various controls as indicated (N = 3). (E) mRNA expression of NEDD4-family E3 ligases in BMDM. Plotted in brown are those ligases that interacted with WBP1L in mass spectrometry experiment (N = 3). (F) Endogenous interaction of WBP1L with WWP1 in BMDM. WBP1L immunoprecipitates from WT or Wbp1l−/− BMDM were immunoblotted with antibody to WWP1 and WBP1L. Input lysates were probed with antibody to WWP1 (N = 3). See also Figure S5
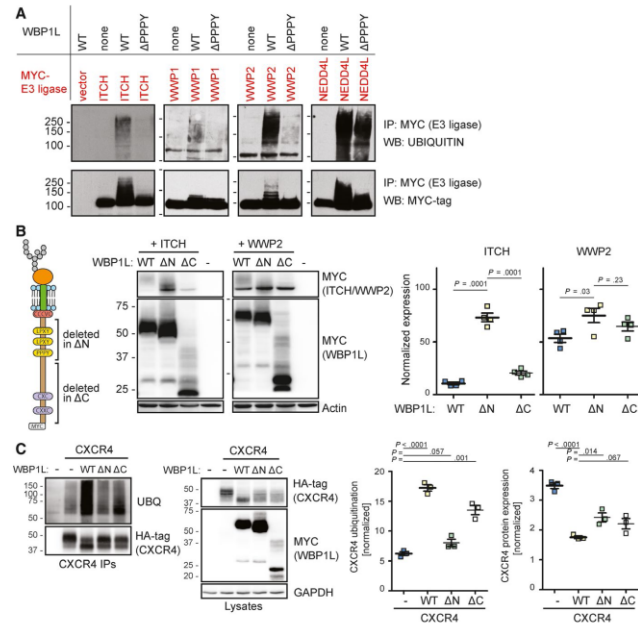
FIGURE 3 WBP1L regulates ubiquitination and expression of NEDD4-family E3 ubiquitin ligases and CXCR4. (A) HEK293 cells were cotransfected with individual Myc-tagged NEDD4-family E3 ubiquitin ligases and non-tagged WBP1L or its mutant lacking PPPY WW domain interacting motif. E3 ligases were immunoprecipitated via the Myc-tag from the lysates of these cells and subjected to immunoblotting with anti-MYC-tag or anti-UBIQUITIN antibody. (B) ITCH and WWP2 stability in HEK293 cells in the presence of WBP1L-MYC, WBP1L ΔC-MYC (deletion of almost entire intracellular part of WBP1L except for WW binding motifs) or WBP1L ΔN-MYC (deletion of WW binding motifs). Lysates from HEK293 cells transfected with ITCH-MYC or WWP2-MYC and WBP1L constructs were immunoblotted with antibody to MYC-tag to visualize ITCH, WWP2 and all forms of WBP1L and with antibody to ACTIN. Quantifications of the data are plotted as values normalized to ACTIN signal and then further normalized to experiment average to allow for comparison among the experiments (N = 3). (C) WBP1L-mediated increase in CXCR4 ubiquitination and down-regulation of CXCR4 protein levels in HEK293 cells. WBP1L-MYC, WBP1LΔC-MYC or WBP1LΔN-MYC were cotransfected with CXCR4-HA followed by CXCR4 imunoprecipitation and immunoblotting with antibodies to ubiquitin or HA-tag. Lysates were probed with antibodies to HA-tag (CXCR4), MYC-tag (WBP1L) or GAPDH (N = 3). For quantification, ubiquitination was normalized to HA-tag (CXCR4) signal (left panel) and CXCR4 expression to GAPDH (right panel). Both were further normalized to experiment average to allow for comparison among the individual experiments

However, this family has nine different members. To investigate whether WBP1L interacts with any of these ligases, we have expressed a FLAG-STREP-tagged WBP1L construct in immortalized monocyte/macrophage progenitors. We have selected this cell type because of a relatively high level of *Wbpl1* mRNA in myeloid progenitors (Figure S1). We isolated the FALG-STREP-tagged construct together with its associated binding partners from the lysates of these cells via a tandem purification on anti-FLAG and Streptactin beads. Mass spectrometry analysis of the isolated material revealed that WBP1L indeed interacts with several members of NEDD4-family. In this particular cell type, WWP2 was the most prominent. However, ITCH, WWP1 and NEDD4L could also be detected in one experiment (Figure 2A). Interestingly, the mass spectrometry signal intensities corresponded to the relative expression levels of these NEDD4-family members in immortalized monocyte/macrophage progenitors (Figure 2B,C). On the

other hand, not all NEDD4-family members expressed in these cells could be co-isolated with WBP1L. These data suggest a certain level of WBP1L selectivity for individual NEDD4-family members.

To find out whether NEDD4-family ligases bind WBP1L via its [L/P]PXY WW domain binding motifs we have co-expressed the two highest scoring NEDD4-family ligases from the mass spectrometry experiment, WWP2 or ITCH, with wild-type WBP1L construct or with mutant WBP1LΔN lacking the membrane-proximal WW domain binding sequences (Figure 2D) in HEK293 cells. These cells allow for relatively high level of overexpression, which was ideal for reliable identification of NEDD4 family binding sites in WBP1L. Both E3 ligases could be readily co-immunoprecipitated with wild-type WBP1L but not with WBP1LΔN (Figure 2D). These data were further confirmed in a similar experiment in J774 macrophage-like cell line, which expresses relatively high level of

ITCH (not shown). The endogenous ITCH could be co-isolated with wild-type WBP1L but not with WBP1LΔN from these cells (Figure S5). To confirm the interaction of WBP1L with a NEDD4-family member at the endogenous protein level, we have selected bone marrow-derived macrophages (BMDM) which express the highest levels of WBP1L among the cell types we have tested so far (Figure 1B). WWP1, which is the most abundant NEDD4-family member in this cell type (Figure 2E), could be co-isolated with WBP1L in this experiment (Figure 2F).

3.3 | WBP1L regulates ubiquitination and expression level of NEDD4-family E3 ubiquitin ligases and of CXCR4

Interaction with WW domain binding motifs is known to result in the activation and autoubiquitination of NEDD4-family ubiquitin ligases.[14,15] To test whether WBP1L can activate NEDD4 family members, we have cotransfected WBP1L-interacting (Figure 2A) NEDD4-family ligases with wild-type WBP1L, or its mutant lacking one of the conserved WW domain binding motifs, into HEK293 cells. This analysis demonstrated that cotransfection with wild-type but not mutant WBP1L resulted in a substantial increase in ubiquitination of all these ligases, which is a sign of their activation (Figure 3A). Published work suggests that in the case of ITCH this ubiquitination results in down-regulation of its protein levels, while WWP2 appears

relatively resistant to this negative feedback regulation. Thus, to further explore the mechanism of how WBP1L regulates these ubiquitin ligases, we co-expressed wild-type WBP1L, WBP1LΔN or WBP1LΔC (lacking C-terminal region of unknown function) with ITCH or WWP2 in HEK293 cells. Co-expression of ITCH with wild-type WBP1L and WBP1LΔC resulted in significantly reduced ITCH protein level when compared to co-expression with WBP1LΔN. As expected, this effect was much more limited in case of WWP2 (Figure 3B).

One of the best-studied targets of NEDD4-family ubiquitin ligases in the haematopoietic system is the chemokine receptor CXCR4. It is involved in the maintenance of haematopoietic stem and progenitor cells and in promoting niche interactions in the bone marrow. It is also thought to support the survival and treatment resistance of leukaemic cells.[16,17] Based on these features, we have selected CXCR4 for a similar set of experiments to test whether WBP1L regulates its protein expression levels and ubiquitination. Indeed, co-expression of WBP1L with CXCR4 in HEK293 cells resulted in increased ubiquitination of CXCR4 (presumably by an endogenous NEDD4-family ligase). This effect was almost completely abolished by mutation of the WW domain binding motifs (WBP1LΔN) while deletion of the C-terminal sequence (WBP1LΔC) had a more limited by reduction in CXCR4 protein levels (Figure 3C). We also observed effect (Figure 3C). CXCR4 ubiquitination was further accompanied that WBP1L co-expression resulted in a striking increase in CXCR4 electrophoretic mobility (Figure 3C). The reason for this mobility shift is at present unknown.
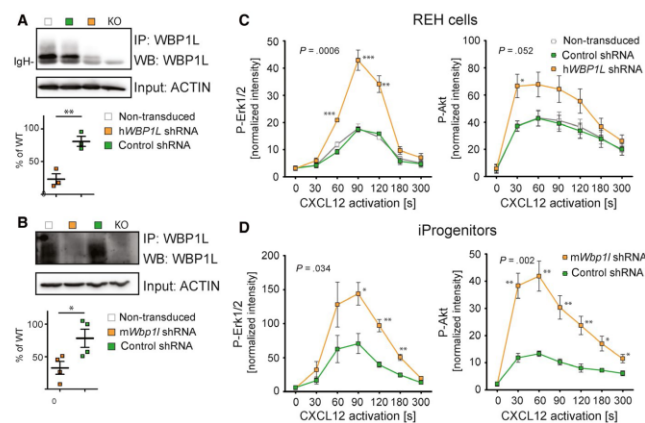

FIGURE 4 ShRNA-mediated down-regulation of WBP1L results in enhanced CXCR4 signalling in human and murine cell lines. (A, B) WBP1L immunoprecipitates from REH cells (A) or immortalized monocyte/macrophage progenitors (B) transduced with *Wbp1l* shRNA were stained with WBP1L antisera to demonstrate WBP1L down-regulation. Equal input of lysates to immunoprecipitation was verified by ACTIN immunoblotting. Quantification of multiple experiments (after normalization to ACTIN signal) was plotted as a percentage of WBP1L expression in non-transduced cells. (C, D) ERK1/2 and AKT phosphorylation downstream of CXCR4 in REH cells (C) and immortalized monocyte/macrophage progenitors (iProgenitors) (D), where WBP1L was down-regulated by shRNA. Cells were stimulated with 100 nmol/L CXCL12, lysed and subjected to Western blot analysis of ERK1/2 and AKT phosphorylation. Data represent mean of fluorescence intensity normalized to GAPDH. The *P*-value was calculated to compare maximum responses of cells transduced with non-silencing control and silencing shRNA. Asterisks denote significant differences in individual time-points. (N = 4)
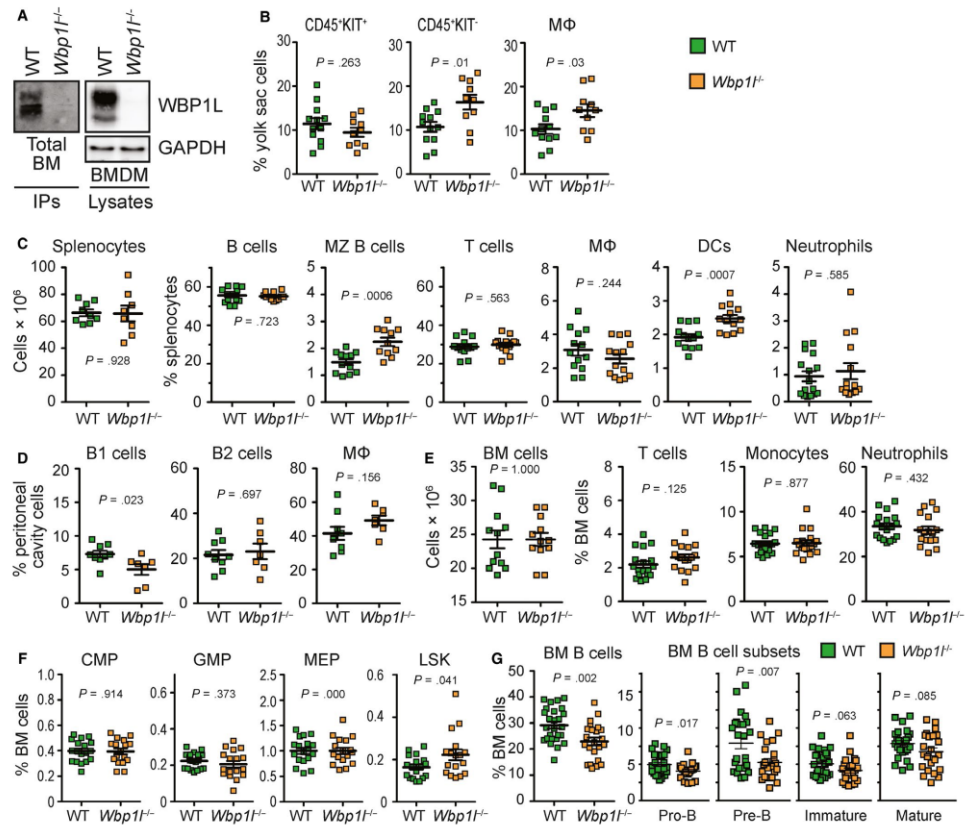
FIGURE 5 Altered leucocyte homeostasis in WBP1L-deficient mice. (A) Western blot analysis of WBP1L immunoprecipitates or whole cell lysates prepared from WT and $Wbp1l^{-/-}$ cells. mOPAL-01/03 antibodies were used for immunoprecipitation and WBP1L rabbit antisera for Western blotting. N = 3 (bone marrow), N = 5 (BMDM). (B) Flow cytometry analyses of E10.5 WT and $Wbp1l^{-/-}$ yolk sac cell subsets. Primitive macrophages were defined as Ter119$^-$ CD11b$^+$ F4/80$^+$. (C) Absolute numbers of splenocytes obtained from WT and $Wbp1l^{-/-}$ mice and flow cytometry analyses of WT and $Wbp1l^{-/-}$ splenocytes defined using the following markers: B cells (B220$^+$), MZ B cells (B220$^+$, AA4.1$^-$, CD23$^{-/low}$, CD1d$^+$), T cells (CD3$^+$), macrophages (F4/80$^+$, CD11b ^{int}), DC (CD11c$^+$, LY6C$^{-/low}$) and neutrophils (LY6G$^+$, CD11b$^+$, LY6C$^-$). (D) Flow cytometry analyses of WT and $Wbp1l^{-/-}$ leucocytes in the peritoneum, defined using the following markers: B1 cells (SSC^{low}, FSC^{low}, B220$^+$, CD23$^{-/low}$), B2 cells (SSC^{low}, FSC^{low}, B220$^+$, CD23$^+$) and macrophages (large peritoneal macrophages, CD11b^{high}, F4/80^{high}). (E) Flow cytometry analyses of WT and $Wbp1l^{-/-}$ bone marrow cell subsets, defined using the following markers: T cells (CD3$^+$), monocytes (LY6C$^+$, CD11b$^+$, LY6G$^-$, CD19$^-$, TER119$^-$, CD3$^-$, NK1.1$^-$), neutrophils (KIT$^-$, B220$^-$, TER119$^-$, CD3$^-$, LY6G^{high}) (F) Flow cytometry analyses of stem and progenitor cells in the bone marrow. Cell subsets were defined using following markers: common myeloid progenitors—CMP (lin$^-$, c-kit$^+$, CD34$^+$, CD16/32$^{neg-low}$, SCA1$^-$), granulocyte-monocyte progenitors—GMP (lin$^-$, KIT$^+$, CD34$^+$, CD16/32^{High}, SCA1$^-$), megakaryocyte-erythroid progenitors—MEP (lin$^-$, KIT$^+$, CD34$^-$, CD16/32$^-$, SCA1$^-$) and LSK (lin$^-$, KIT$^+$, SCA1$^+$). (G) Flow cytometry analysis of bone marrow B cell subsets. B cells (B220$^+$), pro-B cells (CD43$^+$, B220$^+$, IgM$^-$), pre-B cells (CD43$^-$, B220^{low}, IgM$^-$), immature B cells (CD43$^-$, B220^{low}, IgM$^+$) and mature B cells (CD43$^-$, B220^{high}, IgM$^+$)

3.4 | WBP1L inhibits CXCR4 signalling in murine and human cell lines

To analyse the effects of the endogenous WBP1L on CXCR4, we have selected two cell lines where the expression of WBP1L and/ or CXCR4 is highly relevant. These included human leukaemic cell line REH as a representative of $ETV6$-$RUNX1^+$ leukaemia, where we have down-regulated WBP1L by a single shRNA specific for human $WBP1L$ and immortalized murine monocyte/macrophage progenitors as a representative of bone marrow progenitors, where

we used a different shRNA targeting murine *Wbp1l* (Figure 4A,B). After stimulation with CXCR4 ligand CXCL12, these cells showed enhanced activity of downstream signalling pathways, resulting in increased phosphorylation of ERK1/2 and AKT (Figure 4C,D and S6). CXCR7, another known receptor for CXCL12, did not contribute to the signalling output under these conditions (Figure S7). These data demonstrated that WBP1L is involved in the negative regulation of CXCR4 signalling.

3.5 | Altered haematopoiesis in *Wbp1l*-deficient mice

To further analyse the physiological function of WBP1L, we have acquired *Wbp1l*-deficient mouse strain *Wbp1l*[tm2a(EUCOMM)Hmgu] (hereafter referred to as *Wbp1l*^{−/−}) from the International Mouse Phenotyping Consortium. These mice appeared grossly normal and healthy, were born in normal Mendelian ratios and did not express WBP1L protein (Figure 5A).

To characterize the haematopoietic system in *Wbp1l*^{−/−} mice, we have analysed major cell subset frequencies in adult mice and in

embryos. The embryonic haematopoietic cell numbers were grossly normal with small increases in the yolk sac CD45^{+} KIT^{−} cells and CD11b^{+} F4/80^{+} yolk sac macrophages (Figure 5B). In the peripheral tissues of the adult mice, there was a significant increase in marginal zone B cell fraction in the spleen (Figure 5C) and a reduction in B1 cell percentages in the peritoneal cavity (Figure 5D). We also observed increased frequencies of splenic dendritic cells in *Wbp1l*^{−/−} mice (Figure 5C). Otherwise, the frequencies of other leucocyte subsets found in peripheral tissues were normal (Figure 5C,D). Bone marrows from *Wbp1l*^{−/−} animals showed the same cell counts as wild-type bone marrows (Figure 5E). Most of bone marrow cell subsets were also found in normal numbers, including T cells, monocytes, neutrophils (Figure 5E) and the majority of progenitor populations (Figure 5F). However, there were two notable exceptions. First, the overall B cell percentages in the bone marrow were significantly reduced (Figure 5G). The reduction was most pronounced in early developmental stages (pro- and pre-B cells). At the later stages, including immature and mature B cells a similar trend was observed, but it was outside the threshold for statistical significance (*P*-values .06 and .08, respectively) (Figure 5G). The cell cycle of B cell progenitors was not substantially changed with the exception of a very
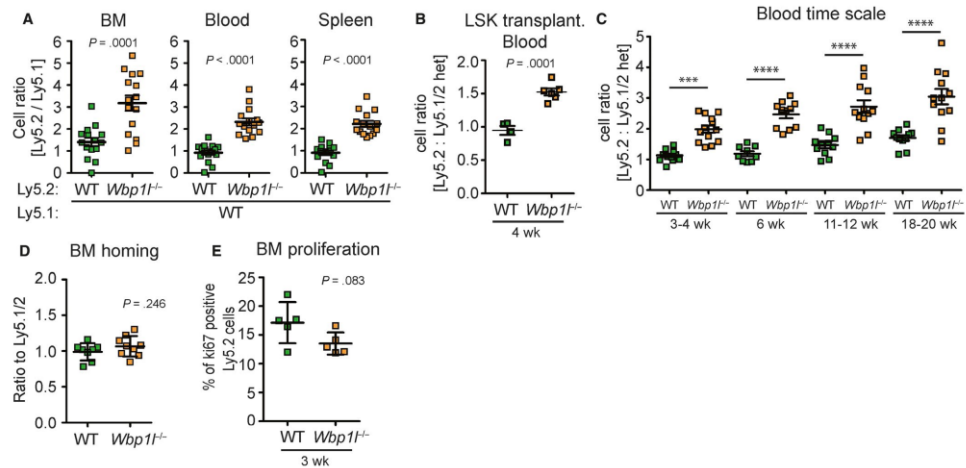

FIGURE 6 Enhanced engraftment of *Wbp1l*^{−/−} bone marrow. (A) Ly5.2[+] bone marrow (WT or *Wbp1l*^{−/−}) was mixed with Ly5.1[+] bone marrow (always WT) in a ratio 1:1 and 2 × 10^{6} cells were transplanted into Ly5.1 lethally irradiated mice. Mice were analysed 2 months post-transplantation. Flow cytometry analyses show the ratio between Ly5.2 and Ly5.1 cells in the bone marrow, blood and spleen. (B) LSK cells sorted from Ly5.2[+] bone marrow (WT or *Wbp1l*^{−/−}) were mixed with LSK from Ly5.1/Ly5.2[+] heterozygous bone marrow (always WT) in a ratio 1:1 and 20 000 cells together with support of 0.5 × 10^{6} Ly5.1 bone marrow cells were injected into tail vain of Ly5.1 lethally irradiated mice. Data represent the ratio between Ly5.2[+] and Ly5.1/Ly5.2^{+} cells detected in the recipient blood 4 wk post injection. One of two independent experiments is shown (N ≥ 8). (C) Ly5.2[+] bone marrow (WT or *Wbp1l*^{−/−}) was mixed with Ly5.1/Ly5.2[+] heterozygous bone marrow (always WT) in a ratio 1:1 and 2 × 10^{6} cells were transplanted into Ly5.1 lethally irradiated mice. At indicated time-points, the ratio between Ly5.2 and Ly5.1/Ly5.2 cells in blood was measured by flow cytometry. (D) Homing of WT and *Wbp1l*^{−/−} bone marrow cells in a competitive set-up. WT or *Wbp1l*^{−/−} bone marrow (Ly5.2[+]) was each combined with WT bone marrow from Ly5.1/Ly5.2[+] heterozygotes in a ratio 1:1 and 2 × 10^{6} cells were injected into the tail vain of sublethally irradiated recipient (Ly5.1[+]). Data represent the ratio between Ly5.2[+] and Ly5.1/Ly5.2^{+} cells detected in the recipient bone marrow 16 h post injection (N ≥ 8). (E) Competitive bone marrow transplantation was performed as in (C) and 3 wk after the transplantation expression of Ki67 proliferation marker was measured in transplanted cells

small but significant increase in G1 phase pre-B cells in *Wbp1l*^{−/−} mice (Figure S8). Second, Lin⁻SCA1⁺KIT⁺ (LSK) cells encompassing early progenitors and stem cells (HSPC) showed slightly but significantly increased percentages in these animals (Figure 5F).

To test their functionality in vivo, we performed a competitive bone marrow transplantation assay, whereby we mixed wild-type or *Wbp1l*^{−/−} Ly5.2 cells with wild-type Ly5.1 bone marrow cells in a 1:1 ratio and transplanted these mixtures into lethally irradiated recipient mice (Ly5.1). Nine weeks later, we have analysed their engraftment. Strikingly, *Wbp1l*^{−/−} bone marrow engrafted significantly better and the ratio between *Wbp1l*^{−/−} and wild-type cells increased from 1:1 to ca 3:1 (Figure 6A), whereas wild-type Ly5.2 and Ly5.1 BM engrafted with equal efficiency. The difference could be observed across all bone marrow leucocyte subsets analysed except for LSK cells, where a similar trend in favour of *Wbp1l*^{−/−} cells was also present but was not statistically significant (Figure S9). The difference was also maintained in the periphery, where the ratio between *Wbp1l*^{−/−} and wild-type cells was roughly 2:1 (Figure 6A). Similar difference in engraftment efficiency was also observed when we transplanted sorted LSK cells in the 1:1 ratio (Figure 6B). Next, we investigated how this ratio changes with time. A significant difference between the engraftment efficiency could be observed as early as 3 weeks after the transplantation and was maintained till at least 18 weeks after the transplantation (Figure 6C). The increased efficiency in the bone marrow engraftment was not the result of increased homing to the bone marrow or increased proliferation, which did not display any alteration (Figure 6D,E). Collectively, these data are showing negative role of WBP1L in HSPC function. Persistence of the engraftment advantage for more than 16 weeks suggests that the haematopoietic system is affected already at the level of haematopoietic stem cells.

3.6 | Compensatory mechanisms restore CXCR4 signalling when WBP1L is lost in the germline, but the effects of WBP1L deficiency on CXCR4 signalling can be observed upon its acute deletion

Part of the data described above are consistent with CXCR4 hyperactivity. However, the same homing capacity of the wild-type and *Wbp1l*^{−/−} bone marrow cells (Figure 6D) is incompatible with enhanced CXCR4 function. These results prompted us to test whether bone marrow cells from *Wbp1l*^{−/−} mice display similar CXCR4 dysregulation as shRNA-treated cell lines. Surprisingly, we did not observe any alterations in CXCL12-triggered ERK phosphorylation in bone marrow cells from *Wbp1l*^{−/−} mice (Figure 7A). This result was in disagreement with our analysis of the effects of shRNA-mediated WBP1L down-regulation in cell lines (Figure 4). To exclude the possibility that enhanced CXCR4 signalling observed there was the result of non-specific off-target effects of *Wbp1l* shRNAs, we expressed shRNA targeting *Wbp1l* in immortalized monocyte/macrophage progenitors from wild-type and *Wbp1l*^{−/−} mice. Because of the absence of WBP1L, only non-specific activity of *Wbp1l* shRNA can be detected in *Wbp1l*^{−/−} progenitors. As
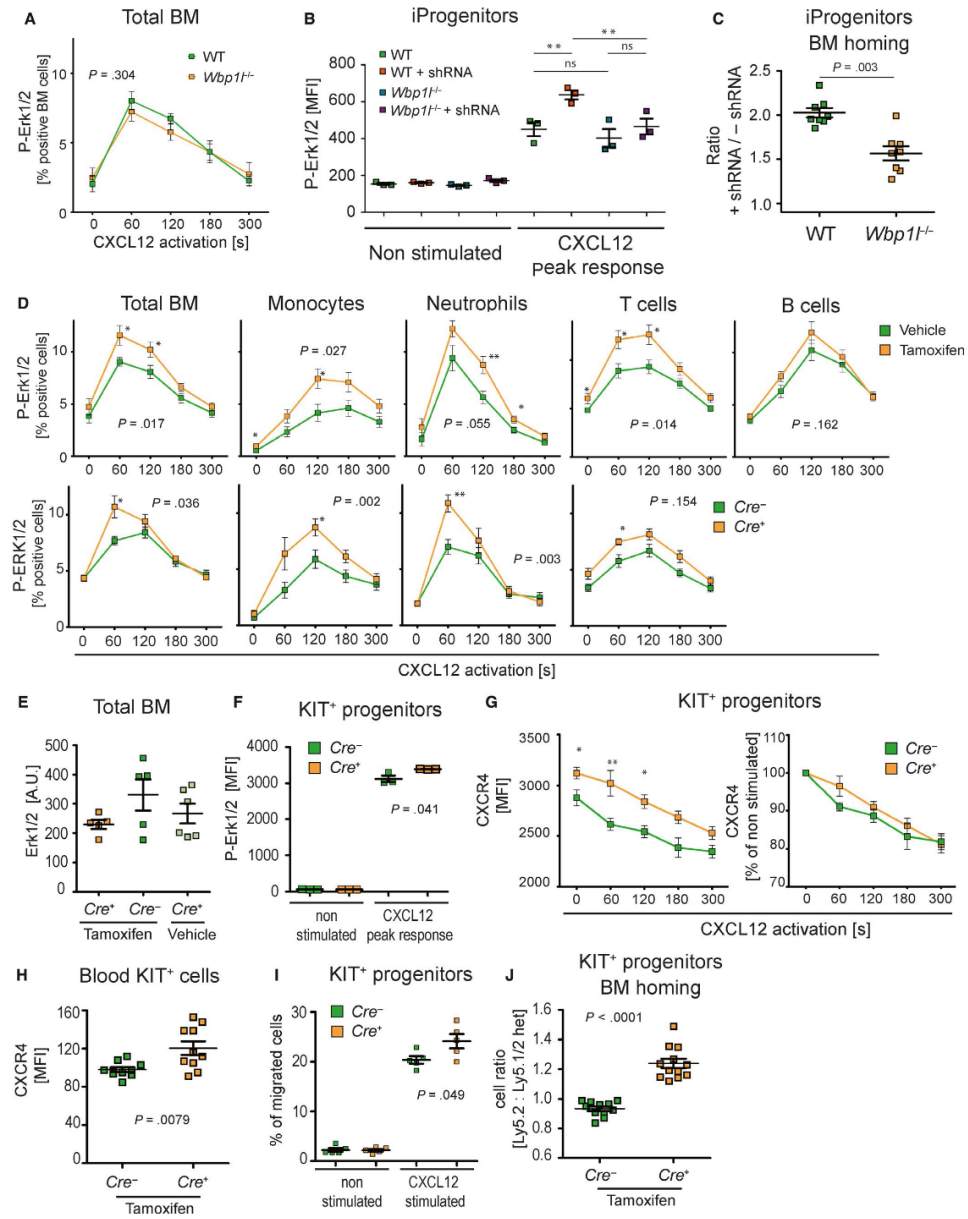
expected, *Wbp1l* shRNA significantly enhanced CXCL12-triggered ERK activation in wild-type cells. On the other hand, only negligible insignificant changes were detected in *Wbp1l*^{−/−} cells (Figure 7B). These results demonstrated that the effects of *Wbp1l* shRNA are dependent on *Wbp1l* and, thus, specific. When we used the same cells in an in vivo homing experiment, we observed that WBP1L down-regulation significantly enhanced bone marrow homing of wild-type cells, when compared to *Wbp1l*^{−/−} cells (Figure 7C). This outcome is consistent with the results of our in vitro analyses showing that WBP1L negatively regulates activity of CXCR4.

To definitely prove the validity of our shRNA data, we have generated a mouse strain *Wbp1l*^{fl/fl}-*CreERT* where the *Wbp1l* gene can be acutely inactivated upon injection of 4OH-tamoxifen. Acute *Wbp1l* deletion in this model resulted in enhanced ERK phosphorylation in response to CXCL12 stimulation in total bone marrow as well as in several major subsets, including T cells, monocytes and neutrophils, whereas in B cells, the difference was small and not statistically significant (Figure 7D and S10). No effects of WBP1L deficiency on total ERK expression were observed (Figure 7E). The enhanced CXCR4 signalling did not translate to any immediate effect on steady-state numbers of major bone marrow and splenic cell subsets (Figure S11A). However, it is likely that only much more substantial increase in CXCR4 signalling would be needed to alter leucocyte bone marrow retention within this timescale.

The data presented above suggested that the effects of WBP1L down-regulation can only be observed after its acute deletion. To further address this possibility, we have established primary culture of isolated KIT⁺ bone marrow cells from *Wbp1l*^{fl/fl}-*CreERT* mice, where *Wbp1l* could be deleted by 4OH-tamoxifen. Importantly, cells cultured outside the bone marrow are not exposed to continuous CXCL12 stimulation and desensitization and are, thus, having high expression of CXCR4 and stronger signalling capacity. In agreement with our previous observations, after acute *Wbp1l* deletion by CRE recombinase (but not after germline deletion), these progenitors showed increased ERK phosphorylation in response to CXCL12 stimulation (Figure 7F and S11B). *Wbp1l* deletion also resulted in an increase in steady-state CXCR4 surface expression with no other effects on the rate of CXCL12-triggered receptor internalization in these cells (Figure 7G and S11C). The same increase in CXCR4 expression was also observed on KIT⁺ progenitors from peripheral blood of animals after acute *Wbp1l* deletion (Figure 7H). Similar, though not significant, trend was also observed when CXCR4 was measured on fixed and permeabilized cells (Figure S11D). Finally, cells with acute *Wbp1l* deletion showed increased migration towards CXCR4 ligand CXCL12 in a transwell assay in vitro (Figure 7I) and increased bone marrow homing efficiency in vivo (Figure 7J). These data confirm that WBP1L negatively regulates CXCR4 expression and signalling in primary cells.

4 | DISCUSSION

Expression of the *WBP1L* gene is heightened in *ETV6-RUNX1*⁺ paediatric BCP-ALL and was shown to correlate with favourable

A Total BM

B iProgenitors

C iProgenitors BM homing

D Total BM · Monocytes · Neutrophils · T cells · B cells

E Total BM

F KIT+ progenitors

G KIT+ progenitors

H Blood KIT+ cells

I KIT+ progenitors

J KIT+ progenitors BM homing

treatment response.[1-3] However, the function of its protein product WBP1L in healthy and leukaemic cells has not been investigated. Here, we attempted to uncover its physiological function. Our initial analysis shows that WBP1L binds several NEDD4-family E3 ubiquitin ligases and its deficiency results in augmented surface expression and signalling of CXCR4, one of their known target proteins.

FIGURE 7 Acute loss of WBP1L results in enhanced CXCR4 signalling but germline deficiency is compensated for. (A) ERK1/2 phosphorylation downstream of CXCR4 in WT and $Wbp1l^{-/-}$ (germline deletion) bone marrow cells. Cells were stimulated with 100 nmol/L CXCL12, fixed, stained for phosphorylated ERK1/2 and analysed by flow cytometry. Data represent percentage of responding cells (N = 6). P-value was calculated for maximum response of WT and $Wbp1l^{-/-}$ cells regardless of the time-point where it was reached. (B) Erk1/2 activation after CXCL12 stimulation (100 nmol/L) of immortalized monocyte/macrophage progenitors (iProgenitors) from WT and $Wbp1l^{-/-}$ mice and of the same cells transduced with $Wbp1l$ shRNA. Erk phosphorylation was measured by flow cytometry of fixed and permeabilized cells stained with fluorescent P-Erk1/2 antibody. Peak response detected during 5 min measurement is shown. Data are represented as medians of fluorescence intensity (N = 3). P-values were calculated using 1way ANOVA with Bonferroni's multiple comparison test. (C) WT cells transduced or not with $Wbp1l$ shRNA were mixed 1:1 and their bone marrow homing ability was analysed as in Figure 6D. As a control $Wbp1l^{-/-}$ cells transduced or not with $Wbp1l$ shRNA and also mixed in a ratio 1:1 were used. Ratios of shRNA transduced and non-transduced cells are plotted for each genotype (n = 8). P-value was calculated for the differences between these two ratios. Significant outliers were discarded based on q test. As not all cells expressed shRNA containing vector after transduction, the true ratio was lower than 1:1 at the time of injection. The final data were normalized to this true ratio. (D) CXCR4 signalling in bone marrow cell subsets after acute deletion of $Wbp1l$. In the top row, $CreERT$ expressing cells treated either with tamoxifen or vehicle (corn oil) are compared. In the bottom row, the comparison is made between tamoxifen-treated $Wbp1l^{fl/fl}$-$CreERT$ and $Wbp1l^{fl/fl}$ (without $CreERT$) bone marrow cells. Cells were stimulated with 100 nmol/L CXCL12, fixed, stained for extracellular markers and intracellular P-ERK and analysed by flow cytometry. Data represent percentage of responding cells from whole bone marrow (N = 7), T cells (CD3+, N = 7/8), monocytes (Ly6C+ Ly6G−, N = 11) and neutrophils (Ly6G+ Ly6C−,N = 7). Significant outliers were discarded based on q test. P-value was calculated for maximum response (regardless of the time-point at which this maximum was reached). In addition, significant differences in individual time-points are labelled with asterisks. (E) Expression of total ERK1/2 in the bone marrow cells where $Wbp1l$ was deleted as in (D). Protein level was measured using Western blot. ERK1 and ERK2 were probed separately and signal was summed and normalized to actin loading control (N ≥ 5) (F). CXCR4 signalling in in vitro 4-hydroxytamoxifen treated KIT+ progenitors isolated from $Wbp1l^{fl/fl}$-$CreERT$ and $Wbp1l^{fl/fl}$ (without $CreERT$) bone marrow. ERK phosphorylation was measured after stimulation with 100 nmol/L CXCL12 by flow cytometry on fixed and permeabilized cells. Peak response detected during 5 min measurement is shown. One of two independent experiments is shown, N = 6. (G) CXCL12-induced changes of CXCR4 surface expression on KIT+ bone marrow progenitors. These cells were isolated from $Wbp1l^{fl/fl}$-$CreERT$ and $Wbp1l^{fl/fl}$ bone marrow, treated with 4-hydroxytamoxifen to induce $Wbp1l$ deletion and stimulated with CXCL12 for indicated time intervals. FACS data are plotted as median fluorescence intensities (left graph) or as percentage of expression level on non-stimulated cells (right graph) (n = 7). (H) CXCR4 expression on KIT+ progenitors detected in the blood of tamoxifen-treated $Wbp1l^{fl/fl}$-$CreERT$ and $Wbp1l^{fl/fl}$ mice. Significant outlier was discarded based on q test (N = 10). (I) Migration of 4-hydroxytamoxifen-treated KIT+ progenitors from $Wbp1l^{fl/fl}$-$CreERT$ and $Wbp1l^{fl/fl}$ mice towards 500 nmol/L CXCR4 in a transwell assay in vitro (N = 5). (J) Ly5.2+ KIT+ progenitors (from $Wbp1l^{fl/fl}$-$CreERT$ or $Wbp1l^{fl/fl}$ mice, treated with 4-hydroxytamoxifen) were mixed 1:1 with Ly5.1/Ly5.2+ heterozygous KIT+ progenitors from WT mice and 10^7 cells were injected into Ly5.1 sublethally irradiated recipients. After 16 h, the ratio between Ly5.2 and Ly5.1/Ly5.2 cells in the bone marrow was measured by flow cytometry (N ≥ 11)

At the organismal level, WBP1L deficiency resulted in perturbations in B cell development and increased ability of bone marrow stem and progenitor cells to reconstitute haematopoietic system after the bone marrow transplantation. In addition, acute $Wbp1l$ deletion resulted in increased progenitor homing to the bone marrow. How much of this phenotype can be attributed to CXCR4 hyperactivity is still an open question. There are at least two other mouse models that show increased CXCR4 activity. One of these strains carries a mutation in CXCR4 that prevents its desensitization and down-regulation ($CXCR4^{WHIM}$). The same mutation in humans causes immunodeficiency known as WHIM syndrome.[18-20] $CXCR4^{WHIM}$ mice display a similar selective dysregulation in the bone marrow B cell compartment as $Wbp1l^{-/-}$ mice with the reduction in B cell percentages that is most profound at the B cell progenitor level.[20] They also show increase in marginal zone B cell percentages. On the other hand, some of their symptoms were not detected in $Wbp1l^{-/-}$ mice, including blood neutropenia and lymphopenia and reduced spleen size.[20] Increased CXCR4 expression and CXCR4-mediated signalling were also observed in mice deficient in the expression of BAR domain containing adaptor protein Missing In Metastasis (MIM). In these animals, leucocyte development and percentages appeared largely normal and no leukopenia has been observed. Rather they showed slightly increased white blood cell counts and splenomegaly.[21,22] Even though MIM deficiency has a number of CXCR4-independent

effects, these data show that enhanced CXCR4 activity does not have to lead to leukopenia in the peripheral tissues, nor to major alterations in leucocyte subset numbers and frequencies in the bone marrow. It is possible that the lack of receptor desensitization rather than alterations in peak signal intensity may be the key factor driving peripheral leukopenia in $CXCR4^{WHIM}$ mice.

Since in mice with germline $Wbp1l$ deletion we have not observed up-regulation in CXCR4 activity, it is difficult to unequivocally answer the question if alterations in $Wbp1l^{-/-}$ B cell development are caused by CXCR4 dysregulation. This phenotype is strikingly similar to the one observed in $CXCR4^{WHIM}$ animals. It is possible that not all haematopoietic cell subsets are able to compensate for the loss of WBP1L. Early B cell progenitors represent a relatively small population, and their WBP1L expression based on the data from ImmGen consortium[23] is similar to other B cell subsets (not shown). The options to analyse their CXCR4 signalling pathways are relatively limited. Those that can be analysed by flow cytometry, including ERK and STAT3 phosphorylation, as well as calcium response appear to be hypo/non-responsive in this particular cell type despite clearly measurable CXCR4 expression (not shown). As a result, B cell progenitors contribute very little to ERK phosphorylation of the entire B cell pool measured in our experiments where the more mature stages dominated the response. The other pathways we were not able to analyse in this relatively rare subpopulation and so it is still

possible that reduction in B cell progenitor numbers in $Wbp1l^{-/-}$ mice is caused by some aspect of CXCR4 signalling, which we could not measure.

WBP1L may also have other functions besides regulation of CXCR4. They may be responsible for a part of the phenotype of WBP1L-deficient cells and animals. WBP1L binds multiple NEDD4 family members and very likely other proteins, which can result in pleiotropic effects on leucocyte biology. It has been shown that in competitive transplantation assay HSPC with only one functional CXCR4 allele perform better than wild-type cells, which perform better than $CXCR4^{WHIM}$ cells, clearly showing an inverse correlation between CXCR4 activity and transplantation efficiency.[24,25] This observation is rather counterintuitive and opposite to the results we obtained with $Wbp1l^{-/-}$ cells. An explanation suggested in these studies was that CXCR4 promotes haematopoietic stem cell quiescence leading to competitive disadvantage when CXCR4 signalling is up-regulated. This leads to the conclusion that though CXCR4 role cannot be completely excluded by our experiments, effects of WBP1L on transplantation efficiency are likely CXCR4-independent. The molecular mechanism of how WBP1L regulates bone marrow engraftment will have to be addressed in future studies. On the other hand, functional effects of acute down-regulation of WBP1L are more clearly connected to CXCR4, leading to increased surface expression of CXCR4, increased CXCR4 signalling and improved homing efficiency, similar to mouse models with increased CXCR4 activity.

It is at present unclear what is the reason for the unequal effects of the acute and constitutive OPAL1 deletion on CXCR4 signalling. We can speculate that WBP1L may be rather general regulator of expression and/or activity of NEDD4 family ligases. However, there are many additional mechanisms regulating these enzymes. In the majority of cases, these might be able to compensate for the loss of WBP1L in the long-term. However, their ability to rapidly react to acute WBP1L loss would likely be more limited, as it may require changes in the gene expression pattern or other time-consuming adaptations.

Another important question is the role that WBP1L potentially plays in leukaemia. The $WBP1L$ gene is a target gene of ETV6, which suppresses its expression.[4] In $ETV6$-$RUNX1^+$ BCP-ALL, one allele of $ETV6$ is inactivated by fusion with $RUNX1$, while the other is often inactivated as well.[26] This could explain the increase of WBP1L expression in $ETV6$-$RUNX1^+$ BCP-ALL. It is also in agreement with our data showing that in REH cells (which already have both $ETV6$ alleles inactivated) $ETV6$-$RUNX1$ genetic deletion did not have any further effect on WBP1L expression. $ETV6$ inactivation likely represents part of the mechanism leading to the development of leukaemia and defining its features. In principle, WBP1L in this context can have two different functions. First, negative regulation of CXCR4 by WBP1L could dampen the interactions of leukaemic (stem) cells with protective bone marrow niches, making them more sensitive to treatment. Second, WBP1L may also have negative effect on leukaemic stem cells similar to its negative regulatory effects on HSPCs that were revealed in our competitive transplantation

experiment. Our data do not specifically address the role of WBP1L in leukaemia. However, the effects of WBP1L deficiency on normal haematopoiesis that we observed here and the fact that WBP1L is an ETV6 target gene make WBP1L a relevant target of future research in this field.

CONFLICT OF INTEREST

The authors confirm that there are no conflicts of interest.

AUTHOR CONTRIBUTIONS

SB, A.D and JK with contribution from MF, PA, JP, TS, NP and TB conducted majority of experiments and data analysis. DG performed microscopy analysis. IS carried out analysis of $Wbp1l^{-/-}$ embryos. OVM and KK analysed palmitoylation of WBP1L. V. Kanderova provided data on WBP1L expression in B cell lines. JS and PS generated ETV6-RUNX1-deficient REH cell line. MBP and MGT generated rabbit antisera to WBP1L. MAJ contributed to design and analysis of homing and competitive transplantation assays. V. Korinek contributed to the generation of $Wbp1l$-CreERT mouse strain. TB with

contribution from SB and AD conceptualized the study, evaluated the data and wrote the paper.

ORCID

Orest V. Matveichuk https://orcid.org/0000-0002-4057-7598
Majd B. Protty https://orcid.org/0000-0001-8992-9120
Tomas Brdicka https://orcid.org/0000-0002-1560-4398

REFERENCES

1. Mosquera-Caro M, Helman P, Veroff R, et al. Identification, validation and cloning of a novel gene (OPAL1) and associated genes highly predictive of outcome in pediatric acute lymphoblastic leukemia using gene expression profiling [abstract]. *Blood*. 2003;102:4a.
2. Holleman A, den Boer ML, Cheok MH, et al. Expression of the outcome predictor in acute leukemia 1 (OPAL1) gene is not an independent prognostic factor in patients treated according to COALL or St Jude protocols. *Blood*. 2006;108:1984-1990.
3. Kanderova V, Kuzilkova D, Stuchly J, et al. High-resolution antibody array analysis of childhood acute leukemia cells. *Mol Cell Proteomics*. 2016;15:1246-1261.
4. Neveu B, Spinella J-F, Richer C, et al. CLIC5: a novel ETV6 target gene in childhood acute lymphoblastic leukemia. *Haematologica*. 2016;101:1534-1543.
5. Lopez RG, Carron C, Oury C, Gardellin P, Bernard O, Ghysdael J. TEL is a sequence-specific transcriptional repressor. *J Biol Chem*. 1999;274:30132-30138.
6. Chakrabarti SR, Nucifora G. The leukemia-associated gene TEL encodes a transcription repressor which associates with SMRT and mSin3A. *Biochem Biophys Res Commun*. 1999;264:871-877.
7. De Braekeleer E, Douet-Guilbert N, Morel F, Le Bris MJ, Basinko A, De Braekeleer M. ETV6 fusion genes in hematological malignancies: a review. *Leuk Res*. 2012;36:945-961.
8. Rasighaemi P, Ward AC. ETV6 and ETV7: Siblings in hematopoiesis and its disruption in disease. *Crit Rev Oncol Hematol*. 2017;116:106-115.
9. Wang LC, Swat W, Fujiwara Y, et al. The TEL/ETV6 gene is required specifically for hematopoiesis in the bone marrow. *Genes Dev*. 1998;12:2392-2402.
10. Hock H, Meade E, Medeiros S, et al. Tel/Etv6 is an essential and selective regulator of adult hematopoietic stem cell survival. *Genes Dev*. 2004;18:2336-2341.
11. Pei J, Grishin NV. Unexpected diversity in Shisa-like proteins suggests the importance of their roles as transmembrane adaptors. *Cell Signal*. 2012;24:758-769.
12. Draber P, Kupka S, Reichert M, et al. LUBAC-recruited CYLD and A20 regulate gene activation and cell death by exerting opposing effects on linear ubiquitin in signaling complexes. *Cell Rep*. 2015;13:2258-2272.
13. Kralova J, Glatzova D, Borna S, Brdicka T. Expression of fluorescent fusion proteins in murine bone marrow-derived dendritic cells and macrophages. *J Vis Exp*. 2018;140:e58081. https://doi.org/10.3791/58081
14. Lorenz S. Structural mechanisms of HECT-type ubiquitin ligases. *Biol Chem*. 2018;399:127-145.
15. Mund T, Pelham HRB. Control of the activity of WW-HECT domain E3 ubiquitin ligases by NDFIP proteins. *EMBO Rep*. 2009;10:501-507.
16. Ayala F, Dewar R, Kieran M, Kalluri R. Contribution of bone microenvironment to leukemogenesis and leukemia progression. *Leukemia*. 2009;23:2233-2241.
17. de Lourdes PA, Amarante MK, Guembarovski RL, de Oliveira CEC, Watanabe MAE. CXCL12/CXCR4 axis in the pathogenesis of acute lymphoblastic leukemia (ALL): a possible therapeutic target. *Cell Mol Life Sci*. 2015;72:1715-1723.
18. Hernandez PA, Gorlin RJ, Lukens JN, et al. Mutations in the chemokine receptor gene CXCR4 are associated with WHIM syndrome, a combined immunodeficiency disease. *Nat Genet*. 2003;34:70-74.
19. Kawai T, Malech HL. WHIM syndrome: congenital immune deficiency disease. *Curr Opin Hematol*. 2009;16:20-26.
20. Balabanian K, Brotin E, Biajoux V, et al. Proper desensitization of CXCR4 is required for lymphocyte development and peripheral compartmentalization in mice. *Blood*. 2012;119:5722-5730.
21. Zhan T, Cao C, Li L, Gu N, Civin CI, Zhan X. MIM regulates the trafficking of bone marrow cells via modulating surface expression of CXCR4. *Leukemia*. 2016;30:1327-1334.
22. Yu D, Zhan XH, Zhao XF, et al. Mice deficient in MIM expression are predisposed to lymphomagenesis. *Oncogene*. 2012;31:3561-3568.
23. Heng TS, Painter MW. The Immunological Genome Project: networks of gene expression in immune cells. *Nat Immunol*. 2008;9:1091-1094.
24. McDermott DH, Gao JL, Liu Q, et al. Chromothriptic cure of WHIM syndrome. *Cell*. 2015;160:686-699.
25. Gao JL, Yim E, Siwicki M, et al. Cxcr4-haploinsufficient bone marrow transplantation corrects leukopenia in an unconditioned WHIM syndrome model. *J Clin Invest*. 2018;128:3312-3318.
26. Sundaresh A, Williams O. Mechanism of ETV6-RUNX1 Leukemia. In: Groner Y, Ito Y, Liu P, Neil JC, Speck NA, van Wijnen A, eds. *RUNX Proteins in Development and Cancer*. Singapore: Springer Singapore; 2017:201-216.

SUPPORTING INFORMATION

Additional supporting information may be found online in the Supporting Information section.

3.4. TOLL-LIKE RECEPTOR SIGNALING IN THYMIC EPITHELIUM CONTROLS THE RECRUITMENT OF CD14^{+} MONOCYTE-DERIVED DCS AND GENERATION OF TREG CELLS

The negative selection of T cells occurs in the thymic medulla where the antigen-presenting cells such as dendritic cells (DCs) or medullary thymic epithelial cells (mTECs) express and present self-antigens (Oukka et al., 1996). This presentation leads to the deletion of self-reactive T-cells (Liston et al., 2003) or their conversion to the T-regulatory cells (Tregs) (Aschenbrenner et al., 2007).

Recent studies showed, that cooperative antigen transfer (CAT) from mTECs to DCs is involved in thymic tolerance (Lancaster et al., 2019; Leventhal et al., 2016). Thymic DCs can be divided into thymus resident Xcr1+CD8a+Sirpa- classical type 1 DCs (cDC1) and DCs with extrathymic origin: B220+ plasmacytoid DCs (pDCs) and Xcr1-CD8a-Sirpa+ migratory classical type 2 DCs (cDC2) (Li et al., 2009). cDCs1 and cDCs2 migrate to the close proximity of mTECs in chemokine dependent manner (Baba et al., 2009; Lei et al., 2011) and CAT from mTECs to the above mentioned DC subsets occurs (Kroger et al., 2017).

Vobořil et. al. showed that mTECs express TLRs, especially TLR9, the stimulation of which leads to the production of chemokines which regulate the influx of a novel monocyte-derived DC (CD14^{+}moDC) into the thymic medulla with its subsequent increase in CAT from mTECs. This also correlated with increased production of Tregs. Correspondingly, the deletion of Myd88 (an adaptor molecule for TLR9 signaling) in TECs resulted in the decreased thymic Treg output. This data suggests, that TLR9/Myd88 signaling in TECs is important in the generation of Treg in the thymus.

Applicant's contribution: Preparation of thymi samples for the cryosections. Optimization of immunostaining. Preparation of representative microscopic images. Microscopical analysis of sections and statistical analysis.

Experimental help during the revision process.

Toll-like receptor signaling in thymic epithelium controls monocyte-derived dendritic cell recruitment and Treg generation

Matouš Vobořil[1], Tomáš Brabec[1], Jan Dobeš[1], Iva Šplíchalová[1], Jiří Březina[1], Adéla Čepková[1], Martina Dobešová[1], Aigerim Aidarova[1], Jan Kubovčiak[2], Oksana Tsyklauri[3], Ondřej Štěpánek[3], Vladimír Beneš[4], Radislav Sedláček[5], Ludger Klein[6], Michal Kolář[2] & Dominik Filipp[1 ✉]

The development of thymic regulatory T cells (Treg) is mediated by Aire-regulated self-antigen presentation on medullary thymic epithelial cells (mTECs) and dendritic cells (DCs), but the cooperation between these cells is still poorly understood. Here we show that signaling through Toll-like receptors (TLR) expressed on mTECs regulates the production of specific chemokines and other genes associated with post-Aire mTEC development. Using single-cell RNA-sequencing, we identify a new thymic CD14+Sirpα+ population of monocyte-derived dendritic cells (CD14+moDC) that are enriched in the thymic medulla and effectively acquire mTEC-derived antigens in response to the above chemokines. Consistently, the cellularity of CD14+moDC is diminished in mice with MyD88-deficient TECs, in which the frequency and functionality of thymic CD25+Foxp3+ Tregs are decreased, leading to aggravated mouse experimental colitis. Thus, our findings describe a TLR-dependent function of mTECs for the recruitment of CD14+moDC, the generation of Tregs, and thereby the establishment of central tolerance.

[1] Laboratory of Immunobiology, Institute of Molecular Genetics of the Czech Academy of Sciences, Prague, Czech Republic. [2] Laboratory of Genomics and Bioinformatics, Institute of Molecular Genetics of the Czech Academy of Sciences, Prague, Czech Republic. [3] Laboratory of Adaptive Immunity, Institute of Molecular Genetics of the Czech Academy of Sciences, Prague, Czech Republic. [4] Genomics Core Facility, EMBL, Services & Technology Unit, Heidelberg, Germany. [5] Czech Centre for Phenogenomics & Laboratory of Transgenic Models of Diseases, Institute of Molecular Genetics of the Czech Academy of Sciences, Prague, Czech Republic. [6] Faculty of Medicine, Institute for Immunology, Ludwig-Maximilans-Universitat, Munich, Germany. ✉email: dominik.filipp@img.cas.cz

The establishment of tolerance is a fundamental attribute of a healthy immune system. Since T cell antigen receptors (TCRs) are generated by random somatic recombination, i.e. could be self or nonself-specific, T cells that express a self-reactive TCR must be removed from the conventional T cell repertoire. The critical part of this process occurs in the thymic medulla where the strength of TCR recognition of self-antigens is probed by various types of antigen presenting cells (APCs), mainly dendritic cells (DCs), B-cells, and highly specialized medullary thymic epithelial cells (mTECs)[1]. mTECs mediate the promiscuous expression of thousands of otherwise strict tissue-restricted self-antigens (TRAs), a large number of which are under the control of the transcriptional regulator Aire[2]. The presentation of TRAs by mTECs can result in either the deletion of self-reactive T cells[3] or their conversion into Tregs[4,5].

It has been recently demonstrated that the process of cooperative antigen transfer (CAT) from mTECs to DCs is essential for the establishment of thymic tolerance[6–11]. The complexity of CAT is foremost due to the heterogeneity of DCs in the thymus. These CD11c^{+} cells are comprised of two major categories: B220^{+} plasmacytoid DCs (pDC) and classical DCs (cDCs), the latter which can be subdivided into Xcr1^{+}CD8α[+]Sirpα[−] classical type 1 DCs (cDC1) and Xcr1^{−}CD8α[−]Sirpα[+] classical type 2 DCs (cDC2)[12,13]. While cDC1 arise primarily in the thymus, cDC2 and pDCs originate extrathymically and then migrate to the thymic medullary region[14,15]. mTEC-derived antigens are transferred both to thymic resident cDC1[6,10] and cDC2[16,17]. Although it has been shown that the migration of cDC1 and cDC2 to the vicinity of mTECs is affected by a gradient of Xcl1[18] and Ccr2/Ccr7 ligands, respectively[19,20], the potential involvement of other chemokines in the regulation of CAT still awaits resolution.

Toll-like receptors (TLRs) sense various immunologically relevant microbial ligands such as lipoproteins, carbohydrates, and nucleic acids. All TLRs, with the exception of TLR3, signal through the adaptor protein, MyD88, which via the activation of the NF-κB pathway induces the expression of pro-inflammatory cytokines, chemokines, and other inflammation-related molecules[21]. While the exact role of non-canonical NF-κB signaling in the development and function of mTECs has been previously demonstrated[22–24], the impact of TLR signaling via the canonical NF-κB pathway in the physiology of mTECs remains undetermined.

Here, we show that, among TLRs, mTECs abundantly express TLR9, and the stimulation of which leads to the influx of Xcr1^{−} Sirpα[+] cDC2 into the thymic medulla. RNA sequencing of stimulated mTECs reveals that the mechanism underpinning this phenomenon is related to the upregulation of a set of chemokines, whose receptors are predominantly expressed by a CD14^{+} subset of thymic DCs, which have been identified as monocyte-derived DCs (CD14^{+}moDC). Furthermore, mice with MyD88-deficient TECs, which exhibit a deficiency in the recruitment of CD14^{+} moDC, also suffer from a decreased thymic Treg output and functionality, which renders the peripheral T cell repertoire prone to colitis induction.

Results

mTECs express a set of TLRs and signaling adaptors. The function of TLR signaling in the physiology of mTECs has not yet been studied in detail[25–27]. We first determined that both mTECs[low] and mTECs[high] subsets (Fig. 1a and Supplementary Fig. 1a) expressed TLR2, 3, 4, and 9 (Fig. 1b). Remarkably, TLR9, which recognizes bacterial, viral or altered DNA[21] and ligands associated with cellular stress[28], is highly expressed by mTECs[high] at levels comparable to thymic cDCs (Fig. 1a, b and Supplementary Fig. 1b). Transcripts of TLR adaptors *MyD88* and *Trif*[21] were also readily detectable (Fig. 1c). Although the levels of TLR4

and TLR9 were higher in mTECs[high], the major producers of Aire, our analysis of Aire^{+/+} and Aire^{−/−} mice revealed that TLRs are expressed in an Aire-independent manner (Fig. 1d).

To assess the significance of TLR/MyD88 signaling in TECs development, we crossed a thymic epithelial cell-specific Foxn1[Cre] driver[29] with a MyD88^{fl/fl} transgenic mice[30] (hereafter called MyD88[ΔTEC]). In comparison to the control, MyD88[ΔTECs] mice showed no significant differences in the frequency of all tested TEC subpopulations (Fig. 1e, f), suggesting that canonical NF-κB signaling through TLRs/MyD88 does not affect mTEC[high] maturation. Similarly, in all mTEC[high] subsets, the expression of CD80, CD86, PD-L1, CD40, and ICOSL on was not altered (Supplementary Fig. 1c). This data demonstrates that TLRs are broadly expressed by mTECs and MyD88-dependent signaling has no apparent impact on TEC subpopulation frequency.

MyD88-dependent chemokine expression in mTECs[high]. Given the high expression of selected TLRs in mTECs^{high} cells, we assessed the impact of the absence of TLR signaling in unperturbed conditions. RNA-sequencing of mTECs[high] (sorted as shown in Supplementary Fig. 1a) from wild type (MyD88^{fl/fl}) and MyD88[ΔTECs] mice revealed MyD88-dependent transcriptional variance (Fig. 2a) defined by 303 differentially expressed transcripts (Fig. 2b and Supplementary Data 1 and 2). While 206 of these transcripts were induced and 97 repressed by MyD88, they were not enriched for Aire-dependent or Aire-independent TRA genes[31] (Supplementary Fig. 2a, left panel). Consistent with the role of TLR/MyD88 signaling in epithelial cells[21], we found several differentially expressed genes (DEGs) which fell into one of two categories: (i) *Il1f6* and *Csf2* cytokines, (ii) *Ccl25*, *Ccl4*, and *Ccl24* chemokines. These mediators act through receptors that are primarily expressed by myeloid cells and DCs[32]. Specifically, IL36R, the receptor for IL1F6, is expressed by DCs and T cells[33] while Csf2r, the receptor for Csf2, is expressed mostly by monocytes, macrophages, and granulocytes[34]. The Ccr9, the receptor for Ccl25, is expressed by both thymocytes and pDCs driving their migration into the thymus[14,35]. Both Ccr5 (receptor for Ccl4) and Ccr3 (receptor for Ccl24) are expressed predominantly on granulocytes and DCs modulating their migration into inflamed tissues[32,36]. qRT-PCR analysis confirmed MyD88-regulated expression of selected genes in mTECs[high] (Fig. 2c). Since the TLRs were postulated to sense both microbial and endogenous molecules[21], we examined which of them could potentially act as a trigger. The analysis of mRNA expression of MyD88-dependent cytokines and chemokines (Fig. 2b, c) in the mTEC[high] population isolated from either Germ-free (GF) or specific-pathogen-free (SPF) mice was comparable (Supplementary Fig. 2b), indicating that these signals are likely of endogenous origin.

Next, we assessed the response of mTECs to TLR/ MyD88 stimulation. Given the high expression of TLR9 (Fig. 1b), we stimulated mTECs[high] from MyD88-deficient (MyD88^{−/−}) and WT (MyD88^{+/+}) mice in vitro with CpG oligodeoxynucleotides (CpG ODN) or PBS. RNA-sequencing revealed significant changes in the transcriptional profile only in MyD88^{+/+} cells. Notably, 347 DEGs were associated with TLR9 stimulation (Fig. 2d, e and Supplementary Data 3 and 4), and of these, 198 were upregulated while 149 were downregulated. However, the pattern of expression of TRA genes remained largely unchanged after in vitro CpG ODN stimulation (Supplementary Fig. 2a, right panel). Importantly, among the most upregulated DEGs were two sets of chemokines: (i) *Cxcl1*, *2*, *3*, and *5*, which signal via the Cxcr2 receptor, expressed predominantly on neutrophils[37] and (ii) *Ccl3*, *5* and *20* which signal via various chemokine receptors, including Ccr1, 3, 5, 6 which are expressed mostly on myeloid
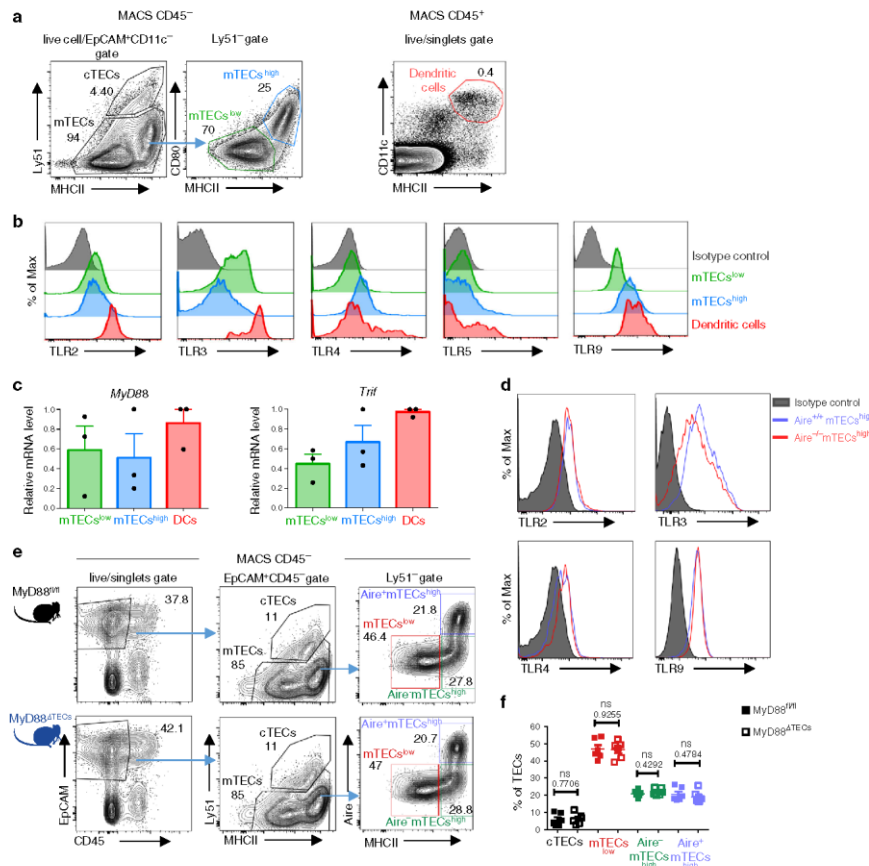
Fig. 1 mTECs express a set of TLRs and their signaling adaptors independently of Aire. a Gating strategy used for the analysis of TEC populations and general thymic conventional DCs. MACS enriched CD45− and EpCAM+CD11c− pre-gated cells were further divided into cTECs (Ly51+), mTECs^low (MHCII^low CD80^low), and mTECs^high (MHCII^high CD80^high). Thymic conventional DCs were gated as CD11c+MHCII+ from the CD45+ fraction. A more detailed gating strategy is found in Supplementary Fig. 1a, b. **b** Representative flow cytometry histograms of TLR expression on mTECs and DCs isolated from the thymus ($n = 3$ independent experiments). **c** MyD88 and Trif mRNA expression is determined by qRT-PCR from FACS sorted mTECs and DCs. The expression is calculated relative to Casc3 and normalized to the highest value within each experiment=1 (mean ± SEM, $n = 3$ samples). **d** Representative flow cytometry histograms of TLR expression on mTECs from Aire+/+ and Aire−/− mice, ($n = 3$ independent experiments). **e** Representative comparative flow cytometry plots of different TEC subpopulations in MyD88^fl/fl and MyD88^ΔTECs mice. **f** Quantification of TEC frequencies from plots in e (mean ± SEM, $n = 6$ mice). Statistical analysis was performed by unpaired, two-tailed Student's t-test, p-values are shown. ns = not significant.

cells[32]. Cytokines (Tnfα, Il-6, Il12a, Il1f6 and Csf2) and other genes (Cd40) were also found to be upregulated (Fig. 2e). The upregulation of Cxcl1 and Ccl5 chemokines after in vitro (Fig. 2f) as well as in vivo intrathymic TLR9 stimulation (Fig. 2g) was confirmed by qRT-PCR analysis. As shown in Supplementary Fig. 2c, repeated intraperitoneal (i.p.) injection of CpG ODN was insufficient for the upregulation of chemokines in mTECs^high. It is of note that in vitro stimulation of TLR4 on mTECs^high by LPS

also resulted in the upregulation of the previously noted chemokines, albeit at a lower level (Supplementary Fig. 2d).

In addition to TLRs, MyD88 also conveys signals generated by IL-1 family cytokines, such as IL-1β, IL-18 or IL-33[38]. Even though the receptors for these cytokines are expressed by mTECs^high (Supplementary Fig. 3a), only in vitro stimulation with IL-1β lead to the upregulation of cytokines and chemokines induced by TLR9 stimulation (Supplementary Fig. 3b).
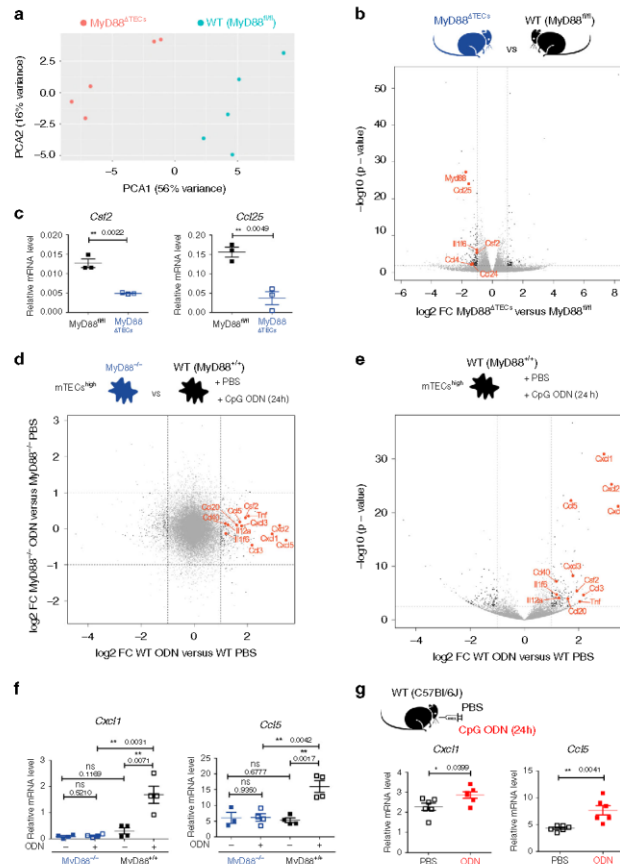
108

Fig. 2 TLR/MyD88 signaling in mTECs[high] drives the expression of cytokines and chemokines. a Principal component analysis of bulk RNA-sequencing data from mTECs[high] (sorted as in Supplementary Fig. 1a) derived from MyD88^{fl/fl} and MyD88[ΔTECs] mice. Data represents the analysis of $n = 5$ samples for each condition. **b** Volcano plot analysis of RNA-sequencing data described in **a**. Fold-change cutoff of log2 = ±1,0 and p-value: 0.05 are marked by dashed lines (also in **d, e**). Differentially expressed genes are depicted in black, genes of interest are in red, and other detected genes in grey. **c** qRT-PCR analysis of relative mRNA expression normalized to Casc3 of genes selected from b (mean ± SEM, $n = 3$ samples). **d** Fold-change fold-change plot of RNA-sequencing data from CpG ODN or PBS in vitro stimulated mTECs[high] (sorted as in Supplementary Fig. 1a) from MyD88^{+/+} and MyD88^{-/-} mice ($n = 4$ samples for each condition). Color code as in **b**. **e** Volcano plot analysis of RNA-sequencing data from d, comparing CpG ODN versus PBS in vitro stimulated mTECs[high] from MyD88^{+/+} mice. Statistical analysis for b, d and e was performed by Wald test, p-value cutoff: 0.05. **f, g** qRT-PCR analysis of Cxcl1 and Ccl5 mRNA expression (normalized to Cacs3) from in vitro (mean ± SEM, $n = 4$ samples) and intrathymically (mean ± SEM, $n = 6$ mice), respectively, CpG ODN or PBS stimulated mTECs[high] from indicated animals. Statistical analysis for **c, f**, and **g** was performed by unpaired, two-tailed Student's t-test, $p \leq 0.05 = *$, $p \leq 0.01 = **$, ns not significant.

Besides chemokines and cytokines, TLR/MyD88 signaling in mTECs[high] (Fig. 2b) also regulated the expression of molecules associated with cornified epithelial pathway[39] (Supplementary Data 1–4). This specifically relates to genes that are associated with post-Aire mTECs[40,41], such as *Krt10*, *Krt77* and *Flg2* (Supplementary

Fig. 3c). Moreover, previously published data has shown the enhanced expression of *Il1f6*, *Cxcl3* and *Cxcl5* in post-Aire mTECs[42]. Thus, we enumerated the total numbers of Involucrin[+]EpCAM^{+} cells in the medullary region of the CpG ODN intrathymically stimulated thymus. We did not observe any changes in the frequency

of general mTECs subsets (Supplementary Fig. 3d) although the total numbers of Involucrin[+] post-Aire mTECs were significantly increased (Supplementary Fig. 3e, f).

Together, these results show that TLR/MyD88 signaling in mTECs under physiological or stimulatory conditions regulates the differentiation of mTEC^{high} cells into Involucrin[+] post-Aire stage. This stage is associated with the expression of a set of chemokines that signal via an overlapping set of chemokine receptors that are primarily expressed by DCs[32].

TLR9/MyD88 signaling in mTECs targets Sirpα[+] cDC2. Migration of different DC subsets into the thymus is orchestrated by distinct chemokines[14,18,19]. Thus, we next assessed which of these subsets would be the target for TLR9/MyD88-induced chemokines in TECs. We sorted three main subsets of CD11c^{+}MHCII^{+} thymic DCs: B220^{+} pDC, Sirpα^{−}Xcr1^{+} cDC1, and Sirpα^{+}Xcr1^{−} cDC2 (Supplementary Fig. 4a), along with Gr-1^{+} granulocytes, CD4 and CD8 single positive thymocytes and performed qRT-PCR analysis of the chemokine receptors indicated above. Remarkably, apart from granulocytes, the chemokine receptors *Cxcr2, Ccr1, 3, 5,* and *6* were mostly expressed by DCs, specifically by cDC2 and pDC (Fig. 3a). This prompted us to quantify the relative frequencies of all thymic DC subsets in MyD88[ΔTECs] in comparison to WT (MyD88^{fl/fl}) mice. In unstimulated conditions, TEC-intrinsic MyD88 signaling did not change the total frequency of CD11c^{+}MHCII^{+} DCs (Fig. 3b, left plot). However, we observed alterations in the frequencies of DC subsets. While cDC1 were increased, the frequencies of pDC and cDC2 were diminished in the MyD88[ΔTECs] thymus (Fig. 3b). In contrast, FACS analysis of TLR9-stimulated thymi revealed a significant increase in cDC2 accompanied by decreased cDC1 in the thymus of WT (MyD88^{fl/fl}) (Fig. 3c and Supplementary Fig. 4b, c) but not MyD88[ΔTECs] animals (Fig. 3c). The frequencies of pDC remained comparable under these two conditions. This demonstrates that the recruitment of cDC2 to the thymus is attributable specifically to TLR9 signaling in TECs (Fig. 3c and Supplementary Fig. 4b). In agreement with medullary localization of cDC2 (Supplementary Fig. 4d), microscopically examined thymi from WT mice stimulated with CpG ODN showed an enrichment of CD11c^{+}Sirpα^{+} cDC2 exclusively in the keratin14-rich medullary region (Figs. 3d, e).

Together, this data suggests that MyD88-driven chemokines expressed by mTECs[high], target receptors on thymic Sirpα[+] cDC2 and mediate their recruitment to the thymic medulla in steady state and TLR9 stimulatory conditions.

TLR9/MyD88 signaling in mTECs recruits CD14^{+}moDCs. Chemokine-dependent migration of DCs to the proximity of mTECs, which underpins the mechanisms of CAT[18], has been shown to be essential for the presentation of mTEC-derived antigens by DCs[6,10]. One prediction from the TEC-dependent TLR/MyD88-induced influx of Sirpα[+]cDC2 to the thymic medulla is that the frequency of CAT to this subset would be enhanced.

To verify this prediction, we crossed Foxn1[Cre] mice with ROSA26[TdTOMATO] leading to TEC-specific, cytoplasmic expression of TdTOMATO (TdTOM) protein in the thymus. In agreement with a previous study[9] and as shown in Supplementary Fig. 5a, we found two major populations of TdTOM^{+} cells: (i) a TdTOM^{high} EpCAM^{+} population which was CD45^{−} and represented TECs expressing TdTOM endogenously (Supplementary Fig. 5b); and (ii) a CD45^{+} TdTOM^{+} population comprised of mainly CD11c^{+} DCs (Supplementary Fig. 5a) which acquired TdTOM via CAT (Fig. 4a). Interestingly, these DCs were enriched for the EpCAM^{+} marker (Fig. 4b) which was likely co-transferred with TdTOM[9]. Bone marrow (BM) chimeras

of lethally irradiated Foxn1[Cre]ROSA26[TdTOMATO] mice reconstituted with WT BM cells showed that around 6% of donor-derived DCs acquired TdTOM (Supplementary Fig. 5c–e). This formally demonstrates that TdTOM is transferred from TECs to DCs.

It has been previously documented that distinct subtypes of thymic DCs vary in their capacity to acquire antigens from TECs[6,10,11,16]. Whereas CAT of TdTOM from TECs to cDC1 and cDC2 is very potent in the Foxn1[Cre]ROSA26[TdTOMATO] system, it is limited in the case of pDC (Fig. 4e, f). This result was also corroborated with the use of BM chimeras which were described above (Supplementary Fig. 5f). Flow cytometry imaging showed that transferred TdTOM in MHCII^{+}CD11c^{+} DCs is localized intracellularly (Fig. 4g).

To determine the heterogeneity of all thymic DC subsets that participate in CAT, we performed single-cell RNA-sequencing (ddSEQ)[43] of Gr-1^{−}CD11c^{+}TdTOM^{+} cells isolated from thymi of Foxn1[Cre]ROSA26[TdTOMATO] mice. Two-dimensional tSNE projection clustering analysis revealed five different clusters of TdTOM[+] DCs (Fig. 5a). Based on their expression profiles and previously described signature genes of cells from mononuclear phagocyte system (MPS)[44], we designated the clusters in accordance with MPS nomenclature[13]: two cDC1 clusters (*Batf3*): a cDC1a (*Ccl5* and *Ccr7*) and cDC1b (*Cd8a, Itgae, Xcr1* and *Ppt1*)[45]; cDC2 cluster (*Sirpα, Mgl2* and *Cd209a*)[12], moDC cluster (*Sirpα, Cd14, Itgam, Cx3cr1* and *Ccr2*)[46]; and one pDC cluster (*Bst2, Ccr9, Siglech,* and *Ly6d*)[14] (Fig. 5b and Supplementary Data 5). This data allowed the clustering of DCs which participate in CAT according to their specific surface markers (Supplementary Fig. 6a). As shown in Fig. 5b, the previously defined thymic moDC subpopulation shared several markers with both cDCs (*Itgax, Itgam, Sirpα,* and *Irf4*) and classical tissue resident macrophages (*Lyz2, Mertk,* and *Mafb*). Due to the high mRNA expression of molecules associated with antigen processing and presentation by moDC subpopulation (Supplementary Fig. 6b), we tested their capacity to present mTEC-derived antigens and activate antigen specific T cells. Specifically, thymic CD14^{+}moDCs isolated from the Aire-HCO mouse model expressing influenza hemagglutinin (HA) under the control of Aire regulatory sequences[47], were co-cultivated with HA-specific CD4^{+} T cell hybridoma cells (A5) carrying a GFP-NFAT reporter[4]. While the result demonstrated that thymic CD14^{+}moDCs can efficiently present mTEC-derived antigens to T cells (Supplementary Fig. 6c), it seems that their previous detection was obstructed by using the previously established gating strategy (Supplementary Fig. 4a), by which they are indistinguishable from a conventional Sirpα[+] cDC2 subset.

Next, we determined which of the five defined thymic DC clusters expressed the receptors for TLR9/MyD88-induced chemokines/cytokines from mTECs (Figs. 2b, d, e). The heat map analysis of chemokine receptors identified by ddSEQ analysis revealed that most of these receptors were expressed by the Sirpα^{+}CD14^{+}moDC cluster (Fig. 5c, left panel). Interestingly, each of the TdTOM^{+} DC clusters expressed a specific set of chemokine receptors (Fig. 5c).

Having characterized the CAT system with participating subsets of DCs in Foxn1[Cre]ROSA26[TdTOMATO] mice, we used it as a read-out to determine the targeting specificity of TEC-dependent TLR9/MyD88 stimulation on these DC subsets. First, in general, TLR9 intrathymic stimulation of Foxn1[Cre]ROSA26[TdTOMATO] mice boosted the frequency of total TdTOM[+] DCs (Fig. 5d left graph and Supplementary Fig. 6d) as well as the mean fluorescent intensity (MFI) of TdTOM in these cells, demonstrating their enhanced rate of CAT under stimulatory conditions (Supplementary Fig. 6e). Second, as predicted, the observed increase in CAT was fully attributable to TdTOM[+]Sirpα[+] DCs and not to other DCs populations (Fig. 5d right graph and Supplementary Fig. 6f). Third, and most importantly, the unsupervised flow cytometry tSNE
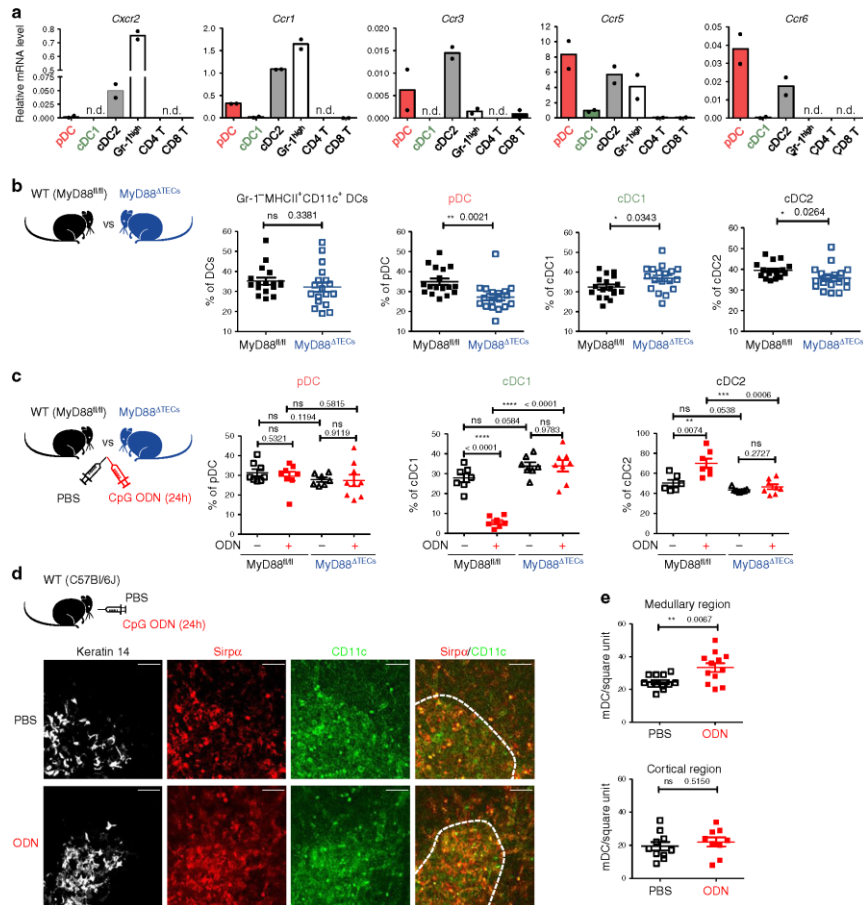
110

Fig. 3 TLR/MyD88 signaling in mTECs^high affects the migration of DCs into the thymic medulla. a qRT-PCR analysis of the relative mRNA expression (normalized to Casc3) of indicated chemokine receptors on FACS sorted populations of thymic DCs; pDC plasmacytoid DCs, cDC1 classical type 1 DC, cDC2 classical type 2 DC, Gr-1^high = neutrophils, CD4 T = CD4+, and CD8 T = CD8+ thymic T cells. Sorting protocol of thymic DC subsets is provided in Supplementary Fig. 4a. T cells were sorted as TCRβ+ and either CD4 or CD8 single positive ($n = 2$ independent experiments). **b** Comparative flow cytometry analysis of total DCs (Gr-1^-CD11c+MHCII+) and different thymic DC subpopulations between MyD88^fl/fl and MyD88^ΔTECs mice enumerated according to gating strategy shown in Supplementary Fig. 4a (mean ± SEM, $n = 17$ for MyD88^fl/fl and $n = 18$ for MyD88^ΔTECs mice). **c** Flow cytometry analysis of different thymic DC populations (gated as in Supplementary Fig. 4a) isolated from CpG ODN or PBS intrathymically stimulated MyD88^fl/fl or MyD88^ΔTECs mice (mean ± SEM, pDC graph: $n = 7$ for ODN^-MyD88^ΔTECs and $n = 8$ for other three displayed items; cDC1 graph: $n = 7$ for MyD88^fl/fl and ODN^-MyD88^ΔTECs and $n = 8$ for ODN+ MyD88^ΔTECs mice; cDC2 graph: $n = 6$ for ODN^-MyD88^fl/fl, $n = 7$ for ODN+MyD88^fl/fl and ODN^-MyD88^ΔTECs and $n = 8$ for ODN+MyD88^ΔTECs mice). Statistical analysis in **b**, **c** was performed by unpaired, two-tailed Student's t-test, $p \leq 0.05 = *$, $p \leq 0.01 = **$, $p \leq 0.001***$, $p < 0.0001 = ****$, ns not significant. **d** Microscopic examinations of thymic sections isolated from CpG ODN or PBS intrathymically stimulated WT mice. Cryosections were stained with keratin 14 (white), Sirpα (red), and CD11c (green). Scale bar represents 50 μm. The white dashed line demarks keratin 14-rich medulla. **e** Quantification of CD11c+Sirpα+ cells in the medullar or cortical region of the cryosections shown in d (mean ± SEM, $n = 12$ counted square unites per medullary region; $n = 10$ and $n = 9$ counted square unites per PBS- and ODN-treated cortical region, respectively. Data are derived from three independent experiments). Statistical analysis was performed by unpaired, two-tailed Student's t-test, $p \leq 0.01 = **$, ns not significant.
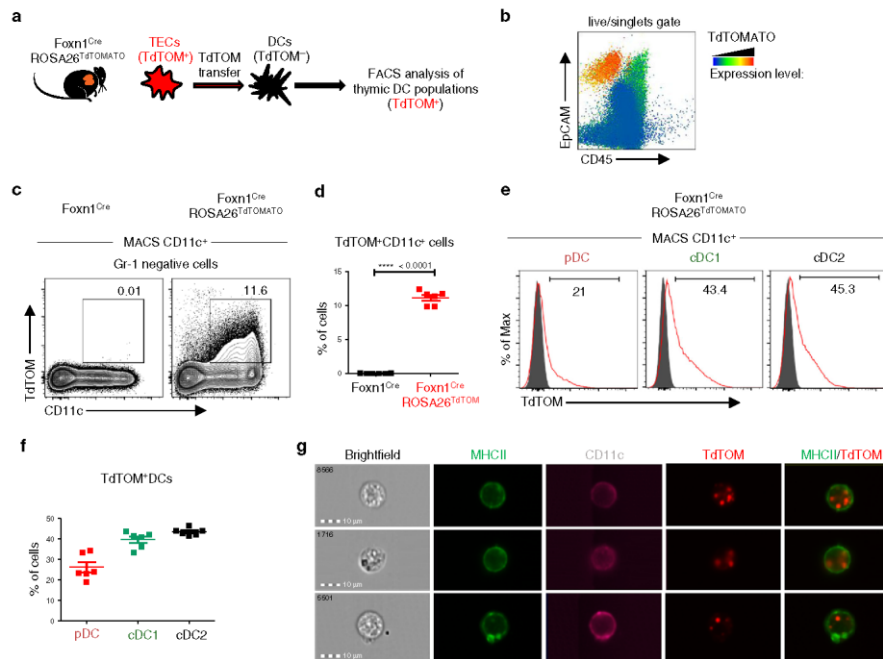
Fig. 4 Foxn1^CreROSA26^TdTOMATO as a model of thymic cooperative antigen transfer. a Experimental design. **b** Flow cytometry heat-map analysis showing the intensity of TdTOM fluorescence among MACS TCRβ-depleted cells from the thymus of the Foxn1^CreROSA26^TdTOMATO mouse. **c** Representative flow cytometry plots comparing the frequency of TdTOM+CD11c+ cells in the thymic MACS-enriched CD11c+ cells between the WT (Foxn1^Cre) and Foxn1^CreROSA26^TdTOM mouse. Cells were pre-gated as live, singlets, and Gr-1-. **d** Quantification of TdTOM+CD11c+ cells from c (mean ± SEM, $n = 6$ mice). Statistical analysis was performed by unpaired, two-tailed Student's t-test, $p < 0.0001 = ****$. **e** Representative flow cytometry histograms showing the frequency of TdTOM+ cells among pDC, cDC1, and cDC2 (gated as in Supplementary Fig. 4a). Gray histograms = Foxn1^Cre (control) mice, red histograms = Foxn1^CreROSA26^TdTOM mice. **f** Quantification of frequencies of TdTOM+ DCs among the indicated DC subsets (mean ± SEM, $n = 6$ mice). **g** Representative images from the Imagestream analysis showing intracellular localization of transferred TdTOM in MHCII+CD11c+ DCs from the thymus of Foxn1^CreROSA26^TdTOMATO ($n = 400$ measured cells).

analysis of the main DC subsets defined by markers revealed by ddSEQ analysis showed that the increase of TdTOM+ DCs was mostly due to the specific enrichment of CD14+moDCs (Figs. 5e, f), which also co-express chemokine receptors for ligands induced by TLR9/MyD88 signaling in mTECs (Figs. 2b, e and 5c). Concomitantly, we observed a decrease in Mgl2+ cDC2, Xcr1+ cDC1b, and B220+ pDC (Fig. 5e, f and Supplementary Fig. 6g). Importantly, and further confirming the need of MyD88 signaling for its recruitment, the decreased frequency of total Sirpα+ DCs in the thymus of non-manipulated MyD88^ΔTECs mice (Fig. 3b) was shown to be accounted specifically by the diminishment of the CD14+moDC subset (Fig. 5g).

To find which of the chemokines described (in Fig. 2b, e) were responsible for CD14+moDC migration to the thymus, we crossed Cxcr2^fl/fl mice with the pan-hematopoietic driver Vav1^Cre to abrogate the signaling of its cognate ligands Cxcl1, 2, 3, and 5 that were among the most upregulated genes in mTECs after TLR9 stimulation. We observed no changes in the recruitment of CD14+moDC after TLR9 stimulation between Cxcr2^fl/flVav1^Cre

and WT mice (Supplementary Fig. 6h). This suggests, that together with ligands of Ccr2, (i.e. Ccl2, 7, 8, and 12)[19], the ligands of Ccr1, Ccr3 or Ccr5, or their combinations[36], regulate the entry of CD14+moDC into the thymic medulla.

Together, TLR9/MyD88-dependent chemokine signaling in mTECs specifically targets the recruitment and subsequent CAT from the mTECs to Sirpα+CD14+moDC subpopulation which exhibits a tangible capacity for antigen presentation.

TLR9/MyD88 signaling in mTECs affects Treg development. Previous studies have suggested that the development of thymic Tregs is dependent on antigen presentation by both mTECs and DCs[6,17,47]. Specifically, antigen presentation by Sirpα+DCs[17] and/or alternatively by CD8α+cDC1[6,10] was implied in the development of organ-specific Tregs. It has been also suggested that the increased ratio of Sirpα+DCs to CD8α+cDC1 leads to an enhanced production of thymic CD25+Foxp3+ Tregs[17,20]. Since a decreased frequency of Sirpα+DCs (Fig. 3b), specifically CD14+moDCs (Fig. 5g) was observed in the thymus of

112
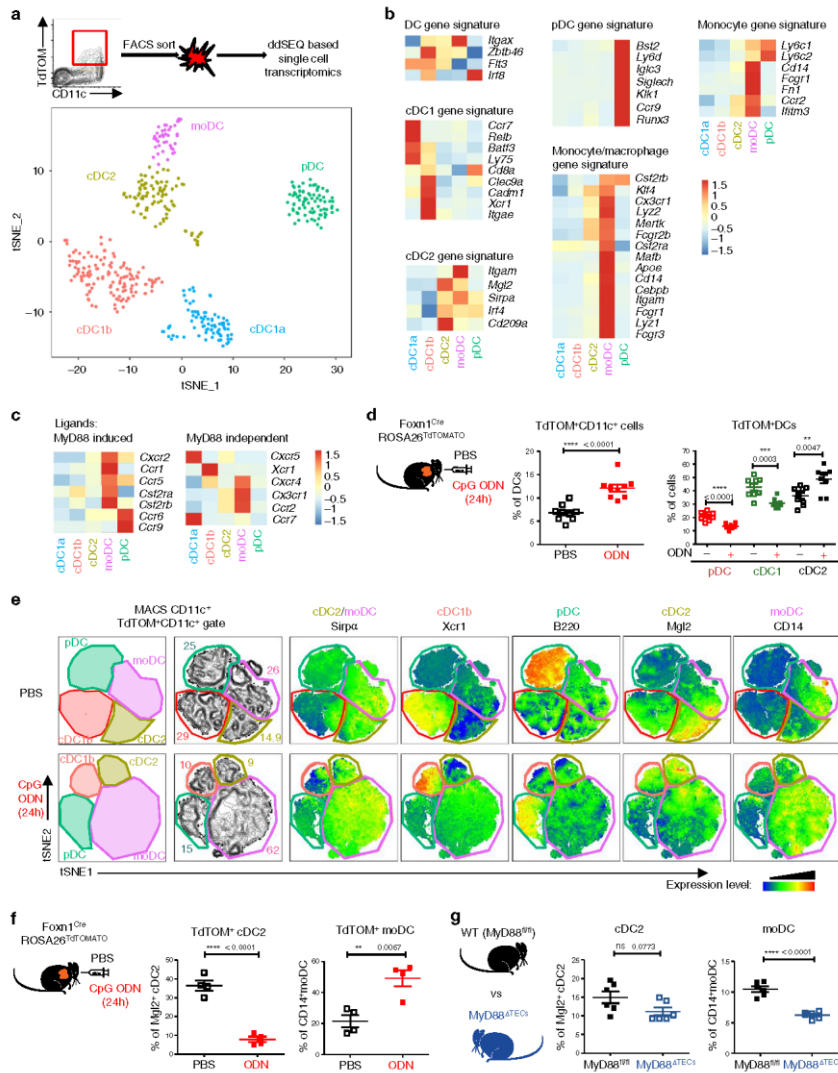
MyD88$^{\Delta TECs}$ mice, we tested whether these effects would impact the development of the major thymocyte populations and Tregs. While the DN (CD8$^-$CD4$^-$), DP (CD8$^+$CD4$^+$), and CD8$^+$ T cells frequencies were comparable between MyD88$^{\Delta TEC}$ and WT mice, CD4$^+$ T cells, and more specifically CD25$^+$Foxp3$^+$ Tregs were significantly reduced in 4-week-old MyD88$^{\Delta TECs}$ mice (Fig. 6a–c and Supplementary Fig. 7a). Since it has been reported that in 4

week-old-mice nearly one half of CD25$^+$Foxp3$^+$ thymic cells consist of mature recirculating Tregs[48,49], we used CD73 protein staining to determine if Tregs reduced in MyD88$^{\Delta TECs}$ mice were newly generated (CD73$^-$) or recirculating (CD73$^+$)[50]. As shown in Fig. 6d, e, the abrogation of MyD88 signaling in mTECs affected mainly the generation of CD25$^+$Foxp3$^+$ thymic Tregs and not their recirculation. On the other hand, the CD25$^+$Foxp3$^+$ thymic Tregs

113

Fig. 5 TLR/MyD88 signaling increases cooperative antigen transfer between TECs and the CD14⁺moDC subpopulation. a Two-dimensional tSNE plot from ddSEQ single-cell RNA-sequencing from FACS sorted Gr-1⁺CD11c⁺TdTOM⁺ DCs from the thymus of Foxn1^{Cre}ROSA26^{TdTOMATO} mice. The color code represents different cell clusters based on the mRNA expression profile of each cell. **b** Heat-map analysis of the expression of signature genes determining each subset defined in **a**. **c** Heat-map analysis of the expression of chemokine receptors by DC subsets defined in **a**. **d** Quantification of TdTOM⁺CD11c⁺ DC subsets (defined as in Supplementary Fig. 4a) in CpG ODN or PBS intrathymically stimulated Foxn1^{Cre}ROSA26^{TdTOMATO} mice (representative flow cytometry plots are shown in Supplementary Fig. 6d, f) (mean ± SEM, $n = 9$ mice). Statistical analysis was performed using unpaired, two-tailed Student's t-test, $p \leq 0.01 = **$, $p \leq 0.001***$, $p < 0.0001****$. **e** Representative flow cytometry tSNE analysis of TdTOM⁺CD11c⁺cell population in PBS or CpG ODN intrathymically stimulated Foxn1^{Cre}ROSA26^{TdTOMATO} mice. tSNE analysis was performed using FlowJO software, based on the FSC-A, SSC-A, CD11c, MHCII, Sirpα, Xcr1, B220, Mgl2 and CD14 markers ($n = 2$ independent experiments). **f** Quantification of frequencies of TdTOM⁺CD14⁺ moDC or TdTOM⁺Mgl2⁺cDC2 from CpG ODN or PBS intrathymically stimulated Foxn1^{Cre}ROSA26^{TdTOMATO} mice (representative flow cytometry plots are shown in Supplementary Fig 6g) (mean ± SEM, $n = 4$ mice). **g** Flow cytometry analysis comparing the frequency of cDC2 (Sirpα⁺Mgl2⁺) and moDC (Sirpα⁺CD14⁺) between MyD88$^{fl/fl}$ and MyD88$^{\Delta TECs}$ mice (mean ± SEM, $n = 6$ mice). Total Sirpα⁺ DC population was gated as shown in Supplementary Fig 4a. Statistical analysis in f and g was performed by unpaired, two-tailed Student's t-test, $p \leq 0.01 = **$, $p < 0.0001****$, ns not significant.

were not reduced in newborn MyD88$^{\Delta TECs}$ (Supplementary Fig. 7b) or GF mice (Supplementary Fig. 7c) when compared to their WT SPF littermates. This, in association with unchanged chemokine expression in mTECs from GF mice, (Supplementary Fig. 2b) further strengthens the notion that the ligands that regulate the mTEC-mediated MyD88-dependent cellularity of Tregs is not likely of exogenous origin.

To further explore the MyD88-dependent regulation of Tregs generation, we tested our prediction that TLR9/MyD88 stimulation of mTECs would lead to the opposite effect, i.e. boosted number of Tregs. Indeed, seven days after intrathymic injection of CpG ODN, we observed a significant increase in the frequency and total number of CD25⁺Foxp3⁺ thymic Tregs (Fig. 6f and Supplementary Fig. 7d–f). Importantly, this increase was completely dependent on TEC-intrinsic MyD88 signaling (Fig. 6f). Compared to the decreased numbers in CD73⁻ Tregs in MyD88$^{\Delta TEC}$, intrathymic injection of CpG ODN led to increased numbers of not only CD73⁻ newly generated Tregs but also recirculating CD73⁺ Tregs (Fig. 6g and Supplementary Fig. 7g). This suggests that there are other mTEC-dependent mechanisms which after CpG ODN stimulation can affect the recirculation of Tregs into the thymus. One outstanding question related to the results from the above experiments (Figs. 3c and 5d–f and Supplementary Fig. 6c) is whether the increased generation of thymic CD25⁺Foxp3⁺CD73⁻ thymic Tregs is dependent on the antigen presenting capacity of DCs. To resolve this query, we intrathymically injected CpG ODN into H2-Ab1$^{fl/fl}$Itgax^{Cre} (H2-Ab1$^{\Delta DCs}$) mice, where antigen presentation by DCs has been abrogated. As demonstrated in Fig. 6h, i and Supplementary Fig. 7h, the presentation of antigen by DCs is essential for the increase in numbers of newly generated CD73⁻ CD25⁺Foxp3⁺ thymic Tregs after TLR9 stimulation.

Next, we tested the physiological consequences of the decrease in production of Tregs in MyD88$^{\Delta TECs}$ mice. We took advantage of a T cell induced colitis model, where the adoptive transfer of naïve, Treg depleted CD4⁺ T cells into Rag1-deficient mice induces severe colitis[51]. In this experimental setup, and as illustrated in Fig. 7a, the i.p. injection of the CD4⁺ T cell population isolated from peripheral lymph nodes of either MyD88$^{\Delta TEC}$ or MyD88$^{fl/fl}$ mice was compared to colitis-inducing transfer of CD4⁺CD45RB^{high}CD25⁻ cells isolated from WT mice.

Strikingly, mice that received CD4⁺ T cells from MyD88$^{\Delta TECs}$ began to lose weight ~4 weeks after adoptive transfer, behaving identically to the positive control. In contrast, mice that received CD4⁺ T cells from WT mice continuously gained weight over time (Fig. 7b). The clinical signs of colitis in mice receiving CD4⁺ T cells from MyD88$^{\Delta TEC}$ and in the positive controls were manifested by the presence of inflammatory infiltrates in the colon lamina propria, increased bowel wall thickness, presence of abscesses in colon tissue (Fig. 7c), increased spleen weight (Supplementary

Fig. 8a, b), and a higher colon weight/length ratio (Fig. 7d and Supplementary Fig. 8a). To confirm the persistence of the transferred T cell population, we also analyzed Tregs frequencies in all conditions. We found that both positive controls and mice that received CD4⁺ T cells from MyD88$^{\Delta TECs}$ had severely diminished Tregs compared to WT controls (Fig. 7e). The very similar phenotype of mice that received CD4⁺ T cells from MyD88$^{\Delta TECs}$ and those which received CD4⁺CD45RB^{high}CD25⁻ suggested, that Tregs in MyD88$^{\Delta TECs}$ were not only reduced in numbers but also functionally altered. Along with the decreased expression of CD25 (Fig. 7f), Tregs from MyD88$^{\Delta TECs}$ mice showed a significantly reduced capacity to suppress the proliferation of OVA-specific OT-II T cells in vitro (Fig. 7g, h) and prevent the early onset of diabetes caused by activated KLGR1⁺ OT-I T cells in a RIP-OVA dependent autoimmune mouse model[52] (Supplementary Fig. 8c–e).

Taken together, these results demonstrate that TLR/MyD88 signaling in TECs affects the development of thymic CD25⁺Foxp3⁺ Tregs. Specifically, in mice with MyD88-deficient TECs, the frequency and functionality of thymic CD25⁺Foxp3⁺ Tregs was decreased and unable to prevent T cell induced colitis.

Discussion

Present study lends a support for the role of TLR signaling in the mechanism of central tolerance. First, we found that mTECs^{high} express TLRs, including TLR9, whose signaling is functionally wired to the expression of chemokines and genes associated with their post-Aire development. Second, the receptors for these chemokines are predominantly expressed by the Sirpα⁺ thymic population of CD14⁺moDCs whose enrichment in the thymus and subsequent CAT is positively regulated by mTEC-intrinsic TLR/MyD88 signaling. Third, TLR/MyD88 signaling in mTECs is important for the proper development of thymic CD73⁻CD25⁺Foxp3⁺ Tregs since its abrogation resulted in a decreased number and the functionality of Tregs, associated with pathological effects in the mouse model of colitis.

The importance of TLR/MyD88 signaling in Aire-dependent autoimmunity was suggested in experiments conducted with MyD88$^{-/-}$Aire$^{-/-}$ double-knockout mice. These mice develop more severe symptoms of autoimmunity than Aire$^{-/-}$ single KO animals indicating the positive regulatory role of MyD88 signals in tolerance induction. Strikingly, neither the enhancement of MyD88 signals by an i.p. injection of TLR ligands, nor their diminishment in mice from GF conditions altered the severity of Aire-dependent autoimmunity[53]. Our data advocates for a scenario in which the worsening of autoimmunity in MyD88$^{-/-}$ Aire$^{-/-}$ mice could be caused by the lack of MyD88 signaling in mTECs^{high}, downregulation of their chemokines needed to
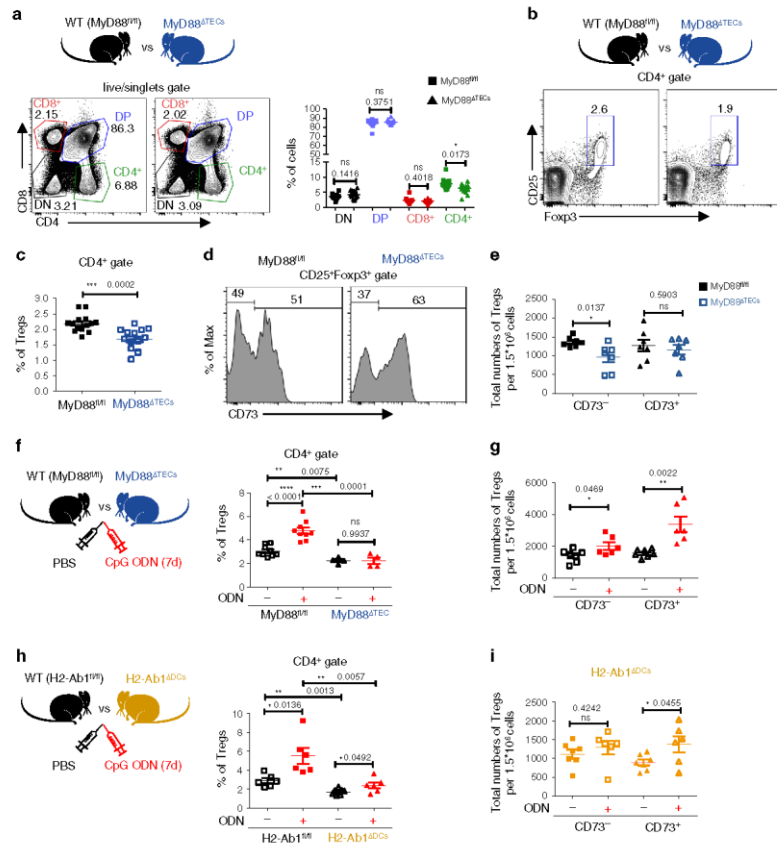
114

Fig. 6 Development of thymic Tregs is impaired in MyD88$^{\Delta TECs}$ mice. a Representative flow cytometry plots (left plot) and their quantification (right plot) comparing the frequencies of main thymic T cell populations between MyD88$^{fl/fl}$ and MyD88$^{\Delta TECs}$ mice (mean ± SEM, $n = 14$ mice). **b** Representative flow cytometry plots comparing the frequencies of CD4$^+$CD25$^+$Foxp3$^+$ thymic Tregs between MyD88$^{fl/fl}$ and MyD88$^{\Delta TECs}$ mice. **c** Quantification of frequencies from b (mean ± SEM, $n = 14$ mice). **d** Representative flow cytometry histograms showing the expression of CD73 by CD4$^+$ CD25$^+$Foxp3$^+$ thymic Tregs (gated as in b). **e** Quantification of the total numbers of CD73$^-$ and CD73$^+$ thymic Tregs from d (mean ± SEM, $n = 7$ mice). **f** Quantification of the frequencies of thymic Tregs from CpG ODN or PBS intrathymically stimulated (7 days) MyD88$^{fl/fl}$ or MyD88$^{\Delta TECs}$ mice (mean ± SEM, $n = 4$ for MyD88$^{\Delta TECs}$ and $n = 9$ for MyD88$^{fl/fl}$ mice). **g** Quantification of the total numbers of CD73$^-$ and CD73$^+$ thymic Tregs from CpG ODN or PBS intrathymically stimulated (7 days) WT (C57Bl/6J) mice (mean ± SEM, $n = 6$ for ODN$^+$ and $n = 7$ for ODN$^-$ mice). **h** Quantification of frequencies of thymic Tregs from CpG ODN or PBS intrathymically stimulated (7 days) H2-Ab1$^{fl/fl}$ or H2-Ab1$^{fl/fl}$Itgax^{Cre} (H2-Ab1$^{\Delta DCs}$) mice (mean ± SEM, $n = 6$ for H2-Ab1$^{fl/fl}$ and ODN$^+$ H2-Ab1$^{\Delta DCs}$ and $n = 7$ for ODN$^-$ H2-Ab1$^{\Delta DCs}$ mice). **i** Quantification of the total numbers of CD73$^-$ and CD73$^+$ thymic Tregs from CpG ODN or PBS intrathymically stimulated (7 days) H2-Ab1$^{\Delta DCs}$ mice (mean ± SEM, $n = 6$ for ODN$^+$ and $n = 7$ for ODN$^-$ mice). Statistical analysis in **a**, c, **e–i** was performed by unpaired, two-tailed Student's t-test, $p \leq 0.05 = *$, $p \leq 0.01 = **$, $p \leq 0.001*** p < 0.0001****$, ns not significant.

recruit CD14$^+$moDCs and, consequently, suboptimal production of thymic Tregs. Consistent with the previous report[53], we confirmed that the extrathymically enhanced (i.p. CpG ODN) or the lack of bacterially-derived MyD88 signals (GF mice) had no effect on the expression level of these chemokines and cytokines in WT mice. This was further corroborated by the fact that GF mice displayed normal numbers of Tregs[50] (Supplementary Fig. 7c).

This data demonstrates that the ligand triggering TLR9/ MyD88 signaling in mTECs^{high} is likely of endogenous thymic-derived origin.

Since MyD88 also conveys signals from the receptors of IL-1 family cytokines (IL-1β, IL-18, IL-33)[38], we tested in vitro whether their signaling in mTECs^{high} could trigger chemokine responses similar to those observed upon TLR9 stimulation. Of
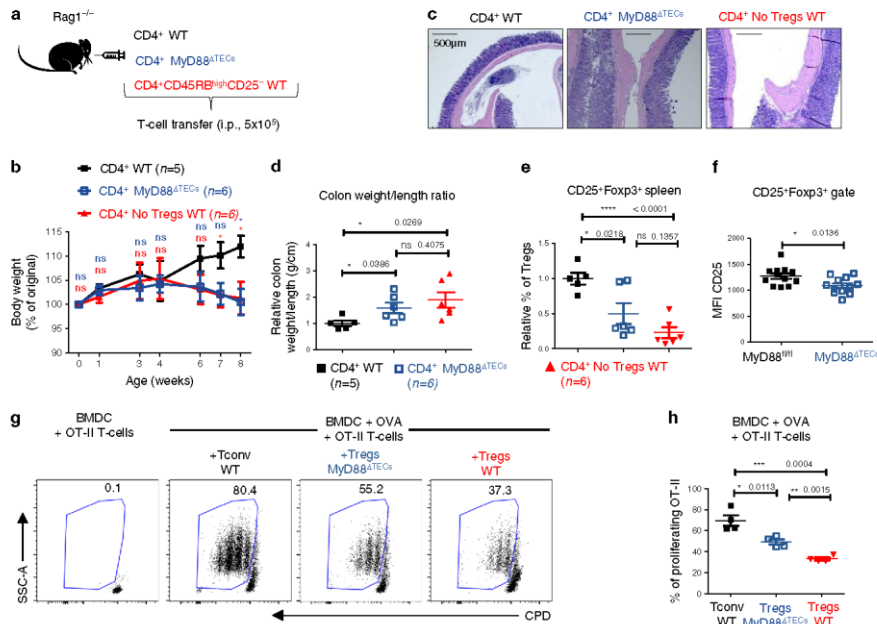
Fig. 7 Tregs from MyD88$^{\Delta TECs}$ mice have reduced suppressive capacity and failed to prevent the T cell induced colitis. a Experimental design of induced colitis. **b** Relative quantification of mice weight normalized to its value on day 0 (100% of original weight) after T cell transfer over the time-course of the colitis experiment (mean ± SEM, $n = 5–6$ mice) Statistical analysis was performed by unpaired, two-tailed Student's *t*-test comparing the relative weight of WT CD4+ with MyD88$^{\Delta TECs}$ CD4+ transferred mice (blue) or with WT CD4+CD45RB^{high}CD25$^-$ transferred mice (red), $p \leq 0.05 = $*, ns not significant. **c** Representative H&E-stained slides of colon sections performed 8 weeks after T cell transfer. Scale bar represents 500 µm ($n = 5$ for CD4+ WT and $n = 6$ for CD4+MyD88 $^{\Delta TECs}$ and CD4+ No Tregs WT mice). **d** Relative quantification (normalized to average of control mice from each experiment) of colon weight/length ratio of T cell induced colitis experimental mice (mean ± SEM, $n = 5–6$ mice). **e** Relative quantification of the frequencies (normalized to average of control mice from each experiment) of CD4+CD25+Foxp3+ Tregs isolated from the spleens of experimental mice 8 weeks after T cell transfer (mean ± SEM, $n = 5–6$ mice). **f** Quantification of the Means fluorescent intensity (MFI) of CD25 protein expression in CD25+Foxp3+ Tregs (gated as in Fig. 6b) in MyD88$^{fl/fl}$ and MyD88$^{\Delta TECs}$ mice (mean ± SEM, $n = 12$ mice) Statistical analysis in **b**, **d–f** was performed by unpaired, two-tailed Student's *t*-test, $p \leq 0.05 = $*, $p < 0.0001$****, ns not significant. **g** Representative flow cytometry plots showing the frequency of proliferating OT-II T cells, co-cultivated with OVA pulsed BMDC and CD4+CD25+ Tregs cells (alternatively with CD4+CD25- Tconv cells, black) isolated from LNs of MyD88$^{fl/fl}$ (WT control, red) or MyD88$^{\Delta TECs}$ (blue) for 72 h. **h** Quantification of frequencies of proliferating OT-II Tcells form h (mean ± SEM, $n = 4$ wells from two independent experiments).

this trio of cytokines, only IL-1β exhibited this capacity. This indicates that IL-1β could act as a co-regulator of chemokines and cytokine expression in mTECs^{high}. However, two observations suggest that TLR9/MyD88 signaling axis can act independently of IL-1β: (i) a direct, in vitro, stimulatory capacity of CpG ODN induces chemokine expression in sorted mTECs^{high}; and (ii) both in vivo intrathymic stimulation of TLR9/MyD88 signaling axis as well as its downregulation in MyD88$^{\Delta TECs}$ cells impacts the recruitment of the very same subsets of CD14+moDCs.

It has been postulated that Aire+ mTECs further differentiate into post-Aire cells, which downregulate the expression of MHCII and Aire, upregulate a set of genes, such as keratins (Krt1, 10, 77) or involucrin and form Hassall's corpuscles[40,41,54]. However, the regulatory mechanism(s) guiding this differentiation process remains poorly understood[55]. Our transcriptomic results are consistent with the idea that TLR/MyD88 signaling establishes an

expression profile that is associated with the differentiation of mTECs^{high} into post-Aire mTECs. Notably, TLR9 stimulation not only increased the number of Involucrin+ post-Aire mTECs (Supplementary Fig. 3e, f), but also lead to the upregulation of cytokines and chemokines (*Il1f6*, *Lcn2*, *Cxcl3*, and *Cxcl5*) associated with Hassall´s corpuscles[42] which attract CD14+moDCs. Together with the fact that they serve as a reservoir of a large amount of Aire-dependent TRAs, post-Aire mTECs could hold central position in the mechanism of transfer of mTEC-derived antigens to thymic DCs.

As described above, TLR/MyD88 signaling in mTECs^{high} drive the expression of chemokines which act on an overlapping set of receptors[32] predominantly expressed by CD14+moDCs (Cxcr2, Ccr1, Ccr3, Ccr5) and pDCs (Ccr5, Ccr6, and Ccr9). A correlative nature between the frequency of CD14+moDC in the thymus of MyD88$^{\Delta TECs}$ and of WT stimulated with CpG, underpins the

116

importance of these chemokines in controlling the migration of these cells into the thymic medulla. However, the deletion of Cxcr2 on hematopoietic cells, the common receptor for Cxcl1, Cxcl2, Cxcl3 and Cxcl5, did not yield any changes in the enrichment of CD14^{+}moDC in the thymus (Supplementary Fig. 6h). This observation, in conjunction with previous reports[18,56], allows one to predict that while the ligands of Ccr3 and/or Ccr5 (Ccl3, Ccl4, Ccl5 or Ccl24) likely regulate the entry of CD14^{+}moDC into the thymus[19], Cxcl-chemokines may regulate the positioning of these cells in close proximity of post-Aire mTECs. Interestingly, with the decreased frequency of CD14^{+} moDCs in the thymus of MyD88[ΔTEC], pDCs were similarly diminished. However, in contrast to CD14^{+}moDCs, the number of pDCs did not increase after TLR9 intrathymic stimulation. This is consistent with the fact that the migration of pDCs to the thymus is driven by Ccl25 (ligand of Ccr9 receptor)[14], the expression of which was diminished in MyD88[ΔTEC] but was not upregulated in WT mTECs after TLR9 stimulation.

It has been previously documented that specific subtypes of thymic DCs vary in their capacity to acquire antigens from TECs. Notably, while the transfer of MHC molecules from TECs to CD8α[+] cDC1 and Sirpα[+]DCs occurred at the same efficiency[16], the transfer of intracellular GFP was restricted mainly to CD8α[+]cDC1[10]. In comparison, our data shows that cytoplasmic TdTOM from Foxn1[Cre]ROSA26[TdTOMATO] could to certain extent, be transferred to all major subtypes of thymic DCs. This may be explained by the robustness of the Foxn1[Cre]-dependent system where, compared to Aire-GFP model, the production of TdTOM is not restricted only to Aire-expressing mTECs but to the entire thymic TEC population. Importantly, since the CAT of TdTOM after CpG ODN intrathymic injection is increasingly targeted to CD14^{+}moDC subpopulation, the efficiency of CAT correlates not only with the broadness of antigen expression but also with the frequency of a given DC subtype in the medulla. On the other hand, since TECs constitute a relatively rare cell population of thymic cells[57], the amount of antigen, which can be potentially transferred to DCs, is fairly limited. This could explain the fact that even when the entire population of thymic DCs is not affected by intrathymic TLR9 stimulation, the frequency of TdTOM^{+} pDCs is significantly decreased, due to the increased competition for TdTOM uptake by CD14^{+}moDCs.

It has become clear that developing thymocytes encounter self-antigens presented by various types of thymic APC, including mTECs[47], B-cells[58], pDCs[14], and cDCs[11,59]. Although the generation of thymic Tregs was shown to be dependent on antigen presentation by both mTECs and DCs[4,47], thymic cDCs seem to be particularly important for this process[6,17,60]. Along with self-antigen presentation, thymic cDCs express high levels of co-stimulatory molecules CD80/86 as well as CD70 which play a crucial role in promoting thymic Treg development[61,62]. Among cDCs, Sirpα^{+}DCs are the most efficient in supporting Treg generation[17,20,63]. In this context, our data demonstrates that the development of thymic CD25^{+}Foxp3^{+} Tregs is boosted by TLR/ MyD88 signaling in TECs, which produce a chemokine gradient driving the migration of CD14^{+}moDCs into the thymus. We also found that mTEC-intrinsic TLR9/MyD88 signaling increased the cell ratio of Sirpα^{+}DCs to Xcr1^{+}cDC1, which correlated with an increased production of thymic Tregs. These findings accurately recapitulate the thymic phenotype of Ccr7^{−/−} mice where the increased ratio of Sirpα[+]DCs to cDC1 correlated with the increased generation of thymic Tregs[20]. This data, together with the fact that abrogation of MHCII-antigen presentation specifically in DCs, resulted in a reduced number of thymic Tregs in unstimulated[17] as well as in CpG stimulated thymus (Fig. 6h), suggest that TLR/MyD88-dependent generation of thymic Tregs is mediated by antigen-presentation by DCs.

Our results also show that TLR/MyD88 signalling in mTECs drives the recirculation of mature CD73^{+}CD25^{+}Foxp3^{+} Tregs into the thymus. Compared to newly generated CD73^{−} Tregs, their increased number in the TLR9 stimulated thymus was not dependent on MHCII presentation by DCs. Together, with the fact that recirculation of CD73^{+} Tregs was not abrogated in MyD88[ΔTECs] mice, suggests that Ccl20, the ligand for Ccr6, which is highly expressed by recirculating Tregs[64] regulates the increased recirculation of CD73^{+}CD25^{+}Foxp3^{+} Tregs into the thymus after TLR9 intrathymic stimulation (Figs. 2d and e).

Altogether, our model proposes that TLR/MyD88 signaling in mTECs regulates the generation of Tregs. The mechanism involves TLR-induced chemokine production and subsequent chemotactic recruitment of CD14^{+}moDC to the thymic medulla, which predicates the developmental output of Tregs. Although this study explores only TLR9 signaling in mTECs, questions surrounding the nature of potential thymic-derived endogenous ligands for TLR/MyD88 signals in mTECs remains enigmatic and warrant further study.

Methods

Mice. A majority of the mice used in this study were of C57BL/6J genetic background and housed in the animal facility at the Institute of Molecular Genetics of the ASCR v.v.i. under SPF conditions. Mice were fed with irradiated standard rodent high energy breeding diet (Altromin 1314 IRR) and given reverse osmosis filtered and chlorinated water ad libitum. Light were adjusted to a 12 h/12 h light/dark cycle; temperature and relative humidity were maintained at 22 ± 1°C and 55 ± 5%, respectively. Experimental protocols were approved by the ethical committee of the Institute of Molecular Genetics and by the ethical committee of the Czech Academy of Science. Aire^{−/−} (B6.129S2-Aire[tm1.1Doi]/J, stock# 004743)[2], Foxn1[Cre] (B6(Cg)-Foxn1[tm3(cre)Nrm]/J, stock# 018448)[29], MyD88^{fl/fl} (B6.129P2(SJL)-Myd88[tm1Defr]/J, stock# 008888), MyD88^{−/−} (B6.129P2(SJL)-Myd88[tm1.1Defr]/J, stock# 009088)[30], Rag1^{−/−} (B6.129S7-Rag1[tm1Mom]/J, stock# 002216)[65], Ly5.1 (B6. SJL-Ptprc[a]Pepc[b]/BoyJ, stock# 002014)[66], Cxcr2^{fl/fl} (C57BL/6-Cxcr2[tm1Rmra]/J, stock# 024638)[67], H2-Ab1^{fl/fl} (B6.129×1-H2-Ab1[tm1Koni]/J, stock# 013181)[68], and Itgax[Cre] (B6.Cg-Tg(Itgax-cre)1-1Reiz/J, stock# 008068)[69] mice were purchased from Jackson Laboratories. Rosa26[TdTOMATO] (B6;129S6-Gt(ROSA)26[Sortm14(CAG-tdTomato)Hze]/J, stock# 007908)[70] and Vav1[Cre] (B6.Cg-Comm d10[Tg(Vav1-icre)A2Kio]/J, stock# 008610)[71] were kindly provided by V. Kořínek (Institute of Molecular Genetics of the ASCR, Prague, Czech Republic). Aire-HCO (Balb/c)[4] were provided by L. Klein. Cd3e[−/−][72], RIP-OVA[73], OT-I[+]Rag2[−/−][74] (all C57BL/6J) were provided by O. Štěpánek. OT-II (B6.Cg-Tg(TcraTcrb)425Cbn/J, stock# 004194)[75] mice were kindly provided by T. Brdička (Institute of Molecular Genetics of the ASCR, Prague, Czech Republic). C57BL/6J GF and control C57BL/6J SPF mice were kindly provided by M. Schwarzer (Institute of Microbiology of the ASCR, Nový Hrádek, Czech Republic. Both GF and control SPF mice were subject to the SSNIPF V1124-300 diet. Thymic cell populations were isolated from 3–6-week-old mice with the exception of newborn mice (4 days old) used in Supplementary Fig. 7b. For the purpose of BM chimera experiments, 5–6-week-old mice were irradiated and analysed between 11 and 13 weeks of age. Comparative analysis used age-matched cohorts regardless of sex and caging. Where possible, littermates were used as the controls. For the purpose of tissue isolation, mice were euthanized by cervical dislocation.

Tissue preparation and cell isolation. Thymic antigen presenting cells, TECs and DCs, were isolated as follows. Thymus was minced into small pieces and treated with Dispase II (Gibco), dissolved in RPMI at concentration 0.1 mg ml⁻¹. Tissue was homogenized by pipetting and after 10 min of incubation (37°C), the supernatant was collected and the reaction was stopped by adding 3% FSC and 2 nM EDTA. The process was repeated until all thymic fragments were digested. For detail description see[76]. For thymic epithelial cells isolation, the whole thymic cell suspension was depleted of CD45^{+} cells by CD45 microbeads staining (Miltenyi biotec). Thymic dendritic cells were isolated using MACS enrichment for CD11c^{+} cells through staining with biotinylated CD11c antibody, followed by Ultrapure Anti-Biotin microbeads staining (Miltenyi biotec). For isolation of T cell, thymus, peripheral lymph nodes (pLN), mesenteric lymph nodes (mLN) or spleen were mechanically mashed through 40 μm Cell strainer (Biologix) and cell suspensions were passed through 50 μm filters (Sysmex). The resulting cell suspension was spun down (4 °C, 400 g, 10 min) and erythrocytes were removed using ACK lysis buffer.

Flow cytometry analysis and cell sorting. Flow cytometry (FACS) analysis and cell sorting were performed using BD LSR II and BD Influx (BD Bioscience) cytometers, respectively. For surface staining, cells were incubated for 20–30 min at 4 °C with the indicated fluorochrome- or biotin-conjugated antibodies. Where necessary, cells were further incubated with streptavidin conjugates for 15 min.

117

Dead cells were excluded using Hoechst 33258 (Sigma) or viability dye eFluor 450 or 506 (eBioscience). For the intracellular staining of Aire and Foxp3, the cells were first stained for the targeted surface molecules, fixed, and permeabilized for 30 min at room temperature (RT) using the Foxp3/Transcription Factor Staining Buffer Set (eBioscience), then stained for 30 min at RT with fluorochrome-conjugated antibodies. FlowJO V10 software (Treestar) and BD PACSDiva™ Software v6.0 for BD™ LSR II (with HTS Option) was used for FACS data analysis including tSNE analysis shown in Fig. 5e. A complete inventory of staining reagents is listed in Supplementary Data 6.

Imaging flow cytometry. Imaging flow cytometry was performed at the Center for Advanced Preclinical Imaging (CAPI) with the use of AMNIS ImageStream X MkII (AMNIS). DCs isolated from Foxn1^{Cre}ROSA26^{TdTOMATO} mice were stained for the surface markers MHCII and CD11c. Dead cells were excluded by Hoechst 33258 staining and bright field analysis. Cells were recorded using 40x magnification. Data was analyzed with Ideas 6.1 software (AMNIS). A complete list of staining reagents can be found in Supplementary Data 6.

In vitro TLRs and cytokines stimulation assays. mTEC^{high} were gated as EpCAM$^+$CD11c$^-$Ly51$^-$MHCII^{high}CD80^{high} and sorted into RPMI media (Sigma) containing 10% FSC and 1% Penicillin/Streptomycin (Gibco). Cells were then cultured in a 96-flat-well plate in 200 µL of 10% FSC RPMI with Penicillin/Streptomycin in the presence of Endotoxin-free TLR ligands (InvivoGen) or recombinant mouse cytokines: TLR9 ligand-CpG ODN (ODN 1826) (5 µM), TLR4 ligand-LPS (1 µg/ml), Il-1β (10 ng/ml), Il-33 (10 ng/ml) (both ImmunoTools) and Il-18 (10 ng/ml) (Biolegend). After 24 h, the supernatant was removed and the cells were resuspended in RNA-lysis buffer. Subsequently, RNA isolation was performed.

In vivo TLR stimulation. For intrathymic injections, mice were anesthetized by i.p. injection of Zoletil (Tiletamine (50 mg/ml) and Zolazepam (50 mg/ml), Virbac) dissolved in PBS at a dose of 50 mg/kg and 10–20 µl of 500 µM CpG ODN (ODN 1826, InvivoGen) or PBS was injected using an insulin syringe (29G) directly into the first intercostal space from the manubrium ~2 mm left of the sternum and 4 mm in depth. The angle of injection was from 25 to 30° relative to the sternum[77]. For systemic TLR9 stimulation, mice were injected by CpG ODN (ODN 1826, InvivoGen) (500 µM) or PBS at day 0 and day 1 into the peritoneum. Mice were then maintained under SPP conditions and euthanized at the indicated time point of an experiment.

Immunofluorescent analysis of thymic cryosections. The thymus was fixed overnight in 4% paraformaldehyde (Sigma) at 4 °C, washed three times in PBS, incubated overnight in 30% sucrose at 4 °C, and finally embedded in OCT compound (VWR). Cryoblocks were cut at 8 µm and blocked with PBS containing 5% BSA (w/v) and 0.1% Triton X-100 for 1 hour at room temperature. Samples were incubated overnight at 4 °C with the following primary antibodies: anti-keratin 14, Sirpa, and CD11c-biotin (Fig. 3d) or anti-Involucrin and anti-EpCAM-APC (Supplementary Fig. 3b). The samples were stained with secondary reagents, Goat anti-rat AF-568, goat anti-rabbit AF-647 and streptavidin FITC or goat anti-rabbit AF-488 for one hour at RT. Sections stained only with secondary reagents were used as negative controls. 4′,6-diamino-2-phenylindole (DAPI) was used to visualize cell nuclei. Stained sections were imaged in Vectashield medium (Vector Laboratories) and imaged using a Dragonfly 503 (Andor)—spinning disk confocal microscope with the immersion objective HC PL APO 20×/0.75. A complete list of staining reagents can be found in Supplementary Data 6. Z-stacks were composed using ImageJ and deconvolution was done by Huygens Professional. CD11c$^+$Sirpa$^+$ double positive cells were counted in multiple 300µm×300µm areas in keratin-14 rich (medulla) and keratin-14 negative (cortex) areas. Counting was done as a blind experiment by three different investigators. Involucrin$^+$EpCAM$^+$ double positive cells were counted as number of cells per thymic medullary region (determined by DAPI staining).

Gene expression analysis by qRT-PCR. Total RNA from FACS-sorted cells was extracted using an RNeasy Plus Micro Kit (Qiagen) and reverse transcribed using RevertAid (ThermoFisher) transcriptase and random hexamers (ThermoFisher). Quantitative RT PCR (qRT PCR) was performed using the LightCycler 480 SYBR Green I Master mix (Roche) on a LightCycler 480 II (Roche). Each sample was tested in duplicate. Threshold cycles were calculated using LightCycler 480 1.5 software. Gene expression was calculated by the relative quantification model[78] using the mRNA levels of the housekeeping gene, Casc3, as a control. Primers were designed using Primer-BLAST (NCBI, NIH). Primers sequences are listed in Supplementary Data 6.

Bone marrow chimera generation. Bone marrow cells were isolated from the *femur* and *tibia* of Ly5.1 mice (CD45.1$^+$) and subsequently depleted of erythrocytes using ACK lysis buffer. Recipient mice (Foxn1^{Cre}ROSA26^{TdTOMATO}, CD45.2$^+$) were irradiated with 6 Gy and reconstituted with 2 × 10^6 donor BM cells. These mice were maintained on water supplemented with gentamycin (1 mg/ml) for 10 days. Three weeks after irradiation, the frequency of blood cell reconstitution

was measured by FACS using anti-CD45.1 and CD45.2 antibodies. If the reconstitution was higher than 80%, mice were euthanized 6 weeks after transfer and subjected to further analysis.

RNA-sequencing and analysis. mTECs were sorted according to the protocol described above and RNA was extracted using a RNeasy Plus Micro Kit (Qiagen). cDNA synthesis, ligation of sequencing adaptors and indexes, ribosomal cDNA depletion, final PCR amplification and product purification were prepared with a SMARTer® Stranded Total RNA-Seq – Pico Input Mammalian library preparation kit v2 (Takara). Library size distribution was evaluated on a Agilent 2100 Bioanalyzer using the High Sensitivity DNA Kit (Agilent). Libraries were sequenced on a Illumina NextSeq® 500 instrument using a 76 bp single-end high-output configuration resulting in ~30 million reads per sample. Read quality was assessed by FastQC (0.11.9). Subsequent read processing including removing sequencing adaptors (Trim Galore!, version 0.4.5), mapping to the reference genome (GRCm38 (Ensembl assembly version 91)) with HISAT2 (2.1.0), and quantifying expression at the genetic level (featureCounts) was done via the SciLifeLab/NGI-RNAseq pipeline [https://github.com/SciLifeLab/NGI-RNAseq]. Final per gene read counts served as an input for differential expression analysis using a DESeq2 R Bioconductor (3.10). Prior to this analysis, genes that were not expressed in at least two samples were discarded. Genes exhibiting a minimal absolute log2-fold change value of 1 and a statistical significance (adjusted p-value < 0.05) between conditions were considered as differentially expressed for subsequent interpretation and visualization. All figures (volcano plots, etc.) were generated using basic R graphical functions. The raw sequencing data were deposited at the ArrayExpress database under accession numbers E-MTAB-8024 (for Fig. 2a, b) and E-MTAB-8025 (for Fig. 2d, e).

Single-cell RNA sequencing. DCs were sorted from Foxn1^{Cre}ROSA26^{TdTOMATO} as Gr-1$^-$CD11c$^+$TdTOM$^+$ (described in detail in Supplementary Fig. 3a and Fig. 4c). Two independent samples (Sample 1 and 2) were used for further analysis. A single-cell library was prepared by Illumina/Bio-Rad single-cell RNA-seq system with a SureCell WTA 3' Library Prep Kit according to the manufacturer's instructions. Total cell concentration and viability was ascertained using a TC20 Automated Cell Counter (Bio-Rad). A ddSEQ Single-Cell Isolator (Bio-Rad) was used to co-encapsulate single cells with barcodes and enzyme solutions for cDNA synthesis. Nextera SureCell transposome solution was used for cDNA fragmentation and ligation of sequencing indexes, followed by PCR amplification and short fragment removal. Finally, library fragment length distribution and concentration were analyzed on a Agilent Bioanalyzer 2100 using a High Sensitivity DNA Kit (Agilent). The resulting libraries were sequenced using a 68/75 paired-end configuration on a Illumina NextSeq® 500 instrument resulting in ~73 million reads per sample.

Single-cell RNA sequencing analysis. The quality of reads was assessed by FastQC. Cell identification was accomplished with cell barcodes and low-expression cells filtering using UMI-tools[79]. The analysis identified 202 cells in Sample 1 and 218 cells in Sample 2. Reads assigned to the selected cells were mapped to the GRCm38 genome assembly (Ensembl version 91) with HISAT2 (2.1.0). Gene expression was quantified using, featureCounts (2.0.0) after deduplication of per-gene assigned read counts by UMIs with UMI-tools. De-duplicated per-gene read counts were imported into R for exploration and statistical analysis using a Seurat[80] package (version 3.0). Counts were normalized according to total expression, multiplied by a scale factor (10,000), and log-transformed. For cell cluster identification and visualization, gene expression values were also scaled according to highly variable genes after controlling for unwanted variation generated by sample identity. Cell clusters were identified based on t-SNE of the first six principal components of PCA using Seurat's method, FindClusters, with a original Louvain algorithm and resolution parameter value of 0.3. To find cluster marker genes, Seurat's method, FindAllMarkers, along with a likelihood ratio test assuming an underlying negative binomial distribution suitable for UMI datasets was used. Only genes exhibiting a significant (adjusted p-value < 0.05) minimal average absolute log2-fold change of 1 between each of the clusters and the rest of the dataset were considered as differentially expressed. For t-SNE expression plots, normalized count data were used. Heatmaps of gene expression per cluster were generated based on gene z-score scaled raw counts. The raw sequencing data was deposited at the ArrayExpress database under accession number E-MTAB-8028.

In vitro antigen presenting assay. For the purpose of antigen presentation assay CD14$^+$moDCs were gated as CD11c$^+$MHCII$^+$B220$^-$Xcr1$^-$Cx3cr1$^+$CD14$^+$ and FACS sorted from Aire-HCO mice into DMEM high-glucose medium (Sigma) supplemented with 10% FCS and 1% Penicillin-Streptomycin (Gibco) and cultivated in a 96 well plate together with the A5 hybridoma cell line (HA-specific CD4 T cell hybridoma cells carrying a GFP-NFAT reporter) at a 1:5 ratio (10 000 of CD14$^+$moDC: 50 000 of A5 cells). As a positive control, CD14$^+$moDCs were pulsed with HA peptide (107-119; customized by Thermofisher) at a concentration of 1 µg/ml. After 20 h, the level of GFP expression by A5 hybridomas was analyzed by flow cytometry.

118

Induction of T cell transfer colitis and histological analysis. FACS-sorted 5×10^5 TCRβ$^+$CD4$^+$CD45RB^{high}CD25$^-$ or complete TCRβ$^+$CD4$^+$ were transferred by i. p. injection into Rag1$^{-/-}$ recipient mice (5-7 weeks old). The weight of mice was recorded weekly to monitor the progress of colitis. Mice were euthanized 8 weeks after transfer[51]. Spleens and colons of the animals were weighed and the length of the colon was measured. For histological analysis PBS washed colons were fixed in 4% paraformaldehyde (Sigma) and embedded into paraffin. Tissue sections were cut into 5μm thin slices, deparaffinized, and stained with hematoxylin and eosin (H&E).

In vitro Tregs suppression assay. BM-derived DCs (BMDCs) were prepared as follows. BM cells were flushed from femur and tibia of WT C57BL/6J mice and cultured in RPMI media (Sigma) containing 10% FSC and 1% Penicillin/Streptomycin (Gibco) supplemented with GM-CSF (5 ng/ml). Fresh media containing GM-CSF was added at day 3 and 5 of cultivation. After 7 days, BMDCs was pulsed with OVA cognate peptide 323-339 (irrelevant OVA 257-264 peptide was used as control) (InvivoGen) at a concentration of 1 μg/ml and co-cultivated with OVA-specific OT-II T cells and Tregs (10 000 BMDCs: 50 000 OT-II T cells: 50 000 Tregs). OT-II T cells were isolated from OT-II+Rag1$^{-/-}$ mice as MACS-enriched CD4$^+$ T cells (CD4$^+$ T Cell Isolation Kit, Miltenyi biotec). CD4$^+$ conventional T cells (Tconv) were used as a negative control. Tregs were isolated from LNs (pLN and mLN) of WT (MyD88$^{fl/fl}$) and MyD88^{ΔTECs} mice using subsequent Auto-MACS (Miltenyi biotec) procedure. CD4-enriched T cells (CD4$^+$ T Cell Isolation Kit, Miltenyi biotec) were stained by anti-CD25 biotin conjugated antibody and CD4$^+$CD25$^+$ Tregs were isolated using Anti-Biotin MicroBeads (Miltenyi biotec). Tconv cells were prepared using Auto-MACS as CD4$^+$CD25$^-$ cells. After 3 days of co-cultivation, cells were stained with anti-Vβ5 and anti-Vα2 antibodies to distinguish OT-II$^+$ T cells. Proliferation was measured by FACS using CPD670 staining.

In vivo model of autoimmune diabetes. Cd3ε$^{-/-}$-RIP-OVA mice (6–8 weeks old) were intravenously injected by MACS enriched CD8$^+$ T cells (5×10^5 cells per mouse) isolated from lymph nodes and spleen of Rip-OVA Ly5.1 (CD45.1$^+$) mice at day 8. After 7 days (day 1) Cd3ε$^{-/-}$-RIP-OVA mice were intravenously injected, FACS sorted CD4$^+$CD25$^+$ Tregs were isolated from LNs (mLN and pLN) of WT (MyD88$^{fl/fl}$), MyD88^{ΔTECs} mice (3×10^5 cells per mouse), OT-I (OT-I$^+$Rag2$^{-/-}$, 100 cells per mouse), and OT-II cells (OT-II$^+$Rag1$^{-/-}$, 1×10^4 cells per mouse). BMDCs (generated as described previously, 10 days of culture, media refreshment at day 4 and 7) were pulsed with OVA peptides (OVA 257–264, 2 mM and OVA 323-339, 100 μM, InvivoGen) in the presence of LPS (100 μg/ml, InvivoGen) for 3 h. In all, 1×10^6 of antigen-stimulated DCs were used for injection (at day 0). Glucose levels were monitored on a daily basis (between day 5 and 14) using test strips (Diabur-Test 5000, Roche or GLUKOPHAN, Erba Lachema, Czech Republic). The animal was considered to have developed autoimmunity when the concentration of glucose in the urine reached ≥10 mmol/l. At day 14, mice were euthanized and the frequency of splenic KLGR1$^+$ OT-1 T cells was measured by flow cytometry.

Statistical analysis. The statistical tests used to analyze the data are indicated in figure legends. Graph construction and statistical analysis were performed using Prism 5.04 software (GraphPad). Statistical analysis of RNAseq and scRNAseq data is indicated in the corresponding method section.

Reporting summary. Further information on research design is available in the Nature Research Reporting Summary linked to this article.

Data availability
The authors declare that all data supporting the findings of this study are available within the article and its supplementary information files or from the corresponding author upon reasonable request. The source data underlying Fig. 1c, f, 2c, f, g, 3a–c, e, 4d, f, 5d, f, g, 6a, c, e–i, 7b, d–h and Supplementary Figs. 2b–d, 3a, b, d, e, 4c, 5e, f, 6c, e, h, 7a–d, f, h and 8b, c, e are provided as a Source Data file. The raw RNA sequencing data are deposited at the ArrayExpress database [https://www.ebi.ac.uk/arrayexpress/] under accession numbers E-MTAB-8024 (Fig. 2a, b), E-MTAB-8025 (Fig. 2d, e) and E-MTAB-8028 (Fig. 5a–c).

References
1. Klein, L., Kyewski, B., Allen, P. M. & Hogquist, K. A. Positive and negative selection of the T cell repertoire: what thymocytes see (and don't see). *Nat. Rev. Immunol.* **14**, 377–391 (2014).
2. Anderson, M. S. et al. Projection of an immunological self shadow within the thymus by the aire protein. *Science* **298**, 1395–1401 (2002).
3. Liston, A., Lesage, S., Wilson, J., Peltonen, L. & Goodnow, C. C. Aire regulates negative selection of organ-specific T cells. *Nat. Immunol.* **4**, 350–354 (2003).
4. Aschenbrenner, K. et al. Selection of Foxp3+ regulatory T cells specific for self antigen expressed and presented by Aire+ medullary thymic epithelial cells. *Nat. Immunol.* **8**, 351–358 (2007).
5. Malchow, S. et al. Aire-dependent thymic development of tumor-associated regulatory T cells. *Science* **339**, 1219–1224 (2013).
6. Perry, J. S. et al. Distinct contributions of Aire and antigen-presenting-cell subsets to the generation of self-tolerance in the thymus. *Immunity* **41**, 414–426 (2014).
7. Leventhal, D. S. et al. Dendritic cells coordinate the development and homeostasis of organ-specific regulatory T cells. *Immunity* **44**, 847–859 (2016).
8. Gallegos, A. M. & Bevan, M. J. Central tolerance to tissue-specific antigens mediated by direct and indirect antigen presentation. *J. Exp. Med.* **200**, 1039–1049 (2004).
9. Koble, C. & Kyewski, B. The thymic medulla: a unique microenvironment for intercellular self-antigen transfer. *J. Exp. Med.* **206**, 1505–1513 (2009).
10. Perry, J. S. A. et al. Transfer of cell-surface antigens by scavenger receptor CD36 promotes thymic regulatory t cell receptor repertoire development and allo-tolerance. *Immunity* **48**, 1271 (2018).
11. Lancaster, J. N. et al. Live-cell imaging reveals the relative contributions of antigen-presenting cell subsets to thymic central tolerance. *Nat. Commun.* **10**, 2220 (2019).
12. Li, J., Park, J., Foss, D. & Goldschneider, I. Thymus-homing peripheral dendritic cells constitute two of the three major subsets of dendritic cells in the steady-state thymus. *J. Exp. Med.* **206**, 607–622 (2009).
13. Guilliams, M. et al. Dendritic cells, monocytes and macrophages: a unified nomenclature based on ontogeny. *Nat. Rev. Immunol.* **14**, 571–578 (2014).
14. Hadeiba, H. et al. Plasmacytoid dendritic cells transport peripheral antigens to the thymus to promote central tolerance. *Immunity* **36**, 438–450 (2012).
15. Bonasio, R. et al. Clonal deletion of thymocytes by circulating dendritic cells homing to the thymus. *Nat. Immunol.* **7**, 1092–1100 (2006).
16. Kroger, C. J., Spidale, N. A., Wang, B. & Tisch, R. Thymic dendritic cell subsets display distinct efficiencies and mechanisms of intercellular MHC transfer. *J. Immunol.* **198**, 249–256 (2017).
17. Leventhal, D. S. et al. Dendritic cells coordinate the development and homeostasis of organ-specific regulatory T cells. *Immunity* **44**, 847–859 (2016).
18. Lei, Y. et al. Aire-dependent production of XCL1 mediates medullary accumulation of thymic dendritic cells and contributes to regulatory T cell development. *J. Exp. Med.* **208**, 383–394 (2011).
19. Baba, T., Nakamoto, Y. & Mukaida, N. Crucial contribution of thymic Sirp alpha+ conventional dendritic cells to central tolerance against blood-borne antigens in a CCR2-dependent manner. *J. Immunol.* **183**, 3053–3063 (2009).
20. Hu, Z. et al. CCR7 modulates the generation of thymic regulatory T cells by altering the composition of the thymic dendritic cell compartment. *Cell Rep.* **21**, 168–180 (2017).
21. Kawai, T. & Akira, S. The role of pattern-recognition receptors in innate immunity: update on Toll-like receptors. *Nat. Immunol.* **11**, 373–384 (2010).
22. Abramson, J. & Anderson, G. Thymic Epithelial Cells. *Annu Rev. Immunol.* **35**, 85–118 (2017).
23. Haljasorg, U. et al. A highly conserved NF-kappaB-responsive enhancer is critical for thymic expression of Aire in mice. *Eur. J. Immunol.* **45**, 3246–3256 (2015).
24. LaFlam, T. N. et al. Identification of a novel cis-regulatory element essential for immune tolerance. *J. Exp. Med.* **212**, 1993–2002 (2015).
25. Bernasconi, P. et al. Increased toll-like receptor 4 expression in thymus of myasthenic patients with thymitis and thymic involution. *Am. J. Pathol.* **167**, 129–139 (2005).
26. Cavalcante, P. et al. Toll-like receptors 7 and 9 in myasthenia gravis thymus: amplifiers of autoimmunity? *Ann. N. Y Acad. Sci.* **1413**, 11–24 (2018).
27. Huang, H. B. et al. TLR4 is constitutively expressed in chick thymic epithelial cells. *Vet. Immunol. Immunopathol.* **158**, 182–188 (2014).
28. Tian, J. et al. Toll-like receptor 9-dependent activation by DNA-containing immune complexes is mediated by HMGB1 and RAGE. *Nat. Immunol.* **8**, 487–496 (2007).
29. Gordon, J. et al. Specific expression of lacZ and cre recombinase in fetal thymic epithelial cells by multiplex gene targeting at the Foxn1 locus. *BMC Dev. Biol.* **7**, 69 (2007).
30. Hou, B., Reizis, B. & DeFranco, A. L. Toll-like receptors activate innate and adaptive immunity by using dendritic cell-intrinsic and -extrinsic mechanisms. *Immunity* **29**, 272–282 (2008).
31. Sansom, S. N. et al. Population and single-cell genomics reveal the Aire dependency, relief from Polycomb silencing, and distribution of self-antigen expression in thymic epithelia. *Genome Res.* **24**, 1918–1931 (2014).

119

32. Griffith, J. W., Sokol, C. L. & Luster, A. D. Chemokines and chemokine receptors: positioning cells for host defense and immunity. *Annu Rev. Immunol.* **32**, 659–702 (2014).
33. Vigne, S. et al. IL-36R ligands are potent regulators of dendritic and T cells. *Blood* **118**, 5813–5823 (2011).
34. Becher, B., Tugues, S. & Greter, M. GM-CSP: from growth factor to central mediator of tissue inflammation. *Immunity* **45**, 963–973 (2016).
35. Zlotoff, D. A. et al. CCR7 and CCR9 together recruit hematopoietic progenitors to the adult thymus. *Blood* **115**, 1897–1905 (2010).
36. Dyer, D. P. et al. Chemokine receptor redundancy and specificity are context dependent. *Immunity* **50**, 378–389.e375 (2019).
37. Belperio, J. A. et al. Critical role for CXCR2 and CXCR2 ligands during the pathogenesis of ventilator-induced lung injury. *J. Clin. Invest.* **110**, 1703–1716 (2002).
38. Fields, J. K., Günther, S. & Sundberg, E. J. Structural Basis of IL-1 Family Cytokine Signaling. *Front Immunol.* **10**, 1412 (2019).
39. Eckhart, L., Lippens, S., Tschachler, E. & Declercq, W. Cell death by cornification. *Biochim Biophys. Acta* **1833**, 3471–3480 (2013).
40. Miller, C. N. et al. Thymic tuft cells promote an IL-4-enriched medulla and shape thymocyte development. *Nature* **559**, 627–631 (2018).
41. Bornstein, C. et al. Single-cell mapping of the thymic stroma identifies IL-25-producing tuft epithelial cells. *Nature* **559**, 622–626 (2018).
42. Wang, J. et al. Hassall's corpuscles with cellular-senescence features maintain IFNα production through neutrophils and pDC activation in the thymus. *Int Immunol.* **31**, 127–139 (2019).
43. Kolodziejczyk, A. A., Kim, J. K., Svensson, V., Marioni, J. C. & Teichmann, S. A. The technology and biology of single-cell RNA sequencing. *Mol. Cell* **58**, 610–620 (2015).
44. Biton, M. et al. T helper cell cytokines modulate intestinal stem cell renewal and differentiation. *Cell* **175**, 1307–1320.e1322 (2018).
45. Ardouin, L. et al. Broad and largely concordant molecular changes characterize tolerogenic and immunogenic dendritic cell maturation in thymus and periphery. *Immunity* **45**, 305–318 (2016).
46. Hettinger, J. et al. Origin of monocytes and macrophages in a committed progenitor. *Nat. Immunol.* **14**, 821–830 (2013).
47. Hinterberger, M. et al. Autonomous role of medullary thymic epithelial cells in central CD4(+) T cell tolerance. *Nat. Immunol.* **11**, 512–519 (2010).
48. McCaughtry, T. M., Wilken, M. S. & Hogquist, K. A. Thymic emigration revisited. *J. Exp. Med.* **204**, 2513–2520 (2007).
49. Thiault, N. et al. Peripheral regulatory T lymphocytes recirculating to the thymus suppress the development of their precursors. *Nat. Immunol.* **16**, 628–634 (2015).
50. Owen, D. L. et al. Thymic regulatory T cells arise via two distinct developmental programs. *Nat. Immunol.* **20**, 195–205 (2019).
51. Mottet, C., Uhlig, H. H. & Powrie, F. Cutting edge: cure of colitis by CD4 +CD25+ regulatory T cells. *J. Immunol.* **170**, 3939–3943 (2003).
52. Drobek, A. et al. Strong homeostatic TCR signals induce formation of self-tolerant virtual memory CD8 T cells. *EMBO J* **37**, e98518 (2018).
53. Gray, D. H., Gavanescu, I., Benoist, C. & Mathis, D. Danger-free autoimmune disease in Aire-deficient mice. *Proc. Natl Acad. Sci. USA* **104**, 18193–18198 (2007).
54. Yano, M. et al. Aire controls the differentiation program of thymic epithelial cells in the medulla for the establishment of self-tolerance. *J. Exp. Med.* **205**, 2827–2838 (2008).
55. White, A. J. et al. Lymphotoxin signals from positively selected thymocytes regulate the terminal differentiation of medullary thymic epithelial cells. *J. Immunol.* **185**, 4769–4776 (2010).
56. Lancaster, J. N., Li, Y. & Ehrlich, L. I. R. Chemokine-mediated choreography of thymocyte development and selection. *Trends Immunol.* **39**, 86–98 (2018).
57. Klein, L. Dead man walking: how thymocytes scan the medulla. *Nat. Immunol.* **10**, 809–811 (2009).
58. Yamano, T. et al. Thymic B cells are licensed to present self antigens for Central T cell tolerance induction. *Immunity* **42**, 1048–1061 (2015).
59. Ohnmacht, C. et al. Constitutive ablation of dendritic cells breaks self-tolerance of CD4 T cells and results in spontaneous fatal autoimmunity. *J. Exp. Med.* **206**, 549–559 (2009).
60. Román, E., Shino, H., Qin, F. X. & Liu, Y. J. Cutting edge: Hematopoietic-derived APCs select regulatory T cells in thymus. *J. Immunol.* **185**, 3819–3823 (2010).
61. Salomon, B. et al. B7/CD28 costimulation is essential for the homeostasis of the CD4+CD25+ immunoregulatory T cells that control autoimmune diabetes. *Immunity* **12**, 431–440 (2000).
62. Coquet, J. M. et al. Epithelial and dendritic cells in the thymic medulla promote CD4+Foxp3+ regulatory T cell development via the CD27-CD70 pathway. *J. Exp. Med* **210**, 715–728 (2013).
63. Proietto, A. I. et al. Dendritic cells in the thymus contribute to T-regulatory cell induction. *Proc. Natl Acad. Sci. USA* **105**, 19869–19874 (2008).
64. Cowan, J. E. et al. Aire controls the recirculation of murine Foxp3. *Eur. J. Immunol.* **48**, 844–854 (2018).
65. Mombaerts, P. et al. RAG-1-deficient mice have no mature B and T lymphocytes. *Cell* **68**, 869–877 (1992).
66. Janowska-Wieczorek, A. et al. Platelet-derived microparticles bind to hematopoietic stem/progenitor cells and enhance their engraftment. *Blood* **98**, 3143–3149 (2001).
67. Liu, L. et al. Functional defect of peripheral neutrophils in mice with induced deletion of CXCR2. *Genesis* **51**, 587–595 (2013).
68. Hashimoto, K., Joshi, S. K. & Koni, P. A. A conditional null allele of the major histocompatibility IA-beta chain gene. *Genesis* **32**, 152–153 (2002).
69. Caton, M. L., Smith-Raska, M. R. & Reizis, B. Notch-RBP-J signaling controls the homeostasis of CD8- dendritic cells in the spleen. *J. Exp. Med* **204**, 1653–1664 (2007).
70. Madisen, L. et al. A robust and high-throughput Cre reporting and characterization system for the whole mouse brain. *Nat. Neurosci.* **13**, 133–140 (2010).
71. de Boer, J. et al. Transgenic mice with hematopoietic and lymphoid specific expression of Cre. *Eur. J. Immunol.* **33**, 314–325 (2003).
72. Sommers, C. L. et al. Function of CD3 epsilon-mediated signals in T cell development. *J. Exp. Med.* **192**, 913–919 (2000).
73. Kurts, C., Miller, J. F., Subramaniam, R. M., Carbone, F. R. & Heath, W. R. Major histocompatibility complex class I-restricted cross-presentation is biased towards high dose antigens and those released during cellular destruction. *J. Exp. Med.* **188**, 409–414 (1998).
74. Palmer, E., Drobek, A. & Stepanek, O. Opposing effects of actin signaling and LPA-1 on establishing the affinity threshold for inducing effector T cell responses in mice. *Eur. J. Immunol.* **46**, 1887–1901 (2016).
75. Barnden, M. J., Allison, J., Heath, W. R. & Carbone, F. R. Defective TCR expression in transgenic mice constructed using cDNA-based alpha- and beta-chain genes under the control of heterologous regulatory elements. *Immunol. Cell Biol.* **76**, 34–40 (1998).
76. Dobeš, J. et al. A novel conditional Aire allele enables cell-specific ablation of the immune tolerance regulator Aire. *Eur. J. Immunol.* **48**, 546–548 (2018).
77. Liu, L. L. et al. A simplified intrathymic injection technique for mice. *Biotech. Histochem.* **87**, 140–147 (2012).
78. Pfaffl, M. W. A new mathematical model for relative quantification in real-time RT-PCR. *Nucleic Acids Res.* **29**, e45 (2001).
79. Smith, T., Heger, A. & Sudbery, I. UMI-tools: modeling sequencing errors in Unique Molecular Identifiers to improve quantification accuracy. *Genome Res.* **27**, 491–499 (2017).
80. Butler, A., Hoffman, P., Smibert, P., Papalexi, E. & Satija, R. Integrating single-cell transcriptomic data across different conditions, technologies, and species. *Nat. Biotechnol.* **36**, 411–420 (2018).

Acknowledgements

Author contributions

M.V. co-designed and conducted the majority of the experiments and wrote the manuscript. T.B., J.D., and J.B. performed some experiments and provided technical help, I.Š. performed microscopic experiments. A.Č., M.D., and A.A. provided technical support for the work. O.T. and O.Š. performed the experiments using mouse diabetic model. M.K. and V.B. performed RNA sequencing. J.K. analyzed RNAseq and scRNAseq data. R.S. and LK provided technical and experimental help, mice and material. D.F. designed experiments, supervised research, and edited the paper.

Competing interests
The authors declare no competing interests.

Additional information
Supplementary information is available for this paper at https://doi.org/10.1038/s41467-020-16081-3.

Correspondence and requests for materials should be addressed to D.F.

Reprints and permission information is available at http://www.nature.com/reprints

Publisher's note Springer Nature remains neutral with regard to jurisdictional claims in published maps and institutional affiliations.

4. GENERAL DISCUSSION

Understanding of the major developmental steps and factors involved in the process of embryonic hematopoiesis and ontogenetical relationships between the progenitors of hematopoietic waves is crucial for further advancement of therapeutic approaches and tools needed for the treatment of hematopoietic diseases and malignancies.

A marker that would specifically label only one embryonic hematopoietic wave is not available. However, experimental separation and isolation of progenitors of a particular wave is of critical importance to characterize molecular processes associated with their emergence, maintenance and function. Our discoveries regarding the origin and appearance of the first hematopoietic cells are based on the premise of our previous study showing that the embryonic macrophages express a battery of TLRs (Balounova et al., 2014), receptors recognizing the PAMPs (Li et al., 2014; Mariano et al., 2014) and DAMPs (Kariko et al., 2004; Liu-Bryan et al., 2005; Shi et al., 2003; Vabulas et al., 2001). At the beginning, we observed that the TLR2 is expressed in E7.5 YS and the emergence of its expression correlates with the presence of hemogenic endothelium in the YS (Ferkowicz et al., 2003; Huber et al., 2004; Tanaka et al., 2012). This knowledge provided a breeding ground for the following research where we asked the question concerning the possibility that the first hematopoietic cells in the YS could express TLR2. Indeed, we showed that YS hematopoietic progenitor cells express the TLR2 from E7.5. Given the general consensus, that the first primitive wave starts at E7.25-E7.5 (Ferkowicz et al., 2003; Isern et al., 2011) the expression of TLR2 at E7.5 YS could indicate that TLR2 marks the formation of the first hematopoietic wave. This assumption would be further supported by the traditional view that the second transient definitive hematopoietic wave (EMPs) arise at E8.25-E8.5 in the YS (McGrath et al., 2015; Palis et al., 1999). In addition, until recently, there was no specific marker which would distinguish the primitive from EMP wave. Both of these YS progenitors share the expression of c-kit (Ferkowicz et al., 2003; Kierdorf et al., 2013; McGrath et al., 2015). When we isolated c-kit$^+$TLR2$^-$ and c-kit$^+$TLR2$^+$ cells from E7.5 YS and perform the *in vitro* clonogenic assay, we found that while TLR2$^-$ population possesses the ability to generate the primitive erythrocytes of the first wave, the

TLR2$^+$ population produced mixed colonies with the erythro-myeloid potential typical for EMPs. This finding showed for the first time that TLR2 marks the appearance of EMP wave in the YS and that the hematopoietic precursors with erythro-myeloid potential emerge one day earlier than previously thought (McGrath et al., 2015; Palis et al., 1999). Based on this data, it seems that the EMP wave emerges in parallel with the first primitive wave, or immediately after. These findings could provide important insight into the origin of tissue-resident macrophages, especially microglia. One theory postulates that microglia originate from the primitive wave which is the first to emerge. That was documented using several inducible mice strains, such as Runx1, Tie2, or c-kit driver (Ginhoux et al., 2010; Sheng et al., 2015). However, we incline to the possibility is that microglia originate from EMPs which coexists with the primitive wave at E7.5 in the YS. These conclusions are also supported by experiments that used a Csf1r reporter mouse in which the expression of the reporter is induced on EMPs and still efficiently labels also microglia (Gomez Perdiguero et al., 2015). Thus, our data support the scenario that microglia are of EMP origin.

To support this hypothesis experimentally, we have generated a constitutively (Tlr2^{Cre}) and hydroxy-tamoxifen (OH) inducible (Tlr2^{CreERT}) mouse strains where the Cre-recombinase is under the control of TLR2 promoter. Using Tlr2^{Cre} mice we have confirmed that the first labeling of YS cells with hematopoietic potential starts at E7.5. In addition, cell labeling using the TLR2 promoter, we showed that TLR2$^+$ EMPs give rise to the myeloid cells in the fetal liver, which is the typical attribute of EMPs.

Interestingly, using the TLR2^{CreERT} we also showed that the early pre-HSCs in AGM are labeled when induced at E8.5 by tamoxifen. This data is in agreement with the report showing the early labeling of pre-HSCs using c-kit reporter mice at the same time (Sheng et al., 2015). It seems that the TLRs program is ontogenically synchronized in YS and AGM hemogenic endothelium during the process of EHT transition despite their origin from the different endothelial cells (Chen et al., 2011; Yokomizo et al., 2019).

To demonstrate the indispensability of the hematopoietic waves during embryonic development, we used the TLR2^{Cre} mouse strain bred with Rosa^{DTA} mouse strain. In this system, the activity of the TLR2 promoter leads to the permanent ablation of TLR2$^+$ cells in the developing embryo. The ablation of TLR2$^+$ cells resulted in the deletion of EMPs and its descendant population together with HSCs, but primitive erythropoiesis stayed intact. These deletional experiments strongly supported the prediction, that the TLR2 is initially activated in EMPs and HSCs but not in the erythroid progenitors of the primitive hematopoietic wave. The constitutive deletion of TLR2$^+$ cells resulted in embryonic lethality at E12.5. However, this cell depletion system displays certain limitations. The active TLR2 promoter activates the DTA constitutively, therefore, we could not declare, if the embryonic lethality is caused by the deletion of EMPs, HSCs, or their combination. For this reason, we generated a novel knock-in mouse strain Tlr2^{Dtr} in which the DTR is under TLR2 promoter. All the cells which express TLR2 on the protein level are efficiently depleted after the administration of DT. The advantage of this system is that the DT acts fast, metabolizes rapidly and thus is removed from the system relatively briskly (Saito et al., 2001). Using this system, we applied the DT twice at E8.5 and E9.5, i.e. at the beginning of the generation of fully developed EMPs, which are phenotypically defined as c-kit$^+$ CD16/32$^+$ CD41$^+$ cells. The DT administration resulted in the deletion of EMPs and its progeny, leaving the primitive erythrocytes intact. On the other hand, the generation of HSCs remained intact. The deletion of EMPs led to the embryonic lethality at the same time as we reported in TLR2^{Cre} Rosa^{DTA} mice. This result suggests that the deletion of EMPs but not HSCs is the reason for embryonic lethality at the indicated time point of development.

It has been shown that TLRs are expressed on adult HSCs in the bone marrow where their stimulation preferentially drives the generation of myeloid cells in inflammatory conditions (De Luca et al., 2009; Megias et al., 2012). Recently it has been shown that inflammatory signaling plays the role in the generation of embryonic hematopoietic cells in zebrafish as well in mice (Espin-Palazon et al., 2014; Li et al., 2014; Mariani et al., 2019; Orelio et al., 2008). Based on these studies, there is the possibility that TLR/Myd88 signaling may play a role in the

proper development of functional hematopoietic cells in the embryo. It is the open question of what could be the TLRs ligand in the aseptic conditions of the uterus. One possibility is that embryonic TLRs sense endogenous ligands originating from an extracellular matrix such as proteoglycans or glycoproteins as was described in adults (Johnson et al., 2002; Okamura et al., 2001). The other scenario may involve exogenous ligands originating from bacteria with the ability to pass through the placenta. The utilization of novel mouse models or germ-free animals may resolve this question.

The seeding of peripheral tissues by hematopoietic cells is a crucial process for the proper development of enlarging embryo and hematopoietic system (Collier, 2001; Ingman et al., 2006; McGrath et al., 2008; Paolicelli et al., 2011; Yosef et al., 2018). It has been shown, that EMPs, pre-macrophages, and macrophages seed the developing embryo based on the CX3CR1 signaling (Stremmel et al., 2018). Another candidate that may be involved in the migration of EMPs and its myeloid descendant population is CXCR4 which is the second most pronounced chemokine receptor after CX3CR1 in the embryo (Mariani et al., 2019). CXCR4 mRNA was firstly identified in early embryos at the end of 20th century (McGrath et al., 1999) and its protein expression was upregulated together with CX3CR on E10.5 macrophages surrounding the AGM region where the endothelial cells in AGM express their ligands and attract them to the AGM region to facilitate the production of transplantable HSC (Mariani et al., 2019). Using the knock-out mice where WBP1L (OPAL1) is deleted and the CXCR4 signaling is enhanced, we decided to measure if the trafficking or the frequencies of the EMPs and macrophages are changed in the embryo from E10.5 to E11.5 where is the peak of the trafficking of these cells from YS to EP (Stremmel et al., 2018). We have found that the frequencies of embryonic macrophages in YS are higher in the embryos lacking the WBP1L compare to the wild-type littermate controls. But the frequencies of macrophages in EP were unchanged. These results suggest that the enhanced CXCR4 expression and its activity plays a role in the generation of embryonic macrophages or that they traffic less from YS to the EP and stay predominantly in YS. The unchanged numbers in the EP may suggest that the EMPs and macrophages from YS migrate to the EP and they proliferate there more than in the

normal conditions and thus compensate for the worsening of the trafficking of EMPs and macrophages from YS to EP.

WBP1L is mainly associated with childhood acute lymphoblastic leukemia and the increase in its mRNA correlates with the favorable outcome of this disease (Ross et al., 2003; Yeoh et al., 2002). The protein regulates the ubiquitination of CXCR4 and its expression. The lack of WBP1L resulted in the CXCR4 enhanced expression and activation. The hyperactivity of CXCR4 signaling resulted in the increased hematopoietic progenitor cell homing to the bone marrow, increased ability of bone marrow stem, and progenitor cells to reconstitute hematopoiesis after irradiation. In addition, the perturbation in B cell development was also observed. Based on these results it seems that enhanced CXCR4 expression and signaling may not play a very important role in macrophage development and trafficking but in the generation of transplantable HSCs which can be applied in human medicine.

At the end, we found that mTECs^{high}, which are known to play an important role in the selection of T cells in the thymus (Hinterberger et al., 2010; Oukka et al., 1996), express a battery of TLRs, specifically TLR9. Its signaling drives the expression of chemokines and genes which are associated with their development into the post-Aire development of mTECs. We showed that the receptors for these chemokines are predominantly expressed by the Sirpα$^+$ CD14$^+$moDCs in the thymus. CD14$^+$moDCs are enriched in the thymus after the TLR9/Myd88 stimulation of mTECs. This stimulation led not only to the enrichment of CD14$^+$moDCs but even the subsequent CAT was observed. We also showed that the TLR9/Myd88 signaling is important for the proper development of thymic CD73$^-$CD25$^+$Foxp3$^+$ Tregs. These findings open the field for a new question regarding the endogenous ligands of TLRs and their influence in the proper development of the hematopoietic system.

Taken together TLR2 expression and its signaling in the immune-privileged tissue (embryo) and in the mTECs raise the question about the endogenous TLRs ligands and its function in the development and homeostatic functions. The utility of germ-free mice may at least in part address these questions.

5. CONCLUSIONS

This paper is based on three original articles: one shared first author and two with the contribution as the co-author. Next on one manuscript which is in revision. In addition, the presented thesis is supported by one paper, related to the TLRs in the intestine. The results can be summed up as follows:

I) Next, we found that the expression of TLR2 on c-kit$^+$ cells allows the discrimination of EMPs from the primitive erythroid wave at E7.5. Using transgenic mice Tlr2^{Cre} and Tlr2^{CreERT} generated in our laboratory we confirmed that these cells give rise to the EMPs and its progeny. Endogenous labeling of cells with an active Tlr2 locus showed, that even embryonic HSCs can be labeled. Both EMPs and HSCs originate from different anatomical locations and different endothelial cells. These findings suggest that the onset of their Tlr2 promoter activity seems to be ontogenically synchronized during EHT.

II) Using the CRISPR/Cas system we generated novel knock-in mouse strain TLR2-RFP-DTR. This mouse strain enables us to delete TLR2$^+$ cells in a time-dependent manner after the administration of DT. We use this tool to delete TLR2 cells during embryonic development. The deletion resulted in a decrease of EMPs and its products, but the HSCs seems to be intact. The deletion of cells resulted in embryonic lethality at E12.5.

III) Regarding the enhanced expression and activation of CXCR4 the frequencies of embryonic macrophages in YS were increased. The perturbation in B cell development increased the ability of HSCs to reconstitute hematopoiesis after transplantation and increased progenitor homing to the bone marrow was described.

IV) We demonstrated, that the TLR9/Myd88 signaling in thymic mTECs is important for the proper generation of thymic CD73$^-$CD25$^+$Foxp3$^+$ Tregs.

6. REFERENCES

Akashi, K., Traver, D., Miyamoto, T., and Weissman, I.L. (2000). A clonogenic common myeloid progenitor that gives rise to all myeloid lineages. Nature *404*, 193-197.

Akira, S. (2006). TLR signaling. Curr Top Microbiol Immunol *311*, 1-16.

Anderson, K.V., Bokla, L., and Nusslein-Volhard, C. (1985). Establishment of dorsal-ventral polarity in the Drosophila embryo: the induction of polarity by the Toll gene product. Cell *42*, 791-798.

Anderson, K.V., and Nusslein-Volhard, C. (1984). Information for the dorsal--ventral pattern of the Drosophila embryo is stored as maternal mRNA. Nature *311*, 223-227.

Anderson, M.S., Venanzi, E.S., Klein, L., Chen, Z., Berzins, S.P., Turley, S.J., von Boehmer, H., Bronson, R., Dierich, A., Benoist, C.*, et al.* (2002). Projection of an immunological self shadow within the thymus by the aire protein. Science *298*, 1395-1401.

Andonegui, G., Zhou, H., Bullard, D., Kelly, M.M., Mullaly, S.C., McDonald, B., Long, E.M., Robbins, S.M., and Kubes, P. (2009). Mice that exclusively express TLR4 on endothelial cells can efficiently clear a lethal systemic Gram-negative bacterial infection. J Clin Invest *119*, 1921-1930.

Applequist, S.E., Wallin, R.P., and Ljunggren, H.G. (2002). Variable expression of Toll-like receptor in murine innate and adaptive immune cell lines. Int Immunol *14*, 1065-1074.

Aschenbrenner, K., D'Cruz, L.M., Vollmann, E.H., Hinterberger, M., Emmerich, J., Swee, L.K., Rolink, A., and Klein, L. (2007). Selection of Foxp3+ regulatory T cells specific for self antigen expressed and presented by Aire+ medullary thymic epithelial cells. Nat Immunol *8*, 351-358.

Azzoni, E., Frontera, V., McGrath, K.E., Harman, J., Carrelha, J., Nerlov, C., Palis, J., Jacobsen, S.E.W., and de Bruijn, M.F. (2018). Kit ligand has a critical role in mouse yolk sac and aorta-gonad-mesonephros hematopoiesis. EMBO Rep *19*.

Baba, T., Nakamoto, Y., and Mukaida, N. (2009). Crucial contribution of thymic Sirp alpha+ conventional dendritic cells to central tolerance against blood-borne antigens in a CCR2-dependent manner. J Immunol *183*, 3053-3063.

Bains, I., van Santen, H.M., Seddon, B., and Yates, A.J. (2013). Models of self-peptide sampling by developing T cells identify candidate mechanisms of thymic selection. PLoS Comput Biol *9*, e1003102.

Baker, B.S., Ovigne, J.M., Powles, A.V., Corcoran, S., and Fry, L. (2003). Normal keratinocytes express Toll-like receptors (TLRs) 1, 2 and 5: modulation of TLR expression in chronic plaque psoriasis. Br J Dermatol *148*, 670-679.

Balounova, J., Splichalova, I., Dobesova, M., Kolar, M., Fiser, K., Prochazka, J., Sedlacek, R., Jurisicova, A., Sung, H.K., Korinek, V.*, et al.* (2019). Toll-like receptor 2 expression on c-kit(+) cells tracks the emergence of embryonic definitive hematopoietic progenitors. Nat Commun *10*, 5176.

Balounova, J., Vavrochova, T., Benesova, M., Ballek, O., Kolar, M., and Filipp, D. (2014). Toll-like receptors expressed on embryonic macrophages couple inflammatory signals to iron metabolism during early ontogenesis. Eur J Immunol *44*, 1491-1502.

Barak, B., Feldman, N., and Okun, E. (2014). Toll-like receptors as developmental tools that regulate neurogenesis during development: an update. Front Neurosci *8*, 272.

Barclay, A.N., and Mayrhofer, G. (1981). Bone marrow origin of Ia-positive cells in the medulla rat thymus. J Exp Med *153*, 1666-1671.

Barclay, A.N., and Mayrhofer, G. (1982). Ia positive cells in the medulla of rat thymus are bone marrow derived. Adv Exp Med Biol *149*, 381-387.

Bertrand, J.Y., Jalil, A., Klaine, M., Jung, S., Cumano, A., and Godin, I. (2005). Three pathways to mature macrophages in the early mouse yolk sac. Blood *106*, 3004-3011.

Bevan, M.J. (1997). In thymic selection, peptide diversity gives and takes away. Immunity *7*, 175-178.

Boehm, T., Scheu, S., Pfeffer, K., and Bleul, C.C. (2003). Thymic medullary epithelial cell differentiation, thymocyte emigration, and the control of autoimmunity require lympho-epithelial cross talk via LTbetaR. J Exp Med *198*, 757-769.

Boiers, C., Carrelha, J., Lutteropp, M., Luc, S., Green, J.C., Azzoni, E., Woll, P.S., Mead, A.J., Hultquist, A., Swiers, G.*, et al.* (2013). Lymphomyeloid contribution of an immune-restricted progenitor emerging prior to definitive hematopoietic stem cells. Cell Stem Cell *13*, 535-548.

Boisset, J.C., van Cappellen, W., Andrieu-Soler, C., Galjart, N., Dzierzak, E., and Robin, C. (2010). In vivo imaging of haematopoietic cells emerging from the mouse aortic endothelium. Nature *464*, 116-120.

Bourke, E., Bosisio, D., Golay, J., Polentarutti, N., and Mantovani, A. (2003). The toll-like receptor repertoire of human B lymphocytes: inducible and selective expression of TLR9 and TLR10 in normal and transformed cells. Blood *102*, 956-963.

Brandt, J.P., and Ringstad, N. (2015). Toll-like Receptor Signaling Promotes Development and Function of Sensory Neurons Required for a C. elegans Pathogen-Avoidance Behavior. Curr Biol *25*, 2228-2237.

Broudy, V.C. (1997). Stem cell factor and hematopoiesis. Blood *90*, 1345-1364.

Busch, K., Klapproth, K., Barile, M., Flossdorf, M., Holland-Letz, T., Schlenner, S.M., Reth, M., Hofer, T., and Rodewald, H.R. (2015). Fundamental properties of unperturbed haematopoiesis from stem cells in vivo. Nature *518*, 542-546.

Collier, R.J. (2001). Understanding the mode of action of diphtheria toxin: a perspective on progress during the 20th century. Toxicon *39*, 1793-1803.

Costa, G., Kouskoff, V., and Lacaud, G. (2012). Origin of blood cells and HSC production in the embryo. Trends Immunol *33*, 215-223.

Crellin, N.K., Garcia, R.V., Hadisfar, O., Allan, S.E., Steiner, T.S., and Levings, M.K. (2005). Human CD4+ T cells express TLR5 and its ligand flagellin enhances the suppressive capacity and expression of FOXP3 in CD4+CD25+ T regulatory cells. J Immunol *175*, 8051-8059.

De Luca, K., Frances-Duvert, V., Asensio, M.J., Ihsani, R., Debien, E., Taillardet, M., Verhoeyen, E., Bella, C., Lantheaume, S., Genestier, L*., et al.* (2009). The TLR1/2 agonist PAM(3)CSK(4) instructs commitment of human hematopoietic stem cells to a myeloid cell fate. Leukemia *23*, 2063-2074.

De Nardo, D. (2015). Toll-like receptors: Activation, signalling and transcriptional modulation. Cytokine *74*, 181-189.

Ding, L., Saunders, T.L., Enikolopov, G., and Morrison, S.J. (2012). Endothelial and perivascular cells maintain haematopoietic stem cells. Nature *481*, 457-462.

Donskoy, E., and Goldschneider, I. (1992). Thymocytopoiesis is maintained by blood-borne precursors throughout postnatal life. A study in parabiotic mice. J Immunol *148*, 1604-1612.

Downs, K.M., and Davies, T. (1993). Staging of gastrulating mouse embryos by morphological landmarks in the dissecting microscope. Development *118*, 1255-1266.

Du, X., Poltorak, A., Wei, Y., and Beutler, B. (2000). Three novel mammalian toll-like receptors: gene structure, expression, and evolution. Eur Cytokine Netw *11*, 362-371.

Eliades, A., Wareing, S., Marinopoulou, E., Fadlullah, M.Z.H., Patel, R., Grabarek, J.B., Plusa, B., Lacaud, G., and Kouskoff, V. (2016). The Hemogenic Competence of Endothelial Progenitors Is Restricted by Runx1 Silencing during Embryonic Development. Cell Rep *15*, 2185-2199.

Ema, H., and Nakauchi, H. (2000). Expansion of hematopoietic stem cells in the developing liver of a mouse embryo. Blood *95*, 2284-2288.

Epelman, S., Lavine, K.J., and Randolph, G.J. (2014). Origin and functions of tissue macrophages. Immunity *41*, 21-35.

Espin-Palazon, R., Stachura, D.L., Campbell, C.A., Garcia-Moreno, D., Del Cid, N., Kim, A.D., Candel, S., Meseguer, J., Mulero, V., and Traver, D. (2014). Proinflammatory signaling regulates hematopoietic stem cell emergence. Cell *159*, 1070-1085.

Feng, L., Ju, M., Lee, K.Y.V., Mackey, A., Evangelista, M., Iwata, D., Adamson, P., Lashkari, K., Foxton, R., Shima, D*., et al.* (2017). A Proinflammatory Function of Toll-Like Receptor 2 in the Retinal Pigment Epithelium as a Novel Target for Reducing Choroidal Neovascularization in Age-Related Macular Degeneration. Am J Pathol *187*, 2208-2221.

Ferkowicz, M.J., Starr, M., Xie, X., Li, W., Johnson, S.A., Shelley, W.C., Morrison, P.R., and Yoder, M.C. (2003). CD41 expression defines the onset of primitive and definitive hematopoiesis in the murine embryo. Development *130*, 4393-4403.

Foldi, I., Anthoney, N., Harrison, N., Gangloff, M., Verstak, B., Nallasivan, M.P., AlAhmed, S., Zhu, B., Phizacklea, M., Losada-Perez, M.*, et al.* (2017). Three-tier regulation of cell number plasticity by neurotrophins and Tolls in Drosophila. J Cell Biol *216*, 1421-1438.

Frame, J.M., Fegan, K.H., Conway, S.J., McGrath, K.E., and Palis, J. (2016). Definitive Hematopoiesis in the Yolk Sac Emerges from Wnt-Responsive Hemogenic Endothelium Independently of Circulation and Arterial Identity. Stem Cells *34*, 431-444.

Fraser, S.T., Isern, J., and Baron, M.H. (2007). Maturation and enucleation of primitive erythroblasts during mouse embryogenesis is accompanied by changes in cell-surface antigen expression. Blood *109*, 343-352.

Fujiwara, Y., Browne, C.P., Cunniff, K., Goff, S.C., and Orkin, S.H. (1996). Arrested development of embryonic red cell precursors in mouse embryos lacking transcription factor GATA-1. Proc Natl Acad Sci U S A *93*, 12355-12358.

Garcia-Porrero, J.A., Godin, I.E., and Dieterlen-Lievre, F. (1995). Potential intraembryonic hemogenic sites at pre-liver stages in the mouse. Anat Embryol (Berl) *192*, 425-435.

Garcia-Porrero, J.A., Manaia, A., Jimeno, J., Lasky, L.L., Dieterlen-Lievre, F., and Godin, I.E. (1998). Antigenic profiles of endothelial and hemopoietic lineages in murine intraembryonic hemogenic sites. Dev Comp Immunol *22*, 303-319.

Ginhoux, F., Greter, M., Leboeuf, M., Nandi, S., See, P., Gokhan, S., Mehler, M.F., Conway, S.J., Ng, L.G., Stanley, E.R.*, et al.* (2010). Fate mapping analysis reveals that adult microglia derive from primitive macrophages. Science *330*, 841-845.

Godfrey, D.I., Kennedy, J., Suda, T., and Zlotnik, A. (1993). A developmental pathway involving four phenotypically and functionally distinct subsets of CD3-CD4-CD8- triple-negative adult mouse thymocytes defined by CD44 and CD25 expression. J Immunol *150*, 4244-4252.

Godin, I.E., Garcia-Porrero, J.A., Coutinho, A., Dieterlen-Lievre, F., and Marcos, M.A. (1993). Para-aortic splanchnopleura from early mouse embryos contains B1a cell progenitors. Nature *364*, 67-70.

Gomez Perdiguero, E., Klapproth, K., Schulz, C., Busch, K., Azzoni, E., Crozet, L., Garner, H., Trouillet, C., de Bruijn, M.F., Geissmann, F.*, et al.* (2015). Tissue-resident macrophages originate from yolk-sac-derived erythro-myeloid progenitors. Nature *518*, 547-551.

Guilliams, M., De Kleer, I., Henri, S., Post, S., Vanhoutte, L., De Prijck, S., Deswarte, K., Malissen, B., Hammad, H., and Lambrecht, B.N. (2013). Alveolar macrophages develop from fetal monocytes that differentiate into long-lived cells in the first week of life via GM-CSF. J Exp Med *210*, 1977-1992.

Hadland, B.K., Varnum-Finney, B., Mandal, P.K., Rossi, D.J., Poulos, M.G., Butler, J.M., Rafii, S., Yoder, M.C., Yoshimoto, M., and Bernstein, I.D. (2017). A Common Origin for B-1a and B-2 Lymphocytes in Clonal Pre- Hematopoietic Stem Cells. Stem Cell Reports *8*, 1563-1572.

Herbomel, P., Thisse, B., and Thisse, C. (1999). Ontogeny and behaviour of early macrophages in the zebrafish embryo. Development *126*, 3735-3745.

Hinterberger, M., Aichinger, M., Prazeres da Costa, O., Voehringer, D., Hoffmann, R., and Klein, L. (2010). Autonomous role of medullary thymic epithelial cells in central CD4(+) T cell tolerance. Nat Immunol *11*, 512-519.

Hoeffel, G., Chen, J., Lavin, Y., Low, D., Almeida, F.F., See, P., Beaudin, A.E., Lum, J., Low, I., Forsberg, E.C.*, et al.* (2015). C-Myb(+) erythro-myeloid progenitor-derived fetal monocytes give rise to adult tissue-resident macrophages. Immunity *42*, 665-678.

Hoeffel, G., Wang, Y., Greter, M., See, P., Teo, P., Malleret, B., Leboeuf, M., Low, D., Oller, G., Almeida, F.*, et al.* (2012). Adult Langerhans cells derive predominantly from embryonic fetal liver monocytes with a minor contribution of yolk sac-derived macrophages. J Exp Med *209*, 1167-1181.

Hogquist, K.A. (2001). Signal strength in thymic selection and lineage commitment. Curr Opin Immunol *13*, 225-231.

Horng, T., Barton, G.M., Flavell, R.A., and Medzhitov, R. (2002). The adaptor molecule TIRAP provides signalling specificity for Toll-like receptors. Nature *420*, 329-333.

Huber, T.L., Kouskoff, V., Fehling, H.J., Palis, J., and Keller, G. (2004). Haemangioblast commitment is initiated in the primitive streak of the mouse embryo. Nature *432*, 625-630.

Hultmark, D. (1994). Macrophage differentiation marker MyD88 is a member of the Toll/IL-1 receptor family. Biochem Biophys Res Commun *199*, 144-146.

Chen, G., Zhuchenko, O., and Kuspa, A. (2007). Immune-like phagocyte activity in the social amoeba. Science *317*, 678-681.

Chen, M.J., Li, Y., De Obaldia, M.E., Yang, Q., Yzaguirre, A.D., Yamada-Inagawa, T., Vink, C.S., Bhandoola, A., Dzierzak, E., and Speck, N.A. (2011). Erythroid/myeloid progenitors and hematopoietic stem cells originate from distinct populations of endothelial cells. Cell Stem Cell *9*, 541-552.

Chen, M.J., Yokomizo, T., Zeigler, B.M., Dzierzak, E., and Speck, N.A. (2009). Runx1 is required for the endothelial to haematopoietic cell transition but not thereafter. Nature *457*, 887-891.

Chiu, S.K., Saw, J., Huang, Y., Sonderegger, S.E., Wong, N.C., Powell, D.R., Beck, D., Pimanda, J.E., Tremblay, C.S., and Curtis, D.J. (2018). A novel role for Lyl1 in primitive erythropoiesis. Development *145*.

Christensen, J.L., Wright, D.E., Wagers, A.J., and Weissman, I.L. (2004). Circulation and chemotaxis of fetal hematopoietic stem cells. PLoS Biol *2*, E75.

Chuang, T., and Ulevitch, R.J. (2001). Identification of hTLR10: a novel human Toll-like receptor preferentially expressed in immune cells. Biochim Biophys Acta *1518*, 157-161.

Ingman, W.V., Wyckoff, J., Gouon-Evans, V., Condeelis, J., and Pollard, J.W. (2006). Macrophages promote collagen fibrillogenesis around terminal end buds of the developing mammary gland. Dev Dyn *235*, 3222-3229.

Isern, J., He, Z., Fraser, S.T., Nowotschin, S., Ferrer-Vaquer, A., Moore, R., Hadjantonakis, A.K., Schulz, V., Tuck, D., Gallagher, P.G.*, et al.* (2011). Single-lineage transcriptome analysis reveals key regulatory pathways in primitive erythroid progenitors in the mouse embryo. Blood *117*, 4924-4934.

Ivanovs, A., Rybtsov, S., Welch, L., Anderson, R.A., Turner, M.L., and Medvinsky, A. (2011). Highly potent human hematopoietic stem cells first emerge in the intraembryonic aorta-gonad-mesonephros region. J Exp Med *208*, 2417-2427.

Jenkins, S.J., Ruckerl, D., Cook, P.C., Jones, L.H., Finkelman, F.D., van Rooijen, N., MacDonald, A.S., and Allen, J.E. (2011). Local macrophage proliferation, rather than recruitment from the blood, is a signature of TH2 inflammation. Science *332*, 1284-1288.

Jiang, Z., Ninomiya-Tsuji, J., Qian, Y., Matsumoto, K., and Li, X. (2002). Interleukin-1 (IL-1) receptor-associated kinase-dependent IL-1-induced signaling complexes phosphorylate TAK1 and TAB2 at the plasma membrane and activate TAK1 in the cytosol. Mol Cell Biol *22*, 7158-7167.

Johnson, G.B., Brunn, G.J., Kodaira, Y., and Platt, J.L. (2002). Receptor-mediated monitoring of tissue well-being via detection of soluble heparan sulfate by Toll-like receptor 4. J Immunol *168*, 5233-5239.

Jung, S., Aliberti, J., Graemmel, P., Sunshine, M.J., Kreutzberg, G.W., Sher, A., and Littman, D.R. (2000). Analysis of fractalkine receptor CX(3)CR1 function by targeted deletion and green fluorescent protein reporter gene insertion. Mol Cell Biol *20*, 4106-4114.

Kariko, K., Ni, H., Capodici, J., Lamphier, M., and Weissman, D. (2004). mRNA is an endogenous ligand for Toll-like receptor 3. J Biol Chem *279*, 12542-12550.

Kawasaki, T., and Kawai, T. (2014). Toll-like receptor signaling pathways. Front Immunol *5*, 461.

Kierdorf, K., Erny, D., Goldmann, T., Sander, V., Schulz, C., Perdiguero, E.G., Wieghofer, P., Heinrich, A., Riemke, P., Holscher, C.*, et al.* (2013). Microglia emerge from erythromyeloid precursors via Pu.1- and Irf8-dependent pathways. Nat Neurosci *16*, 273-280.

Kingsley, P.D., Malik, J., Fantauzzo, K.A., and Palis, J. (2004). Yolk sac-derived primitive erythroblasts enucleate during mammalian embryogenesis. Blood *104*, 19-25.

Klein, I., Cornejo, J.C., Polakos, N.K., John, B., Wuensch, S.A., Topham, D.J., Pierce, R.H., and Crispe, I.N. (2007). Kupffer cell heterogeneity: functional properties of bone marrow derived and sessile hepatic macrophages. Blood *110*, 4077-4085.

Klein, L., Klein, T., Ruther, U., and Kyewski, B. (1998). CD4 T cell tolerance to human C-reactive protein, an inducible serum protein, is mediated by medullary thymic epithelium. J Exp Med *188*, 5-16.

Komai-Koma, M., Jones, L., Ogg, G.S., Xu, D., and Liew, F.Y. (2004). TLR2 is expressed on activated T cells as a costimulatory receptor. Proc Natl Acad Sci U S A *101*, 3029-3034.

Kondo, M., Weissman, I.L., and Akashi, K. (1997). Identification of clonogenic common lymphoid progenitors in mouse bone marrow. Cell *91*, 661-672.

Kroger, C.J., Spidale, N.A., Wang, B., and Tisch, R. (2017). Thymic Dendritic Cell Subsets Display Distinct Efficiencies and Mechanisms of Intercellular MHC Transfer. J Immunol *198*, 249-256.

Kumaravelu, P., Hook, L., Morrison, A.M., Ure, J., Zhao, S., Zuyev, S., Ansell, J., and Medvinsky, A. (2002). Quantitative developmental anatomy of definitive haematopoietic stem cells/long-term repopulating units (HSC/RUs): role of the aorta-gonad-mesonephros (AGM) region and the yolk sac in colonisation of the mouse embryonic liver. Development *129*, 4891-4899.

Lancaster, J.N., Thyagarajan, H.M., Srinivasan, J., Li, Y., Hu, Z., and Ehrlich, L.I.R. (2019). Live-cell imaging reveals the relative contributions of antigen-presenting cell subsets to thymic central tolerance. Nat Commun *10*, 2220.

Lathia, J.D., Okun, E., Tang, S.C., Griffioen, K., Cheng, A., Mughal, M.R., Laryea, G., Selvaraj, P.K., ffrench-Constant, C., Magnus, T.*, et al.* (2008). Toll-like receptor 3 is a negative regulator of embryonic neural progenitor cell proliferation. J Neurosci *28*, 13978-13984.

Lavin, Y., Winter, D., Blecher-Gonen, R., David, E., Keren-Shaul, H., Merad, M., Jung, S., and Amit, I. (2014). Tissue-resident macrophage enhancer landscapes are shaped by the local microenvironment. Cell *159*, 1312-1326.

Lei, Y., Ripen, A.M., Ishimaru, N., Ohigashi, I., Nagasawa, T., Jeker, L.T., Bosl, M.R., Hollander, G.A., Hayashi, Y., Malefyt Rde, W.*, et al.* (2011). Aire-dependent production of XCL1 mediates medullary accumulation of thymic dendritic cells and contributes to regulatory T cell development. J Exp Med *208*, 383-394.

Leow-Dyke, S., Allen, C., Denes, A., Nilsson, O., Maysami, S., Bowie, A.G., Rothwell, N.J., and Pinteaux, E. (2012). Neuronal Toll-like receptor 4 signaling induces brain endothelial activation and neutrophil transmigration in vitro. J Neuroinflammation *9*, 230.

Leventhal, D.S., Gilmore, D.C., Berger, J.M., Nishi, S., Lee, V., Malchow, S., Kline, D.E., Kline, J., Vander Griend, D.J., Huang, H.*, et al.* (2016). Dendritic Cells Coordinate the Development and Homeostasis of Organ-Specific Regulatory T Cells. Immunity *44*, 847-859.

Li, J., Park, J., Foss, D., and Goldschneider, I. (2009). Thymus-homing peripheral dendritic cells constitute two of the three major subsets of dendritic cells in the steady-state thymus. J Exp Med *206*, 607-622.

Li, J.Y., Liu, Y., Gao, X.X., Gao, X., and Cai, H. (2014). TLR2 and TLR4 signaling pathways are required for recombinant Brucella abortus BCSP31-induced cytokine production, functional upregulation of mouse macrophages, and the Th1 immune response in vivo and in vitro. Cell Mol Immunol *11*, 477-494.

Liston, A., Lesage, S., Wilson, J., Peltonen, L., and Goodnow, C.C. (2003). Aire regulates negative selection of organ-specific T cells. Nat Immunol *4*, 350-354.

Liu-Bryan, R., Scott, P., Sydlaske, A., Rose, D.M., and Terkeltaub, R. (2005). Innate immunity conferred by Toll-like receptors 2 and 4 and myeloid differentiation factor 88 expression is pivotal to monosodium urate monohydrate crystal-induced inflammation. Arthritis Rheum *52*, 2936-2946.

Liu, G., and Zhao, Y. (2007). Toll-like receptors and immune regulation: their direct and indirect modulation on regulatory CD4+ CD25+ T cells. Immunology *122*, 149-156.

Liu, L., Papa, E.F., Dooner, M.S., Machan, J.T., Johnson, K.W., Goldberg, L.R., Quesenberry, P.J., and Colvin, G.A. (2012). Homing and long-term engraftment of long- and short-term renewal hematopoietic stem cells. PLoS One *7*, e31300.

Lugus, J.J., Park, C., Ma, Y.D., and Choi, K. (2009). Both primitive and definitive blood cells are derived from Flk-1+ mesoderm. Blood *113*, 563-566.

Luis, T.C., Luc, S., Mizukami, T., Boukarabila, H., Thongjuea, S., Woll, P.S., Azzoni, E., Giustacchini, A., Lutteropp, M., Bouriez-Jones, T.*, et al.* (2016). Initial seeding of the embryonic thymus by immune-restricted lympho-myeloid progenitors. Nat Immunol *17*, 1424-1435.

Lux, C.T., Yoshimoto, M., McGrath, K., Conway, S.J., Palis, J., and Yoder, M.C. (2008). All primitive and definitive hematopoietic progenitor cells emerging before E10 in the mouse embryo are products of the yolk sac. Blood *111*, 3435-3438.

Mariani, S.A., Li, Z., Rice, S., Krieg, C., Fragkogianni, S., Robinson, M., Vink, C.S., Pollard, J.W., and Dzierzak, E. (2019). Pro-inflammatory Aorta-Associated Macrophages Are Involved in Embryonic Development of Hematopoietic Stem Cells. Immunity *50*, 1439-1452 e1435.

Mariano, V.S., Zorzetto-Fernandes, A.L., da Silva, T.A., Ruas, L.P., Nohara, L.L., Almeida, I.C., and Roque-Barreira, M.C. (2014). Recognition of TLR2 N-glycans: critical role in ArtinM immunomodulatory activity. PLoS One *9*, e98512.

Mass, E., Ballesteros, I., Farlik, M., Halbritter, F., Gunther, P., Crozet, L., Jacome-Galarza, C.E., Handler, K., Klughammer, J., Kobayashi, Y.*, et al.* (2016). Specification of tissue-resident macrophages during organogenesis. Science *353*.

Mass, E., Jacome-Galarza, C.E., Blank, T., Lazarov, T., Durham, B.H., Ozkaya, N., Pastore, A., Schwabenland, M., Chung, Y.R., Rosenblum, M.K.*, et al.* (2017). A somatic mutation in erythro-myeloid progenitors causes neurodegenerative disease. Nature *549*, 389-393.

Mayerova, D., and Hogquist, K.A. (2004). Central tolerance to self-antigen expressed by cortical epithelial cells. J Immunol *172*, 851-856.

McCabe, A., and MacNamara, K.C. (2016). Macrophages: Key regulators of steady-state and demand-adapted hematopoiesis. Exp Hematol *44*, 213-222.

McCarthy, G.M., Bridges, C.R., Blednov, Y.A., and Harris, R.A. (2017). CNS cell-type localization and LPS response of TLR signaling pathways. F1000Res *6*, 1144.

McGrath, K.E., Frame, J.M., Fegan, K.H., Bowen, J.R., Conway, S.J., Catherman, S.C., Kingsley, P.D., Koniski, A.D., and Palis, J. (2015). Distinct Sources of Hematopoietic Progenitors Emerge before HSCs and Provide Functional Blood Cells in the Mammalian Embryo. Cell Rep *11*, 1892-1904.

McGrath, K.E., Frame, J.M., Fromm, G.J., Koniski, A.D., Kingsley, P.D., Little, J., Bulger, M., and Palis, J. (2011). A transient definitive erythroid lineage with unique regulation of the beta-globin locus in the mammalian embryo. Blood *117*, 4600-4608.

McGrath, K.E., Kingsley, P.D., Koniski, A.D., Porter, R.L., Bushnell, T.P., and Palis, J. (2008). Enucleation of primitive erythroid cells generates a transient population of "pyrenocytes" in the mammalian fetus. Blood *111*, 2409-2417.

McGrath, K.E., Koniski, A.D., Malik, J., and Palis, J. (2003). Circulation is established in a stepwise pattern in the mammalian embryo. Blood *101*, 1669-1675.

McGrath, K.E., Koniski, A.D., Maltby, K.M., McGann, J.K., and Palis, J. (1999). Embryonic expression and function of the chemokine SDF-1 and its receptor, CXCR4. Dev Biol *213*, 442-456.

Medvinsky, A., and Dzierzak, E. (1996). Definitive hematopoiesis is autonomously initiated by the AGM region. Cell *86*, 897-906.

Medzhitov, R., Preston-Hurlburt, P., and Janeway, C.A., Jr. (1997). A human homologue of the Drosophila Toll protein signals activation of adaptive immunity. Nature *388*, 394-397.

Megias, J., Yanez, A., Moriano, S., O'Connor, J.E., Gozalbo, D., and Gil, M.L. (2012). Direct Toll-like receptor-mediated stimulation of hematopoietic stem and progenitor cells occurs in vivo and promotes differentiation toward macrophages. Stem Cells *30*, 1486-1495.

Mendelson, A., and Frenette, P.S. (2014). Hematopoietic stem cell niche maintenance during homeostasis and regeneration. Nat Med *20*, 833-846.

Merad, M., Manz, M.G., Karsunky, H., Wagers, A., Peters, W., Charo, I., Weissman, I.L., Cyster, J.G., and Engleman, E.G. (2002). Langerhans cells renew in the skin throughout life under steady-state conditions. Nat Immunol *3*, 1135-1141.

Mikkola, H.K., Fujiwara, Y., Schlaeger, T.M., Traver, D., and Orkin, S.H. (2003). Expression of CD41 marks the initiation of definitive hematopoiesis in the mouse embryo. Blood *101*, 508-516.

Mucenski, M.L., McLain, K., Kier, A.B., Swerdlow, S.H., Schreiner, C.M., Miller, T.A., Pietryga, D.W., Scott, W.J., Jr., and Potter, S.S. (1991). A functional c-myb gene is required for normal murine fetal hepatic hematopoiesis. Cell *65*, 677-689.

Mukouyama, Y., Chiba, N., Mucenski, M.L., Satake, M., Miyajima, A., Hara, T., and Watanabe, T. (1999). Hematopoietic cells in cultures of the murine embryonic aorta-gonad-mesonephros region are induced by c-Myb. Curr Biol *9*, 833-836.

Muller, A.M., Medvinsky, A., Strouboulis, J., Grosveld, F., and Dzierzak, E. (1994). Development of hematopoietic stem cell activity in the mouse embryo. Immunity *1*, 291-301.

Munoz-Espin, D., Canamero, M., Maraver, A., Gomez-Lopez, G., Contreras, J., Murillo-Cuesta, S., Rodriguez-Baeza, A., Varela-Nieto, I., Ruberte, J., Collado, M.*, et al.* (2013). Programmed cell senescence during mammalian embryonic development. Cell *155*, 1104-1118.

Muzio, M., Ni, J., Feng, P., and Dixit, V.M. (1997). IRAK (Pelle) family member IRAK-2 and MyD88 as proximal mediators of IL-1 signaling. Science *278*, 1612-1615.

Nagai, Y., Garrett, K.P., Ohta, S., Bahrun, U., Kouro, T., Akira, S., Takatsu, K., and Kincade, P.W. (2006). Toll-like receptors on hematopoietic progenitor cells stimulate innate immune system replenishment. Immunity *24*, 801-812.

Ninomiya-Tsuji, J., Kishimoto, K., Hiyama, A., Inoue, J., Cao, Z., and Matsumoto, K. (1999). The kinase TAK1 can activate the NIK-I kappaB as well as the MAP kinase cascade in the IL-1 signalling pathway. Nature *398*, 252-256.

North, T.E., de Bruijn, M.F., Stacy, T., Talebian, L., Lind, E., Robin, C., Binder, M., Dzierzak, E., and Speck, N.A. (2002). Runx1 expression marks long-term repopulating hematopoietic stem cells in the midgestation mouse embryo. Immunity *16*, 661-672.

Ogawa, M., Tajima, F., Ito, T., Sato, T., Laver, J.H., and Deguchi, T. (2001). CD34 expression by murine hematopoietic stem cells. Developmental changes and kinetic alterations. Ann N Y Acad Sci *938*, 139-145.

Okamura, Y., Watari, M., Jerud, E.S., Young, D.W., Ishizaka, S.T., Rose, J., Chow, J.C., and Strauss, J.F., 3rd (2001). The extra domain A of fibronectin activates Toll-like receptor 4. J Biol Chem *276*, 10229-10233.

Okun, E., Griffioen, K.J., Son, T.G., Lee, J.H., Roberts, N.J., Mughal, M.R., Hutchison, E., Cheng, A., Arumugam, T.V., Lathia, J.D.*, et al.* (2010). TLR2 activation inhibits embryonic neural progenitor cell proliferation. J Neurochem *114*, 462-474.

Orelio, C., Haak, E., Peeters, M., and Dzierzak, E. (2008). Interleukin-1-mediated hematopoietic cell regulation in the aorta-gonad-mesonephros region of the mouse embryo. Blood *112*, 4895-4904.

Oukka, M., Cohen-Tannoudji, M., Tanaka, Y., Babinet, C., and Kosmatopoulos, K. (1996). Medullary thymic epithelial cells induce tolerance to intracellular proteins. J Immunol *156*, 968-975.

Palis, J. (2014). Primitive and definitive erythropoiesis in mammals. Front Physiol *5*, 3.

Palis, J., Robertson, S., Kennedy, M., Wall, C., and Keller, G. (1999). Development of erythroid and myeloid progenitors in the yolk sac and embryo proper of the mouse. Development *126*, 5073-5084.

Palladino, M.A., Savarese, M.A., Chapman, J.L., Dughi, M.K., and Plaska, D. (2008). Localization of Toll-like receptors on epididymal epithelial cells and spermatozoa. Am J Reprod Immunol *60*, 541-555.

Paolicelli, R.C., Bolasco, G., Pagani, F., Maggi, L., Scianni, M., Panzanelli, P., Giustetto, M., Ferreira, T.A., Guiducci, E., Dumas, L.*, et al.* (2011). Synaptic pruning by microglia is necessary for normal brain development. Science *333*, 1456-1458.

Patni, S., Wynen, L.P., Seager, A.L., Morgan, G., White, J.O., and Thornton, C.A. (2009). Expression and activity of Toll-like receptors 1-9 in the human term placenta and changes associated with labor at term. Biol Reprod *80*, 243-248.

Perdiguero, E.G., and Geissmann, F. (2016). The development and maintenance of resident macrophages. Nat Immunol *17*, 2-8.

Perdiguero, E.G., Klapproth, K., Schulz, C., Busch, K., de Bruijn, M., Rodewald, H.R., and Geissmann, F. (2015). The Origin of Tissue-Resident Macrophages: When an Erythro-myeloid Progenitor Is an Erythro-myeloid Progenitor. Immunity *43*, 1023-1024.

Perry, J.S.A., Lio, C.J., Kau, A.L., Nutsch, K., Yang, Z., Gordon, J.I., Murphy, K.M., and Hsieh, C.S. (2014). Distinct contributions of Aire and antigen-presenting-cell subsets to the generation of self-tolerance in the thymus. Immunity *41*, 414-426.

Pijuan-Sala, B., Griffiths, J.A., Guibentif, C., Hiscock, T.W., Jawaid, W., Calero-Nieto, F.J., Mulas, C., Ibarra-Soria, X., Tyser, R.C.V., Ho, D.L.L.*, et al.* (2019). A single-cell molecular map of mouse gastrulation and early organogenesis. Nature *566*, 490-495.

Plein, A., Fantin, A., Denti, L., Pollard, J.W., and Ruhrberg, C. (2018). Erythro-myeloid progenitors contribute endothelial cells to blood vessels. Nature *562*, 223-228.

Price, A.E., Shamardani, K., Lugo, K.A., Deguine, J., Roberts, A.W., Lee, B.L., and Barton, G.M. (2018). A Map of Toll-like Receptor Expression in the Intestinal Epithelium Reveals Distinct Spatial, Cell Type-Specific, and Temporal Patterns. Immunity *49*, 560-575 e566.

Pudney, J., He, X., Masheeb, Z., Kindelberger, D.W., Kuohung, W., and Ingalls, R.R. (2016). Differential expression of toll-like receptors in the human placenta across early gestation. Placenta *46*, 1-10.

Riccioli, A., Starace, D., Galli, R., Fuso, A., Scarpa, S., Palombi, F., De Cesaris, P., Ziparo, E., and Filippini, A. (2006). Sertoli cells initiate testicular innate immune responses through TLR activation. J Immunol *177*, 7122-7130.

Rock, F.L., Hardiman, G., Timans, J.C., Kastelein, R.A., and Bazan, J.F. (1998). A family of human receptors structurally related to Drosophila Toll. Proc Natl Acad Sci U S A *95*, 588-593.

Rolls, A., Shechter, R., London, A., Ziv, Y., Ronen, A., Levy, R., and Schwartz, M. (2007). Toll-like receptors modulate adult hippocampal neurogenesis. Nat Cell Biol *9*, 1081-1088.

Ross, M.E., Zhou, X., Song, G., Shurtleff, S.A., Girtman, K., Williams, W.K., Liu, H.C., Mahfouz, R., Raimondi, S.C., Lenny, N.*, et al.* (2003). Classification of pediatric acute lymphoblastic leukemia by gene expression profiling. Blood *102*, 2951-2959.

Saito, M., Iwawaki, T., Taya, C., Yonekawa, H., Noda, M., Inui, Y., Mekada, E., Kimata, Y., Tsuru, A., and Kohno, K. (2001). Diphtheria toxin receptor-mediated conditional and targeted cell ablation in transgenic mice. Nat Biotechnol *19*, 746-750.

Shechter, R., Ronen, A., Rolls, A., London, A., Bakalash, S., Young, M.J., and Schwartz, M. (2008). Toll-like receptor 4 restricts retinal progenitor cell proliferation. J Cell Biol *183*, 393-400.

Sheng, J., Ruedl, C., and Karjalainen, K. (2015). Most Tissue-Resident Macrophages Except Microglia Are Derived from Fetal Hematopoietic Stem Cells. Immunity *43*, 382-393.

Shi, Y., Evans, J.E., and Rock, K.L. (2003). Molecular identification of a danger signal that alerts the immune system to dying cells. Nature *425*, 516-521.

Schulz, C., Gomez Perdiguero, E., Chorro, L., Szabo-Rogers, H., Cagnard, N., Kierdorf, K., Prinz, M., Wu, B., Jacobsen, S.E., Pollard, J.W.*, et al.* (2012). A lineage of myeloid cells independent of Myb and hematopoietic stem cells. Science *336*, 86-90.

Silva-Santos, B., Pennington, D.J., and Hayday, A.C. (2005). Lymphotoxin-mediated regulation of gammadelta cell differentiation by alphabeta T cell progenitors. Science *307*, 925-928.

Silver, L., and Palis, J. (1997). Initiation of murine embryonic erythropoiesis: a spatial analysis. Blood *89*, 1154-1164.

Sioud, M., Floisand, Y., Forfang, L., and Lund-Johansen, F. (2006). Signaling through toll-like receptor 7/8 induces the differentiation of human bone marrow CD34+ progenitor cells along the myeloid lineage. J Mol Biol *364*, 945-954.

Spangrude, G.J., Heimfeld, S., and Weissman, I.L. (1988). Purification and characterization of mouse hematopoietic stem cells. Science *241*, 58-62.

Stremmel, C., Schuchert, R., Wagner, F., Thaler, R., Weinberger, T., Pick, R., Mass, E., Ishikawa-Ankerhold, H.C., Margraf, A., Hutter, S.*, et al.* (2018). Yolk sac macrophage progenitors traffic to the embryo during defined stages of development. Nat Commun *9*, 75.

Stritesky, G.L., Xing, Y., Erickson, J.R., Kalekar, L.A., Wang, X., Mueller, D.L., Jameson, S.C., and Hogquist, K.A. (2013). Murine thymic selection quantified using a unique method to capture deleted T cells. Proc Natl Acad Sci U S A *110*, 4679-4684.

Takahashi, K., Yamamura, F., and Naito, M. (1989). Differentiation, maturation, and proliferation of macrophages in the mouse yolk sac: a light-microscopic, enzyme-cytochemical, immunohistochemical, and ultrastructural study. J Leukoc Biol *45*, 87-96.

Takeda, K., Kaisho, T., and Akira, S. (2003). Toll-like receptors. Annu Rev Immunol *21*, 335-376.

Tanaka, Y., Hayashi, M., Kubota, Y., Nagai, H., Sheng, G., Nishikawa, S., and Samokhvalov, I.M. (2012). Early ontogenic origin of the hematopoietic stem cell lineage. Proc Natl Acad Sci U S A *109*, 4515-4520.

Tanaka, Y., Sanchez, V., Takata, N., Yokomizo, T., Yamanaka, Y., Kataoka, H., Hoppe, P.S., Schroeder, T., and Nishikawa, S. (2014). Circulation-independent differentiation pathway from extraembryonic mesoderm toward hematopoietic stem cells via hemogenic angioblasts. Cell Rep *8*, 31-39.

Taoudi, S., and Medvinsky, A. (2007). Functional identification of the hematopoietic stem cell niche in the ventral domain of the embryonic dorsal aorta. Proc Natl Acad Sci U S A *104*, 9399-9403.

Tenor, J.L., and Aballay, A. (2008). A conserved Toll-like receptor is required for Caenorhabditis elegans innate immunity. EMBO Rep *9*, 103-109.

Tober, J., Koniski, A., McGrath, K.E., Vemishetti, R., Emerson, R., de Mesy-Bentley, K.K., Waugh, R., and Palis, J. (2007). The megakaryocyte lineage originates from hemangioblast precursors and is an integral component both of primitive and of definitive hematopoiesis. Blood *109*, 1433-1441.

Travnickova, J., Tran Chau, V., Julien, E., Mateos-Langerak, J., Gonzalez, C., Lelievre, E., Lutfalla, G., Tavian, M., and Kissa, K. (2015). Primitive macrophages control HSPC mobilization and definitive haematopoiesis. Nat Commun *6*, 6227.

Truman, L.A., Ford, C.A., Pasikowska, M., Pound, J.D., Wilkinson, S.J., Dumitriu, I.E., Melville, L., Melrose, L.A., Ogden, C.A., Nibbs, R., *et al.* (2008). CX3CL1/fractalkine is released from apoptotic lymphocytes to stimulate macrophage chemotaxis. Blood *112*, 5026-5036.

Tsai, F.Y., Keller, G., Kuo, F.C., Weiss, M., Chen, J., Rosenblatt, M., Alt, F.W., and Orkin, S.H. (1994). An early haematopoietic defect in mice lacking the transcription factor GATA-2. Nature *371*, 221-226.

Vabulas, R.M., Ahmad-Nejad, P., da Costa, C., Miethke, T., Kirschning, C.J., Hacker, H., and Wagner, H. (2001). Endocytosed HSP60s use toll-like receptor 2 (TLR2) and TLR4 to activate the toll/interleukin-1 receptor signaling pathway in innate immune cells. J Biol Chem *276*, 31332-31339.

van Furth, R. (1980). The mononuclear phagocyte system. Verh Dtsch Ges Pathol *64*, 1-11.

van Furth, R., and Cohn, Z.A. (1968). The origin and kinetics of mononuclear phagocytes. J Exp Med *128*, 415-435.

Willenborg, S., Lucas, T., van Loo, G., Knipper, J.A., Krieg, T., Haase, I., Brachvogel, B., Hammerschmidt, M., Nagy, A., Ferrara, N.*, et al.* (2012). CCR2 recruits an inflammatory macrophage subpopulation critical for angiogenesis in tissue repair. Blood *120*, 613-625.

Yamamoto, M., Sato, S., Hemmi, H., Hoshino, K., Kaisho, T., Sanjo, H., Takeuchi, O., Sugiyama, M., Okabe, M., Takeda, K.*, et al.* (2003a). Role of adaptor TRIF in the MyD88-independent toll-like receptor signaling pathway. Science *301*, 640-643.

Yamamoto, M., Sato, S., Hemmi, H., Uematsu, S., Hoshino, K., Kaisho, T., Takeuchi, O., Takeda, K., and Akira, S. (2003b). TRAM is specifically involved in the Toll-like receptor 4-mediated MyD88-independent signaling pathway. Nat Immunol *4*, 1144-1150.

Yeoh, E.J., Ross, M.E., Shurtleff, S.A., Williams, W.K., Patel, D., Mahfouz, R., Behm, F.G., Raimondi, S.C., Relling, M.V., Patel, A.*, et al.* (2002). Classification, subtype discovery, and prediction of outcome in pediatric acute lymphoblastic leukemia by gene expression profiling. Cancer Cell *1*, 133-143.

Yokomizo, T., and Dzierzak, E. (2010). Three-dimensional cartography of hematopoietic clusters in the vasculature of whole mouse embryos. Development *137*, 3651-3661.

Yokomizo, T., Watanabe, N., Umemoto, T., Matsuo, J., Harai, R., Kihara, Y., Nakamura, E., Tada, N., Sato, T., Takaku, T.*, et al.* (2019). Hlf marks the developmental pathway for hematopoietic stem cells but not for erythro-myeloid progenitors. J Exp Med *216*, 1599-1614.

Yokota, T., Huang, J., Tavian, M., Nagai, Y., Hirose, J., Zuniga-Pflucker, J.C., Peault, B., and Kincade, P.W. (2006). Tracing the first waves of lymphopoiesis in mice. Development *133*, 2041-2051.

Yona, S., Kim, K.W., Wolf, Y., Mildner, A., Varol, D., Breker, M., Strauss-Ayali, D., Viukov, S., Guilliams, M., Misharin, A.*, et al.* (2013). Fate mapping reveals origins and dynamics of monocytes and tissue macrophages under homeostasis. Immunity *38*, 79-91.

Yosef, N., Vadakkan, T.J., Park, J.H., Poche, R.A., Thomas, J.L., and Dickinson, M.E. (2018). The phenotypic and functional properties of mouse yolk-sac-derived embryonic macrophages. Dev Biol *442*, 138-154.

Yoshimoto, M., Porayette, P., and Yoder, M.C. (2008). Overcoming obstacles in the search for the site of hematopoietic stem cell emergence. Cell Stem Cell *3*, 583-586.

Zarember, K.A., and Godowski, P.J. (2002). Tissue expression of human Toll-like receptors and differential regulation of Toll-like receptor mRNAs in leukocytes in response to microbes, their products, and cytokines. J Immunol *168*, 554-561.

Zhao, J., Chen, X., Song, G., Zhang, J., Liu, H., and Liu, X. (2017). Uhrf1 controls the self-renewal versus differentiation of hematopoietic stem cells by epigenetically regulating the cell-division modes. Proc Natl Acad Sci U S A *114*, E142-E151.

Zhou, F., Li, X., Wang, W., Zhu, P., Zhou, J., He, W., Ding, M., Xiong, F., Zheng, X., Li, Z.*, et al.* (2016). Tracing haematopoietic stem cell formation at single-cell resolution. Nature *533*, 487-492.

Zhu, J.W., Li, Y.F., Wang, Z.T., Jia, W.Q., and Xu, R.X. (2016). Toll-Like Receptor 4 Deficiency Impairs Motor Coordination. Front Neurosci *10*, 33.

Zovein, A.C., Hofmann, J.J., Lynch, M., French, W.J., Turlo, K.A., Yang, Y., Becker, M.S., Zanetta, L., Dejana, E., Gasson, J.C.*, et al.* (2008). Fate tracing reveals the endothelial origin of hematopoietic stem cells. Cell Stem Cell *3*, 625-636.